Simulation of hydration and formation of structure in hardening cement-based materials

K. van Breugel

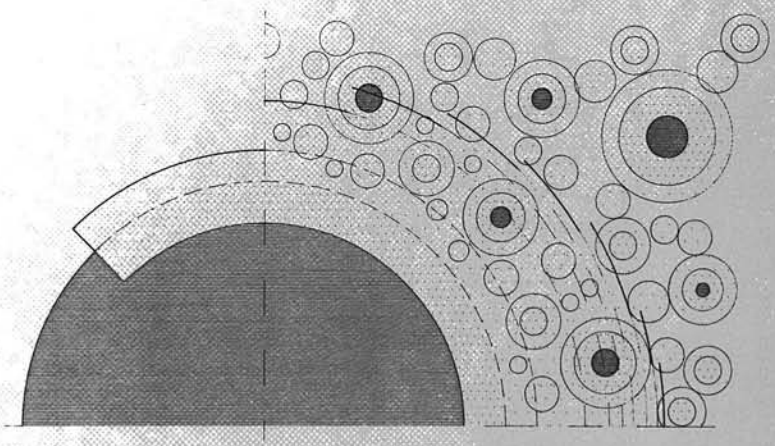

Hymostruc

697130

Simulation of Hydration and Formation of Structure in Hardening Cement-Based Materials

Second Edition

Bibliotheek TU Delft

C 0003813903

HYMOSTRUC

2414
541
2

"Where were you when I laid the foundations of the earth?
Tell me, if you know so much".
Job 38:4a

Simulation of Hydration and Formation of Structure in Hardening Cement-Based Materials

Second Edition

Revised version of the author's PhD-Thesis

by

Klaas van Breugel

Published and distributed by:

Delft University Press
Mekelweg 4
2628 CD Delft
The Netherlands
Telephone: +31 15 2783254
Fax: +31 15 2781661
E-mail: DUP@DUP.TUDelft.NL

ISBN / 90-407-1621-8

Copyright c 1997 by K. van Breugel

All rights reserved. No part of the material protected by this copyright notice may be reproduced or utilized in any form or by any means, electronic or mechanical, including photocopying, recording or by any information storage and retrieval system, without permission from the publisher: Delft University Press.

Printed in the Netherlands

TABLE OF CONTENTS page

Preface to the first edition xiii
Preface to the second edition xv

PART I: LITERATURE STUDY

Chapter 1. INTRODUCTION

1.1 General scope of the project 3
1.2 Survey of field of interest 3
1.3 Aims and outline of the project 6
1.4 Research strategy and built-up of the report 9

Chapter 2. CHEMICAL AND GRANULAR CHARACTERISTICS OF CEMENT

2.1 General 11
2.2 Cement composition 11
2.2.1 Mineral composition of raw materials 11
2.2.2 Clinker composition 11
2.2.3 Clinker composition. Accuracy considerations 13
2.2.4 Effect of particle size on compound composition 15
2.2.5 Gypsum 16
2.3 Granular characteristics of cement 17
2.3.1 General 17
2.3.2 Particle shape 17
2.3.2.1 Relationship between particle shape and particle size 17
2.3.2.2 Sphere-shaped versus cube-shaped particles 18
2.3.3 Particle size distribution 18
2.3.3.1 General 18
2.3.3.2 Mathematical expressions for particle size distributions 19
2.3.3.3 Minimum particle size 22
2.3.4 Specific surface 23
2.3.4.1 General 23
2.3.4.2 Determination of specific surface 23
2.3.4.3 Effect of minimum particle size on specific surface 24
2.3.4.4 Effect of gypsum of specific surface 25
2.3.4.5 Significance of granular features for evaluation of hydration data 25
2.4 Cement characteristics. Discussion and concluding remarks 26

Chapter 3. ASPECTS OF HYDRATION OF CEMENT-BASED MATERIALS

3.1	General	29
3.2	Chemical reactions of Portland cement and cement constituents	29
3.3	Heat of hydration	30
3.3.1	Determination of heat of hydration. Measuring methods	30
3.3.1.1	Adiabatic calorimetry. Accuracy	30
3.3.1.2	Isothermal calorimetry. Accuracy	31
3.3.2	Maximum heat of hydration. General calculation format	32
3.3.3	Heat of hydration of constituents	32
3.3.4	Predicted maximum heat of hydration. Accuracy	33
3.3.5	Degree of heat liberation. Accuracy	34
3.4	State of water	36
3.4.1	Classification of types of water	36
3.4.2	Chemically bound water	37
3.4.2.1	General aspects	37
3.4.2.2	Determination of chemically bound water $\hat{W}n$	38
3.4.2.3	Maximum chemically bound water $\hat{W}n$. General calculation format	39
3.4.2.4	Prediction of maximum chemically bound water $\hat{W}n$	39
3.4.2.5	Relative amount of chemically bound water. Accuracy and reliability	40
3.4.3	Physically bound water	41
3.4.4	Free water	42
3.5	Hydration mechanisms	42
3.5.1	Topochemical and through-solution reactions	42
3.5.2	Clinker hydration versus hydration of individual constituents	43
3.5.2.1	Rate of reaction of individual constituents	43
3.5.2.2	Independent hydration concept	44
3.5.2.3	Equal fractional rates (EFR-concept)	44
3.5.3	Hydration mechanisms. Discussion	45
3.6	Stages in cement hydration	47
3.6.1	General	47
3.6.2	Early period	47
3.6.3	Middle period	50
3.6.4	Late period	50
3.7	Chemical composition of reaction products	52
3.7.1	Survey of literature data	52
3.7.2	Chemical composition of reaction products. Discussion	53
3.8	Degree of hydration	54
3.8.1	Definitions	54
3.8.1.1	General	54
3.8.1.2	Parameters to indicate the degree of hydration	55
3.8.1.3	Degree of hydration - Definitions. Discussion	57
3.8.2	Cessation of the hydration process	57
3.8.2.1	Ultimate degree of hydration. Some observations	57
3.8.2.2	Ultimate degree of hydration. Theoretical considerations	58
3.8.3	Paste curing versus mortar and concrete curing	60
3.9	Chemistry-oriented aspects of hydration. Summary and discussion	61

Chapter 4. FORMATION OF STRUCTURE AND STRENGTH DEVELOPMENT

MORPHOLOGY-RELATED ASPECTS

4.1	General	63
4.2	Colloidal aspects in the early period of hydration	63
4.2.1	Stability of colloidal cement dispersion systems	63
4.2.1.1	Early electrostatic repulsion	64
4.2.1.2	Van der Waals attraction	65
4.2.1.3	Stereological implications of colloidal considerations	66
4.3	Morphology of hydration products	66
4.3.1	Classification of reaction products	66
4.3.1.1	Ettringite	67
4.3.1.2	Calcium silicate hydrates	68
4.3.1.3	Calcium hydroxide crystals	69
4.3.1.4	Stoichiometry of the physical composition of hydration products	69
4.3.2	Factors affecting morphology	70
4.3.3	Morphology - Miscellaneous	71
4.3.3.1	Average and minimum sizes of gel particles	71
4.3.3.2	Morphological stability	72
4.4	Formation of structure	72
4.4.1	Formation of basic skeleton	72
4.4.2	Inner and outer product	74
4.4.3	Gel characteristics	74
4.4.3.1	Gel porosity	74
4.4.3.2	Specific surface of gel	75
4.4.3.3	Gel density	75
4.4.4	Paste characteristics	77
4.4.4.1	General	77
4.4.4.2	Porosity and pore size distribution	77
4.4.4.3	Factors affecting porosity and pore size distribution	78
4.4.5	Aspects of structure formation and strength development in pastes	81
4.4.5.1	Physico-Chemical aspects	81
4.4.5.2	Development of microstructure and strength. Stereological aspect	82
4.5	Paste strength and influencing factors	83
4.5.1	General	83
4.5.2	Cement fineness and particle size distribution	83
4.5.3	Temperature effects	85
4.5.4	Water/cement ratio	86
4.5.5.	Cement composition	86
4.6	Paste strength versus strength of concrete and mortar	88
4.7	Matrix-aggregate interfacial phenomena	89
4.7.1	General	89
4.7.2	Thickness of the matrix-aggregate interface layer	89
4.7.3	Structural and morphological aspects of the interface layer	90
4.7.4	Degree of hydration in the interfacial zone	92
4.7.5	Matrix-aggregate interface aspects of strength development	92

4.8 Volumetric considerations of hydrating pastes 93
4.9 Strength laws. Macro level 94
4.9.1 General 94
4.9.2 Strength-porosity concept (f/P-relationship) 94
4.9.3 Gel-space ratio concept 96
4.9.4 "Degree-of-hydration" concept 97
4.9.5 Maturity laws 98
4.9.6 Strength laws. Discussion 98
4.10 Structure formation and strength development. Summary and Discussion 99

Chapter 5. CEMENT HYDRATION AND FORMATION OF MICROSTRUCTURE

KINETICS AND RATE FORMULAE

5.1 Kinetics and Rate Formulae. An introductory survey of models 103
5.2 Overall kinetics 105
5.2.1 Review of rate equations 106
5.2.2 Overall kinetics. Discussion 108
5.3 Particle kinetics 109
5.3.1 Phase-boundary reactions 109
5.3.2 Diffusion controlled reactions 111
5.3.3 Particle kinetics. Discussion 115
5.4 Hybrid kinetic models 116
5.4.1 Effect of particle size distribution on the overall rate of hydration 116
5.4.2 Relative humidity and gel-space ratio as rate determining factors 120
5.4.3 Kinetic models allowing for chemical composition of the cement 122
5.4.4 Overall, particle and hybrid kinetic models. Intermediate evaluation 124
5.5 Integrated kinetic models 126
5.5.1 Concepts put forward by Frohnsdorf et al. and Jennings 126
5.5.2 Preliminary Delft-studies 127
5.5.2.1 General 127
5.5.2.2 Stereological aspects of hydration and formation of structure 127
5.5.2.3 Effect of particle interaction on rate of hydration 130
5.5.2.4 Parameter studies carried out using HYDRASIM 131
5.5.2.5 Preliminary Delft-studies. General discussion, Evaluation and Outlook 133
5.6 Temperature dependency of rate processes 134
5.6.1 General 134
5.6.2 Temperature parameters 135
5.6.2.1 Temperature sensitivity factor "g" 135
5.6.2.2 Activation energy concept 137
5.6.2.3 Rate concept proposed by Röhling 139
5.6.2.4 Relationship between g-factor and AE-values 141
5.6.3 Temperature effects. Discussion 141
5.7 Models for kinetics. Summary and concluding remarks 142

PART II: HYMOSTRUC

Chapter 6. HYMOSTRUC: SIMULATION MODEL FOR CEMENT HYDRATION AND FORMATION OF STRUCTURE

Theoretical Part

6.1	General	145
6.2	Stereological aspects. "Cell" definition	145
6.2.1	Particle size distribution	145
6.2.2	Specific surface	147
6.2.3	Paste characteristics	147
6.2.4	Cell definition. Cell volume and particle spacing	148
6.2.5	Cell density	149
6.3	The spherical cell	150
6.3.1	Smeared-out and discrete cell density	150
6.3.2	Shell density. Volumetric considerations and conversion factor	151
6.4	Interaction mechanisms	154
6.4.1	Introductory remarks and basic assumptions	154
6.4.1.1	Spatial distribution of particles	154
6.4.1.2	Basic assumptions	155
6.4.2	"Particle expansion" during hydration	156
6.4.3	Embedded and free particles	160
6.4.4	Embedded centre-plane area and contact area	162
6.5	Rate of hydration	163
6.5.1	Particle shape effect	163
6.5.1.1	Particle shape effect in case of phase-boundary reaction	163
6.5.1.2	Particle shape effect in case of diffusion controlled reaction	164
6.5.2	Rate of penetration	166
6.5.2.1	Basic rate equation	166
6.5.2.2	Basic rate factor K_0 and K_1 and transition thickness δ_{tr}	167
6.5.3	Degree of hydration: Particle -, Cell - and Overall hydration	169
6.5.4	Effects of particle interaction on the rate of penetration	170
6.5.4.1	Increased shell expansion	170
6.5.4.2	Water withdrawal by embedded particles. Reduction factor $\Omega_1(x,\alpha_{x,j})$	171
6.5.5	Effect of water shortage in the pore system.	173
6.5.5.1	Porosity and pore size distribution	173
6.5.5.2	Maximum pore size ϕ_{max}	174
6.5.5.3	State of water in pore system. Reduction factor $\Omega_2(\alpha_j)$	176
6.5.5.4	Total capillary pore wall area $A_{por}(\alpha)$	177
6.5.5.5	Wet pore wall area $A_{wat}(\alpha)$. Reduction factor $\Omega_2(\alpha)$	178
6.5.5.6	Reduction factor $\Omega_2(\alpha)$. Indicative values	181
6.5.6	Effect of decrease of water content. Reduction factor $\Omega_3(\alpha)$	182
6.5.6.1	General	182
6.5.6.2	Pore water chemistry and rate of reaction. Some considerations	183
6.5.7	Water shortage effects. A comparison of different concepts	186

6.5.7.1	General	186
6.5.7.2	Water shortage concepts. HYMOSTRUC versus Röhling	186
6.5.7.3	Water shortage concepts. HYMOSTRUC vs. "Relative Humidity Concept".	187
6.6	Temperature effects	190
6.6.1	General	190
6.6.2	Net temperature effect. Determination of apparent activation energy	190
6.6.2.1	Isothermal tests carried out by Lerch and Ford	190
6.6.2.2	Temperature function $F_1(T)$. Implementation in HYMOSTRUC	195
6.6.3	Morphology and structure related temperature effects on reaction rate	196
6.6.3.1	General considerations	196
6.6.3.2	Determination of ν-factor as a function of curing temperature	197
6.6.3.3	Temperature function $F_2(T)$. Implementation in HYMOSTRUC	198
6.6.4	Temperature rise in Adiabatic Tests	199
6.7	Chemical composition of the cement as rate controlling factor	200
6.7.1	General considerations	200
6.7.2	Model parameters K_0 and δ_{tr} as function of cement composition	201
6.8	HYMOSTRUC - Theoretical part. Summary	202
6.9	HYMOSTRUC - Condensed flow chart	203

Chapter 7. HYMOSTRUC: MODEL FEATURES

7.1	General	207
7.2	Clustering of particles. Reduction of the number of free particles	207
7.3	Rate of hydration	208
7.3.1	Particle hydration versus overall hydration	208
7.3.2	Embedding of particles and shell expansion	209
7.3.3	Effects of embedding of particles on the rate of hydration	211
7.3.3.1	Shell expansion and water withdrawal caused by embedded particles	211
7.3.3.2	Influence of water/cement ratio on the effect of embedded particles	211
7.3.3.3	Water withdrawal mechanism. The partition factor $\Omega_1(.)$	212
7.3.4	Water shortage effects. The reduction factor $\Omega_{23}(\alpha)$	213
7.3.5	Rate of penetration	215
7.3.5.1	Basic rate factor K_0	215
7.3.5.2	Development of rate of penetration with elapse of time	215
7.3.6	Effect of transition thickness δ_{tr} on the course of the hydration curve	216
7.4	Strength considerations	217
7.4.1	General	217
7.4.2	Amount of embedded particles and strength development	218
7.4.2.1	Embedded cement volume	218
7.4.2.2	Embedded centre-plane area or contact surface area	219
7.4.3	Embedded cement and strength development. Effect of w/c ratio	219
7.4.4	Interparticle versus transparticle fracturing	221
7.5	Interface phenomena	223
7.5.1	Potentialities of HYMOSTRUC for quantitative analysis of "Wall Effects"	223
7.5.2	Paste density at the matrix-aggregate interfacial zone	225
7.5.3	Hydration in the interfacial zone	226
7.5.4	Strength considerations in view of interface phenomena. Discussion	228

Chapter 8. NUMERICAL EVALUATION PROGRAM FOR DETERMINATION OF MODEL PARAMETERS

Accuracy Considerations and Predictability

8.1	General	229
8.2	Effect of chemical composition of the cement on model parameters	229
8.2.1	Tests of Lerch and Ford	229
8.2.2	Model parameters for alite and belite hydration	231
8.2.3	Chemical clinker composition. Discussion	231
8.3	Effect of cement fineness and particle size distribution on model parameters	233
8.3.1	Tests of Keienburg	233
8.3.2	Effect of the particle size distribution	235
8.3.2.1	Tests of Frigione et al.	235
8.3.2.2	Tests carried out by Locher et al.	236
8.3.3	Cement fineness and particle size distribution. Discussion	237
8.4	Effect of water/cement ratio. Isothermal tests	238
8.4.1	Tests of Danielsson	238
8.4.2	Tests of Frigione et al.	239
8.4.3	Effect of water/cement ratio. Discussion	239
8.5	Effect of temperature. Isothermal tests	240
8.5.1	Tests of Lerch and Ford	240
8.5.2	Tests of Rakel	242
8.5.3	Isothermal temperature effects. Summary and discussion	244
8.6	Adiabatic and semi-adiabatic curing	245
8.6.1	Adiabatic tests	245
8.6.2	Semi-adiabatic tests	247
8.6.3	Adiabatic tests. Discussion	250
8.7	Model parameters: quantitative values and accuracy. Discussion	251
8.7.1	Basic rate factor K_0	251
8.7.2	Transition thickness δ_{tr}	253
8.7.3	Coefficients β_1 and β_2	254
8.8	Predictability	255
8.8.1	Introductory considerations	255
8.8.2	Prediction of adiabatic hydration curves	255

PART III: APPLICATIONS, EVALUATION AND SUMMARIES

Chapter 9. PRACTICAL APPLICATION OF HYMOSTRUC. RELIABILITY

9.1	General	259
9.2	Macro-Level Calculations. Program features of TEMPSPAN	259
9.3	Macro-Level calculations. Case-study	260

9.3.1 Construction and mix data 260
9.3.2 Case study. Results 261
9.3.3 Probability of cracking 262
9.4 Discussion 264

Chapter 10. CONCLUSIONS AND RECOMMENDATIONS

10.1 Objectives of the study 265
10.2 Conclusions 265
10.3 Recommendations 267

Chapter 11. EXTENDED SUMMARY

11.1 General 269
11.2 Goals 269
11.3 Structure formation and strength development. Basic concept 269
11.4 Kinetics of particle growth and formation of microstructure 270
11.5 Factors affecting the rate of hydration 273
11.5.1 Chemical aspects 273
11.5.2 Particle size distribution 273
11.5.3 Effect of water/cement ratio and state of water 274
11.5.4 Temperature effects 276
11.6 HYMOSTRUC. Independent model parameters 278
11.6.1 General 278
11.6.2 Values of independent model parameters 278
11.7 Applications 279
11.7.1 Strength development 279
11.7.2 Fracture modes in hardening cement pastes 279
11.7.3 Interface phenomena. Porosity 280
11.7.4 Temperature predictions in concrete structures 281
11.7.5 Probability of cracking 282
11.8 Reliability considerations 283
11.9 Working with HYMOSTRUC 285

SUMMARY 287

SAMENVATTING 289

REFERENCES 291

NOTATIONS AND SYMBOLS 303

ACKNOWLEDGEMENTS 305

PREFACE TO THE FIRST EDITION

Now more than ever, is the time to focus research in the building industry on the control of all those processes which can or do affect the quality of our technical achievements. Inferior quality of products implies, in essence, a waste of scarce materials and energy. In this respect one should bear in mind that, in comparison with other industrial activities, the building industry is one of the most demanding branches insofar material use and energy consumption is concerned. Society can, therefore, substantially benefit from even relatively small savings of materials and energy in this industry.

Another most challenging research aim that is currently a focus of attention concerns the development of high-performance and tailor-made materials. Besides realization of unconventional structural designs, economic material use and reduction of maintenance costs are aimed at with the use of these new materials.

Rational judgement of the quality of a product and whether savings of materials and energy are possible or not, as well as the development of high-performance materials, should be based on a clear understanding of the material behaviour at different morphological levels. This holds for all materials and not in the least for cement-based materials. Among the possible methods to investigate the extremely complex structure and structural development of cement-based materials, computer-based material simulations have become increasingly important. It is virtually inconceivable that the mutual interferences of processes and mechanisms occurring in hardening and hardened cement-based systems could ever be described comprehensively without the help of advanced computer facilities.

The recognition of both the complexity of processes and mechanisms responsible for the development of material properties and the vast potential of computer simulations has taken shape in what is nowadays known as Computational Materials Science. As far as the potential of computer simulations is concerned, the possibility to synthesize information from different disciplines should be considered as one of the most challenging features of this modern research technique. It is this potential of computer simulations which make them a most valuable tool for bridging the gaps between different research disciplines and between theory and engineering practice.

The present thesis is an example of what can be achieved in the field of computational materials science, i.e. with numerical modelling of hydration and structural development in cement-based materials. The complexity of the subject, viz. the mutual interference of granular, stereological, physio-chemical and colloidal aspects of the processes and mechanisms involved in hydration and structural development, *as well as* the relevancy of adequate simulation models for *practical engineering purposes*, are outlined in Part I of the thesis. This part is written as a condensed state-of-the-art of these aspects, including a critical evaluation of the implications for mathematical modelling. It is explained why and how, at the present state of knowledge, rigorous systematization of information generated in individual disciplines is required in order to develop adequate algorithms with which the mutually interfering processes and mechanisms can be described.

A reader who is already familiar with the complexity of the subject and with the problems of mathematical modelling of hydration and structural development in particular, can go to the heart of the matter immediately by starting in Part II of this report. In this

second part a detailed description of a simulation model, denoted with the acronym **HYMOSTRUC**, is given. It further comprises an evaluation of the consistency and, particularly, the *predictability* of the model, as well as a case study showing the potential of the model to serve practical engineering purposes.

A short general discussion and a list of conclusions and recommendations, as well as an extended summary of the whole report, are presented in Part III of this thesis.

With this particular format of the report attempts have been made to explain the potential of computer simulations for both fundamental research purposes and engineering practice for people who are active in different disciplines involved or interested in hydration and microstructural development in cement-based materials. In no way this thesis claims to be comprehensive in the sense that all relevant aspects have been dealt with exhaustively. The results of this study, however, convincingly demonstrate that computer simulations of complex processes and mechanisms have a great potential. There is no doubt that future developments in materials science and engineering practice will be stamped significantly by an increasingly important role of these simulations. It is the author's wish that further progress in computational material science may receive some stimulus from the present study.

Delft, October 1991

PREFACE TO THE SECOND EDITION

Many reactions on the first of edition of this thesis have inspired the author to publish this second edition. Another reason for reprinting the thesis is that it serves as a reference work for a number of studies performed, or in progress, at the Delft University of Technology concerning the properties of concrete at early ages and the extension of the simulation program HYMOSTRUC presented in this book. Moreover, since the program has become available as a commercial software package, the original model description should be available for potential users.

In this second edition minor changes have been carried through. Some corrections in the text have been conducted and obvious misprints have been removed. The contents of the report, however, has been left largely unchanged. This in spite of the fact that much most worthwhile research has been done since the first edition of the thesis was published in 1991. Although these recent research achievements will not be reviewed in detail in this book, a few noteworthy studies and developments will still be mentioned. Worthwhile to mention are, first of all, the NIST-studies in the United States. These studies have meanwhile resulted in a large number of publications by Garboczi[1]) and co-workers. For a nice review of the present state of development of the NIST model reference is made here to a recent article of Bentz[2]). In that article it is shown how the digital-image-based model developed at NIST is capable to allow for a variety of physical and chemical aspects of hydration and microstructural development in a fundamental way. Besides the NIST-studies the work of a number of Japanese researchers and research groups must be mentioned. In 1994 Kishi[3]) presented a model for hydration of blended cement. In a more recent paper Maekawa[4]) has emphasized the mutual interaction of different mechanisms and processes, which have to be considered in the early stage of hydration and should, therefore, also be addressed in advanced microstructural models.

In the proceedings[5]) of a NATO-workshop on modelling of microstructure in cement-based systems, held in Saint-Rémy-les-Chevreuse (Fr), current research on modelling of

---

[1]) Garboczi, E.J., Bentz, D.P. (1992) *Computer-based models of the microstructures and properties of cement-based materials*. 9th Int. Conf. Chem. of Cement, New Delhi, Vol. VI, 3-15.

[2]) Bentz, D.P. (1997) *Three-dimensional Computer Simulation of Portland Cement Hydration and Microstructure Development*. J. Am. Ceram. Soc., 80, [1], 3-21

[3]) Kishi, T., Maekawa, K. (1994). *Thermal and Mechanical Modelling of Young Concrete Based on Hydration Process of Multi-Component Cement Minerals*. Proc. Int. RILEM Symposium on Thermal Cracking in Concrete at Early Ages, Munich, 11-18.

[4]) Maekawa, K., Chaube, R.P., Kishi, T. (1995) *Coupled mass transport, hydration and structure formation thoery for durability design of concrete structures*. Proc. Int. Workshop on Rational Design of Concrete Structures, Hakodate, Japan.

[5]) Jennings, H., Kropp, J., Scrivener, K. (1994) *The Modelling of Microstructure and Its Potential for Studying Transport Properties and Durability*, Kluwer Academic Publishers, NATO ASI Series E., Vol. 304, 558 p.

hydration and microstructure in the USA, France, Denmark, Sweden, Switzerland and The Netherlands are presented. In these proceedings a number of quite different approaches is presented, showing the complexity and multi-disciplinarity of the subject in a convincing way.

In The Netherlands further studies on different aspects of numerical simulation of hardening cement-based systems were performed at the Delft University of Technology. Research topics are moisture transport in hardening paste, more in particular in the "ribbon paste", volume changes due to self-desiccation[6]), and modelling of the influence of microstructural changes on creep and relaxation in hardening paste and concrete[7]). In these studies the HYMOSTRUC model presented in this book is the starting point for the simulation of both the evolution of the hydration process and the microstructure. In the framework of these studies the original HYMOSTRUC program has been extended substantially. These extensions concern the spatial distribution of the particles in the paste, thermodynamic principles and a more sophisticated interpretation of the calculated interaction between hydrating cement particles.

The simulation program HYMOSTRUC is commercially available since 1995. In the autumn of 1997 the new release will be issued. This 3.1-version runs under WINDOWS 95. Extensions of the HYMOSTRUC program are under development. These extensions concern the development of mechanical properties and of autogenous shrinkage due to self-desiccation.

Delft, September 1997

---

[6]) Koenders, E.A.B. (1997) *Simulation of volume changes in hardening cement-based materials*. PhD-thesis, Delft, 171 p.

[7]) Lokhorst, S.J. (1997) *Deformational Behaviour of Concrete Influenced by Hydration-Related Changes of the Microstructure*. TU-Delft.

PART I

Literature Study

Survey and Evaluation

Introduction

Chemical and Granular Characteristic of Cement

Aspects of Hydration of Cement-Based Materials

Microstructure and Strength Development

Kinetics and Rate Formulae for Hydration and Microstructural Development

1 INTRODUCTION

1.1 General Scope of the Project

From decades of practical experience as well as from theoretical considerations it is well known that the *quality* of concrete largely depends on, first of all, the water/cement ratio, but also on the magnitude of temperatures and thermal stresses in the concrete's early life. In order to enhance the quality and performance of the concrete, control of these temperatures and associated thermal stresses is a major item in today's engineering practice. For quantification of the effectiveness of technological and technical measures that can be applied for improving quality, i.e. to reduce thermal stresses and the probability of cracking, numerical simulation techniques are judged to have become of paramount importance. Simulation programs should be able to predict the development of hydration temperatures, strength, stresses and the risk of early thermal cracking.

In a short survey of this field of interest, it will appear that control of temperatures, strength, stresses and the probability of cracking have been points of concern of engineers and designers from the beginning of concrete engineering. Some distinct trends in computer-aided quality control and simulation techniques will be highlighted in this survey. Against the background of this survey the particular aims of this study will be defined.

1.2 Survey of Field of Interest

Thermal Effects in Hardening Concrete

Tetmayer [587] was probably one of the first who recognized the importance of thermal effects in early-age concrete and carried out temperature measurements as early as 1883. Since Tetmayer's measurements many authors have discussed thermal problems. Major items in these discussions, of which many date back to the late twenties and early thirties, referred to either optimization of pouring sequences in view of reducing maximum hydration temperatures in mass concrete structures like dams, economical formwork removal, or avoidance of thermal cracking [88,169,290]. Thermal problems and recommendations for formwork removal in *thin* and *slender* elements were discussed in the forties by Forbrich [169], while the number of recent reports on this subject shows an enormous growth [230, 252,360,613]. In the last decade the risk of thermal cracking has been discussed particularly in connection with *durability*. Incompatibility of thermal deformations of the cement matrix and aggregate and the associated risk of microcracking and loss of durability has pushed forward the need for control of maximum temperatures during the concrete's early life [251,257,429,643]. A sub-item in this respect refers to the *avoidance of frost damage* in early-age concrete [118,170,340,360,361]. More recently, the consequences of early thermal cracking and associated loss of durability have been discussed in view of the *shortage of raw materials* [584].

Temperature and Strength: Predictive Methods

The first attempts to predict hydration temperatures in hardening concrete have been ascribed to Yoshida and date back to 1921 *(Ibid. [563])*. A *graphical method* for the prediction of maximum temperatures has been elaborated by Werner. His method has been applied successfully for the prediction of the maximum temperature in the piers of the Väster Bridge in Stockholm *(Ibid. Forsen [171])*. Several *analytical methods* for the determination of temperature fields were proposed and discussed in the thirties [89,105,373, 402]. Almost all those methods were based on the differential equation of Fourier:

$$\frac{(\partial T)}{(\partial t)} = a_c * [\frac{(\partial^2 T)}{(\partial x^2)} + \frac{(\partial^2 T)}{(\partial y^2)} + \frac{(\partial^2 T)}{(\partial z^2)}] + Q(t,x,y,z) \qquad (1.1)$$

where a_c [m^2/s] is the coefficient of thermal diffusivity of concrete, T [°C] the temperature, x,y,z are the coordinates of a particular point in the structure and Q(t,x,y,z) [J/g] is the heat liberation function. The latter function is, in essence, also a function of the reaction temperature, i.e. the initial temperature of the mix.

In the framework of this study the heat liberation function is of particular interest. Several authors have proposed to approximate the real (adiabatic) heat liberation curve by an exponential function [237,261,311] (Fig. 1.1):

$$Q(t) = Q^{max} * (1 - \exp(-r.t)) \qquad [J] \qquad (1.2)$$

where Q(t) is the heat of hydration liberated at time t, Q^{max} the heat of hydration when hydration has practically ceased and r an empirical constant. In order to account for the typical S-shape of the actual hydration curve a function is preferred of the form [236]:

$$Q(t) = Q^{max} * \exp(-(\tau/t)^{\beta}) \qquad [J] \qquad (1.3)$$

with Q(t) and Q^{max} as in eq. (1.2), whereas τ and β are empirical constants.

In the early applications of the Fourier function the hydration curves (1.2) and (1.3) were considered to be independent of the place in the structure. As early as 1937, however, Carlson [89] pointed out that the heat liberation curve Q(t) will be affected by the actual reaction temperatures in the concrete, which are not known at the outset of the calculation. Rastrup [477] was probably the first who actually took the influence of the reaction temperature on the rate of reaction, and hence on the rate of heat of liberation, into account. In a step-by-step calculation procedure the effect of the actual reaction temperature was accounted for according to considerations put forward by Van 't Hoff (see Section 5.6). A most important feature in Rastrup's approach was that not only the temperature of the concrete was obtained, but *also the degree of hydration*. This at least on the condition that the degree of hydration can be equalized with the degree of heat liberation (see Section 3.3.5 and 3.8). The degree of hydration is, in turn, an important, if not the *most* im-

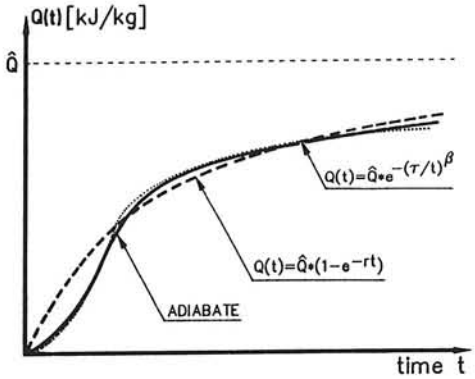

Fig. 1.1 Mathematical functions used to approximate adiabatic hydration curves.

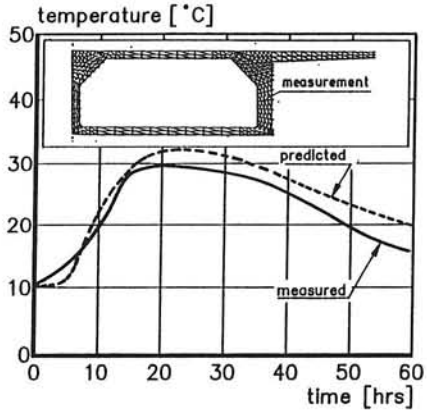

Fig. 1.2 Calculated and measured temperatures in a box-girder bridge [230].

portant parameter for the characterization of the continuously changing material properties like the strength and stiffness of a hardening cement-based material [68,295] [1]).

After Rastrup's pioneering work, several authors have worked from a similar angle. Similar in the sense that they, in one way or another, explicitly accounted for the *temperature sensitivity* of the cement, i.e. for the effect of the actual curing temperature on the rate of hydration [66,313,486,499]. An important conclusion that can be drawn from a comparison of a large number of predicted temperatures with measurements on site is that nowadays temperature predictions are possible with a high accuracy [66,148,361,362]. To illustrate this see Fig. 1.2, which shows the measured and predicted temperatures in a box-girder bridge recently built in Amsterdam [230]. Also strength predictions, based on experimentally determined correlations between strength and degree of hydration, gave reasonable results [262] (see also Section 4.9.4).

Stress Prediction and Risk of Cracking

The subsequent and inevitable step in view of quality control in early-age concrete refers to the prediction of thermal stresses. Although stress calculations in hardening concrete have been carried out since 1938 [90], it cannot be stated that stress calculation procedures have reached a mature state yet: stress calculations are still considered to be very complicated [311,550] or even beyond our present ability [360]. The major problem refers to the quantification of both early-age plastic deformations and early-age relaxation. A number of

---

1) The use of the degree of hydration as the key-parameter for describing the evolution of the materials properties in hardening concrete has strongly been emphasized by G. De Schutter in his PhD-thesis: *Fundamental and practical study of thermal stresses in hardening mass concrete elements*, Gent (B), 2 Volumes, 364 p. + Appendices (in Dutch).

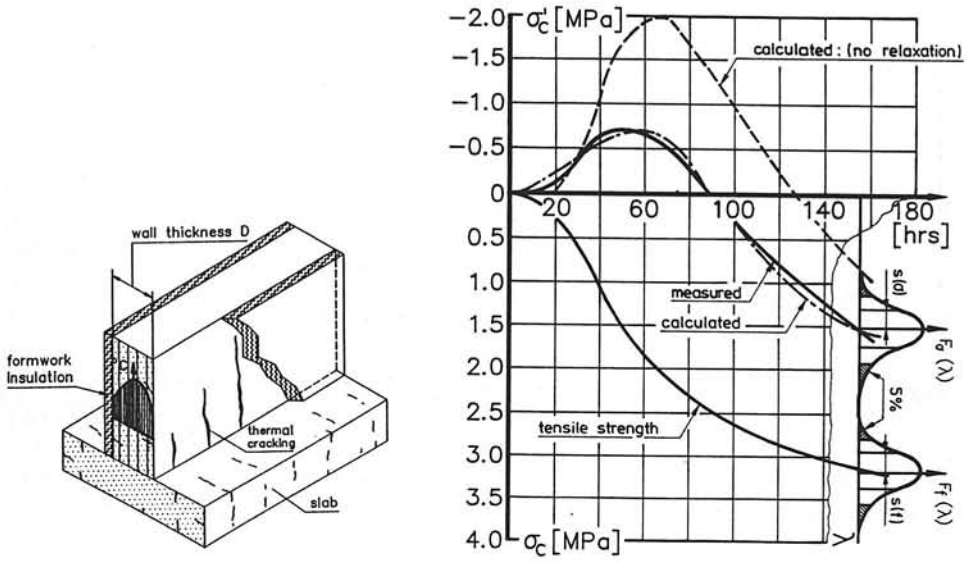

Fig. 1.3 Stresses, strength and risk of cracking in hardening concrete [68].

simplified calculation procedures have been proposed in which the effect of early-age relaxation is allowed for by reducing the modulus of elasticity in the early stage of the hydration process [24,246]. More sophisticated calculation procedures have been elaborated by Emborg [152,153] and recently by Laube [329]. A relaxation formula which explicitly allows for the effect of the hydration process on stress relaxation was proposed by the author in the early eighties [67,68]. Promising results were obtained for both calculated thermal stresses and the probability of cracking (Fig. 1.3). Predictions of early-age creep, also based on calculation procedures in which the progress of the hydration process was explicitly accounted for, were promising as well [372,607]. The importance of explicit allowance for structural formation, and thus implicitly for the development of the degree of hydration, in creep functions for early-age concrete has recently been supported by Bažant [31].

1.3 Aims and Outline of the Project

From the foregoing survey it is evident that for both temperature and strength calculations, as well as for the prediction of stresses and the risk of cracking, the degree of hydration must be considered as a most important factor. The degree of hydration is the parameter which indicates the amount of liberated heat as well as the physico-chemical and geometrical constitution of the cement paste. The accuracy and reliability of macro-level models for temperature, strength and stress calculations, therefore, largely depend on the accuracy with which the degree of hydration can be determined. Besides inaccuracies in the calcu-

lated degree of hydration, strength and stress predictions can also suffer from a lack of fundamental knowledge with respect to the *correlation* between the degree of hydration and associated structural formation, on the one hand, and strength and stress development, on the other.

The complexity of the correlation between structural formation and development of material properties, as well as the need for further research on this topic, has been emphasized by several authors [117,257,315,345,440,445,599]. With regard to the reason for the absence of models in which the progress of the hydration process and the development of material properties are considered comprehensively, we are inclined to fall in with Shein [536] and Daimond [139] when they, each in a different way, point out that it might be *the lack of fundamental rigour* in defining the relevant characteristics of the starting materials and of the hydration products *rather than a lack of information about individual processes and mechanisms* to which this absence must be attributed. This lack of rigour causes a kind of status quo as far as mathematical modelling of hydration processes and structural formation is concerned. This status quo in turn means that a lot of the most interesting information in micro[2]) and meso[*]) level research is not transferred to the macro[*]) or engineering level.

The present study must be regarded as an attempt to bridge the gap between these research levels. Among the possible ways to bridge this gap it was decided to develop a computer-based simulation model[3]). This choice was considered evident in the light of the complexity of the subject, i.e. of the many interfering processes and mechanisms that has to be allowed for and which can hardly be dealt with comprehensively without the use of the computer.

The position of this simulation model in the field of interest as described in the preceding Section is diagrammatically shown in Fig. 1.4. The model, called **HYMOSTRUC**, the acronym for **HY**dration, **MO**rphology and **STRUC**ture development, can be considered as the pendant of a number of experimental tests which are required to generate the input for macro-level calculations of hydration temperatures, strength and stresses in concrete structures. These experiments comprise the determination of adiabatic curves, as well as the relationship between the degree of hydration and strength development.

The particular aims of the present research project and of the simulation model in particular are defined now as follows:

1. *Development of a simulation model with which adiabatic and/or isothermal hydration curves of cement-based materials can be predicted. These curves could serve as input for numerical evaluation of thermal effects in hardening concrete structures.*
2. *The simulation model should take into consideration mutual interferences between the hydration process and the development of microstructure. Morphological features, particularly temperature-related ones, should be dealt with.*

---

2)*) In this report the definitions for micro-, meso- and macro-level are according to Wittmann [624].

3) Strictly speaking the term "simulation model" is a somewhat tautological term. However, since the term is quite current in the technical literature it has sometimes been used in this report

3. *The correlation between structural development (as it will be considered in the model) and the development of material properties shall be evaluated.*
4. *In view of the desired applicability of the results in engineering practice indications shall be given about the reliability and accuracy of the predictions.*

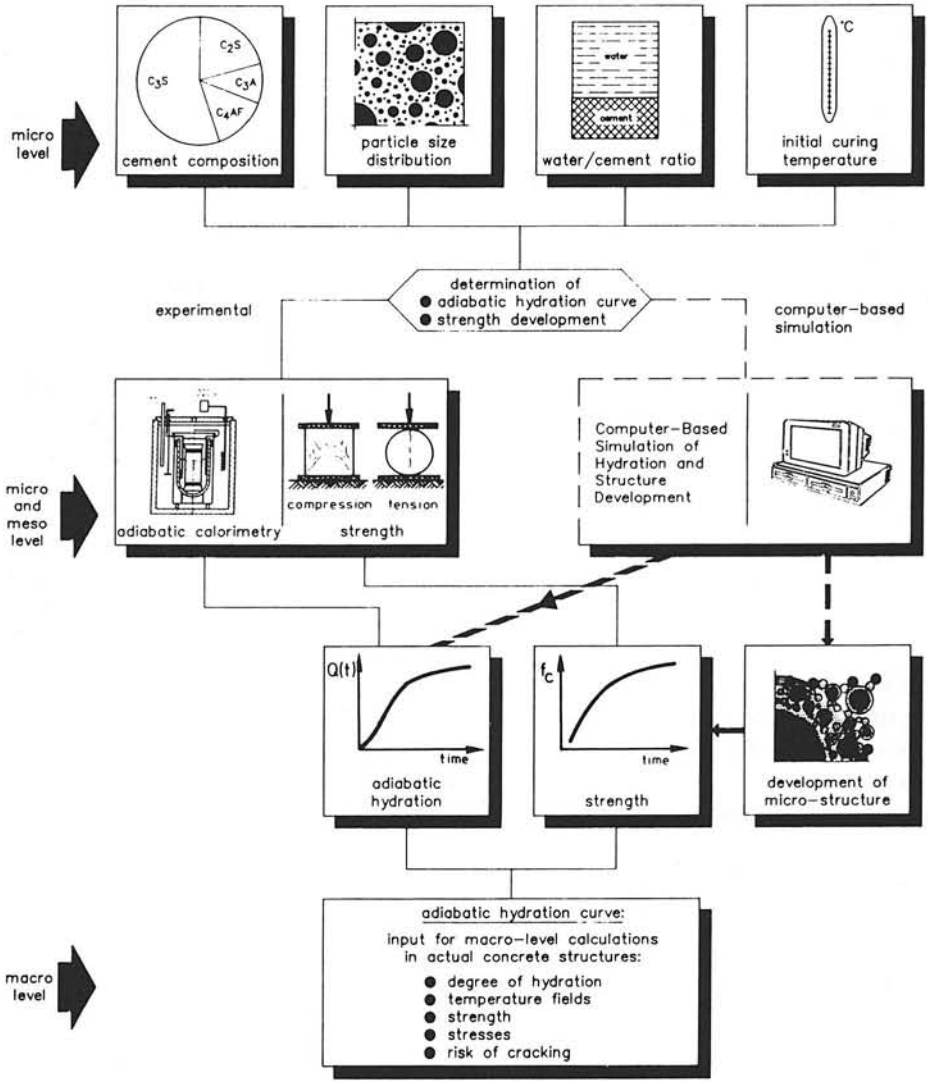

Fig. 1.4 Schematic representation of the field of interest and the position of the model, i.e. HYMOSTRUC, presented in this study.

With regard to aforementioned points the following additional remarks are made:

- The model shall be able to allow for the effects of the cement composition, the particle size distribution of the cement, the water/cement ratio and the curing temperature during the hydration process and the development of material properties. This implies that the *chemical, physical, granular* and *stereological* aspects of both the hydration process and structure formation shall be modelled explicitly.
- Main emphasize will be on hydration of systems based on Portland cement.
- In order to enhance the applicability in engineering practice the simulation model should be developed preferably for a Personal Computer environment.

1.4 Research Strategy and Set-Up of the Report

With respect to the strategy followed in this study, it was decided to base ourselves mainly on the experimental data presented in the literature. This policy has certainly been inspired by Diamond [141] and Shein [536], when they both emphasized the need of research that aims at making the huge files of available experimental data operative rather than generating more "experiment-bound" information. A small number of tests has nevertheless been carried out in order to have at least one set of data of which detailed information about the specimens and test conditions would be at our disposal.

In order to establish and to judge the consistency of the simulation model that will be developed one actually has to descend to the *meso-*, the *micro-* and even the *nano-level*, i.e. the levels at which the physico-chemical and stereological aspects of the hydration process and structural formation are formulated. The chemical and granular characteristics of Portland cement - to which we will restrict ourselves - are reviewed in Chapter 2. Chapter 3 deals with hydration concepts and mechanisms, including considerations con-

		Ch. 1. Introduction
PART I	Survey and evaluation of literature	Ch. 2. Cement Characteristics Ch. 3. Hydration Mechanisms Ch. 4. Microstructure and Strength Ch. 5. Kinetics / Rate Formula
PART II	HYMOSTRUC: Outline of the simulation model	Ch. 6. HYMOSTRUC: Theoretical Part Ch. 7. Model Features Ch. 8. Model Evaluation / Predictability
PART III		Ch. 9. Practical Application Ch. 10. Conclusions and Recommendations Ch. 11. Extended Summary

Fig. 1.5 Structure of the report - schematic.

cerning the accuracy with which the degree of hydration can be determined. Chapter 4 discusses some morphological features and the most relevant aspects of structure formation. This chapter gives due attention to the stereological aspect of both bulk hydration and matrix-aggregate hydration. Strength aspects will be dealt with as well. Kinetic models will be reviewed in Chapter 5.

The information discussed and evaluated in the Chapters 2 to 5, i.e. PART I of the report, constitutes the starting point for a detailed presentation of HYMOSTRUC in PART II, which covers the Chapters 6 to 8. The theoretical background of the simulation model is presented in Chapter 6, whereas some particular features of HYMOSTRUC are discussed in Chapter 7. In Chapter 8 an evaluation program is carried out in which the potential of HYMOSTRUC to approximate, i.e. to simulate and predict, hydration data are shown.

The hydration data was obtained from literature and selected so as to guarantee that in our simulations a wide range of particle size distributions, cement compositions, water/cement ratios and curing conditions. The evaluation program includes the determination of the so-called "independent model parameters", of which the values were not known at the outset of the program. Chapter 9 presents a case study, which illustrates the practical relevance and reliability of HYMOSTRUC. Emphasis is placed on the influence of inaccuracies and uncertainties in the independent model parameters on the calculated probability of thermal cracking in hardening concrete walls. Conclusions and recommendations are presented in Chapter 10. The main features of the simulation model are presented in an extended summary in Chapter 11. The report closes with short summaries in English and Dutch. The set-up of the report has been summarized diagrammatically in Fig. 1.5.

2 CHEMICAL AND GRANULAR CHARACTERISTICS OF CEMENT

2.1 General

In the introduction it has been mentioned already that both hydration of cement and formation of structure exhibit a chemical, physical and a granular and stereological aspect.

Considerations concerning the *chemical* aspect require information about the chemical composition of the cement. Since we intend to model the hydration process as a function of, among other things, the chemical composition of cement, several relevant chemistry-related aspects of the raw material will be discussed in this chapter. Due attention will be given to the accuracy with which the clinker composition of cement can be determined.

Considerations on the *stereological* aspect of both the hydration process and structural formation require information on the *granular features* of the cement, viz. the *particle shape* and the *particle size distribution*. A clear picture of the granular features of cement will turn out to be essential for a correct interpretation of experimental data concerning the degree of hydration, penetration depths, diffusion coefficients, hydration mechanisms, etc.

2.2 Cement composition

2.2.1 Mineral Composition of Raw Material

In the raw material from which Portland cement clinker is made, i.e. limestone and clay, four *major oxides* are found, viz. calcium oxide (CaO), silicium oxide (SiO_2), aluminium oxide (Al_2O_3) and ferrite oxide (Fe_2O_3). The most important *minor oxides* are magnesium oxide (MgO), potassium oxide (K_2O) and sodium oxide (Na_2O). Further sulphates (SO_3) are present, mainly in the form of potassium and sodium sulphates. The SO_3 content deserves special attention since this oxide, together with added gypsum, regulates the progress of the hydration process in the early stages of hardening. Other minor oxides like TiO_2, Mn_2O_3 and Pb_2O_5 are of less importance as far as the very purpose of this study is concerned. For specific features and effects of minor oxides and for the desirable and/or permissible quantities of the latter in raw mixes, reference is made to the literature [97, 263]. Fig. 2.1 shows the range of percentages of major oxides generally found in ordinary Portland cement. The proportional variation in the amounts of minor oxides is generally much higher than the variation in major oxides.

2.2.2 Clinker Composition

Burning, partial melting and sintering of the mix of raw material results in a clinker of which the four major minerals are tricalcium silicate (C_3S), dicalcium silicate (C_2S), tricalcium aluminate (C_3A) and tetracalcium aluminate ferrite (C_4AF). Their percentages in

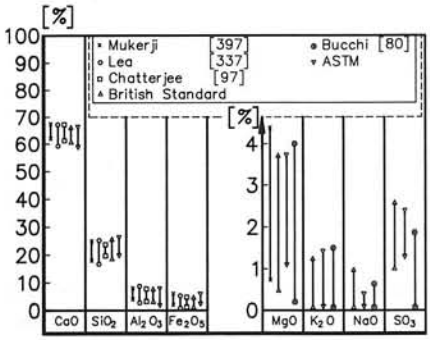

Fig. 2.1 Chemical composition of raw materials of ordinary Portland cement.

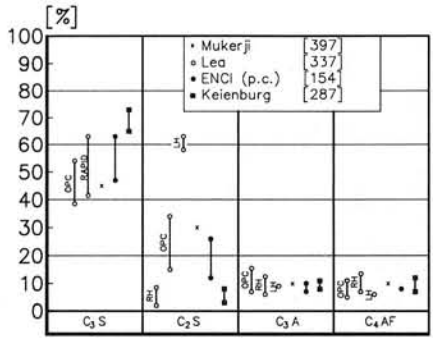

Fig. 2.2 Mineral composition of Portland clinker: low heat, moderate heat and rapid hardening.

Portland cement clinker are shown in Fig. 2.2, whereas Fig. 2.3 gives an impression of the distribution of the minerals in a clinker particle. The major minerals will generally contain small amounts of impurities. C_3S with small amounts of Fe, Al, Mg, Cr and Zn is called alite [242]. Impure C_2S is known as belite and β-C_2S, whereas impure C_4AF and C_3A is called celite [242,337]. The presence of impurities in the major constituents means that hydration data obtained from artificially prepared clinkers of pure constituents cannot unconditionally be applied to Portland cements. This even holds for the hydration characteristics of clinker made from impure compounds, since the hydration of individual impure compounds is different from hydration of these compounds in Portland cement [337,630].

Besides the four major constituents, the clinker may contain small amounts of minor constituents like Na_2SO_4, NC_8A_3 and $KC_{23}S_{12}$, and some free calcium oxide (CaO) and magnesium oxide (MgO).

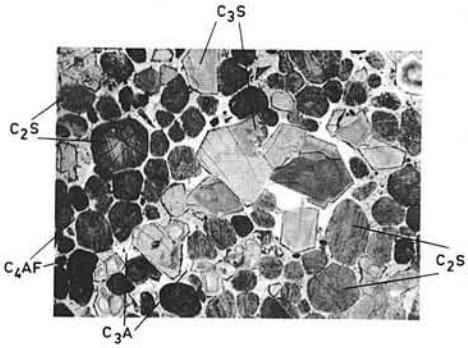

Fig. 2.3 Distribution of minerals in a clinker particle (taken from [122]).

The final clinker composition depends on the mineral composition of the raw material and the technical manufacturing conditions, such as the homogeneity of the mix of oxides, the characteristics of the fuel, the heating regime and the cooling process and the method of storage of the clinker [310]. Particularly the cooling history may have a significant influence on the final composition of the clinker [337,397].

2.2.3 Clinker Composition. Accuracy Considerations

General

Methods for the determination of the degree of hydration require information about the chemical composition of the cement. The degree of hydration can be determined, for example, by dividing measured values of either the liberated heat or the chemically bound water by the theoretical maximum values of these quantities (Section 3.8). These maximum values can be calculated from the chemical composition of the clinker. The *accuracy* and *reliability* of these values are directly dependent on the accuracy with which the chemical composition has been determined. As will be shown in the following, the chemical clinker composition as determined by different methods may deviate quite substantially. Information about the accuracy and reliability with which the chemical clinker composition can be determined is, therefore, of great importance in view of both accuracy considerations and the interpretation of experimental data.

For the determination of the chemical composition of the cement clinker two basically different approaches exist, viz., the *indirect* and the *direct* methods. The indirect or mathematical methods are most attractive for desk research purposes. Direct or experimental methods are considered to be more accurate but tend to be tedious and laborious and are, therefore, expensive [7]. Direct methods have the advantage that they inherently account for the effect of the cooling history on the final clinker composition.

Indirect Methods

The first and most often quoted mathematical procedure for the determination of the compound composition was proposed by Bogue in 1929 [60]. With the original version of his calculation procedure the amounts of C_3S, C_2S, C_3A and C_4AF were obtained. Modifications of the Bogue method and even fundamentally differently based calculation procedures have been proposed by, among others, Lea [337], Newkirk [401], Locher [349] and Glauser [193-195]. Major points of difference referred to the extent to which the effect of minor constituents and the burning and cooling processes were taken into account [195, 211,348,398,401,457].

Results of compound calculations according to different procedures are shown in Fig. 2.4. The calculations refer to two Dutch Portland cements, viz. a coarse A and a fine C cement with mineral compositions as shown in the inserts of the figure. As a general trend it can be observed that the C_3S content according to Bogue and Lea is substantially lower than according to Locher and Glauser. With respect to the C_2S content the reverse appears to be the case. Similar results have been reported by Roth [504] for completely different cements. It should further be noted that the calculated cement composition is very sensi-

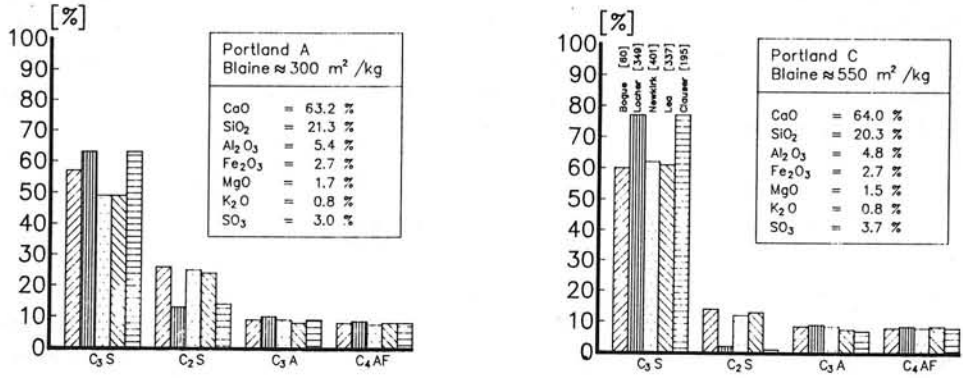

Fig. 2.4 Clinker compound composition of two Dutch cements as calculated according to different authors.

tive to small variations in the mineral composition of the cement (compare the calculated composition of Type A and Type B cement). This very much complicates theoretical considerations concerning modelling of the hydration process as far as the chemical aspect is concerned!

Deviations between different methods and inaccuracies of the Bogue method have been reviewed by Aldridge [7], Locher [349] and by Bogue himself (in [340]). After evaluating a number of calculation methods, Aldridge concluded that none of the methods proposed so far can be considered a significant improvement of the classic Bogue method (Gutt and Nurse in [7]). Locher [349] concluded in a similar way that, although the Bogue composition was *not* very accurate, it could nevertheless be used for a rough indication of the predominant chemical characteristics of the cement.

As will be discussed in more detail in Chapter 8, the C_3S content is an important quantity with which one of the main model parameters appears to be distinctly correlated. Hence it is of paramount significance to know how accurately the C_3S content of the cement can be determined. An indicator of this accuracy is the *multi-method standard deviation* that can be deduced from the calculated C_3S contents in the Portland cement A and C, presented in Fig. 2.4. For the C_3S contents mean values of 56% and 67% are found with multi-method standard deviations of 6% and 10%, respectively.

Direct Methods

Direct methods for the determination of the compound composition are the electron microscopy [231], X-ray diffraction spectroscopy and X-ray fluerence analysis. The potentialities of microscopic methods have been discussed by Gille [188] and Kramer [310]. It has been found that the C_3S content obtained with microscopic methods are higher than the Bogue values [7,312,349]. According to Knofel et al. [300] the microscopic C_3S content are even up to 30%(!) higher than according to Bogue. X-ray techniques have been said to require more research in order to obviate the major drawbacks of this method [7].

Direct versus Indirect Methods

According to Odler et al. [414] it is hard to say which method yields the most realistic results. All currently used methods would suffer from method-bound systematic and non-systematic errors. Harrisson et al. [231] found the results obtained by electron-optical analysis to be systematically better than those obtained with the Bogue method. Aldridge, on the other hand, is quite clear in stating that of all methods only the microscopic method gives accurate results [7]. He also found a pretty good correlation between the microscopic C_3S content and the corresponding Bogue value. Apart from the good correlation between Bogue values and microscopically obtained data, it was because microscopic determinations were tedious and lengthy and most of the cement literature describes ce-ment in terms of the Bogue composition, that Aldridge recommended the use of the Bogue method.

In view of the observed differences between the results obtained with the direct and indirect methods and the associated risk of wrong interpretations of test results, information about the clinker composition should always refer to the applied measurement and calculation methods. The consequences of inaccuracies and uncertainties in the theoretical compound composition in view of the reliability of predictive mathematical models for cement hydration will be discussed in Chapter 3.

It is noticed that the procedure for determination the compound composition proposed by Taylor in [583] has not been dealt with in this thesis. In future studies his method will be considered as well.

2.2.4 Effect of Particle Size on Compound Composition

The chemical composition of cement particles is slightly dependent on the particle size. Small cement particles generally contain more C_3S and less C_2S than large particles [342, 501,564,600,609,615,629]. According to Matouschek [371] the amount of C_3S decreased from 54% to 44% for particle sizes in the range from 0 to 60 μm, whereas the C_2S content increased from 25% to 36%. For small particles Czernin [120] found an increase in insoluble matter, a substantial decrease in the silica modulus and a considerable increase in alkalies. Beke et al. [36] clearly showed that the differences in particle composition are attributable to differences in grindability of the individual clinker compounds. β-C_2S was found to be less grindable than pure C_3S, while C_4AF and C_3A showed an intermediate behaviour. Also the experimental work of Kayser [284] has convincingly shown that the grinding process is responsible for the observed deviations in the chemical composition of particles of various sizes. Frigione et al. [176] found that fine material contains more C_3S and C_4AF and less C_2S and C_3A than coarser material. Similar results were found by Ritzmann [492].

An effect of the particle size on the chemical composition has also been found by Locher [351], but less pronounced than, for example, by Matoushek, and even with a tendency contradictory to the results of other researchers. Locher's results are shown in Fig. 2.5, together with those of Ritzmann. The chemical composition of fine particles was found hardly to deviate from that of course particles. Locher explained his observations by

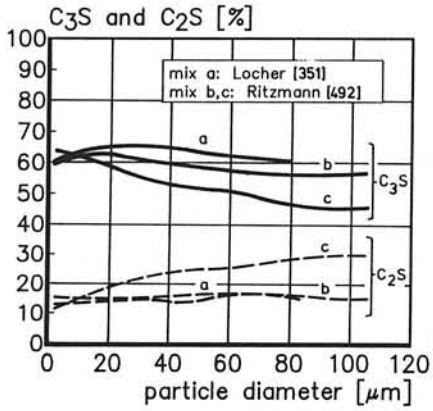

Fig. 2.5 Effect of particle size on chemical composition.
Data from Locher [351] (curves a) and Ritzmann [492] (curves b and c).

the formation of conglomeration-type particles: clusters built up of fine particles having the fine particle's composition.

Contradictory results have also been reported by Beke [34]. He found that for a C_3S content of the bulk material of 60% the C_3S content in the fraction 0-3 μm would be dramatically lower, viz. 27%. For the C_2S content of the bulk cement 13.3% was found, whereas for the fraction 0-3 μm a C_2S content of 35% would hold.

In the light of these contradictory observations, it is not very difficult to follow Brown et al. [73], who recently stated that the relationship between particle size and particle composition is still not well understood and should be the object of further research. In this research due attention should be paid to the interpretation problems. In this respect it is worthwhile to note that according to Sarkar [515] the effect of C_3S content on the hydration reaction is outweighed in importance by the effect of the particle size.

2.2.5 Gypsum

In order to regulate the rate of early reactions, a small amount of gypsum is added to the cement [521]. The amount of gypsum is generally expressed in SO_3 equivalents. The most commonly-used sulphate source is gypsum, $CaSO_4.2H_2O$, equivalent with 0.47 g SO_3 per gram gypsum. Another sulphate source frequently mentioned in the literature is anhydrite ($CaSO_4$), whereas aphtitalite ($3K_2SO_4.\ Na_2SO_4$) and syngenite ($CaSO_4.K_2SO_4.H_2O$) are two less frequently mentioned sources [568]. The often mentioned hemihydrate ($CaSO_4.{}^1/_2H_2O$) is, in essence, not an added sulphate source, but a product formed during the manufacturing process of clinker plus gypsum ($CaSO_4.2H_2O$).

The optimum gypsum content depends on the fineness and the compound composition of the cement and the solubility of the sulphate source. Anhydrite, for example, is less ra-

pidly soluble than gypsum. The optimum will, therefore, be higher in case of anhydrite than in case of gypsum. Indicative values for the optimum SO_3 content in view of strength development are discussed in Section 4.5.5.

2.3 Granular Characteristics of Cement

2.3.1 General

Already in the early stage of modern cement technology, much attention has been paid to the particle size distribution of the cement. At first the discussions focused on the relationship between the particle size distribution and the attainable maximum strength, whereas at present ecological aspects are also explicitly considered. Here we restrict ourselves to the remark that all research on the relationship between strength and the granular features of the cement has revealed that the *particle size distribution* rather than the *fineness*, i.e. the *specific surface*, of the cement is a predominant parameter for both strength development and ultimate strength. The pronounced influence of the granular properties on strength and strength development, and implicitly on the hydration process and structural formation, requires due attention to these properties.

2.3.2 Particle shape

2.3.2.1 Relationship between Particle Shape and Particle Size

Cement particles are often considered to be spheres. In reality, however, the particles have an irregular, angular shape (Fig. 2.6). That this should be so can easily be understood when bearing in mind that grinding of cement clinker is, in essence, a process of breaking larger particles into smaller ones. This process of fracturing inevitably results in the for-

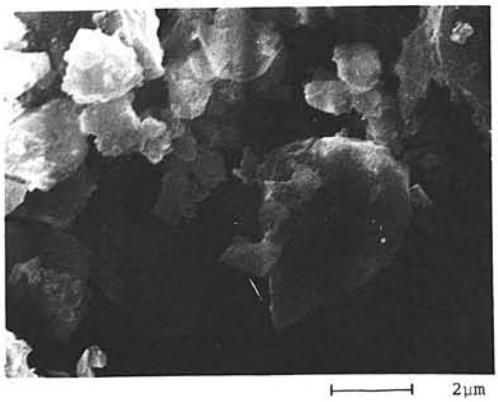

Fig. 2.6 Particle shape of dry Portland cement powder. Note the pronounced difference in particle size. Taken from [424].

mation of non-spherical particles. The degree of angularity of individual particles will depend on the fracturing mechanism.

Wieland [615] has suggested two different mechanisms of fracturing, viz. a *beating friction* mechanism. The beating mechanism would occur down to a particle size of 30 to 35 μm, while further fracturing would be caused by the friction mechanism. Contrary to the beating mechanism the friction mechanism would generate more round-shaped particles. Helmuth [238] considers the particle shape as a function of random multiple fracturing of the poly-mineral clinker during grinding. The ultimate result of the fracturing process is particles with shapes varying from somewhat rounded to more angular grains.

A consequence of Wieland's suggestion of two different fracturing mechanisms is that the particle shape depends on the particle size. A relationship between particle size and particle shape has also been presumed by Keienburg [287].

In the absence of detailed information on this topic the particle shape will be assumed to be independent of the particle size.

2.3.2.2 Sphere-Shaped versus Cube-Shaped Particles

As suggested in the preceding section, the fracturing process actually excludes the formation of spherical particles. Fracture surfaces are most probably more or less flat and a cube-like particle shape seems to be more realistic than a sphere-like shape. In one of his papers, Knudsen [302] has indeed adopted the cube-like particle shape.

When adopting a cubic shape of the cement particles one still has to decide which dimension of the cube should be considered as the *characteristic* particle size. Three possibilities are shown in Fig. 2.7. Either the rib size of the cube, the surface plane diagonal or the body diagonal of the cube could be considered as characteristic for a cubic particle. It is obvious that for the proposed particle shapes the specific surfaces [m^2/kg] will differ quite significantly. In the legend of Fig. 2.7 this is shown in tabular form. In the bottom line of the legend the specific surface of samples with the indicated particle shape is given as a percentage of the specific surface of samples which consist of spherical particles. From these values it is evident that the specific surface is a parameter which merely *indicates* the fineness of a cement, but cannot be considered as the *absolute particle surface area*. In Section 2.3.4 this subject will be dealt with in more detail.

2.3.3 Particle Size Distribution

2.3.3.1 General

The particle size of ordinary Portland cement varies between 0 and 150 μm. Methods for the determination of the particle size distribution of a poly-size material have been discussed extensively in the literature [4,243,337,640]. Currently used are the sedimentation-based methods [347,609], Laser diffraction [207,421], air separator, optical microscopy

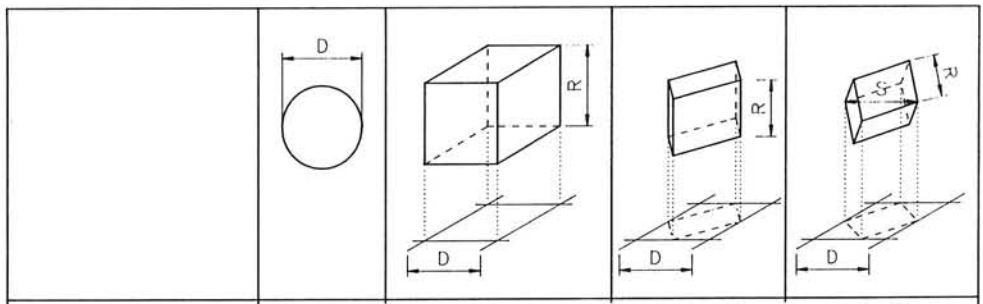

Characteristic particle size	D=R	R=D	$R={}^1/_2.D.2^{1/2}$	$R={}^1/_3.D.3^{1/2}$
Particle volume	${}^1/_6.\pi D^3$: 1 g	D^3	${}^1/_4.D^3.2^{1/2}$	${}^1/_9.D^3.3^{1/2}$
Particle surface	$\pi.D^2$	$6.D^2$	$3.D^2$	$2.D^2$
Number of particles with same volume as sphere	1	0.52	1.48	2.72
Specific surface	$\pi.D^2$	$6.D^2$	$6.D^2.2^{1/2}$	$6.D^2.3^{1/2}$
Relative specific surface	100%	100%	141%	173%

Fig. 2.7 Comparison of particle shapes and corresponding specific surfaces.

[255] and the Coulter Counter [70,210].

As pointed out by Werner et al. [612] in 1928 already, sedimentation methods do not consider the actual angular shape and size of the particles, but the equivalent diameters of spherical particles. In essence, all other methods also transfer actually measured particle sizes into spherical particle characteristics, i.e. an equivalent particle diameter. Undoubtedly this is a simplification of reality. In the case of mathematically modelling the granular aspect of the hydration process, however, it will be very difficult to benefit from more detailed information about the actual shape and size of the cement particles. For workable mathematical expressions for the description of the particle shapes the transfer from the actual irregular particle shape into more regular shapes is almost inevitable. The simplifications concerning the actual particle shape and particle size, however, should be borne in mind when hydration data has to be interpreted.

2.3.3.2 Mathematical Expressions for Particle Size Distributions

In his extensive work on small particle statistics, Herdan [240] gives a large number of expressions with which the particle size distribution of ground materials can be described. One of the most frequently used expressions for the particle size distribution of cement is the Rosin-Rammler function. This function, originally used to describe the particle size distribution of ground coal, runs as follows [502]:

$$G(x) = 100\ (\ 1 - e^{-bx^n}) \qquad (2.1)$$

where: $G(x)$ = percentage by mass passing the sieve with diameter x [%]

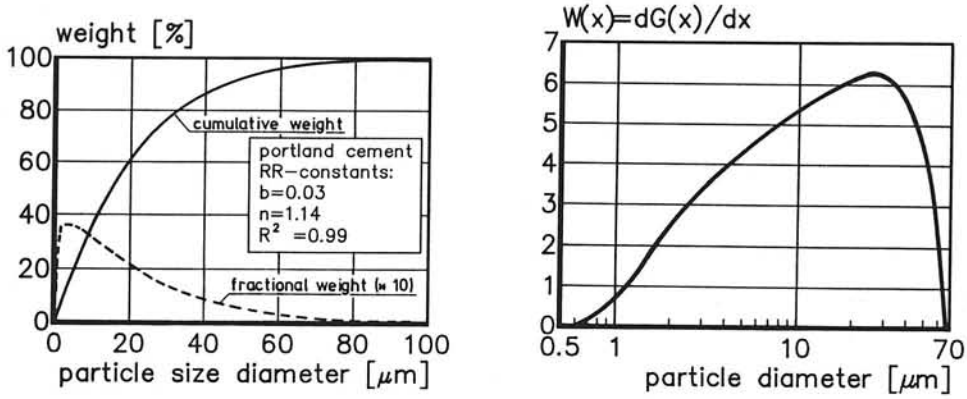

a. Dutch Portland cement A (ENCI)

b. Data of Locher [347].

Fig. 2.8 Cumulative and fractional weight distribution of a Portland cement.

x = characteristic particle size [μm]
b,n = constants

Examples of the actual and R-R approximated particle size distribution of an ordinary Portland cement are shown in Fig. 2.8. The analytically approximated fractional weight distribution W(x), i.e. the first derivative of G(x), is indicated as well. According to Rosin [502] deviations between actual and approximated particle size distribution were in the order of 3 percent. He further found that the R-R function could also be applied to the particle size distribution of blast furnace cement, albeit that then the deviations between theoretical and actual particle size distributions are greater. Probably the main advantage of the R-R function is that it comprises only two constants. This significantly simplifies evaluation and interpretation of test results.

Shortly after Rosin's publication in 1933, Anderegg [14] observed that the R-R function incorrectly suggests that the particle size distribution of cement would be a continuous one. In practice the fractions in the range from 10 to 20 μm would generally be less than indicated using the R-R function, while the actual amount of cement in the range from 20 to 50 μm would exceed the R-R values.

Discontinuities in the particle size distribution of cement have been investigated more thoroughly by Wieland [615] and Grant [207]. Shortcomings of the R-R function have also been discussed by Beke [33] and Rumpf [508]. Moreover, one has to reckon with considerable changes in the particle size distribution in the last decade due to the introduction of less energy demanding grinding techniques [383,519].

Apart from the occasionally rather poor approximation of the actual particle size distribution the R-R function is unattractive in case one would stick to pure analytical evaluations. In Section 2.3.4.2 there will be returned to this subject in more detail.

With the particular aim to get rid of the mathematical complications inherent in the use of the R-R function, several alternatives have been proposed, for example a power function [508], a Weibull distribution (Ibid. [73]), or a logarithmic Gaussian error function [565]. Again with the aim to simplify mathematical evaluation Kundsen [302] proposed a modified form of a function originally applied by Gille, viz.:

$$G(x) = 1 - \frac{C}{C-B} * e^{-Bx} + \frac{B}{C-B} * e^{-Cx} \tag{2.2}$$

This function was said to give a very good fit of the actual particle size distribution down to a particle size x=0.1 μm. A drawback of expression (2.2) is that the two constants in this expression each appear more than once, which makes this expression less transparent.

Although it might be true that with expression (2.2) the *cumulative* weight distribution is described accurately, it is still questionable whether the *fractional* weight distribution is accurately described as well. Most probably this will not be the case. For an accurate approximation of the *actual* fractional weight distribution, the application of a polynomial or a Fourier series has to be considered [187]. Apart from a better approximation of the actual particle size distribution, the adoption of a polynome or a Fourier series will certainly simplify mathematical evaluations. The drawback, however, is again the insertion of many constants, which makes this approach less attractive and less transparent. For this reason polynomes and Fourier series will not be explored further in this study.

Criteria for Choosing Mathematical Distribution Functions

For the final choice of a mathematical function for the particle size distribution, several aspects should be taken into account.

In the first place the required accuracy with which the particle size distribution is approximated should be judged *in connection with* the accuracy with which the particle *shape* can be established.

Secondly one has to realize that the particle size distribution is only one on the many parameters which determine the progress of the hydration process and the development of material properties. This means that the effect of inaccuracies in the description of the particle size distribution on the hydration process should be judged in connection with the effect of inaccuracies and uncertainties with which other relevant mechanisms are described. Parametric sensitivity studies revealed that a less accurate description of the *tails* of the particle size distribution does not significantly affect the mathematically obtained hydration data. This can easily be understood when bearing in mind that, firstly, the small fractions form only a minor percentage of the total amount of cement and, secondly, the small particles will be completely dissolved very quickly. Inaccuracies attributable to an inadequate description of the small fractions will therefore be relatively small and limited to the very early stage of the hydration process when structural and strength formation are still negligible.

For these two reasons it is considered admissible to adopt the R-R function for further theoretical considerations. Adoption of the R-R function has the great advantage that only

two constants are required to characterize the particle size distribution [187,383]. Another advantage is that, since in most of the cement literature the particle size distribution is described in terms of the R-R distribution, a comparison of the literature data with experimentally or mathematically obtained results can easily be made.

The drawback of the complexity of mathematical evaluations with the R-R function in a purely *analytical* approach can easily be overcome by changing to a *numerical* approach for integration and differentiation procedures. With the presently available advanced computer facilities this change-over is self-evident. As will be discussed later on, the numerical approach also significantly increases the possibility to allow for a large number of hydration and hydration-related features, which almost inevitably have to be disregarded if a strictly analytical approach is adopted.

Finally, from a scientific point of view it should be realized that the R-R function is not merely a phenomenological description of the particle size distribution. As explained by Beke [37], when discussing Aljawdin's work *(Ibid. [442])* on fracturing of poly-size material, the R-R function has a sound physical basis. The latter argument does not unconditionally guarantee a higher accuracy, but has the advantage of being consistent with fundamental considerations on the fracturing process.

2.3.3.3 Minimum Particle Size

Contrary to what is indicated by most mathematical functions for the particle size distribution there does exist a minimum particle size. Values for the minimum particle size are mentioned in the range from 0.03 to 0.4 μm (Table 2.1). The theoretical amount of cement belonging to fractions below the minimum particle size is not a significant portion of the total weight of the cement. The fine material, however, substantially contributes to the specific surface of the cement.

If the cement properties are related to the specific surface of the cement it becomes of paramount importance to define very clearly which particle size must be considered as the minimum particle size [130]. Since the experimental determination of the minimum parti-

Table 2.1 Minimum particle size x_0 according to several authors.

Author	ref.	min. particle size x_0 [μm]	comment
Andreasen et al.	[15]	0.1	Wet grinding procedure
Ramler	[475]	0.1	*Ibid. Beke [33]*
Matoushek	[371]	0.4	
Keienburg	[287]	0.1	From literature survey
Sarkar	[515]	0.311	SEM - technique
Gille	[187]	0.05 - 0.1	
Haegermann	[222]	0.03 - 0.12	*Ibid. Lea [337]*

cle size is quite complex and the accuracy is still questionable, Rammler [475] has proposed that the minimum particle size be defined as the one corresponding to the 0.5% undersize weight distribution. This approach has the advantage of flexibility in the sense that for fine cements the minimum particle size will be smaller than for coarse cements, which is likely to occur in practice.

2.3.4 Specific Surface

2.3.4.1 General

The specific surface of cement is defined as the surface area per unit weight. The specific surface of proprietary Portland cements varies from 250 m^2/kg for a coarse cement to 550 m^2/kg for a fine cement.

The specific surface is a function of both the particle shape and the particle size distribution. In Section 2.3.2.2 it has already been explained that the characterization of the particle shape and particle size significantly affects the considerations concerning the specific surface area. In Section 2.3.3 it was further observed that expressions used for the description of the particle size distribution might exhibit substantial deviations from the actual particle size distribution [207,615]. In view of these facts it is not surprising that the specific surface areas calculated using different methods show a wide scatter. For one single cement Gründer and Tabbah [217] have reported surface areas ranging from 127 to 639 m^2/kg when different measurement methods are applied. Hence it is evident that the specific surface of cement is a *method-dependent* cement characteristic. Thus to avoid dramatic misinterpretations, extreme caution must be exercised when using experimental and literature data in theoretical considerations.

2.3.4.2 Determination of Specific Surface

Indirect Methods

The specific surface of a poly-size material can be determined by multiplying the number of particles in each fraction by the surface area of one single particle and adding up these products for all the fractions. Particles are often considered to be spheres, whereas the particle size distribution can be described explicitly with, for example, the R-R function.

Measuring methods which implicitly allow for the particle size distribution have been proposed by Lea and Nurse (see [337,433]), Blaine [56] and Wagner [609]. The ratio between the Blaine and the Wagner surface is generally found to be about 2 [243,299,578, 342], although ratios between 1 and 2.5 have been reported as well [491]. The two methods differ in the adopted minimum particle size. Wagner assumes the average diameter of particles in the range from 0 to 7.5 μm to be 3.75 μm. Lea [337] has judged this assumption to be too rough for an accurate calculation of the specific surface since it is mainly the fine material that forms a major percentage of the specific surface. According to Grindrod [210] more than 70% of the specific surface of an ordinary cement must be

attributed to particles smaller than 3.5 μm. Particles smaller than 1.25 μm would still form 45% of the total surface area.

As observed in Section 2.3.3.2, mathematical evaluations using the R-R function can become quite cumbersome. Among others, Sylvan [565] and Meric [383] have pointed to analytical complications with integrating either an R-R function G(x) or a fractional weight distribution W(x) with respect to the particle diameter x. These integrals have to be determined in order to find the specific surface of the cement. Starting from the R-R function (2.1) the specific surface SS would follow from:

$$SS = \int_{x=x_0}^{x=\infty} \frac{3.b.n.}{\rho_{ce}} * x^{n-2} * e^{-bx^n} dx \qquad (2.3)$$

where ρ_{ce} is the specific mass of the cement. For a discussion about the analytical difficulties reference is made to lit. [383,565]. The most convenient way to get rid of the tough analytical difficulties is to determine the specific surface by numerical integration of eq. (2.3).

Direct Methods

Methods for the determination of the specific surface which account for the actual particle shape are the *adsorption or direct methods*. For the determination of adsorption surfaces of anhydrous cement nitrogen, argon or krypton can be applied as adsorbents [604]. The adsorption method, originally proposed by Brunauer, Emmett and Teller and hence known as the BET-method, yields specific surfaces significantly exceeding the Blaine surfaces. Rakel [472] determined a ratio between BET- and Blaine surfaces of 2.07 to 3.4. From data reported by Lea [337] a ratio between BET- and Wagner surfaces can be deduced of about 4.4. With a Blaine/Wagner ratio of 2 this corresponds to the BET/Blaine ratio 2.2.

According to Sebok [528] the BET values do not only depend on the granular features of the cement, but also on the chemical composition of the clinker. This effect will not be considered in further detail in this study.

2.3.4.3 Effect of Minimum Particle Size on Specific Surface

In Section 2.3.3.3, as well as in the preceding Section, it has been noted that the fine material forms a large percentage of the specific surface. The influence of the small particle fractions on the specific surface has been investigated for three Dutch cements, viz. Portland cement Type A, B and C with nominal Blaine surfaces of about 275, 350 and 550 m^2/kg, respectively. The particle size distributions of these cements are given in Fig. 2.9 together with the R-R constants b and n. In the calculations sphere-shaped particles were assumed. For cement Type B the influence of the fine material, i.e. of the assumed minimum particle size, on the calculated specific surface is shown in Fig. 2.10. Grindrod's statement that particles <3.5 μm form 70% of the specific surface of an ordinary ground cement is in good agreement with the percentages deduced from the curves in Fig. 2.10.

2.3.4.4 Effect of Gypsum on Specific Surface.

The gypsum which is added to the cement is generally finer than the pure cement. According to an often applied rule of thumb each percent (by weight) of added gypsum is responsible for an increase of the specific surface of the mix by about 10 m^2/kg [427]. Data given by Keienburg [287] shows that the addition of gypsum caused an increase of the specific surface of 5 to 6 m^2/kg per percent added gypsum.

2.3.4.5 Significance of Granular Features for Evaluation of Hydration Data

From both a theoretical point of view (Section 2.3.2.1) and microscopic observations it is evident that the assumption of sphere-shaped particles for the determination of the specific surface as adopted in most of the indirect methods can be expected to *underestimate* the actual surface area. It seems obvious, therefore, to consider the experimentally obtained adsorption surface areas as being closer to reality than, for example, the Blaine surfaces, since the former do implicitly allow for the effect of the particle shape.

The fact that the actual cement surface area is two to three times higher than the Blaine surfaces is of great importance for the interpretation of hydration data. The lower the specific surface, the higher the thickness δ_{in} of the cement layer involved in the reaction process should be in order to reach a certain degree of hydration. Moreover, the smaller the surface area, the more rapid the increase of the thickness of the layer of reaction products around a hydrating particle, the degree of hydration of particles with different surface areas being the same. The foregoing is explained schematically in Fig. 2.11. For a spherical and a prismatic particle the penetration depth δ_{in} and the total thickness of the layer of hydration products δ have been determined as a function of the degree of hydration. The dimensions of the prismatic particle have been chosen to obtain a ratio of the specific surfaces of the spherical and the prismatic particle of about 1.75. In Fig. 2.11b and 2.11c the relative and absolute increase of the penetration depth is shown as a function of the degree

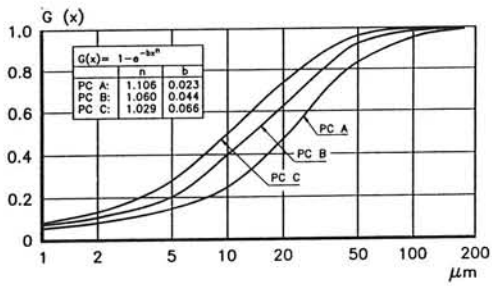

Fig. 2.9 Particle size distribution of Dutch cements Type A, B and C. (coarse, medium and fine)

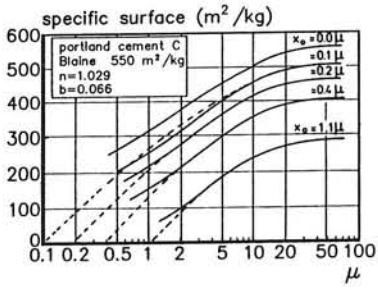

Fig. 2.10 Calculated specific surface of Portland cement C (fine cement). Minimum particle size x_0 μm.

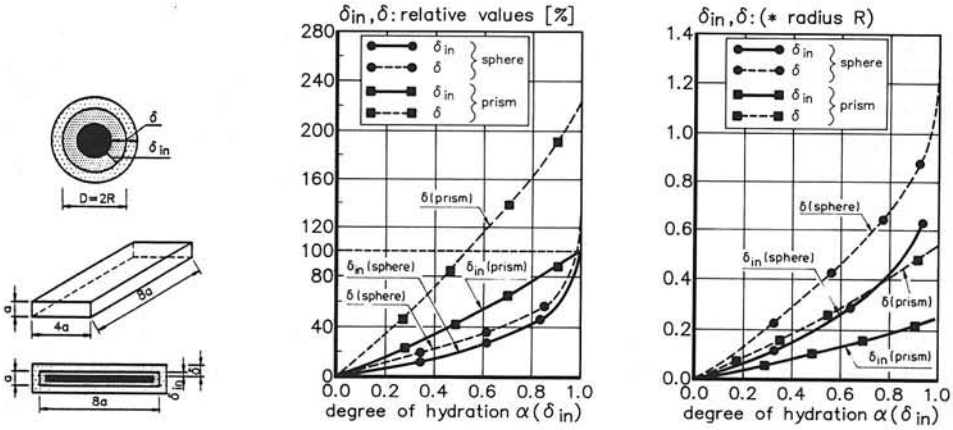

a. b. c.

Fig. 2.11 Relationship between degree of hydration and penetration depth and thickness of product layer for spherical and prismatic particles.

a. Spherical and prismatic particle: schematic.
b. Proportional increase of penetration depth δ_{in} and product layer δ.
c. Increase of penetration depth δ_{in} and product layer δ as related to the radius R of the spherical particle.

of hydration. Fig. 2.11c shows that for an arbitrary degree of hydration, for example α=0.5, the absolute value of the penetration depth of the spherical particle is twice the penetration depth of the prismatic particle. Assuming a ratio between the volume of the reaction products and the reacted cement of ν=2.2 [462], it also appears that the thickness of the layer of hydration products surrounding the anhydrous core of the spherical particle will be about 1.7 times larger than the layer which surrounds the prismatic particle.

Since the thickness of the product layer determines which reaction mechanism is activated (see Chapter 6), an inaccurate determination of the specific surface might result in misinterpretation of hydration data and hence of presumed reaction mechanisms.

2.4 Cement Characteristics. Discussion and Concluding Remarks

Chemical Composition of Portland Cement

The clinker composition of a cement is a function of the mineral composition of the raw materials. Small deviations in the mineral composition and burning conditions significantly influence the clinker composition. In this respect all mathematical methods for the determination of the clinker composition quoted in Section 2.2 show the same tendencies, albeit that the absolute values of calculated clinker compositions reveal substantial deviations.

The most often applied mathematical procedure, viz. the Bogue method, *underestimates* the actual amount of C_3S and *overestimates* the actual C_2S content.

None of the predictive mathematical methods for the determination of the compound composition considers the evident dependence of this composition on the particle size. The difference between the C_3S content of small and large particles can reach up to 10...20%. Differences in the C_2S content of small and large particles have been reported of the same order of magnitude. Differences of this order of magnitude can be expected to affect the rate of hydration in the different stages of the hydration process substantially. Ignoring these differences can result in misinterpretations of hydration data.

Particle Size Distribution

Contrary to what the majority of current mathematical functions for the particle size distribution suggest, the actual particle size distribution of cement may exhibit some discontinuities. As long as mathematical functions for the cumulative weight distribution of cement do not account for these discontinuities, it is highly questionable whether it would be worthwhile to try to achieve a very high correlation of these functions with the actual cumulative weight distributions. The Rosin-Rammler function, although probably less accurate in the fine particle range, is therefore considered to be accurate enough for the mathematical description of the particle size distribution.

Particle Shape and Specific Surface

From both a theoretical point of view and microscopic observations it is evident that cement particles are not spherical. This is further confirmed by adsorption measurements of the specific surfaces of cement. The latter adsorption data show the "actual" surface areas to be 2 to 3 times the Blaine surfaces. The latter are based on spherical particle considerations. Actual particle shapes significantly deviating from a spherical shape can have significant consequences in the interpretation of hydration data. Misinterpretations with respect to hydration depths, thickness of the layer of hydration products, hydration mechanisms and diffusion coefficients have to be expected.

3 ASPECTS OF HYDRATION OF CEMENT-BASED MATERIALS

3.1 General

From the extensive literature surveys on hydration mechanisms and structure development in the proceedings of the International Conferences on the Chemistry of Cements [114, 538,581] it is quite obvious that cement hydration and structural formation must be considered as mutually interdependent. The chemical aspect of the hydration process is generally discussed under the heading "Hydration mechanisms". The physical and stereological aspects are generally emphasized in discussions about structural formation and strength development. Since the chemical, physical and stereological aspects of the hydration process, intimately interfere throughout the hydration process a completely separate survey of these aspects is hardly possible. However, in line with previous practice, separate surveys of the chemistry-oriented aspects of the hydration process, on the one hand, (this chapter) and structural formation and strength development, on the other, (Chapter 4) have been carried out. The major aim of these surveys is to make clear to what extent and in which stage of the hydration process the chemical, physical and stereological aspects interfere most intensively and require, as it has been called in this study, "integrated modelling" of the processes and mechanisms involved. The term "integrated" will be explained in Chapter 5.

3.2 Chemical Reactions of Portland Cement and Cement Constituents

On contact with water Portland cement particles start to dissolve and react with water under formation of hydration products. The main reactions of the individual cement constituents with water are [155,583,622] [1]):

$$C_3S + xH \rightarrow C_2S + CH + (x\text{-}1)H \tag{3.1a}$$
$$2C_2S + 4H \rightarrow C_3S_2H_3 + CH \tag{3.1b}$$
$$2C_3S + 6H \rightarrow C_3S_2H_3 + 3CH \tag{3.1c}$$
$$C_3A + 6H \rightarrow C_3AH_6 \tag{3.1d}$$
$$C_3A + 3C\underline{\bar{S}} + 32H \rightarrow C_3A3C\underline{\bar{S}}H_{32} \tag{3.1e}$$
$$C_3A3C\underline{\bar{S}}H_{32} + C_3AH_6 \rightarrow 3C_3AC\underline{\bar{S}}H_{14} + H \tag{3.1f}$$
$$C_4AF + 19H \rightarrow C_4AH_{19} + F \tag{3.1g}$$

For reactions of minor constituents, although not insignificant as far as their influence on the hydration process and the development of material properties is concerned, reference is made to the literature [97,142].

The reaction of cement with water is accompanied by *liberation of heat* and *chemical*

---

[1]) Notation in cement chemistry: C = CaO, S = SiO_2, A = Al_2O_3, F = Fe_2O_3, H = H_2O

and physical binding of water. Both the amounts of liberated heat and bound water relative to the maximum amounts of these quantities in the case where all the cement has reacted, can be considered as indicators of the degree of hydration. Other methods for monitoring the progress of the hydration process, for example microwave techniques [199] and shrinkage measurements [142], will be briefly dealt with in Section 3.8.

Since an accurate prediction of the degree of hydration is one of the main purposes of this project, it is worthwhile to consider the accuracy with which the degree of hydration can be approximated by either the degree of heat liberation or the amount of bound water. Accuracy considerations will therefore be given due attention in the Sections 3.3 and 3.4.

3.3 Heat of Hydration

3.3.1 Determination of Heat of Hydration. Measuring Methods

The most commonly used experimental methods for the determination of the heat of hydration are the adiabatic method, on the one hand, and isothermal methods like the heat of solution method and conduction calorimetry on the other. For a detailed description of these methods reference is made to the literature [8,29,252,282]. Here only some remarks are made concerning the accuracy of the different methods and a comparison of them in view of accuracy considerations is dealt with in the Chapters 8 and 9.

3.3.1.1 Adiabatic Calorimetry. Accuracy

Adiabatic heat measurements are most convenient for producing continuous heat of hydration curves under curing conditions close to or almost identical with mass curing. Many authors have judged this to be a major advantage of this method, since it enhances the possibility of direct application of the results for practical purposes [29,66,92,252,290]. Adiabatic hydration curves would be the most suitable starting point for temperature calculations in hardening structures. The fact that hydration of cement in concrete and mortar develops differently from that in neat pastes (see Section 3.8.3) has been mentioned as another reason why adiabatic calorimetry is judged to be of great practical importance [92].

Accuracy

The high accuracy that can be reached with adiabatic calorimetry has been mentioned by Meissner in 1933 already [379]. Particularly in the most interesting stage of the hydration process, i.e. up to about 7 days, accurate information is obtained. From 7 days onwards the accuracy decreases. For the majority of practical purposes, however, this does not constitute a serious problem.

Alègre [8] mentioned a systematic error at 8 days in the order of 2°C. This can be estimated to be equivalent with an error of about 4%. Adiabatic hydration curves are re-ported to be reproducible within a scatter zone of ±0.15°C, equivalent with a coefficient of variation of 0.25...0.6% [92]. In a Round Robin test, conducted in the framework of RILEM-

committee TC 119, a multi-laboratory standard deviation was computed at 3.8°C [2]).

Adiabatically determined maximum heats of hydration tend to be lower than the calculated maximum values [92]. This can most probably be attributed to incomplete hydration of the cement in the adiabatic test.

3.3.1.2 Isothermal Calorimetry. Accuracy

Conduction Calorimetry

One of the major drawbacks of adiabatic calorimetry is that the effect of the curing temperature on the rate of hydration is implicitly measured. This poses difficulties with respect to the interpretation of results in terms of hydration mechanisms. For research on reaction kinetics the isothermal method is, therefore, more widely employed [470,513]. The conduction method is one of the currently utilized isothermal methods. Just like the adiabatic calorimeter the conduction calorimeter produces continuous heat liberation curves. The maximum values for the liberated heat of hydration obtained with the conduction calorimeter are higher than those measured adiabatically [92]. The formation of different hydration products, including changes (decrease) in the specific heat of the hydration products, are responsible for the observed phenomenon (see also Sections 6.6.4 and 8.6.1).

Accuracy

For the standard deviation of the conduction calorimeter values have been reported of 1.9 J/g at 3 days up to 4.0 J/g at 7 days, corresponding to a coefficient of variation of 1% (Q_3=220 J/g) and 1.5% (Q_7=280 J/g), respectively [293]. Cembureau [95] reports standard deviations of 3.1 J/g and 2.9 J/g at 3 and 7 days respectively, whereas the multi-laboratory standard deviations would vary between 8.5 J/g and 12.2 J/g.

Heat of Solution Method

The heat of solution method gives the heat of hydration at discrete points of time. The method is very convenient for routine work and is relatively inexpensive, but suffers from several chemistry-related complications [92,293,514]. Its main advantage is its applicability for long-term measurements.

Accuracy

According to Catharin the accuracy is ±13 J/g, equivalent to a coefficient of variation ±3% [92]. Earlier Woods (1932) had mentioned an accuracy of ±6 J/g [626]. These values are in good agreement with those of Alègre, who found an error of ±13 J/g. A literature review carried out by Alègre shows coefficients of variation at 28 days from 0.8 to 8% [8]. Estimating the amount of liberated heat at 28 days Q_{28} at 350 J/g, a standard deviation of 3 to 28 J/g has to be considered. Recently Killoh [293] concluded that the minimum

---

[2]) Koenders, E.A.B., Breugel, K. van (1994). *Numerical and experimental adiabatic hydration curve determination*. Proc. Int. RILEM symposium Thermal Cracking in Concrete at Early Ages, Munich, Ed. Springenschmid, 3-12.

standard deviation that is likely to be achieved would be about 6 J/g, a value in good agreement with the early results of Woods in 1932. The "multi-laboratory standard deviation" was reported to range between 6.7....39.7 J/g [94], whereas the ASTM standard mentions a value of 16.9 J/g [18].

According to Killoh, the standard deviation for the conduction calorimeter is about 5 times lower at 3 days and 3 times lower at 7 days than for the heat of solution data. He further found an excellent agreement between the heat of solution data and those obtained with the conduction calorimeter. From experimental work carried out by Lerch et al. [342] it can be deduced, however, that the conduction calorimeter yields values about 5% higher than obtained with the heat of solution method (Q_3 of 25 cements, cured at 21°C).

3.3.2 Maximum Heat of Hydration. General Calculation Format

The total amount of heat measured at macro level is the sum of mainly the heat of chemical reaction and heat of adsorption, the latter being about 25% of the total heat [462]. The potential heat of hydration, i.e. the amount of heat liberated when all the cement has reacted, can be calculated from the clinker composition of the cement provided that the heats of hydration of the individual constituents are known and superposition of the individual heats of hydration is justified. For the maximum heat of hydration of Portland cement the following calculation format has been proposed [601]:

$$Q^{max} = q_1.(C_3S) + q_2.(C_2S) + q_3.(C_3A) + q_4.(C_4AF) + q_5.(C) + q_6.(MgO) \qquad (3.2)$$

with:	Q^{max}	= maximum amount of heat liberated at complete hydration	[J/g]
	$q_1 ... q_2$	= heat of hydration of the constituents considered (Table 3.1)	[J/g]
	(...)	= content of constituents of the cement considered	[g]

The accuracy of the calculated heat of hydration depends on the accuracy with which the clinker composition has been determined, on the one hand, (Chapter 2), and the accuracy of the heats of hydration of the constituents, on the other.

3.3.3 Heat of Hydration of Constituents

With respect to the maximum heat of hydration of the constituents of cement, the published data shows a fairly consistent picture. An extract of the published data is given in Table 3.1. Differences are generally due to either the applied measuring methods or the extent to which the effect of minor compounds and/or the presence of glass were considered [2,337,340,631].

Particular attention must be given to the heat of hydration of C_3A. C_3A reacts with gypsum under formation of ettringite and liberation of ≈624 J/g C_3A [340]. This amount of heat should be added to the 866 J/g C_3A liberated during the conversion of ettringite into stable monosulphate, totalling 1,490 J/g. In order to account for the fact that not all the

C_3A will react with gypsum an apparent heat of hydration of 1,350 J/g is generally adopted. This value is in good agreement with the results of a least square analysis carried out by Verbeck et al. [601].

With respect to the data in Table 3.1 it is further commented that the heat of hydration of $KC_{23}S_{12}$ is, at least at later ages, equal to the heat of hydration of C_2S. $KC_{23}S_{12}$, although quite a different product, but formed instead of C_2S, can therefore be considered as C_2S as far as heat liberation is concerned [401]. In more general terms Lea [337] has also mentioned the similar behaviour of these two products.

3.3.4 Predicted Maximum Heat of Hydration. Accuracy

According to the calculation format (3.2) the maximum heat of hydration of two Portland cements, indicated as cement A and C, has been determined. The mineral composition of the cements is given in the inserts of Fig. 2.3. The compound composition of these cements was calculated according to the methods proposed by Bogue, Lea, Newkirk, Locher and Glauser (Chapter 2). For the heats of hydration q_1 ... q_6 of the constituents the values were used as given in Table 3.1. Results are shown diagrammatically in Fig. 3.1.

From a straightforward statistical evaluation of the calculated heat of hydration data of these two cements mean values of 476 J/g and 502 J/g with standard deviations of 34 J/g and 33 J/g, i.e. coefficients of variation of 7.1% and 6.6%, were obtained. In these calculations two degrees of freedom are allowed for, viz. the calculation procedures for, firstly, the clinker composition and, secondly, the heat of hydration. For each calculated coefficient of variation only one single cement was considered. Yong [631] calculated a coefficient of variation by simply choosing the clinker composition as a degree of freedom. From his analysis, in which 20 cements were involved, coefficients of variation were de-

Table 3.1 Relative contribution to heat of hydration of clinker compounds [J/g]

Author	ref.	q_1 C_3S	q_2 C_2S	q_3 C_3A	q_4 C_4AF	q_5 free C	q_6 MgO	$KC_{23}S_{12}$	NC_8A_3
Woods	[626]	570	260	840	125	---	---	---	---
Bogue	[58]	500	260	866	125	---	---	---	---
Lerch et al.	[340]	500	260	866[1])	420	1166	850 [2])	---	---
Thorwaldson	[589]	---	---	---	1166	---	---	---	---
Chatharin	[93]	500	251	1340	420	1172	---	---	---
Adam	[2]	---	---	500 /	170 /	840	---	---	500/
		---	---	630	290	1256	---	---	630
Newkirk	[401]	560	1360	300	---	---	---	310	1205

[1]) Accounting for reaction of tricalcium aluminate hydrate and gypsum. Some extra 624 J/g SO_3 must be considered [340].

[2]) Taken from literature (see [340]).

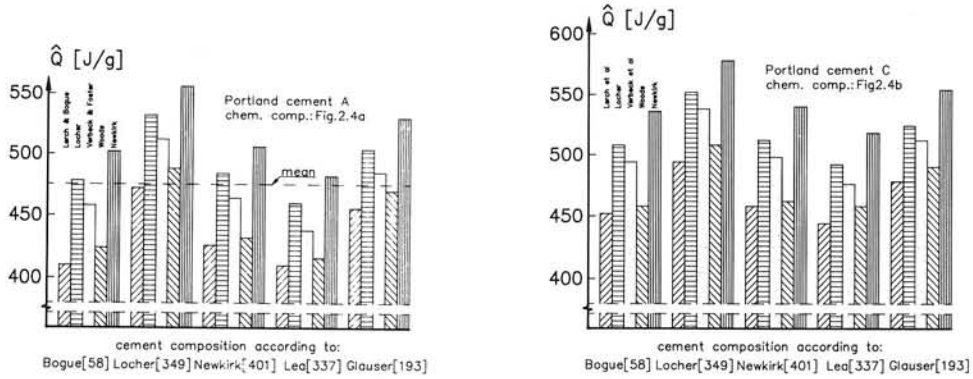

Fig. 3.1 Predicted heat of hydration of two Portland cements A and C. Clinker composition calculated according to different authors (Chapter 2, Fig. 2.4).

duced in the range from 1.5 to 4%. The major cause of scatter originated from the influence of alkalies. For practical purposes a coefficient of variation of 4% was recommended.

In conclusion it can be stated that:

1. Compound compositions determined according to different calculation formats can result in differences in the calculated maximum heat of hydration of up to 70...90 J/g (Fig. 3.1). Disregarding the effect of a particular calculation format can introduce significant errors and misinterpretations of test results concerning, for example, the degree of hydration (also Section 3.3.5).
2. Once having chosen a calculation format for the determination of the maximum heat of hydration, a coefficient of variation of about 4% for the obtained values should be considered.

3.3.5 Degree of Heat Liberation. Accuracy

For many practical and research purposes it is convenient to approximate the degree of hydration $\alpha(t)$ with the degree of heat liberation $\alpha(Q(t))$, viz.:

$$\alpha(t) \approx \alpha(Q(t)) = \frac{Q(t)}{Q^{max}} \tag{3.3}$$

where $Q(t)$ is the heat liberated at time t. To what extent this approximation of the degree of hydration with the degree of heat liberation is justified will be discussed in more detail in Section 3.8.1.2. In the following only the accuracy with which the degree of heat liberation can be determined will be dealt with.

The absolute error $\Delta\alpha(t)$ of the degree of heat liberation calculated according to eq. (3.2)

can be approximated with:

$$\Delta\alpha(t) = \alpha(t) * [\frac{\Delta Q(t)}{Q(t)} + \frac{\Delta Q^{max}}{Q^{max}}] \tag{3.4}$$

Let us assume the absolute error $\Delta Q(t)$ and ΔQ^{max} to be equivalent with the five percent fractile of $Q(t)$ and Q^{max}, respectively. For the absolute deviations from the best possible values for $Q(t)$ and Q^{max} it follows:

$$\Delta Q(t) = 1.64 * 0.6\% = 1\% \qquad (0.6\%;\ \text{see Section 3.3.1.1})$$

and:

$$\Delta Q^{max} = 1.64 * 4.0\% = 6.5\% \qquad (4.0\%;\ \text{see Section 3.3.4})$$

For the absolute error $\Delta\alpha(t)$ it follows:

$$\Delta\alpha(t) = 0.075\ \alpha(t)$$

If both the intermediate and maximum amounts of heat of hydration were determined with the conduction calorimeter and were found to be 210 J/g at 7 days and 420 J/g at complete hydration with standard deviations of 3 J/g at 7 days and 4 J/g at complete hydration, the absolute error $\Delta\alpha(t_7)$ calculated according to the foregoing format would be 3.6%, or 0.036*210=7.6 J/g. The latter value can be estimated as the minimum possible error, i.e. the best possible result.

Against the background of these accuracy considerations, it is worthwhile to realize that *predictive models*, which can generate heat liberation curves, and hence curves for the degree of hydration, with an accuracy of 3.6...7.5% as related to the mean value of a series of experimental results, can be considered as equally reliable. Individual predictive models can only be further improved if it was possible, for example, to quantify explicitly the influences of minor constituents on the heat liberation and the hydration process. As long as these effects cannot be modelled reliably, one has to consider a scatter in the experimentally obtained results as indicated. This must be considered as important information in view of the evaluation program that will be executed and discussed in Chapter 8.

Further it is emphasized that in order to obtain reliable values for the degree of hydration, the intermediate and maximum amounts of heat of hydration should preferably be determined according to one and the same experimental method. This would eliminate one of the major sources of inaccuracy.

Assuming a linear relationship between the degree of hydration and compressive strength (see Chapter 4), the standard deviation of the theoretical strength will be equal to that of the degree of hydration, i.e. 3.6...7.5%. In this respect it is interesting to bear in mind that the standard deviation of the cube compressive strength for one and the same cement, i.e. one and the same concrete mix, obtained under laboratory conditions generally varies between 3...5% [529,557]. The order of magnitude of these values can serve

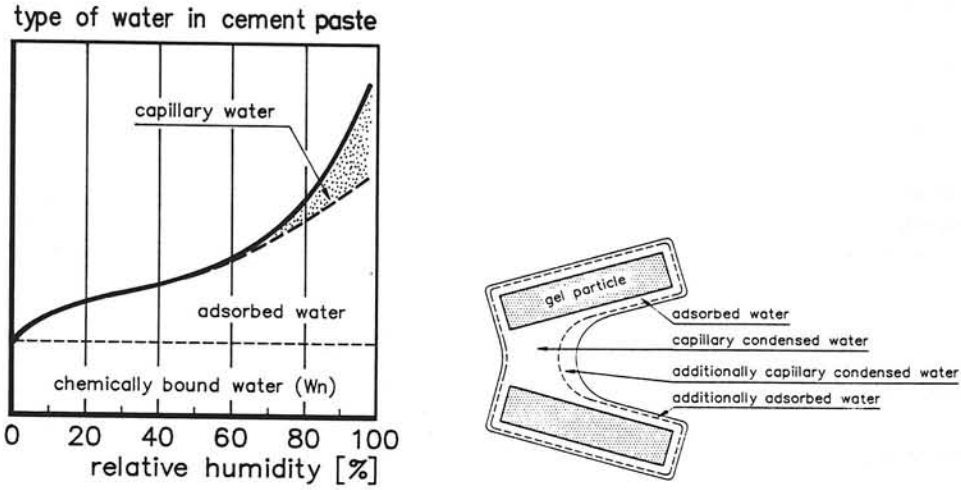

Fig. 3.2 Distribution of water in cement paste as a function of the relative humidity.
a. Diagrammatical representation of types of water in cement paste.
b. Schematic representation of adsorption isotherms including capillary condensation (after [533]).

as a reference if we are to calculate the theoretical probability of early-age cracking in an actual concrete structure. For these calculations the main strength and the standard deviation of the strength should be known. In Chapter 9, where an example of such a calculation is presented, we will cover this subject in more detail.

3.4 State of Water

3.4.1 Classification of Types of Water

In a hydrating water/cement system the water is present in *roughly* three different forms, viz. *chemically bound water, physically bound water* and *free* or *capillary water.* As shown diagrammatically in Fig. 3.2a, the amount of physically and capillary water strongly depends on the relative humidity in the pore system. For a relative humidity in the range from 0% to 20...30% (which is not a practical situation in normally cured pastes!), the pore walls of the pore system, i.e. the surfaces of the colloidal hydration products, are covered with one single mono-molecular layer of water with a thickness of about 3 Å [155] (Note: A water molecule is considered to be a sphere with a diameter of 2.76 Å [214]). With increasing relative humidity the thickness of the adsorption layer increases up to about 8 to 9 Å at a relative humidity of 70...80% [467]. This is equal to the thickness of three mono-molecular water layers. At places where the gel particles are at short distances from each other capillary condensation will occur as indicated in Fig. 3.2b.

Table 3.2 Classification of water according to different authors.

Author	ref.	pore diameter ϕ 0.01 0.1 1.0 10 100 10^3 [µm] / 1 10 100 10^3 10^4 10^5 10^6 10^7 [Å]
Powers et al.	[462]	non-evap./ comb. or fixed water | evaporable water: water that evaporates on drying at 25°C in evacuated desiccator over a system of magnesium perchlorate: $Mg(ClO_4).2H_2O + Mg(ClO_4).4H_2O$
Richartz et al.	[490]	Gel water (or "Zwischenschichtwasser"): evaporates on vacuum drying
Hansen	[229]	non-evap. | evaporable water = gel water + capillary water
Taylor	[582]	water in crystalline phase / water in gel / adsorbed or monolayer water / water in micropores / water in larger pores
Dorner et al.	[143]	adsorbed water freez. at -160°C | structure water RH: 60-90% | cap. condensed water freez. at -15°C | bulk water freezing temperature = 0°C
Several authors	[55,75,266, 510,637]	* Division between different types of water is *not* sharp * Part of hydrate water is evaporable * Measuring method strongly influences the experimentally obtained results

According to Dorner [143] pores with a diameter of 60 to 200 Å will remain filled with water at a RH=60...90%. These values are in fairly good agreement with those of Chatterji [99], according to whom - in agreement with Wittmann [620] - the adsorbed water film at 100% RH could reach a thickness of about 250 µm.

In a parallel classification, a distinction has been made between evaporable and non-evaporable water. The classification of water as proposed by different authors has been summarized in Table 3.2.

3.4.2 Chemically Bound Water

3.4.2.1 General Aspects

At complete hydration of cement, an amount of water of about 22%...25% of the weight of the anhydrous cement is chemically bound to the cement [289,462]. In this form, which actually includes water molecules which are most tightly adhered to the surfaces of reaction products, it is considered to be an inherent part of the solid matter. The resulting volume of the reaction products is less than that of the summarized volumes of the constituents cement and water. This volume reduction is equivalent with 18% to 26% of the volume of the chemically bound water [111,120,462].

3.4.2.2 Determination of Chemically Bound Water Wn

The non-evaporable water is defined as the part of the total water content that is lost, i.e. has chemically reacted with the cement, when a specimen, which has been brought to the "bare surface condition", is ignited at 1,000°C [387]. This bare surface condition can be obtained with one of the following methods [387,462]:

1. *Oven drying at 105°C (O-drying)*
2. *Drying at room temperature over magnesium perchlorate (P-drying);*
3. *Drying under vacuum by the dry-ice method (D-drying);*

According to Mills [387] the non-evaporable water content determined according to the O-drying method is about 11% less than the P-drying values and 3% less than the D-drying values. Lea [337] has emphasized the influence of the height of the ignition temperature on the non-evaporable water content, whereas Rechenberg discussed the pros and cons of several measurement methods, such as the Penfield[3]) method [241,344,441,480].

Table 3.3 summarizes values of non-evaporable or combined water as reported by different authors. Differences in measuring methods and curing conditions sometimes allow for great differences in these values. An increase of the w/c ratio has been reported to increase the non-evaporable water content [250,309,503]. Some authors, however, could not find a significant effect of this parameter [351]. Curing at elevated temperatures would result in a decrease of the non-evaporable water content [309,420].

From foregoing considerations it must be evident that, in order to avoid misinterpretations of literature and experimental data, the drying method and the ignition temperature should always be indicated!

Table 3.3 Chemically bound water $\hat{W}n$ [g/g] according to different authors.

Author	ref.	C_3S	Portl. cement	Comments / Drying methods
Powers et al.	[462]	0.23	0.21 -0.25	P- and D-drying (Ibid. [351])
Locher	[351]	0.21	---- ----	Vacuum drying (D-drying)
Brunauer et al.	[76]	0.204	---- ----	Ibid. Le Sueur [335]
Locher	[355]	0.21	---- ----	
Mills	[387]	---- - ---	0.24 -0.26	O-drying
Odler et al.	[410]	---- - ----	0.20 -0.22	Am. cements Type I and III
Odler et al.	[413]	---- - ----	0.20 -0.22	Review of different authors
Le Sueur et al.	[335]	0.26 -0.30	---- -----	O-drying in dry N-atmosphere

[3]) Penfield method: Applied in the experimental evaluation program discussed in Chapter 8.

Table 3.4 Chemically bound water of constituents [g/g].

Author	ref.	w_1 C_3S	w_2 C_2S	w_3 C_3A	w_4 C_4AF	Comment
Powers et al.	[462]	0.187	0.158	0.665	0.213	paste 0.5 yr old
Copeland et al.	[112]	0.228	0.680	0.429	0.132	paste 1.0 yr old
		0.234	0.178	0.514	0.158	paste 6.5 yr old
		0.230	0.196	0.522	0.109	paste 13 yr old

3.4.2.3 Maximum Chemically Bound Water $\hat{W}n$. General Calculation Format

A general format for calculating the maximum amount of chemically bound water has been put forward by, among others, Copeland et al. [112]:

$$\hat{W}n = w_1*(C_3S) + w_2*(C_2S) + w_3*(C_3A) + w_4*(C_4AF) \tag{3.5}$$

with: $\hat{W}n$ = maximum chemically bound water at complete hydration [g/g]
$w_{1...4}$ = chemically bound water of individual constituents [g/g]
(...) = content of major constituents of the cement considered [g]

Values for the amounts of chemically bound water w_i (i=1,2,3,4) of the individual constituents as proposed by different authors are given in Table 3.4.

3.4.2.4 Prediction of Maximum Chemically Bound Water $\hat{W}n$

For the two Portland cements A and C, considered earlier in Section 3.3.4, the maximum amounts of chemically bound water have been calculated according to expression (3.5). The results are shown diagrammatically in Fig. 3.3. From a statistical evaluation similar to that carried out for the maximum heat of hydration data the mean values and standard deviations of the maximum amount of chemically bound water can be calculated. Mean values for Wn were found to be 0.219 g/g and 0.229 g/g with standard deviations 0.0047 g/g and 0.0038 g/g for cements A and C, respectively. The corresponding coefficients of variation are 2.2% and 1.7%. A comparison of these coefficients with those obtained for the maximum heats of hydration, i.e. 7.1% and 6.6%, reveals that the calculated maximum chemically bound water seems to be less susceptible to the method according to which the clinker composition is determined.

From the standard deviations of the chemically bound water of the constituents, Copeland computed the coefficient of variation for the maximum amount of chemically bound water of Portland cement clinker at 7.3% to 5.5% [112], which is close to the coefficients of variation found for the heat of hydration values (Section 3.3.5). These values can be

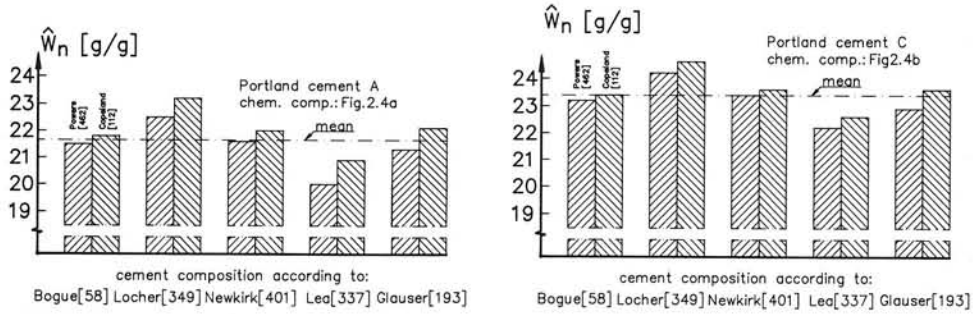

Fig. 3.3 Calculated maximum values of chemically bound water of two Dutch Portland cements A and C. Clinker composition according to different authors (Chapter 2, Fig. 2.4)

compared with the coefficient of variation of 4% recommended by Yong [631] for the accuracy with which the heat of hydration could be determined for any arbitrarily chosen clinker composition.

3.4.2.5 Relative Amount of Chemically Bound Water. Accuracy and Reliability

Particularly for theoretical and research purposes the relative amount of chemically bound water, i.e.

$$\alpha(Wn(t)) = \frac{Wn(t)}{\hat{W}n} \tag{3.6}$$

is often used as a measure of the degree of hydration $\alpha(t)$. With respect to the reliability and accuracy of this concept it should first of all be emphasized that substantial errors can be introduced when data obtained according to the O-, P- and D-drying methods are confused. This might already give rise to an error in the relative amount of chemically bound water, and hence in the degree of hydration, of up to 10% (Section 3.4.2.2). Further it can easily be seen that the accuracy with which the relative amount of chemically bound water $\alpha(Wn(t))$ is calculated can never exceed the accuracy of the quantities involved in eq. (3.6). Assuming a coefficient of variation for Wn-measurements of about 1.5%, and for the calculated maximum amount of chemically bound water of 5.5% (see Section 3.4.2.4), the coefficient of variation of $\alpha(Wn(t))$ would amount to 7%, which is similar to the estimated accuracy with which the degree of heat liberation can be determined (Section 3.3.4.3).

3.4.3 Physically Bound Water

As can be deduced already from Fig. 3.2 the amount of physically bound or adsorbed water actually depends on the relative humidity in the pore system. As a rough guide value for the amount of physically bound water a value of 15% of the weight of the anhydrous cement is generally adopted [289,462]. Together with the amount of chemically bound water, i.e. about 25% of the weight of the anhydrous cement (Section 3.4.1), the amount of water required for complete hydration would be about 40% of the weight of the cement.

An adsorbed water layer with a thickness of 8 to 9 Å, i.e. the adsorption layer that remains at a relative humidity of about 80%, is thick enough to fill the gel pores with a diameter of about 20 Å almost completely with water. Assuming the 20 Å pores to be characteristic of the gel (Fig. 3.4 and Section 4.4.4), it can be concluded that under normal curing conditions the gel is completely saturated. This part of the physically bound water is, therefore, considered to be part of the gel which is not available for further hydration.

Due to strong adhesion forces a densification of the gel water by about 10% has been assumed [462]. For most practical applications, however, and also for the theoretical considerations in this report, the specific volume of the gel water will be taken as unity.

Several authors have observed that the borderline between chemically and physically bound water is not a very sharp one [75,356,582]. A more diffuse borderline originates from the fact that the pore structure is a continuous one and does not reveal a discontinuity at a pore size of 20 Å, which could have established a pronounced difference between physically and chemically bound water.

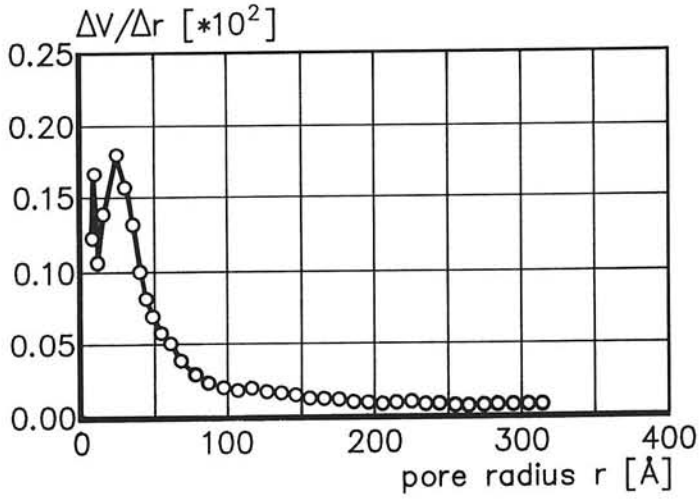

Fig. 3.4 Micro-pore distribution in cement paste specimen (After [623]). German Portland cement PZ 375. Curing temperature T=20°C, wcr=0.4.

3.4.4 Free Water

Water that is removed by heating of cement paste up to 105°C is generally identified as free water. Water molecules of this free water are considered to behave like in bulk water. Within the definition of free water Dorner [143] further distinguishes between bulk water (in pores ϕ>0.2 μm), capillary water (in pores 0.01 μm <ϕ<0.2 μm) and structured water. Structured water is accommodated in the smaller pore regions with 0.006 μm<d<0.02 μm.

Free water is often equalized with evaporable water. This water is assumed to be available for further hydration of the cement. Similar to what has been observed with respect to the borderline between chemically and physically bound water, the borderline between evaporable and non-evaporable water is not a very distinct one either [510]. Part of the evaporable water (which includes the physically bound water [464]) has been found to behave as a structural component of some hydrates, viz. the innermost adsorbed water layers.

3.5 Hydration Mechanisms

3.5.1 Topochemical and Through-Solution Reaction

The debate on whether cement hydration proceeds topochemically or according to a through solution mechanism dates back to the very beginning of cement chemistry. The subject is of significant importance in view of mathematical modelling of both the hydration process and structural formation.

Topochemical Concept (see Fig. 3.5a)
Immediately after the first contact of the cement with water a calcium-rich silicious clinker would liberate Ca^{++} ions into the solution. A calcium-poor skeleton is left which reacts with the calcium-rich solution which is accompanied by swelling of the hydration products compared with the original volume of the anhydrous cement.

The topochemical concept was launched by Michaelis [384] at the beginning of this century. Since then topochemical phenomena have been reported for the hydration of both C_3S [197,218,229] and Portland cement [131,279,294].

a. Topochemical reaction

b. Through-solution mechanism

Fig. 3.5 Schematic representation of proposed hydration mechanisms (after [294]).

Through-solution concept (see Fig. 3.5b)
In the through-solution concept dissolution of the anhydrous grain after contact of the cement with water is considered to be followed by hydration in the solution. The hydration products then precipitate on the grain surface.

The through-solution concept was first formulated by Le Chatelier [334] for plaster and Portland cement in the first decade of this century. The concept has been supported by, among others, Regourd et al. [481], Brunauer [75] and Gauglitz [183], Williamson [616] and Dron et al. [145].

Simultaneously Operating Mechanisms
According to Neville [400] the controversy between the topochemical and through-solution concept can largely be reduced to a matter of terminology. Shebl et al. [535] explains that hydration of C_3S involves both through-solution reactions and topochemical reactions (solid-state reaction). The water/solid ratio would be an important factor in this respect. For low water/solid ratios the reaction would be predominantly topochemical, whereas for high water/solid ratios the through-solution mechanism would be more important. Both reactions could occur simultaneously.

The concept of simultaneously operating mechanisms is plausible indeed if the *outer products*, i.e. the products which are formed *outside* the original grain boundaries in a relatively water-rich environment, are formed by a through-solution mechanism, while the *inner products*, formed *inside* the original grain boundaries, are the result of a topochemical reaction [124,569].

From a literature survey on this topic Daimon [124] concluded that it is very difficult to determine which mechanism has occurred. The fact that we are dealing with a poly-size system significantly contributes to the complexity of the subject. Probably the effect of the particle size distribution also explains why Kalousek [276] found many contradictions between different authors on this point.

3.5.2 Clinker Hydration versus Hydration of Individual Constituents

3.5.2.1 Rate of Reaction of Individual Constituents

The rates of reaction of individual constituents differ quite significantly. For C_3S and C_2S the rates of hydration are shown in Fig. 3.6 (from Lea [337]). The hydration data found by different authors were determined by either X-ray diffraction measurements of the remaining unhydrated material or measurements of combined water. Although there is, for several reasons, a substantial scatter in these hydration curves, there nevertheless remains a quite distinct difference between the rates of hydration of the individual compounds. Similar conclusions also hold for the hydration of C_3A and C_4AF.

It is to be expected that the rate of hydration of cement will somehow be a function of the rates of reaction of the individual constituent phases. The question whether and to what extent individual constituents hydrate either independently from each other (Independent Hydration Concept) or at Equal Fractional Rates (EFR-concept) is the subject of the

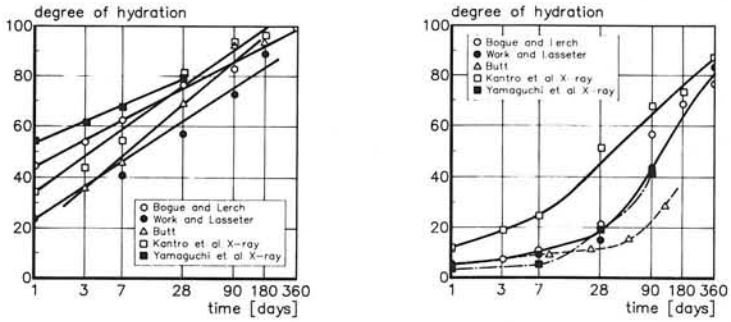

a. C_3S-hydration

b. C_2S-hydration

Fig. 3.6 Rate of hydration of different pastes according to several authors (from [337]).

next section. This question is of paramount importance in view of mathematical modelling of the hydration process of a poly-mineral material like cement.

3.5.2.2 Independent Hydration Concept

In the independent hydration concept, schematically shown in Fig. 3.7a, any interaction between hydrating constituents is disregarded. Independent hydration of constituents is the basis of Parrott's hydration model [435]. In order to substantiate the effectiveness of his approach Parrott refers to, among others, Odler et al. [416], according to whom belite hydrates independently from other compounds. Also non-uniformity of the rate of reaction of poly-mineral particles as observed by several authors might be interpreted as an argument in favour of the Independent Hydration Concept [381,509,596].

Independent hydration of constituents is one of the main presuppositions of the application of least square analysis of hydration data. This mathematical technique has frequently been used in the past for the determination of the rate of hydration of constituents in a poly-mineral system [401,601,626].

3.5.2.3 Equal Fractional Rates (EFR-concept)

One of the first representatives of the EFR-concept was Brownmiller [74]. From microscopic observations he concluded to the evidence of a gradual, uniform reduction of the particle size as hydration proceeds (see Fig. 3.7b). Any channelling of water into the grains to hydrate the more reactive constituents was not noticed. In a discussion with Brownmiller, Rexford [489] stated that hydration would indeed take place at a comparatively uniform overall rate, which affected all of the cement compounds of a cement particle more or less simultaneously. Further support for the EFR-concept came from Greene [209], Powers [462], Verbeck [601], Zur Strassen [645] and Frigione [176].

3.5.3 Hydration Mechanisms. Discussion

Copeland has critically pointed to the contrast between the assumptions underlying the Equal Fractional Rate concept, on the one hand, and the least square analysis, and implicitly the Independent Hydration Concept, on the other, and stated that *"one or both of these assumptions would prove incorrect [214]"*. In the light of this statement the work of Bentur et al. [41], Yamaguchi [630] and Lehmann [338] is worth mentioning.

Bentur found that with the presence of C_2S the hydration of C_3S increased. This phenomenon was assumed to be attributable to an increase of the effective water/C_3S ratio for which the slowly reacting C_2S was said to be responsible. Although the interaction was quite convincing, there still remained a marked difference in the rate of hydration of the two compounds (Fig. 3.8).

Yamaguchi [630], who investigated the effect of gypsum on the rate of hydration of synthetic and commercial cements, clearly showed that the rate of hydration of individual constituents was different for different mixes (Fig. 3.9). His results convincingly show the existence of interactions between the hydrating constituents, but also a distinct difference between the degrees of hydration of the constituents.

According to Lehmann [338] independent hydration of compounds can occur in the early stage of hydration, whereas at later stages, when the reactions become more and more diffusion controlled, hydration of different compounds would proceed at equal fractional rates. Zur Strassen [645] also considered diffusion of ions through the thickening shell of reaction products as a reasonable explanation for hydration at equal fractional rates at later stages.

Putting together all this information it can be concluded that in a polymineral system, hydration of individual constituents proceeds *neither* at equal fractional rates *nor* independently from each other. Apart from interactions of a purely *chemical* nature at least two sources of *physical* interaction appear to exist, viz.:

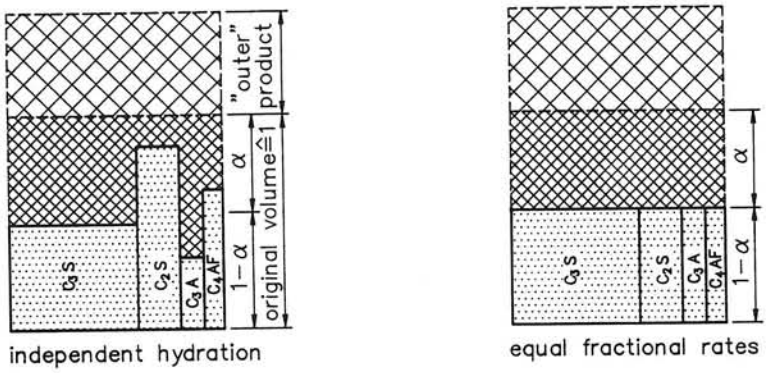

a. Independent Hydration

b. Equal Fractional Rates

Fig. 3.7 Schematic representation of Independent Hydration Concept and hydration at Equal Fractional Rates.

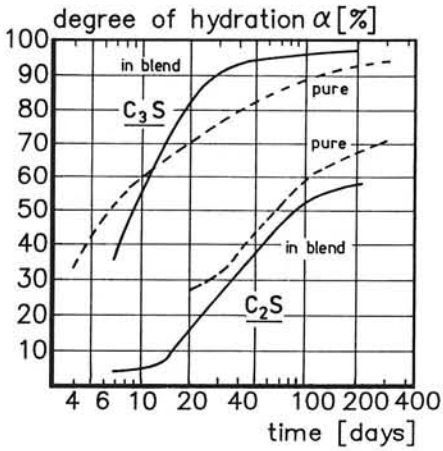

Fig. 3.8 Rate of hydration of C_3S: as pure constituents and in a 50/50 blend [41].

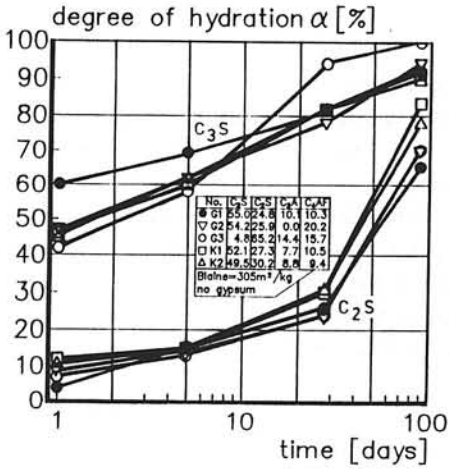

Fig. 3.9 Rate of hydration of constituents, affected by the clinker composition [630].

1. *Changes in the effective constituent/water ratio, caused by differences in the rates of hydration of the individual constituents;*
2. *Diffusion processes, which would be responsible for a more equal rate of hydration of the individual constituents at later - diffusion-controlled - stages of the hydration process.*

The evidence of interactions make us reluctant to adopt the independent hydration concept. At any rate this concept requires corrections for the existence of interactions in order to avoid misinterpretations of experimentally and theoretically obtained hydration data. Attempts to model the interactions between hydrating constituents, however, will soon lead to great difficulties. The subject has been discussed by many authors, but at present no universally accepted model is available that comprehensively and consistently describes how individual compounds interfere. The role of gypsum and alkalies in the hydration process further enhances the complexity of the subject. Meanwhile it should be born in mind that allowing for an increasing number of interactions (and hence of model parameters) in order to create more reliable predictive models can indeed result in a very good fit of test results, but still without offering any reliable ground for the correctness of the way in which the interactions had been modelled. In this respect it is worth while to quote Bezjak when he stated *".. any mathematical modelling that takes into account a great number of parameters can fit well any hydration-time relationship [53]. ..... Such a good fit, however, will not represent in itself a reliable proof of the correctness of the model [55]".* This somewhat sceptical, but nevertheless realistic attitude may, of course, not prevent us from allowing for those interactions and parameters of which the significance has been demonstrated and quantified explicitly in the past.

3.6 Stages in Cement Hydration

3.6.1 General

The hydration of Portland cement exhibits several subsequent stages with marked differences in the rate of reaction. Detailed characteristics of these stages, their duration and rate-controlling mechanisms, mainly depend on the clinker composition of the cement, the particle size distribution, the water/cement ratio and the curing temperature. A typical shape of the hydration curve of Portland cement is shown in the insert of Table 3.5. The table schematically summarizes how several authors have distinguished different stages of the hydration process. In this report the classification will be used a proposed in the recent work of Jennings et al. [267] and Scrivener [524], viz. the *early, middle* and *late period.*

3.6.2 Early Period

On contact with water cement grains immediately start to react. This early reaction period, which lasts for only a few minutes [538,541,566], is termed the pre-induction period. In this early stage C_3A and, to a minor extent, C_3S are the most active components. Calcium ions (Ca^{++}) go into solution and start to form a saturated solution. After a few min-

Table 3.5 Classification of stage of the hydration process according to different authors.

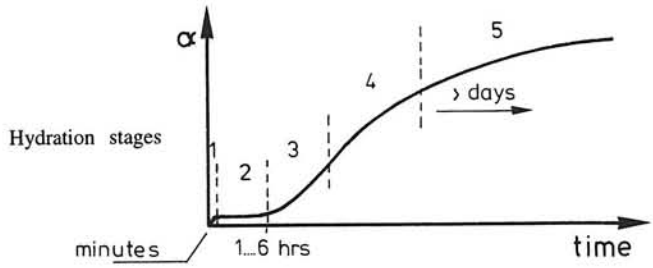

Author	ref.	product					
Kondo et al.	[307]	C_3S	① pre-induction	② induction	③ acceleration	④ deceleration	⑤ remarkable deceleration
Skalny	[538]	C_3S	pre-induction	induction	acceleration	deceleration	
Skalny et al.		p.c	pre-induction	induction	post-induction (diffusion controlled stage)		
Shebl et al.	[535]	C_3S				hydration completed	jennite / tobermorite formation
Jennings et al. Scrivener	[267] [524]	p.c	Early period ≈ 3 hrs	Middle period 3 to 20...30 hrs	Late period > 30 hrs		

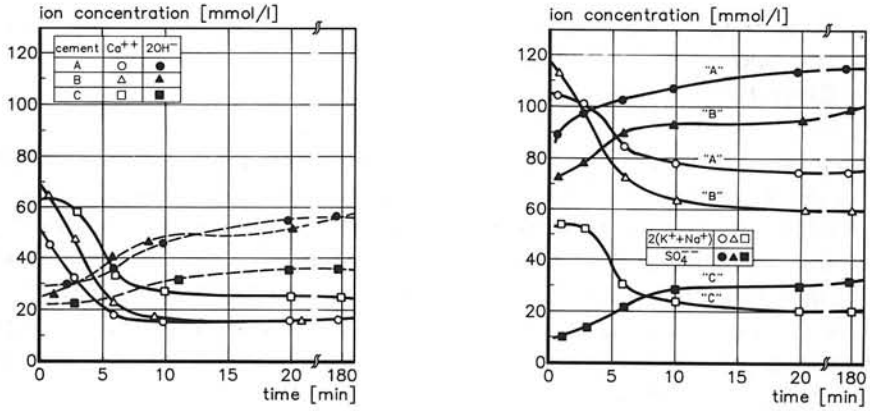

a. C_3S (I) hydration

b. C_3S (II) hydration

Fig. 3.10 Changes in the pore water composition in the early stage of hydration. Three different cements (after Fujii, et al. [180]). wcr=0.5

utes a Ca^{++} concentration of 20 to 30 mmol/l is reached [172,179,233,403,541,597]. Mean while other ions are formed as well, viz. Si, OH^-, SO_4^{--}, K^+ and Na^+. The ion concontration will depend on, among other things, the chemical composition of the cement and the presence of admixtures [181,413].

An example of the effect of the cement composition on the early ion concentrations is shown in Fig. 3.10. For three different cements Fig. 3.10a shows Ca^{++} and OH^- concentration, whereas the SO_4^{--} and (K^++Na^+) concentrations are shown in Fig. 3.10b. The figures show that after a few minutes a stable concentration is reached which remains so for a period of at least 180 minutes.

Figure 3.11 shows the Ca^{++} concentrations measured in the pore water of two C_3S

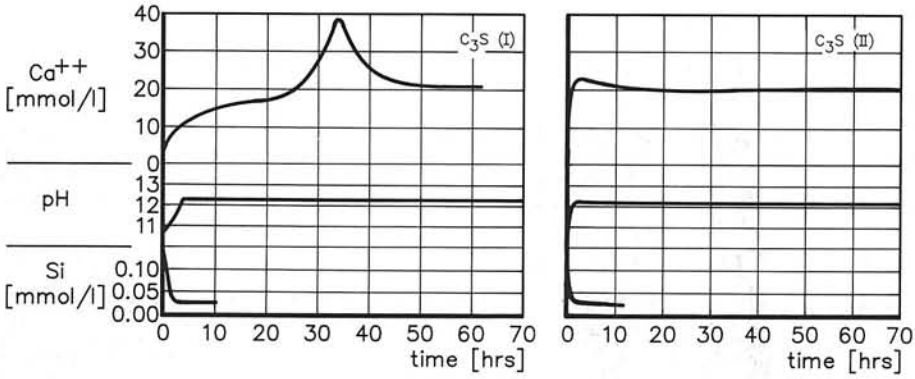

Fig. 3.11 Pore water composition in two different C_3S pastes (Slegers et al. [541]).
a (left) : C_3S (I), doped with 0.5% B_2O_3
b (right): C_3S (II), manufactured from pure limestone and silica gel.

pastes. The C_3S material was manufactured differently, causing marked differences in the Ca^{++} concentrations. In these tests the Ca^{++} concentration of about 20 mmol/l remains constant for at least 70 hours.

The effect of the pH on the early Ca^{++} and silicate concentration is shown in Fig. 3.12a and b. The observations refer to C_3S (alite) with a water/solid ratio of 500.

The rapid early reactions in the first few minutes are followed by a period of low reactivity. This period is known as the *induction period* or *dormant stage*. The length of this period depends on the fineness of the cement, the temperature and the chemical composition of the cement (including the gypsum content and admixtures [413]). The dormant stage will generally not exceed 5 hours. From the figures 3.10 to 3.12 it can be concluded that during this period the chemical composition of the aqueous phase will remain more or less constant.

Several explanations proposed for the observed early hydration behaviour and for the mechanism which would cause the end of the dormant stage have been discussed by Bensted [39]. Two of the most often mentioned concepts, viz. the "membrane or protective layer concept" and the concept of "delayed nucleation and growth" will be discussed briefly in the following.

Membrane or protective layer concept

In the membrane or protective layer concept the anhydrous cement grains are assumed to be covered with reaction products which prevent further reactions from taking place. Several authors hold the view that the first reaction products form only *locally* on the grain surface [166,381]. Others presume the formation of a gelatinous layer or membrane over the whole particle surface [22,212,413,473]. In both cases coverage of active surfaces prevents further hydration.

For the mechanism that would cause the end of the dormant stage several theories exist. According to the *osmotic pump theory* osmotic pressure at the inside of the membrane results in rupture of the membrane thus clearing the way for subsequent rapid reactions

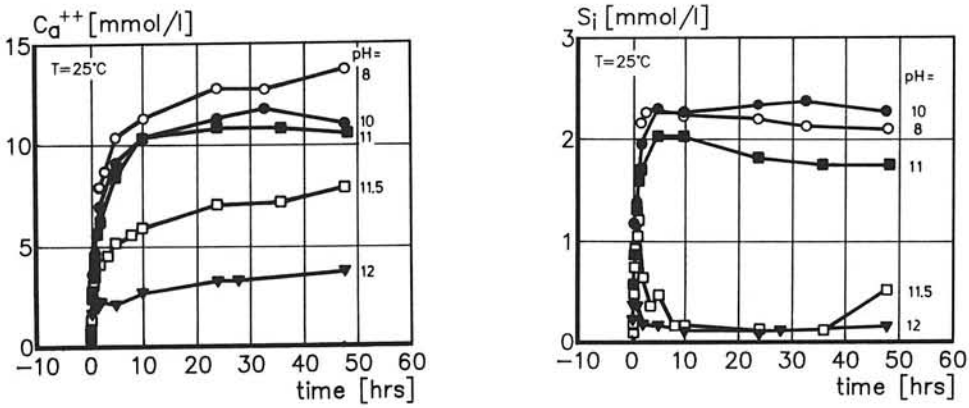

a. Ca^{++} concentration

b. Si concentration

Fig. 3.12 Effect of pH on the aqueous phase in a water-alite system (after [474]).

[265]. Ludwig [356] has proposed a *mechanism of rupturing* and subsequent healing of the protective membrane until all the *gypsum* needed for the healing process is used up. His theory explains why the duration of the dormant stage depends on the amount of gypsum and the specific surface of the cement [8,504]. Others have proposed a change in permeability of the protective layer to cause the end of the dormant stage [106,272,308,473, 552].

Delayed nucleation and growth concept

In the concept of delayed nucleation and growth Ca^{++} and OH^{-} ions would dissolve slowly, giving off little heat, until sufficient supersaturation is attained to overcome nucleation difficulties [566,581,586,634].

Fierens [165] assumes that the existence of a potential barrier prevents nucleation at the grain surface. Nucleation could occur as soon as the reaction products have reached a critical size and *Van der Waals attraction* commences to dominate the *repulsion forces* (see also Section 4.2).

3.6.3 Middle Period

The middle period starts when the mechanism which had prevented rapid hydration during the preceding stage has lost its basis for continuing existence. A mechanism starts that can be described as a transport of ions to and from the surface of the anhydrous particles through a gradually thickening shell that forms around the anhydrous core. The shells grow outward and reach a thickness of 0.5 to 1.0 μm after about 12 hours hydration. When growing outward the shells of adjacent grains interlock. On macro scale this interlocking is observed as development of strength and stiffness. According to Taylor [581] the reactions would develop mainly according to a through-solution mechanism in this stage.

For the duration of the middle period (for guidance: up to 24 to 48 hours), the ion concentration will be almost constant (see Figures 3.10 to 3.12). A slight decrease of the Ca^{++} concentration, however, may have already commenced.

3.6.4 Late Period

In the late period the reactions gradually become more and more diffusion-controlled. Meanwhile the ion concentration in the aqueous phase significantly changes. For an ordinary Portland cement the development of the ion concentration over the first 1,000 hrs is shown in Fig. 3.13. This figure shows that in the period from 24 to 100 hrs, i.e. only in the late phase of the middle period and early phase of the late period, the ion concentration in the aqueous phase has reached a new state of equilibrium. Obviously, gradual change from a surface reaction to a diffusion controlled reaction coincides with the change in the chemical composition of the pore water. This observation has interesting consequences for the mathematical modelling of the hydration process in this stage. In Section

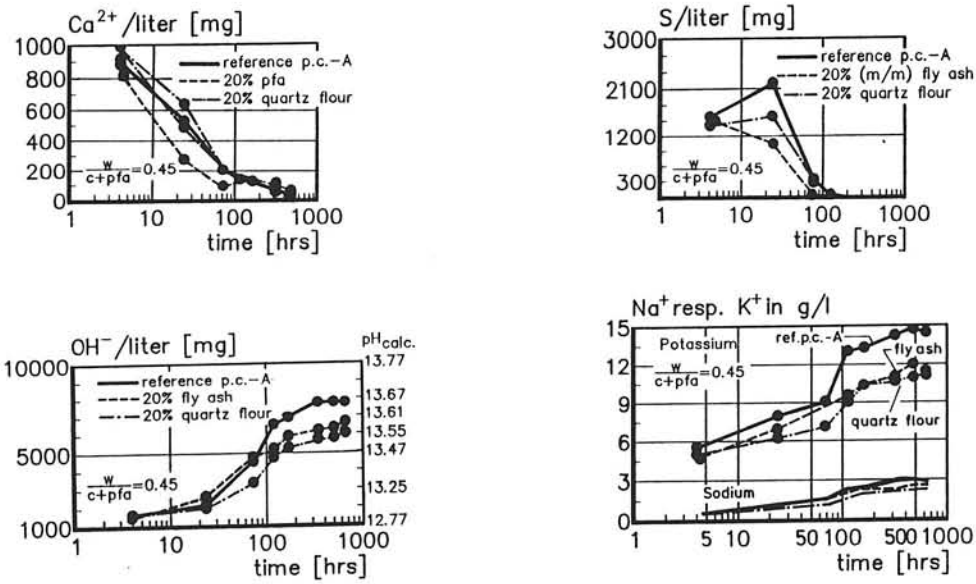

Fig. 3.13 Change in ion concentration in pore water of hydrating Portland cement paste over a 1,000 hours period (after Fraay [172]).

6.5.6 we will cover this point in more detail.

With respect to the formation of CSH during the late period three different mechanisms have been proposed:

1. Further *outward growth* of the shell of hydration products. The shell becomes less porous while its thickness increases up to about 8...10 μm at 7...14 days.
2. Inward growth of the shell. Anhydrous cores dissolve, leaving a space between the remaining anhydrous cement core and the shell. At 4 days this space would be ≈3 μm. After 4 days the inward growth of the shell overtakes the retreat of the anhydrous core and the space is gradually filled up [266]. Grains smaller than 15...20 μm hydrate completely before the space has been entirely filled. In this case cavities might be left of up to 5 μm [469]. The mechanisms considered under 1 and 2 are both assumed to be through-solution mechanisms [581].
3. Continuing hydration of still unhydrated cores would now proceed mainly topochemically [524,581]. In Section 4.4.2 this point will be covered in more detail when discussing the classification of hydration products into inner and outer products.

The foregoing classification of hydration stages can serve as a starting point for a more detailed discussion about some of the relevant topics concerning morphology, structural formation and strength development in Chapter 4.

3.7 Chemical Composition of Reaction Products

3.7.1 Survey of Literature Data

Otherwise than might have been suggested using eq. 3.1a...g, the hydrate composition is not constant. The hydrate composition, indicated by the C/S ratio, appears to vary quite significantly from less than 1 up to 3 or even 4 [395]. For C_3S-pastes the C/S ratios have been reported in the range from 1.4 [278] to 3.63 [138]. Since it is generally assumed that from the chemical composition of the hydration products information can be deduced about the relevant hydration mechanisms, it is considered useful to dwell at this point for a moment.

Glasser et al. [191], in a review of hydrate composition produced by C_3S, concluded to a C/S ratio of 3 at the interface with the unreacted core and a decrease of this value to probably below 1 in the liquid phase. According to Menetrier et al. [380] the high C/S ratio of 3 would drop to 2.6...2.7 very quickly, viz. only a few seconds after contact with water. The C/S ratio would pass through a minimum of 2.2...2.5 and then increase again up to 2.8...2.9. From then on the C/S ratio would continuously decrease to a value of about 2.0 and 1.5 after 10 and 30 minutes, respectively.

In fairly good agreement with Glasser and Menetrier, Bombed [61] concluded that three phases with different C/S ratios can be distinguished:

1. A thin layer, 0.1...to 0.2 μm, with a C/S ratio equal to the starting material, e.g. C/S=3 in the case of hydration of C_3S.
2. Formation of an unstable hydrate with a low C/S ratio of 0.8...1.5;
3. Formation of a stable gel with C/S=1.5...2.0.

Effect of water/cement ratio

For a C_3S-paste the C/S ratio increased with decreasing water/solid ratio. For a w/c ratio exceeding 0.6 the effect on the C/S ratio was found to be less pronounced [351].

For cement pastes with w/c ratio's from 0.3 to 0.6 the composition of the reaction products would not change significantly in the period from 3 days up to 23 years [581]. Similar observations were made by Stucke et al. [562], who found that the C/S ratio of CSH-II [4]) would even be independent of the w/c ratio.

Effect of degree of hydration

Several authors have pointed to the effect of the degree of hydration on the hydrate composition [78,138,351,484]. With increasing degree of hydration the C/S ratio would increase as well. However, a decrease in the average C/S ratio with increasing hydration has been reported as well [106,277,307]. Moreover, in some investigations the C/S ratio of hydrates formed from C_3S appeared to be almost independent of the degree of hydration [413,351].

---

[4]) CSH-I = $C_{0.8\text{-}1.5}SH_x$; CSH-II = $C_{1.5\text{-}2.0}SH$ [219].

Effect of temperature.
In several papers Odler et al. have reported on a noticeable effect of the temperature on the composition of the reaction products [409,418]. According to Menetrier et al. [380] the C/S ratio would be lower at low temperatures than at high temperatures. Some data published by Zur Strassen *(Ibid [350])*, however, showed that the effect of temperature on the C/S ratio would be rather weak.

Inner and outer product
According to Daimon [124] the C/S ratio of the inner product is higher than that of the outer product. For C_3S pastes Stucke et al. [562] observed a C/S ratio of the inner product of about 1.9, while for the outer product a ratio of 1.6 would hold. Rayment et al. [479] could distinguish inner and outer products only in cement containing unhydrated alite. The outer product had a mean C/S ratio of 2.6 to 2.7. Even in a fully reacted paste Taylor et al. [581] still distinguished inner and outer products.

In contrast with these observations, Rodger [495] could not find any difference in the C/S ratios of inner and outer products in a two year old C_3S paste. Rodger's observation of similar composition of outer and inner product is in line with Odler's finding that the chemical composition of the hydration products remained fairly constant throughout the hydration process [413].

3.7.2 Chemical Composition of Reaction Products. Discussion

In this discussion an attempt will be made to deduce some information about the hydration mechanisms that might have occurred during the reaction process. Particular attention will be given to what has been observed with respect to the chemical composition of the inner and outer products.
There seems to be a high degree of consensus about the fact that:

1. Inner product is formed topochemically and exhibits a relatively high C/S ratio and no big portlandite crystals;
2. Outer product has a relatively low C/S ratio and is formed predominantly by a through-solution mechanism. This would also, at least in part, explain the evident effect of the w/c ratio on the hydrate composition. Large portlandite crystals are found as well;
3. A pronounced difference in the C/S ratios of inner and outer product in *not* observed in more mature pastes.

The observed difference in the C/S ratios of inner and outer product *in the early stage* of the hydration process and the absence of a distinct difference in C/S ratios between inner and outer product in more *mature pastes* can most probably be attributed to intensive merging of outer product of expanding particles and, what is considered to be of even more importance, to a *mechanism of embedding of smaller particles in the outer shell of larger particles*. This "embedding mechanism", to be discussed in more detail in Chapter

6, explains why the distinction between inner and outer product loses part of its original markedness in more mature pastes. The outer shell of large particles, in which small particles are embedded exhibiting both inner and outer product features, is likely to have a C/S ratio somewhere between that of an outer and inner product.

From the foregoing evidence, it can be deduced that for a - to a certain extent - homogeneous gel, possible initial differences in the chemical composition between inner and outer products gradually vanish due to merging, i.e. embedding mechanisms. The formation of a more or less homogeneous gel can justify an approach for modelling the hydration process such that, at least in the first instance, processes and mechanisms can be ignored which might have caused differences in the chemical composition of the hydration products.

It is remarked that with the aforementioned evidence for a homogeneous gel the chemical structure of the reaction products, i.e. the arrangements of molecules in tobermorite-like and jennite-like structures, has in fact not been defined. It would bring us beyond the scope of this thesis to enter into this field in more detail. For a more detailed discussion about this most complex topic reference is made to the proceedings of the First International Workshop on Hydration and Setting, Dijon, 1991 (among others: Nonat [403]).

3.8 Degree of Hydration

3.8.1 Definitions

3.8.1.1 General

To what extent the hydration process has proceeded is usually indicated with the term "degree of hydration". For several reasons an unambiguous definition of the degree of hydration is hard to give, if not impossible. The ultimate stage of complete hydration has trivially been defined as the stage in which all the cement has reacted. Although trivial, it is still not easy to determine when in a poly-size and poly-mineral specimen all the material has reacted. In this respect one should remember that the chemical composition of cement particles varies with the particle size (Chapter 2) and that different constituents do not hydrate at the same rate. Moreover, different constituents neither produce equal amounts of heat of hydration nor do they bind equal amounts of water per unit weight. *In spite of all these difficulties we are nevertheless inclined to define the degree of hydration $\alpha(t)$ as the ratio between the amount of cement that has reacted, i.e. that has been dissolved, at time t relative to the original amount of cement.* In other words (see also [439]):

$$\alpha(t) = \frac{\textit{amount of cement that has reacted at time } t}{\textit{total amount of cement at time } t=0} \tag{3.7}$$

The charm of this definition is, as will be shown in subsequent chapters, its relative convenience in the case of considerations concerning the stereological aspects of structural

formation. For the determination of the amount of cement that has actually reacted Tsumura [596] has recommended röntgenographic techniques to be most reliable.

3.8.1.2 Parameters to Indicate the Degree of Hydration [5])

Parameters that can be used to indicate or approximate the actual degree of hydration as defined with eq. (3.7) are [83]:

1. Liberated heat of hydration:	$\alpha(t) = Q(t)/Q^{max}$	(3.8a)
2. Amount of chemically bound water:	$\alpha(t) = Wn(t)/\hat{W}n$	(3.8b)
3. Chemical shrinkage [121,185,185,305]	$\alpha(t) = \varepsilon(t)/\varepsilon^{max}$	(3.8c)
4. Amount of $Ca(OH)_2$:	$\alpha(t) = V_{CH}(t)/\{V_{CH}\}^{max}$	(3.8d)
5. Specific surface of the cement paste:	$\alpha(t) = SS(t)/\hat{S}S$	(3.8e)
6. Strength:	$\alpha(t) = f(t)/f^{max}$	(3.8f)
7. Dielectric properties of the cement		(3.8g)

In addition to what has been said in Section 3.3.5 and 3.4.2.5 about the accuracy with which the degree of hydration could be approximated by either the degree of heat liberation or the amount of chemically bound water the following comments can be made.

Liberated heat of hydration
As early as the early thirties the liberated heat of hydration has been used as an indicator of the degree of hydration [342,626]. According to Lehmann et al. [338] there exists an excellent linear relationship between these two quantities. Discrepancies between the degree of hydration and the degree of heat liberation, however, have been reported by Bombed [61], Daimon et al. [125] and Brown et al. [72]. The relationship between degree of hydration and degree of heat liberation has been found to be affected by the curing temperature [184,409].

Chemically bound water
According to Le Sueur et al. [335] a linear relationship exists between the amount of combined water and the degree of hydration determined using QXRD. This conclusion is in line with earlier work by Powers and Brownyard [462]. They found a constant ratio between the amount of water required to cover the hydration products with one single monolayer of water and the amount of non-evaporable, chemically bound water. This constant ratio suggests that the chemically bound water is a reliable indicator of the amount of cement that has reacted, even for a poly-mineral material like cement. The linear relationship is applicable from 1 day up to complete hydration. From the latter observation the conclusion has been drawn that from 1 day hydration onward the nature of the hydration pro-

---

[5]) For recent detailed studies on parameters to identify the degree of hydration, see K.O. Kjellsen in *Quantitative analysis of the major phases in sulfate-resistant cement silica fume systems by SEM, ^{29}Si NMR and XRD methods*, CBI report 2:97, Swedish Cement and Concrete Research Institute, 55 p.

ducts would remain the same (also [410]).

Several authors have found a very good linear correlation between the heat of hydration and the amount of non-evaporable water. This suggests the two parameters to be equivalent as far as their applicability as hydration parameters is concerned. According to Bombed [61], however, the non-evaporable water concept would yield more reliable values than the heat of hydration concept. Deviations from a linear relationship between the degree of hydration and Wn-values have to be expected for low hydration values [338, 355]. Also for very high degrees of hydration, $0.95<\alpha<1.0$, the $Wn(t)/\alpha(t)$ - relationship would be less distinct [338]. According to Granju et al. [206] deviations of more than 10% should be reckoned with.

Amount of $Ca(OH)_2$

According to Le Sueur et al. [335] there exists a linear relationship between the development of the degree of hydration and the formation of calcium hydroxide (CH). The amount of calcium hydroxide could even be a more reliable indicator of the degree of hydration than the heat of hydration [61]. Odler et al. [418], on the contrary, report on deviations of $CH(t)/\alpha(t)$ values with other measurements of up to 30%, which substantially weakens the latter statement.

Specific surface of gel

The assumption of a characteristic porosity of the hydration products (see Chapter 4) allows for the correlation between the internal surface of the hydration products with the degree of hydration. The relationship has been investigated and subsequently discussed and supported by Jaspers [262], Venaut [600] and Powers et al. [462].

Chemical shrinkage

Chemical shrinkage is a phenomenon inherent in the hydration process and as such it can serve as an indicator of the degree of hydration [121,185,305,434]. With this method the determination of the degree of hydration is reduced to a geometrical, i.e. a stereological problem, viz. the determination of the volume associated with the volume reduction of the reaction products relative to the total volume of the constituent phases. The method requires due attention for the effect of the size of the samples from which the measurements are taken, since suction of water from outside into the core of the sample can require quite a long period of time [121]. Knudsen [305] and Geiger et al. [185] have shown that chemical shrinkage measurements can successfully be used as indicators of the degree of hydration, provided that the method is executed under well-defined test conditions.

Dielectric properties of hydrated cement

For a continuous and non-destructive monitoring of the hydration kinetics and the degree of hydration, micro-wave techniques can be applied [199]. The method relies on the fact that the dielectric properties of hydrating cement are closely related to its *free water content*. The method is expected to have great potential to follow the hydration of various cements and hydraulic binders with and without chemical admixtures. The method seems of particular interest for monitoring early hydration processes.

3.8.1.3 Degree of Hydration - Definitions. Discussion

Statements with regard to the accuracy, reliability or adequateness of the foregoing definitions presuppose an absolute and exact reference. Daimon [125] has suggested that for a reliable picture of the stage of the hydration process, several indicators should be con-sidered simultaneously. The "reference" would then exist of a kind of "weighted average". From a theoretical standpoint such a reference might be attractive, from a practical point of view, however, it is not, since it would require a huge experimental effort to establish such a weighted average. It must be admitted, however, that the reference chosen in this study (expression (3.7)) is not free from several inherent difficulties either. In this respect it might be interesting to note that there is a tendency to question the significance of the expression "degree of hydration" rather than to look for an unambiguous definition. The reason for this is the very complex and heterogeneous character of the hydration process [119]. Copeland has summarized it in this way [112]:

> *"Since the major phases hydrate at fractional rates different from each other, one may question the significance of the expression degree of hydration as applied to cement and the meaning of terms such as maturity factor for pastes, mortars and concrete. These concepts are important practically, even though they cannot be precisely defined theoretically".*

Copeland further stated that in view of the theoretical difficulties associated with the definition of the degree of hydration, on the one hand, and the approximate linearity between non-evaporable water content, heat of hydration and surface area of the cement paste, on the other hand, any of these quantities can be used as an estimate of the degree of hydration of cement (see also Section 3.8.1.2, Kjellsen[5])).

3.8.2 Cessation of the Hydration Process

3.8.2.1 Ultimate Degree of Hydration. Some Observations

For complete hydration of an ordinary Portland cement a w/c ratio of about 0.4 would theoretically be sufficient [462,635]. According to Rossler et al. [503] complete hydration of cement would even be possible for ω_0=0.22 (X-ray measurements). Rossler comments that this is substantially less than the generally considered value of 0.4, but did not give an explanation for this discrepancy. Glasser et al. [190] has mentioned a critical w/c ratio for complete hydration of 0.24, which is in close agreement with Rossler's values. High maximum values for the degree of hydration in low w/c ratio pastes have also been reported by Odler et al. [410], viz. α=0.64 and 0.83 for ω_0=0.2 and 0.3, respectively.

In contrast with the aforementioned observations Catharin [92] states that for complete hydration, a w/c ratio even greater than 0.5 is required. Catharin's statement is supported by Moore [395], who stated that complete hydration of an ordinary cement hydrating at ω_0=0.5 would take more than ten years. Cement of normal fineness would not hydrate

completely at normal w/c ratio in periods of time up to 100 years. In an almost 100 year old concrete Mallinson [367] indeed found large cores of unhydrated cement. Only a narrow rim, about 10 μm thick, of hydrated material was found.

The degree of hydration at 28 days hydration of cement in ordinary concrete mixes cured under site conditions would be about 0.6 to 0.8 [190,281,611], whereas in a 10 year old cement paste the degree of hydration was found to be about α=0.7 [507]. These figures suggest that in the case of curing under site conditions, mechanisms are at work that prevent the hydration process to proceed into high α-regions.

3.8.2.2 Ultimate Degree of Hydration. Theoretical Considerations

Two quantities have turned out to be of predominant importance in view of the ultimate degree of hydration, viz.:

1. *Amount of water available for the reaction with the cement, i.e. available as a reaction medium.*
2. *Space available for deposition of hydration products (Powers et al. [462]).*

Sufficiency of water

As observed in Section 3.8.2.1, complete hydration of cement is generally assumed to require a w/c ratio of about 0.4. According to Young et al. [632] hydration ceases when the amount of water is insufficient to form a saturated CSH. A minimum water/cement ratio of 0.42 would be required for complete hydration.

In the case of *sealed curing* the ultimate degree of hydration α that can be reached for w/c ratios below 0.4 has straightforwardly been estimated using the equation:

$$\alpha_u = \omega_0 * [k_0 + k_1]^{-1} \tag{3.9}$$

where k_0=0.25 refers to the required amount of chemically bound water [g/g cement] and k_1=0.15 to the amount of physically bound water [g/g cement].

In the case of *saturated curing* the initial w/c ratio needed to attain complete hydration can be somewhat smaller since the volume reduction of the reaction products relative to the volumes of the constituent phases enables an intake of water from the outside. For the maximum degree of hydration it can be derived:

$$\alpha_u = \frac{\omega_0}{(k_0+k_1) - k_0*(v_w-v_n) + k_1*(v_w-v_{gw})} \tag{3.10}$$

where: $v_{..}$ = specific volume of free water (index w), non-evaporable water (index n) and gel water (index gw).
Note: The value for v_n, i.e. v_n = 0.75 cm^3/g, is a notional one!

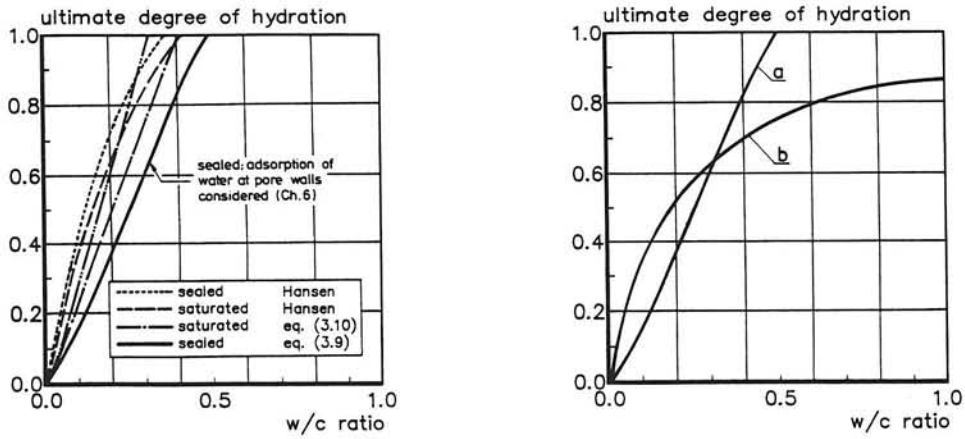

a. After Hansen and eqns (3.9) and (3.10)

b. After Mills and author

Fig. 3.14 Maximum degree of hydration as a function of the water/cement ratio
a. Data from Hansen [226] (curve b) and according to eq. (3.9) and (3.10).
b. Data after Mills [387] and the author (Section 6.5.5.6; curve a).

For v_w=1 cm^3/g, v_n=0.75 cm^3/g (a notional value!; see Section 3.4.2.1) and v_{gw}=1.0 cm^3/g and values for k_0 and k_1 as adopted in eq. (3.9) it follows that in the case of saturated curing an initial w/c ratio ω_0=0.3375 would be sufficient for complete hydration. Fig. 3.14a shows the ultimate degree of hydration a as a function of the initial w/c ratio for both sealed and saturated curing calculated according to eq. (3.9) and (3.10). Curves presented by Hansen [226], based on similar considerations as indicated above, are inserted as well.

Relative humidity

In the preceding section, and explicitly in the derivation of the expressions (3.9) and (3.10), the amount of physically bound water was assumed to be a fixed percentage of the cement weight that has reacted. In Section 3.4.3 it has been observed, however, that the amount of physically bound or adsorbed water depends on the relative humidity in the pore system. As will be explained in more detail in Chapter 6, mathematical evaluation of the effect of a remaining adsorption layer on the pore walls of the capillary pores will significantly affect the value of the ultimate degree of hydration. In Fig. 3.14b, curve a, the ultimate degree of hydration is calculated using the assumption that the pore walls of the capillary pores remain covered with a 9 Å thick adsorption layer. This is the thickness of the adsorption layer that remains when the relative humidity in the pore system drops down to 70...80% (see Fig. 3.2a and Fig. 6.14).

More detailed research on the effect of the relative humidity on the hydration process has revealed that hydration at low relative humidities results in a densification of the hydration products which surround the anhydrous cores. Early drying of young pastes at

115°C has even been found to result in an irrecoverable densification of the hydration products preventing the hydration process to continue [619]. Catharin [93] also considered the effect of early drying. He also expressed his doubts as to whether subsequent addition of water could restart the hydration process. Several authors have stated that there is hardly any hydration at relative humidities below about 70-80% [244,271,438] and hydration is negligible below RH=30% [463].

Accessibility of water and "space" considerations

The bases for the equations (3.9) and (3.10) are *volumetric considerations*, i.e. the presence of a certain amount of water in the porous cement paste. Presence of water, however, does not imply that the *distribution* of water in the cement paste is such that all cement particles will hydrate completely. The formation of an increasingly dense shell of hydration products around the larger particles will significantly reduce the rate of hydration and may even prevent the transport of ions to and from the surface of the anhydrous grains. Hence, the practical use of equations (3.9) and (3.10) is limited. Moreover, as Powers [462] has pointed out already, hydration would stop when the space available for accommodation of new hydration products becomes too small. These considerations have been implicitly recognized in Mills' phenomenological equation for the ultimate degree of hydration [397]:

$$\alpha_u = \frac{1.031 * \omega_0}{0.194 + \omega_0} \tag{3.11}$$

The ultimate degree of hydration according to this equation is shown in Fig. 3.14b (curve b). Although this equation can be considered to give a better approximation of the ultimate degree of hydration actually reached in practice, it should be borne in mind that it does not allow for the effect of the *type* of cement and, what is of more importance, the *fineness* of the cement. The coarser the cement, the lower the maximum degree of hydration will be.

3.8.3 Paste Curing versus Mortar and Concrete Curing

According to Catharin the degree of hydration of pastes and mortar would be about the same [93], whereas for complete hydration of cement in concrete a slightly higher w/c ratio seemed to be required [92]. Karsch et al. [282] found that the heat of hydration measured from mortars is higher than measured from pastes. According to Roth [504] the degree of hydration in mortar could exceed that of a paste by 10%. In agreement with Karsch and Roth, Locher [355] found that hydration of cement in mortar and concrete proceeds significantly faster than in neat pastes. Faster hydration of cement in the presence of aggregates might be attributed to easier water supply via the porous matrix-aggregate interfacial zone (see also [355] and Section 4.7).

3.9 Chemistry-Oriented Aspects of Hydration. Summary and Discussion

Major points in this discussion refer to the hydration mechanisms and the accuracy with which predictions of the degree of hydration are possible.

Maximum heat of hydration of a poly-mineral material
The potential heat of hydration of a clinker can be calculated from the clinker compound composition. It is evident that inaccuracies in the calculated compound composition will be transferred to the calculated potential heats of hydration of the cement. One should be very careful, therefore, with theoretical considerations in which heat of hydration data obtained according to different methods are used. Two potential sources of error should be considered. The first one refers to inaccuracies in the calculated compound composition of the cement and the second to the mathematical procedure to calculate the heat of hydration as a function of this compound composition. For a randomly generated set of potential heat of hydration data, random in the sense that the data was calculated according to different mathematical methods and subsequently applied to compound compositions which in turn were calculated according to different methods, standard deviations were obtained with an order of magnitude of 6 to 7%. These values must be considered as a warning against an uncritical use of current mathematical methods rather than figures which reflect the actual scatter in the potential heat of hydration of a certain cement. In this respect it should be noted that the differences in potential heat of hydration as calculated according to different mathematical methods show a *systematic* character. This implies that as long as one single calculation format is applied for the determination of the potential heat of hydration, the standard deviation will be substantially smaller than the one obtained from multi-method data. This is a most important fact since otherwise it would become very hard to achieve reliable predictions for the development of mechanical properties in cement-based materials.

Maximum amount of chemically bound water of a poly-mineral material
A similar reasoning as devoted to the potential heat of hydration also holds for the chemically bound water. The calculated potential amount of chemically bound water at complete hydration suffers from the inaccuracies in the clinker compound composition, on the one hand, and the inaccuracies inherent in mathematical methods for the determination of the amount of chemically bound water in a poly-mineral material, on the other. It was found, however, that the standard deviation calculated from randomly generated chemically bound water data, random in a similar sense as outlined in the preceding section with respect to the calculated heat of hydration data, is smaller than the standard deviation calculated from the heat of hydration data, viz. ≈2% relative to ≈7%. The conclusion seems to be justify that the calculated potential amount of chemically bound water is less susceptible to variations in the compound composition of the cement.

Hydration mechanisms
Hydration mechanisms of Portland cement have been investigated for the past hundred years or so, but are still not clearly understood [473]. Against the background of the great

differences in hydration features of individual constituents, the linearity between non-evaporable water content, liberated heat of hydration and surface area of the porous cement paste might be interpreted as supporting the concept of hydration at equal fractional rates. Also C/S ratios independent of the degree of hydration as observed by Odler et al. [431], Rodger's observation that the C/S ratio of inner and outer products in a mature paste do not differ and several observations showing a concentric inward growth of the reaction front in hydrating cement particles, can be interpreted as arguments in favour of the equal fractional rate concept. Adoption of the equal fractional rates concept, however, without making allowance for the evident differences in the rate of hydration of individual constituents would mean an unacceptable misjudgment of an extensive amount of experimental data which do indeed exhibit independent hydration features.

One step in view of "reconciliation" that what is in essence irreconcilable exists in the recognition that the degree of hydration is an *apparent*, *overall* or *global* value, representing a certain *average* of the degrees of hydration of the individual constituents. This, however, is no more than a first step and in fact no more than a matter of wording without doing anything to obviate the complications encountered in modelling. The adoption of an apparent degree of hydration has nevertheless the advantage that the definition of the degree of hydration as formulated with expression (3.7) still holds. A more substantial point of reconciliation would exist, in our opinion, in defining the *rate of penetration of a uniform reaction front in a cement particle as a function of the chemical composition of the cement.* This point will be covered in more detail in Chapters 6 and 8.

Degree of hydration

The degree of hydration, defined as the relative amount of cement that has reacted, can be approximated by, for example, either the degree of heat liberation or the relative amount of chemically combined water. While doing this one should be aware of two sources of error. Firstly, the format used for the determination of the maximum values of the heat of hydration or the amount of chemically bound water and, secondly, the methods used for the determination of the intermediate values of the heat of hydration or the chemically bound water. From preliminary accuracy considerations it seems justified to state that for the accuracy with which the degree of hydration can be determined a coefficient of variation of about 5% is applicable. The coefficient of variation allows for the effect of alkalies and other minor constituents which complicate the determination of both the maximum values of the heat of hydration and the chemically bound water, on the one hand, and for the limited accuracy with which intermediate values of the quantities observed can be determined. This coefficient of variation presupposes the application of one single format for the determination of the maximum and intermediate values of the parameters. When different calculation formats are used for the *maximum values* and different measuring methods for *intermediate values* for the quantities observed, the multi-method coefficient of variation will exceed 7.5%. *Systematic errors* in the degree of hydration in the order of 10% have to be considered in case different methods are used.

4 FORMATION OF MICROSTRUCTURE AND STRENGTH DEVELOPMENT
MORPHOLOGY-RELATED ASPECTS

4.1 General

During the hydration process the hydration products make mutual contacts and build up a three-dimensional network structure around the still hydrating anhydrous cores. On macro scale this process of structural formation is observed as the development of material properties like strength, hardness, stiffness and permeability. Some basic features of structural formation and strength development will be reviewed in this chapter. The relationship between microstructure and macro-properties has been studied for several decades already. Less explored is the interrelationship between structural formation and rate of hydration. As we will see in Chapter 5 the majority of kinetic models for cement hydration are based on detailed descriptions of the hydration processes which are supposed to occur in individually hydrating sphere-shaped particles. Any physical interaction between hydrating particles is generally not considered in these models. Disregarding the interaction between the hydrating particles implies that these models are, by definition, inadequate to describe the development of material properties, since these properties are closely connected with the increasing interaction between the hydrating particles. Moreover, the physico-geometrical interactions between hydrating particles might affect the progress of the hydration process itself to a considerable extent. Hence, disregarding these interactions may lead to misinterpretation of observed hydration phenomena.

The intensity of the particle interaction depends, among other things, on the particle size distribution of the cement and the w/c ratio. In other words, the interaction is stereologically determined. In this chapter the stereological aspect of hydration and structure formation will, therefore, be considered explicitly and not only for bulk paste, but also for the paste-aggregate interface.

4.2 Colloidal Aspects in the Early Period of Hydration

4.2.1 Stability of Colloidal Cement Dispersion Systems

In Chapter 2 it has been shown that the particle size of proprietary cements ranges from about 0.5 to 150 μm. In pastes manufactured with w/c ratios between 0.4 to 0.6, the mean distance between particles belonging to the same fraction is of the same order of magnitude. Indicative values of the initial centre-to-centre distances of the cement particles are shown in Fig. 4.1 (see also Section 5.5.2.2). The average interparticle spacing, or "hydraulic radius", ranges from 1 to 2 μm [617] (hydraulic radius = water volume divided by the total surface area of the cement). The small value of the hydraulic radius is predominantly caused by the small particle fractions, which fractions form the major part of the specific surface of the cement. On contact with water these small particles will soon dissolve completely, thus clearing the way for reaction products to grow in size beyond the

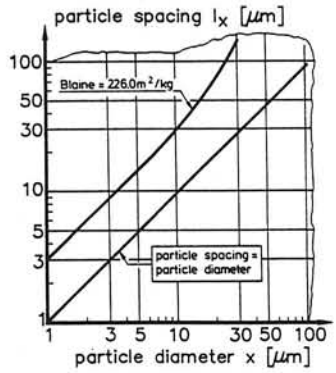

Fig. 4.1 Initial centre-to-centre distances of cement particles in a paste with w/c ratio ω_0=0.4 and a coarse cement, i.e. Blaine 226 m^2/kg (calculated after Section 5.5.2).

value of the initial hydraulic radius.

Characteristic sizes of reaction products range from 0.01 μm up to even 100 μm (see Section 4.3). A system of which the dimensions of the elementary particles have the indicated order of magnitude belongs to the family of colloidal systems [175]. In such colloidal systems the specific colloidal features like interparticle electrostatic repulsion and Van der Waals attraction have to be considered. Colloidal phenomena play a most important role in mature pastes [445,608,621]. For the present we are interested particularly in the effect colloidal repulsion and attraction forces might have on the particle spacing of the cement immediately after addition of water. The major reason for considering the initial colloidal phenomena refers to one of the main assumptions in the computer simulations presented in Chapter 6, i.e. the assumption of a homogeneous, stable dispersion of cement particles in the cement-water system as diagrammatically shown in Fig. 4.2a. Whether this assumption is justified will be examined in the next three Sections. Only the main conclusions of some preliminary investigations on this point will be presented.

4.2.1.1 Early Electrostatic Repulsion

On contact with water cement particles commence to dissolve. At first it is mainly the C_3A that reacts, soon followed by C_3S. Within a very short time, i.e. a few minutes at most, a saturated Ca^{++} solution is formed with an initial Ca^{++} concentration of 20 mmol/l and a corresponding OH^- concentration (Section 3.6). Although it is a simplification of reality, the paste can be considered as a system in which the cement particles have a resulting negative charge. Depending on the character of the electrolyte and the particle distance, electrostatic repulsion forces might be responsible for separation of the particles in this initial phase. Repulsion effects of any significance have to be expected if the particle spacing "s" is less than about four times the Debye-length k^{-1} [428]. The Debye-length is

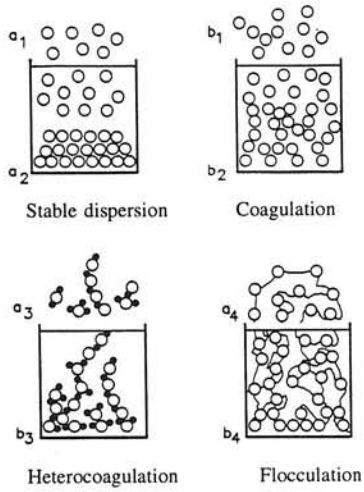

Fig. 4.2 States of colloidal dispersions ($a_{1,2,3,4}$) and settled volumes ($b_{1,2,3,4}$) [428,614].

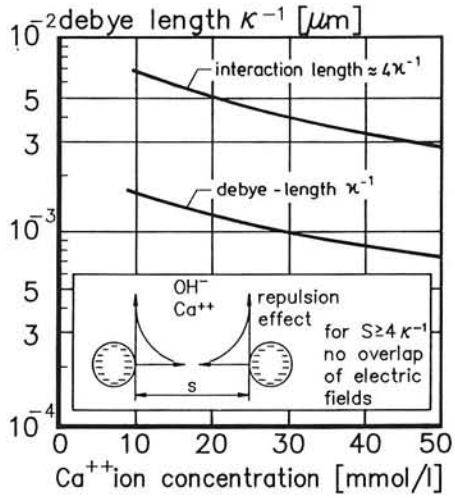

Fig. 4.3 Debye (interaction) length k^{-1} as a function of the Ca^{++} ion concentration.

the distance from the electrically charged surface over which the potential falls off with 1/e times its initial value.

In Fig. 4.3, generated on the basis of the formulae given by Frens [175], Ottewill [428] and Heinz [234], the Debye-length is expressed as a function of the calcium ion concentration. The minimum particle spacing $s=4/k^{-1}$ required for substantial repulsion effects is indicated as well. For an initial calcium concentration of 20 mmol/l repulsion effects have to be expected if the particle spacing becomes less than 50 Å (0.0050 μm). This is much less than the initial average particle spacing of about 1 to 2 μm. These preliminary investigations seem to indicate that electrostatic repulsion effects between cement particles will not be significant. A subsequent conclusion, actually associated with the previous one, could be that early expansion of a colloidal cement-water system can most probably not be attributed to these repulsion effects. For early volume expansion, see also Section 4.8.

4.2.1.2 Van der Waals Attraction

If solid particles approach each other Van der Waals attraction forces occur. The significance of Van der Waals forces in colloidal systems is generally expressed in terms of potential energy V_p according to [175,234,428]:

$$V_p = - A.r * (12.s)^{-1} \tag{4.1}$$

where V_p is the potential energy of interaction (attraction), A the Hamaker constant

(5.10^{-20} J), r the particle radius and s the particle spacing. The significance of early particle attraction was investigated for a cement-water system with a w/c ratio ω_0=0.4. It was found that immediately after addition of water to the cement the system could be considered as a *low energy system*, in which the interparticle attractive forces do not play a significant role.

4.2.1.3 Stereological Implications of Colloidal Considerations

Predominant repulsion forces would have been the precondition of a stable dispersion, whereas predominant attraction forces would have just caused significant flocculation of the cement particles. From the preliminary calculations presented in the foregoing no evidence for substantial effects of either repulsion or attraction forces could be deduced. The absence of analytical evidence for either important repulsion or attraction forces leads us to presume that in cement-water systems both dispersion-like and flocculation-like phenomena might be present. The literature on this point seem to bear out this presumption. A more or less stable dispersion has been considered by Shebl [535] and Steinour [555]. Several authors, however, have pointed to agglomeration of small particles and adherence of small particles to large particles [3,137,140,187,351,524]. Pommersheim [453] even suggests that it would be more accurate to use the particle size distribution of the flocculated particles in considerations on the effect of particle size effects on hydration kinetics.

Since the percentage of the small particles that coagulate or adhere to larger particles is relatively small, it is still assumed justified to ignore the effect of it on the initial spatial distribution of the cement particles. Positively stated, the cement particles will be assumed to be dispersed predominantly homogeneously in the system.

The question whether a homogeneous or a random distribution of the cement particles should be considered will be dealt with in more detail in Chapter 6. For the importance of colloidal effects on structural formation in later stages of the hydration process reference is made to Section 4.4.5.1.

4.3 Morphology of Hydration Products

4.3.1 Classification of Reaction Products

Hydration products are reported to look like fibres, needles, rosettes, rods, tubes, pherulitic particles, cigar- and tree-shaped particles, crumpled sheets or foils, tabulated structures, spicules, spins, acicular particles, prismatic crystals, globules, hemispheres and scales [59,81,137,280,315,581,632]. The shape and sizes of these particles depends on the chemical composition of the cement, the presence of gypsum and additives [30], the degree of hydration [278,339], the w/c ratio, the curing temperature and external pressure. With respect to their physico-chemical composition three main products are generally distinguished, viz.:

1. Ettringite (AFt);
2. Calcium silicate hydrates (CSH);
3. Calcium hydroxide (CH)

The formation of these products during the hydration process is diagrammatically shown in the well-known schematic presentation of Fig. 4.4.

4.3.1.1 Ettringite

Ettringite particles are generally found in the shape of needles with a length up to 10 μm and 0.25 μm in diameter [214,521]. In a supersulphated cement ettringite crystals of even 120 μm long and 2 to 3 μm thick have been observed [385]. Unlike CSH particles ettringite needles do not branch [137].

Whether ettringite is formed topochemically or by a through-solution mechanism is still a point of controversy. According to Schwiete et al. [521] ettringite is formed topochemically on the C_3A surfaces. Mehta [375], on the contrary, concludes from the observed crystal formation in originally water filled spaces that a through-solution mechanism must have been at work. An important factor in this context is the Ca^{++} concentration in the pore water. High lime concentration promotes the topochemical mechanism, whereas a low Ca^{++} concentration tends to result in a through-solution mechanism. Since the Ca^{++} concentration is not a constant but varies with elapse of the hydration process, both mechanisms are likely to occur but refer to different stages of the hydration process.

With lapse of time ettringite is converted into monosulphate (Fig. 4.4) [1]). The volume

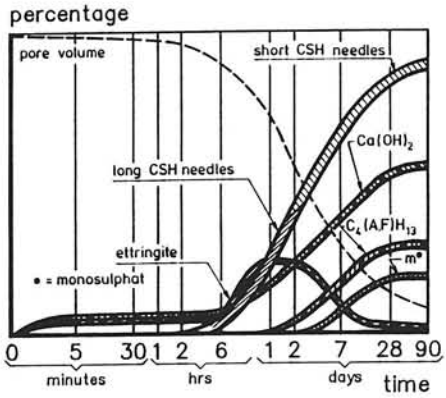

Fig. 4.4 Schematic presentation of the formation of individual hydration products [354].

[1]) The formation of monosulphate in present commercial cements could not be established by Kuzel [321]. This would jeopardize the conversion of ettringite into monosulphate to be the cause of changes in the strength as suggested by several authors.

occupied by monosulphate is about 2.5 times less than that of ettringite [274]. The volume changes associated with the conversion of ettringite into monosulphate (AFm) might somehow affect the strength of a paste (see Section 4.5.5).

4.3.1.2 Calcium Silicate Hydrates

The calcium silicate hydrates, or CSH gel, have a highly amorphous morphology. Several authors have assumed similarities between CSH gel and the natural minerals tobermorite and jennite [182,577]. Diamond [137] and Richartz et al. [490] have pointed out that identification of CSH gel with aforementioned minerals is strictly speaking not correct. Diamond alternatively distinguishes between four major morphological appearances of the CSHs [137,140]. His classification still holds quite well and is a good starting point for further considerations. The major features of this classification will briefly be summarized in the following (see also Fig. 4.5a-d; (with thanks for permission for reproducing the photos)).

Type I: elongated fibres
Elongated fibres, 0.5 - 2 μm long, 0.2 μm across. Some are hollow [490] but most of them are solid [137,140].

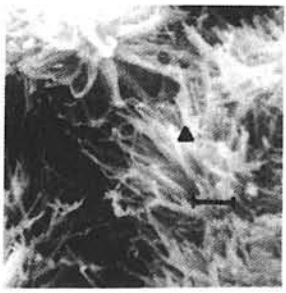

Fig. 4.5a "Type I" CSH gel structure.
SEM: pcp, ω_0=0.6, t=185d, T=40°C [137].

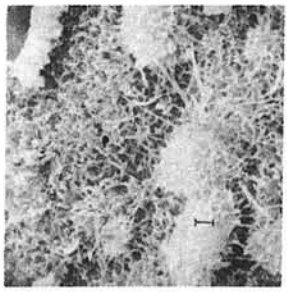

Fig. 4.5b "Type II" CSH gel structure.
SEM: pcm, ω_0=0.6, t=14d, T=24°C [137].

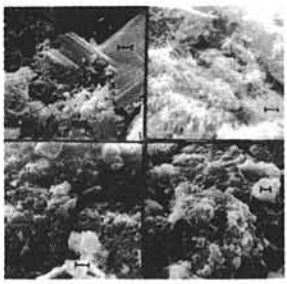

Fig. 4.5c Type III CSH gel structure.
SEM: various pcp [137].

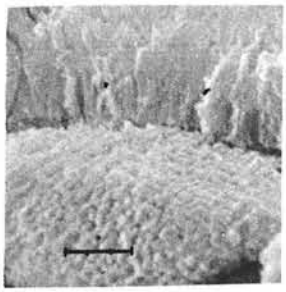

Fig. 4.5d Type IV CSH gel structure.
SEM: pcp, ω_0=0.6, t=2d, T=60°C [137].

Type II: reticular network
Interlocking structure of "honeycomb morphology". Unlike Type I particles and ettringite needles, the Type II particles branch every half micrometer or so. Thus a continuous interconnected reticular network is formed in three directions. Similar morphological appearances were found by Lawrence et al. [331].

In addition to Diamond's classification Barnes [25] also considered a product which he indicated as Type IIA particles: equant grains with typical dimensions of about 0.5 μm. This product also shows similarities with Diamond's Type III product.

Type III: Equant grains
Equi-dimensional particles, i.e. particles with equal dimensions in all directions. The irregular equant or flattened particles would have a characteristic size of no more than 0.3 μm across. Some sub-particles tend to be rather well rounded and are close to being equant.

Type IV: Inner product
A product with either regular pores or close packed equant grains. The grain size (or pore separation) is typically about 0.1 μm. *Assemblages* of CSH particles may reach sizes ranging from several tens to hundreds of microns. Assemblages of this size thus appear to have the same order of magnitude as the original cement particles.

According to Budnikov et al. [81] the primary structural element of the gel is an amorphous *globular* particle. Acicular and generally elongated new formations would only play a subsidiary role. They were assumed to result from disintegration of samples. Sphere shaped reaction products have already been considered by Bogue [59], and later by a number of other researchers [42,81,366,559].

4.3.1.3 Calcium Hydroxide Crystals

Calcium hydroxide, about 10% to 20% of the gel [137,642], is generally found in crystalline form. An amorphous, poorly crystalline nature of CH particles has been reported as well [81,150,213,317]. When CH is deposited in empty spaces, well-built crystals are formed. In the vicinity of aggregate surfaces, however, the morphological characteristics of CH can be very complex [137].

CH crystals can develop into particles with sizes several orders of magnitude larger than CSH particles. Crystal sizes up to 100 μm and even 1,000 μm have been mentioned [137, 637], so substantially exceeding the mean size of CSH particles and of the original anhydrous cement grains.

4.3.1.4 Stoichiometry of the Physical Composition of Hydration Products

In a more or less mature paste reaction, products can be regarded as "solid solutions" of CSH and CH [101]. These *fused* reaction products are generally assumed to have constant

stoichiometric physical composition, i.e. a constant morphological appearance. Particularly at later stages the reaction products are considered to be almost identical [120]. In this respect also El-Jazairi's observations that hydration products are produced in very much the same relative proportions at all stages of the hydration process and also over a wide range of w/c ratios are worthy of note [151]. His observations are in agreement with, at any rate not in contradiction with, Powers' concept of a constant density of the gel [462].

It is emphasized here that the concept of a constant morphological appearance of the reaction products, and this in combination with a constant relative proportion in which the reaction products are formed in subsequent stages of the hydration process, is of great significance in view of mathematical modelling of both the diffusion controlled stage of the hydration process and structure development!

4.3.2 Factors Affecting Morphology

Temperature

In 1982 it was Roy [507] who observed a ring-wise variation in the character of the reactions products in a 10 year old C_3S-paste. These rings were interpreted as: *"annual rings, which may represent higher rates of hydration during summer than during winter season"*. Though the remarkable interpretation of the observed phenomena might be questionable, it is quite obvious from this and other observations, that the reaction temperature influences the morphology of the reaction products. And this can again affect the structural and physical properties of the cement paste [41,61,297,299,418].

According to Ludwig et al. [356] hydration at elevated temperatures results in an *increase* of the size of the hydration products. It was suggested that the increase in size of the formed crystals is proportional to the increase in curing temperature. Ludwig's observations are in agreement with those of Bernal et al. [47]. Similar observations have been reported by Regourd et al. [482]. CSH particles formed at 200°C were shorter and more intensively merged than particles formed at 80°C. According to Mori et al. [396], investigating temperature effects on hydration of C_3A-gypsum pastes, ettringite crystals formed at low temperatures were finer and formed a more compact coating around the anhydrous particles compared with ettringite formed at higher temperatures.

In contrast with these observations are those of Richartz et al. [490], Locher [349], and Walz et al. [610], who found that curing at low temperatures resulted in more well-developed and larger reaction products. Long, defect-free crystals formed at low temperatures have also been reported by Keil [288]. High temperatures, on the contrary, would result in a more coarse crystal structure.

Water/Cement and Water/Solid Ratio

The higher the water/cement ratio the more space is available for reaction products to grow undisturbedly. Particularly in the early stage of hydration when ettringite needles are formed, the available space determines the morphology of the reaction products [220,375]. In a water-rich C_3A + gypsum system long, slender ettringite particles up to 100 μm have been observed, whereas at low w/c ratios short prismatic crystals were found, 1 μm long

and 0.25 μm thick [375].

It is also possible that differences in the pore water composition, resulting from differences in the w/c ratio, affect the morphological appearance of the reaction products. In the previously cited sources, however, the morphological differences of the hydration products were more or less exclusively related to differences in spatial constraints at different water/cement ratios.

Foregoing observations can be considered to be more or less representative of the effect of the w/c ratio on the morphology of hydration products of ordinary cements, particularly of the CH crystals.

Effect of Gypsum

The morphology of pure C_3S gel can be described by a fibrous structure of rolled sheets, while in the presence of gypsum small platelets are predominant [115]. Morphological changes occur when the SO_3 content exceeds 2%. An increase of the gypsum content results in a decrease of the average length of the ettringite needles from 0.5 μm to 0.1 μm [357]. Menetrier et al. observed little effect due to the gypsum on the reaction products in the early phase of hydration, and at later stages no significant effect was found [382]. Only a minor effect of gypsum on the morphology of reaction products has been reported by Ciach et al. [102].

Additives/Admixtures

According to Ciach et al. [102] admixtures do not significantly influence the final morphology of cement pastes. Odler et al. [412] and Khalil et al. [292], who investigated the effect of lignosulphate and CLS admixtures, did not observe noticeable changes in the morphology of hydration products either. For certain admixtures modifications of the outermost CSH gel growing into the capillary pore space has been found [632]. Some retarders would result in a more open porosity of the structure built up by the reaction products [523].

4.3.3 Morphology - Miscellaneous

4.3.3.1 Average and Minimum Sizes of Gel Particles

Since the CSHs form the major proportion of the gel, it can be reasonably assumed that the average sizes of the reaction products is dominated by the CSH-particle size. For the order of magnitude of particle sizes formed by hydration of both Portland cement and blast furnace cement Dorner et al. [143] gives 0.01 μm, whereas Richartz et al. [490] and Grudemo [215] have mentioned CSH particle sizes ranging from 0.002 to 0.1 μm. CSHs with an average length of 1 μm have been reported as well [81]. Powers [465] has mentioned an average size of gel products of 0.01 to 0.015 μm. A particle size of 0.001 to 0.002 μm can be considered as an absolute minimum. Characteristic sizes of CH crystals vary from 10 μm to 1 mm, whereas the calcium aluminate crystals range from 1 to 10 μm

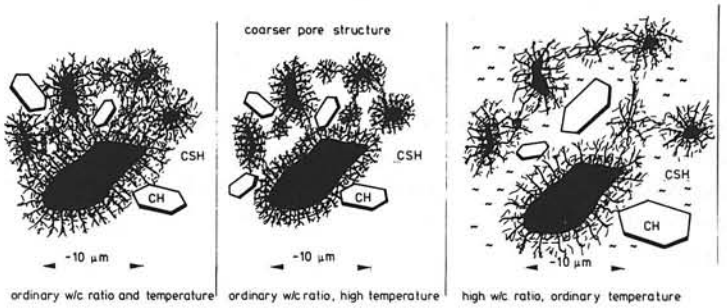

Fig. 4.6 Morphological features and formation of structure: schematic representation. Effect of w/c ratio and curing temperature.

[637]. A schematic representation of the morphological features, including the effects of water/cement ratio and curing temperature, is given in Fig. 4.6.

4.3.3.2 Morphological Stability

With lapse of time, hydration products tend to convert into products with a different morphological appearance. The transformation from ettringite into monosulphate has been mentioned in Section 4.3.1.1 (see also Section 4.3.1.1, footnote [1])). Crystallization of CH and polymerization of CSH has been reported to occur over a period of at least 15 years [81,150,217,317,367,526]. With the exception of the ettringite-monosulphate conversion, the time dependent morphological changes can be assumed not to play a significant role in the first 28 days of hydration; the period in which about 80% of the ultimate degree of hydration is reached. Since we are mainly interested in the early mechanisms of structural formation in this study, these time dependent transformations in mature pastes will be further disregarded.

4.4 Formation of Structure

4.4.1 Formation of Basic Skeleton

Geometrical and Morphological Aspects

A schematic representation of the formation of structure as proposed by Locher et al. [354] is shown in Fig. 4.7. Reaction products formed at the surface of cement particles in the early stage of hydration generally consist of very small needles (ettringite) of 0.25 by 0.05 µm (Fig. 4.7a). After one hour of hydration these needles have developed to a size of 1 by 0.1 µm [521]. In subsequent stages of the hydration process ettringite needles may continue to grow and reach a length of 2 to 3 µm [214] and even up to 10 µm [637].

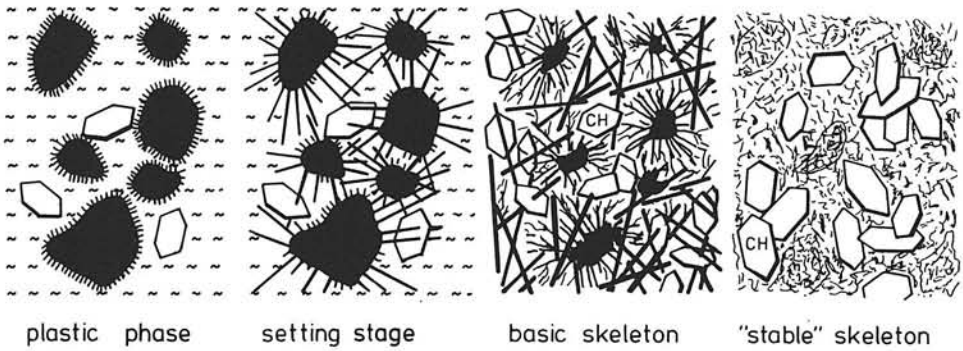

Fig. 4.7 Formation of reaction products and build-up of structure (after Locher [354]).

While growing they gradually bridge the interparticle distances of about 1 to 2 μm, forming a spatial network (Fig. 4.7b). With the formation of this network the position of the cement particles in the cement/water system is established.

In the early stage of the hydration process the formation of clusters of needle-like particles has been observed [113]. Probably the rapid dissolution of small particles - particles up to about 2 μm - allow for this clustering to a great extent. As the hydration process progresses these clusters interlock and grow together. Meanwhile CSH particles are formed radiating out from active centres into the water filled pores, building up an increasingly dense, three dimensional network [490,618]. The characteristic fibril size of the CSHs in this stage of the reaction process is about 1 μm in length with a diameter of 0.01 μm. Plate-shaped CSH particles would have sizes of the same order of magnitude [81]. CH crystals are formed mainly in empty spaces and can develop into very large particles which envelop the hydrating cement particles [124].

The basic skeleton is formed between 7 and 28 days [102,405] (Fig. 4.7c). As the hydration process further progresses the reaction products hardly grow in size, but new particles are formed, similar in size to those formed earlier [110,120,462]. These new products settle in the empty space within the spatial network originally built up by the ettringite needles [102] (Fig. 4.7c,d).

Hadley Grains

Worthy of note, but hard to take into account in a mathematical model is the formation of "Hadley grains": hollow shells of reaction products, obviously formed as the result of a relatively rapid dissolution of the anhydrous core and subsequent outward diffusion of the ions into the solution [28,226,468,633] (see also Fig. 4.8a). The formation of Hadley grains is a phenomenon typical of cement hydration. For compound hydration it has not been observed so far [269]. Scrivener and Pratt observed the formation of monosulphate inside Hadley grains, which at least make us aware to the most complex mechanisms and processes that are operative during hydration [525].

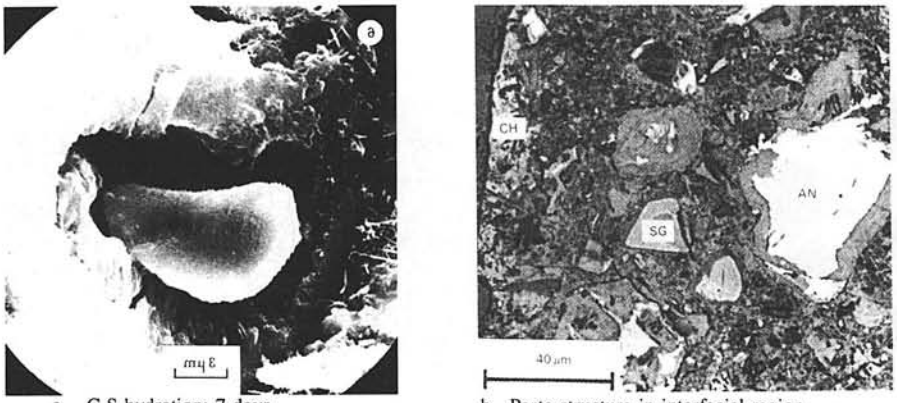

a. C_3S hydration: 7 days

b. Paste structure in interfacial region

Fig. 4.8 Shape of partly hydrated C_3S (7 days, [469]) and of cement particles [527]. AN = anhydrous cement. SG = slag.

4.4.2 Inner and Outer Product

Probably Taplin [569] was the first who introduced the concept of inner and outer product. The outer product, formed outside the original grain boundaries, would be less dense than the inner product formed inside these boundaries. A difference in density of inner and outer product particularly holds in the early phase of hydration. During the hydration process this difference gradually vanishes due to volume constraints and associated merging of the outer product of expanding particles [123,205]. This merging effect might be the reason why a distinct boundary between inner and outer product is not always observed, and at any rate is hard to distinguish [140,331].

With regard to the mechanism according to which the outer and inner product is formed it seems evident that outer product is formed by a through-solution mechanism, whereas inner product is formed topochemically.

According to Daimon [125] the transformation of anhydrous C_3S grains into CSH gel occurs without a change in the shape of the grain. This statement can be substantiated by many photos of partly hydrated grains (Fig. 4.8). The statement does not hold for particles smaller than about 3 µm. These particles completely dissolve [318,526] and only form an outer product which precipitates at the surface of large particles [618]. Preservation of the particle shape has also been observed in the case of hydrating cement particles [140].

4.4.3 Gel Characteristics

4.4.3.1 Gel Porosity

The hydration products with an average particle size of 0.002 to 0.100 µm build up a porous matrix with a minimum pore size of about 0.002 µm. This minimum pore size

follows from the minimum space needed for nucleation and crystal growth [462,386]. Wider pores are considered to be "unstable", since in these pores new hydration products can be formed [462]. The porous matrix built up by the hydration products, including the pore water, is termed "gel". The solid structure of hydration product, i.e. the structure that remains after removal of the water from the gel pores, is called the *xerogel* [25,622].

Powers et al. [462] have assumed the minimum pore size of 0.002 μm to be characteristic for the gel. In good agreement with this value Neville [400] gives characteristic sizes of the gel pores from 0.0015 to 0.002 μm. According to Richartz et al. [490] and Diamond [137] the size of the gel pores would depend on the particle size distribution of the cement, the initial w/c ratio and the presence of external pressure. Young et al. [637] considered it plausible that the micro-porosity of the CSH gel decreases with increase of the degree of hydration. Due to all these factors the gel pores would range from 0.002 to 0.1 μm, i.e. sizes similar to those of the average gel particles.

The gel porosity is assumed to be fairly constant throughout the hydration process and is generally estimated at about 28% [226,462]. The concept of a constant and characteristic gel porosity is in harmony with the assumed constant geometrical stoichiometric appearance of hydration products [110].

4.4.3.2 Specific Surface of Gel

The assumption of a constant gel porosity and a constant geometrical stoichiometric appearance of hydration products is further substantiated by the observation that the specific surface of the gel is fairly constant throughout the hydration process [462]. The measured absolute value of the specific surface strongly depends, however, on the measurement method [604]. Specific surfaces are reported from 150...300 m^2/g for D-dried samples [35, 558] to up to 1000 m^2/g for cement paste in a saturated condition [35,137]. The decrease of the specific surface as found in pre-dried samples must be attributed to coarsening of the structure due to the collapse of pores [137,164,532,624] Curing at elevated temperatures results in a decrease of the specific surface [418,420].

4.4.3.3 Gel Density

The ratio of the volume of the expanded porous gel relative to that of the original cement values has been reported to range from 2.06 to 2.20 [35,400,462,558]. For a specific weight of the unhydrated cement of ρ_{ce}=3.1 g/cm^3, a w/c ratio for complete hydration of cement of 0.4 and an increase of the volume of the gel relative to that of the unhydrated cement as just indicated, the gel density can be computed at 2.07 to 1.97 g/cm^2. In these calculations it is assumed that the density of the inner and outer product is identical. In view of the mechanisms according to which these two types of product are formed it is questionable whether this assumption is correct. The concept of a characteristic and constant porosity of gel, however, indeed sustains the assumption of a constant gel density. Granju et al. [205] do not distinguish between inner and outer product either. He states

that the major part of the gel, outside as well as inside the boundaries of the initial anhydrous grains, is made from dense gel.

The measured gel density tends to be somewhat higher than the calculated densities. This difference, as well as the scatter in density measurements, can largely be traced back to differences in the way in which the free capillary water is removed from the sample [161,309]. Moreover, the w/c ratio, the degree of hydration, temperature, external pressure and the amount of gypsum affect the gel density.

Effect of Water/Cement Ratio, i.e. "Initial Porosity"

The gel density is found to increase with decreasing w/c ratio [162,227,487] (see also Table 4.1). Hydration under pressure in low porosity pastes could allow for this [545]. The solid density of the hydration product, on the contrary, was found to increase with an increase in the w/c ratio [227].

Effect of degree of hydration

As the hydration process progresses the gel density has been found to increase [204,487, 495,545]. Soroka et al. [545] assume that a similar mechanism occurs here as in the case of low porosity pastes, i.e. hydration under pressure due to spatial constraints.

Effect of gypsum

Some contradictory results on the effect of SO_3 on the gel density have been reported by Soroka [546,547]. Experimental work carried out in 1986 did not reveal any effect of the SO_3 content on the gel density. Earlier data [546], suggesting that gypsum would influence the quality of the gel due to an effect on the density, were not confirmed by these later tests.

Table 4.1 Gel density data according to different authors.

Author	ref.	wcr	gel density [g/cm^3]		Comment
			C_3S	pcp	
Powers et al.	[462]	0.4	1.97		ρ_{ce}=3.1 g/cm^3
Koster et al.	[309]	0.3-0.8	2.65-2.15		paste
Feldmann	[159]		0.5-0.8	2.44-2.25	paste; dried at RH=11%
		0.5-0.8	2.25-2.25		paste; D-dried samples
		5.0	2.38-2.30		bottle hydrated
Hansen et al.	[228]	0.4-0.75		2.34-2.28	paste
Young et al.	[635]	0.4	2.39		RH = 0%
		0.4	2.18		RH = 11%
Young et al.	[637]		2.15		*Ibid. Hansen [228]*
Soroka et al.	[545]			2.14-2.34	initial porosity variable

4.4.4 Paste Characteristics

4.4.4.1 General

Foregoing considerations concerning gel characteristics will be extended now with a survey of paste characteristics. Particular attention will be given to the porosity of the paste, since a large number of engineering properties of cement-based materials have appeared to be closely related to this parameter [129]. Progress in modelling of the performance of cement-based materials is, in turn, likely to be closely linked to a better understanding of the formation of the pore structure and of the pore structure itself [437].

4.4.4.2 Porosity and Pore Size Distribution

The pore volume V_{por} [cm^3/g] is generally defined as the initial paste volume minus the volume of solid material, i.e. the total volume of remaining anhydrous cement grains and the xerogel. The non-evaporable water Wn is considered as part of the solid mass. Porosity P [cm^3/cm^3] is defined as the ratio between pore volume V_{por} and initial paste volume V_{pa}.

The pore system in cement paste consists of pores in the range of 10...20 Å to 10^7 Å. Several authors assume a continuous pore size distribution [307,386,490]. Furthermore, there is a good general agreement concerning a subdivision into different classes of pores,

Table 4.2 Classification of pores - schematic representation / nomenclature.

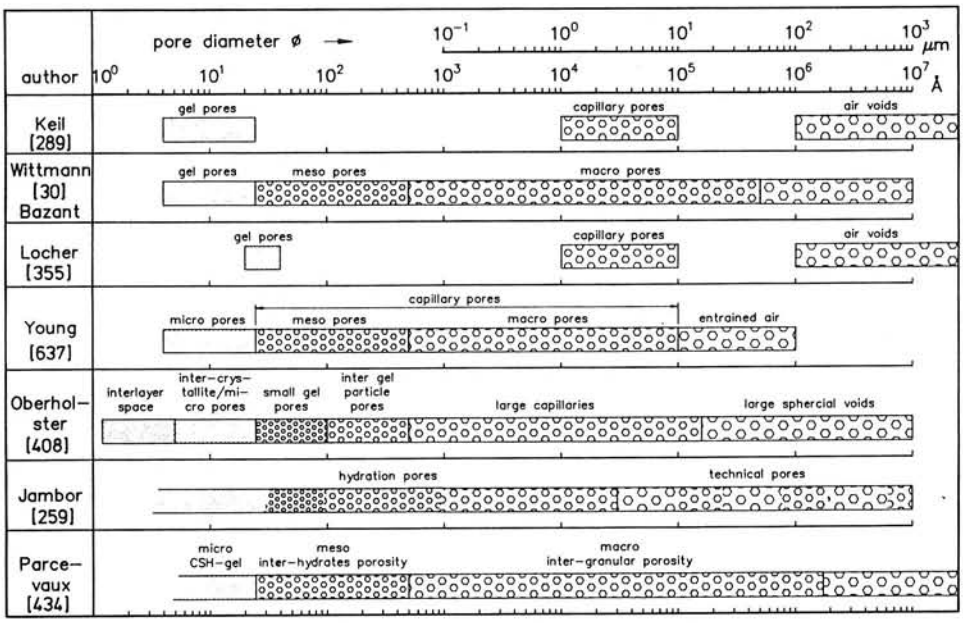

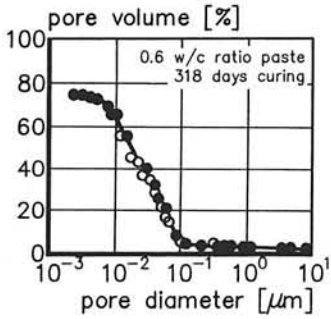

Fig. 4.9 Pore size distribution of cement paste; a typical curve [136].

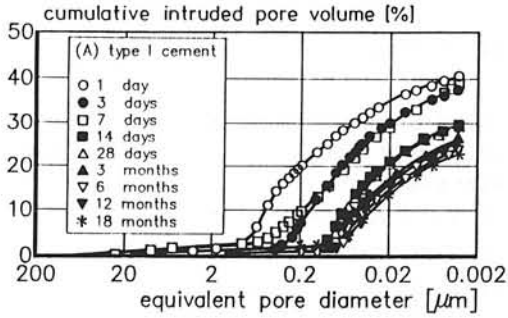

Fig. 4.10 Pore size distribution: Effect of degree of hydration [163].

viz. *gel pores, capillary pores* and *air voids*. The range of pore sizes characteristic for different pore classes as proposed by different authors is given schematically in Table 4.2. A typical pore size distribution of a cement paste is shown in Fig. 4.9.

It has been emphasized by several authors that all methods for the determination of the porosity and the pore size distribution suffer from different kinds of experimental difficulties [100,129,291,405,532,624]. High pressure mercury intrusion, for example, would significantly damage and coarsen the pore structure [164]. Also the manner of water removal has turned out to influence the measured porosity considerably [129,254,503]. Simplifications in the interpretation of experimental data, for example the assumption of cylindrical pore shapes instead of irregular shapes [522,637], results in the need for caution with respect to porosity measurement.

In order to avoid these experimental difficulties it has been suggested to refrain from these methods and concentrate on consistent *mathematical procedures* for the determination of *porosity* [274]. Such procedures, however, will fail as soon as information about the pore size *distribution* is required. These mathematical procedures, therefore, give only limited solace. In view of the experimental difficulties, simplifications and associated interpretation problems it must be emphasized that pore size distributions, however derived, should be considered as *comparative* rather than *absolute* [253,316].

4.4.4.3 Factors Affecting Porosity and Pore Size Distribution

According to Diamond [137] porosity and the pore size distribution are not intrinsic features of hydration products. Both are functions of w/c ratio and degree of hydration and are strongly influenced by application of pressure. Curing conditions and cement composition influence the porosity and pore size distribution as well. For the effect of pressure on the pore structure reference is made to the literature [19,316]. The effects of degree of hydration, w/c ratio, temperature, cement composition and particle size distribution will be reviewed in the following.

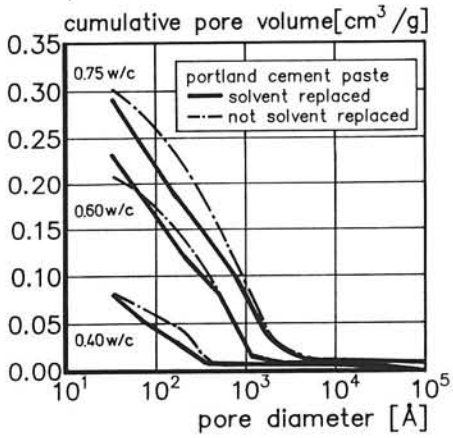

Fig. 4.11 Effect of w/c ratio on the pore size distribution and pore volume (Hansen [228]). MIP-measurements.

Degree of Hydration

As the hydration process progresses the total porosity of cement paste decreases [129]. A general trend is that the volume of the large pores significantly decreases, whereas the proportional amount of the small pores (<100 Å) dramatically increases [537]. The reduction of the volume of large pores is predominant in the early stage of hydration [109]. An increase of the volume of the small pores, i.e. in the range <37...500 Å, was not found by Shi-Ping et al. [537]. His observations might be in agreement with those of Mehta et al. [376], who explain that, at first, hydration products are formed in larger pores (>1320 Å) and later on in the smaller ones, thus leaving - in the first instance - the volume of the small pores more or less constant. Once the larger spaces, i.e. voids >1320 Å, are filled, further hydration would affect the entire pore size distribution. A similar mechanism for pore size reduction during the hydration process has been postulated by Parrott et al. [436].

A representative picture of the effect of hydration on the pore size distribution is shown in Fig. 4.10. It shows that the shape of the curves remains fairly constant. According to Parcevaux this is applicable *regardless* of the curing conditions and stage of hydration process. Similar results were obtained by Efes [147], Whiting et al. [614], Fraay [172] and many others. As will be discussed in Chapter 6, the approximately constant slope of the pore size distribution substantially simplifies mathematical modelling of the effect of changes in the porosity on the rate of hydration.

Water/Cement Ratio

According to Odler et al. [411] a high w/c ratio results in a higher volume of *all* pore groups, whereas only a slight effect on the distribution of the volume of pores in different

sizes occurs. Insofar as there *is* an effect, one should reckon with a proportional increase in the volume of the smaller pores with decreasing w/c ratio [169,595]. An increase of the w/c ratio would result in an increase of the portion of the larger pores [316,595], i.e. an increase of the mean pore size [537]. The effect of the w/c ratio on the pore size distribution is illustrated in Fig. 4.11.

Temperature

For relatively low w/c ratio pastes and temperatures up to 60°C there is only a minor effect of the temperature on the pore structure [401,507]. For C_3S/C_2S blends with ω_0=0.4 Bentur et al. [41] found an increase of the macro porosity and a decrease of the meso and micro porosity without any change in total porosity for a temperature increase from 25°C to 65°C. Trettin et al. [595], on the contrary, reports on an increase of the pore volume with pores <20 Å.

According to Odler et al. [420] an increase of the temperature would yield a narrower pore size distribution, i.e. a decrease of the portion of both small and large pores, while at the same time the position of the maximum of the distribution curve changed only insignificantly. Curing at low temperatures would result in an increase of the width of the pores [41].

Cement Composition

Effects of the type of cement on the pore structure have been reported by Uchikawa [598] and Lach et al. [322]. The latter author even states that the chemical and mineralogical composition and the fineness of the cement influence the initial porosity more than the time of curing. According to Berger et al. [44] C_2S pastes tend to a higher capillary porosity than C_3S pastes, while the porosity of a C_2S/C_3S blend was found to range somewhere in between. Berger suggests that this observation could be explained by the fact that more of the CSH particles in C_2S are loosely packed outer products which would increase the volume of meso pores at the expense of micro pores. The capillary porosity of Portland cement paste tends to be smaller than that of pure compounds, especially at high degrees of hydration.

Particle Size Distribution of Cement. Addition of Ultra Fines

With increasing fineness of the cement the volume of smaller pores increases [322,595]. Maybe more important than the *fineness* of the cement is the packing of the cement. With denser packing the pore volume decreases [391].

Addition of silica fume (SF) (particle diameter 0.1...1.0 μm) results in a denser paste, a reduction of the volume of large pores and hence a reduction of the average pore size [3,190,365,391]. The reduction of the pore size and densification of the paste can partly be traced back to a denser packing of the particles [328,527]. The fact that SF acts as nucleation centres in the water-rich spaces left by the cement particles is probably a more important factor in this respect.

4.4.5 Aspects of Structural Formation and Strength Development in Pastes

4.4.5.1 Physico-Chemical Aspects

In the foregoing some morphological and geometrical aspects of structural formation in gel and pastes were considered. This Section deals with some basic ideas with respect to mechanisms which actually cause the strength of the structure.

Immediately after mixing with water the cement particle spacing is generally so large that Van der Waals attractive forces which might bind the cement particles together are negligibly small as far as structural formation is concerned (see Section 4.2). With the dramatic decrease of the average size of the gel particles relative to the original cement particles and the associated increase in specific surface of the gel, the Van der Waals forces can no longer be ignored. Van der Waals attraction between the colloidal gel particles are of predominant importance in Michaelis' concept of strength development [384]. Wittmann [622] has mentioned Ernsberger and France to have been the first who have experimentally showed colloidal effects to occur in cement paste in 1945. The role of colloidal effects and Van der Waals forces, or *secondary bonds*, have since then been considered by many authors [445,467,548,621]. Secondary bonds can be considered as one of the corner stones of the "Munich model" [523]. According to Beaudion et al. [32] secondary bonds play a predominant role in strength considerations.

Besides these secondary bonds, *primary* or *chemical bonds* have to be considered [288, 445,462,637]. Some authors hold the view that chemical bonds are of primary importance for strength development [157,163]. Wittmann [622] assumes that primary and secondary bonds both contribute to the mutual coupling of gel particles for fifty percent each.

The possible contribution to strength of primary bonds has been thoroughly investigated by Chatterji [98,99]. He tried to calculate the probability of chemical bonds of randomly growing crystals. Chatterji concluded that chemical bonding could only play a minor role in the structure of a cement paste. Inspired by ideas of Mills, Kawamura carried out similar statistical evaluations [283,388]. Kawamura came to the qualitative conclusion that strength depends on the number of gel particles which are not in contact with others.

Some of the presuppositions of Chatterji's probabilistic approach as well as his conclusions have been criticized by Diamond [139]. In line with Diamonds reservedness with respect to the statement that chemical bonds would play a minor role Budnikov astutely noted that if *only* adhesion plays a role it would be difficult to explain the high water resistance of cement-based materials [81].

After having discussed Chatterji's work and that of many others, Diamond concludes that in the present state of knowledge not much reliable or even useful information concerning the bonds between particles has been acquired [139]. In similar words Pancrazi et al. [431] stated that the precise nature of the interparticle bonds is still in a stage of hypothesis. As long as the true nature of the atomic arrangements of CSH gel is still an open question and quantification of the relative contributions of primary and secondary bonds to strength seems to be beyond what is possible at the moment, one shall have to revert to *models* with which reality is approximated in a qualitatively reasonable and mathematically workable way.

4.4.5.2 Development of Microstructure and Strength. Stereological Aspect

Several authors have circumvented the fundamental question of which type of bonds between gel particles exist or dominate and have concentrated on the *number of contact points* and the *magnitude of contact surfaces* between hydrating particles rather than on the chemical or physical nature of the bonds [107,204,331,346,449,485]. Assuming the nature of interparticle bonds to remain the same throughout the hydration process - which is not more than a working hypothesis - this approach is certainly very attractive in view of mathematical modelling. This basically stereological approach becomes even more attractive if we adopt the "unstable pore concept" as proposed by Powers et al. [462]. From this concept Cranju et al. [205] concluded to a regular concentric outward growth of hydrating cement particles. Thinking along a scenario of expanding particles, structural formation can be considered as a mechanism of increasingly intensive interference between growing particles.

It is not only unsolved difficulties of a physico-chemical nature as discussed in Section 4.4.5.1 which pushes research towards a more stereology-oriented approach. The evident effect of the particle size distribution on structural formation - i.e. of the spatial position of hydrating particles and hydration products relative to each other - also calls for increased attention to stereological considerations [490,594]. Henk [239] even states explicitly that strength development is, in essence, a geometrical problem. His statement can easily be substantiated by referring to the strength development of low porosity pastes. The fact that in these pastes high strength values are reached at relatively low degrees of hydration can be attributed to a great extent to the initial dense packing of the cement particles which results in only small amounts of gel being required for "gluing" the hydrating particles together [47,355,505].

Another reason why stereological considerations must be given due attention refers to observations concerning fracture surfaces in hardening pastes. These surfaces show that with increasing degree of hydration the fracture path changes from predominantly *interparticle* to predominantly *transparticle* (Fig. 4.12). This change takes place between 7 and 14 days, depending on the initial w/c ratio [43,107,123]. Young and Berger [43] observed

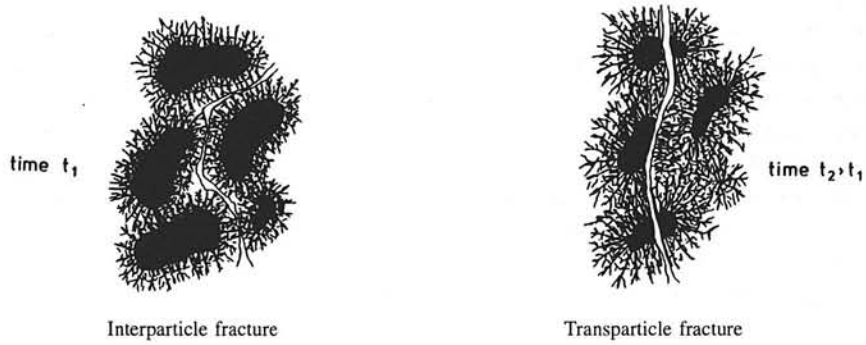

Fig. 4.12 Schematic representation of change of fracture mode from interparticle to transparticle during the hydration process.

a change of the fracture mode at a degree of hydration of about 40 to 50%. These observations are conceivable against the background of the increasingly intensive merging of hydration products on the gradually growing contact surfaces. At first, when only few contact points between expanding particles are formed, the interparticle fracture mode will require least energy. At later stages, when large contact surfaces are formed, the strength of the gel may exceed the strength at either the interface between the gel and the anhydrous core of the hydrating cement particle or, in the case of the formation of Hadley grains, the strength of the gel in a sphere-shaped shell around the anhydrous core. The latter fracture mode is illustrated in Fig. 4.12. In Chapter 7 this topic will be addressed again when discussing the potential of HYMOSTRUC to simulate the change of fracture mode quantitatively.

The emphasis on the stereological aspect of both structural formation and strength development does not suggest that physico-chemical aspects are of minor importance. The stereology-oriented approach, however, is assumed to be capable, in essence, to explain many phenomena with respect to the effect of particle size distribution and water/cement ratio on structural formation and strength development which cannot be explained merely from physico-chemical considerations. Moreover, explicit modelling of contact surfaces as envisaged in a stereological approach is assumed also to enable mathematical modelling of the influence of the geometrical interference of hydrating particles on the rate of hydration.

4.5 Paste Strength and Influencing Factors

4.5.1 General

It is a matter of fact that much research on strength development in hydrating pastes has been done in the absence of a satisfactory theoretical basis of the strength producing mechanisms [445,605]. The predominantly phenomenological approach has nevertheless provided us with an extensive file of experimental data with respect to the effect of several parameters on strength development and ultimate strength of cement paste, mortars and concrete. This data can serve as a most valuable reference to which more fundamental strength and simulation models can be tuned.

Parameters which have revealed to be of predominant importance for strength development are largely the same as those which affect the pore structure of the cement paste discussed in Section 4.4.4.3. The main conclusions of past investigations on these parameters are summarized in the following Sections.

4.5.2 Cement Fineness and Particle Size Distribution

A huge file of data on the effect of the fineness and particle size distribution of the cement on strength development and ultimate strength was generated in the thirties [201,217, 235,476,629]. One of the major topics in those days was the efficiency of different types

of cement mills, i.e. the optimum ratio between potential strength of the cement, on the one hand, and the required energy to grind the cement to its optimum fineness, on the other [16,35,245,399]. More recently this optimum is investigated in view of ecological considerations [103].

Already in the early thirties it was found that the often assumed correlation between the specific surface SS of the cement and produced strength did not hold satisfactorily [173, 318]. The poor correlation between the specific surface and strength has since then been confirmed by many authors [245,404,427,492,540]. A better correlation exists between strength and the *mean particle size* of the cement [399]. Most promising, however, are those studies in which the whole particle size distribution is considered. From a large number of studies on the correlation between strength and particle size distribution the main conclusions are as follows.

* Particles in the range from 5...30 μm produce the highest strength. Hraste [247] refers to 17 authors to substantiate this conclusion. Particles larger than 50...60 μm are irrelevant in view of early strength and have been considered merely as expensive aggregates [494,629]. A certain percentage of particles >30 μm might nevertheless be efficient for reaching a high ultimate strength [448] [2]). Even particles >63 μm have been mentioned to have a distinct function in view of strength development [285]. The fractions with particles from 10...25 μm, however, are undeniably most effective and have, therefore, been termed "Fleur du Ciment" [576].
* A steep slope of the particle size distribution generally entails higher strength in the *intermediate* stages of the hydration process, the specific surface being the same [34,103, 320,353,448].
* According to Locher et al. [352] the particle fractions <3 μm are important for high early strength, whereas for high 28-day and high ultimate strength the fractions 3...9 μm and higher are more important. A similar trend has been found by Venaut [600], according to whom the fraction 5...7 μm was responsible for high 1-2 day strength, 20...25 μm for the 7 day strength and 25...30 μm for optimum 28 day strength. Particles >40 μm only contributed to the strength after several years. The 28 day strength would benefit most from the fractions 5...10 μm and 10...30 μm [247].
* The highest *ultimate strength* is obtained using a cement with a wide particle size distribution, a low amount of fine particles and a low w/c ratio [318,605].

It has been pointed out by several authors that the effect of the particle size distribution on the strength can largely be traced back to the effect of the particle size distribution on the degree of hydration [353,399,427].

---

[2]) See also B.J. Dagleish et al., 1992, Proc. RILEM Int. Conference on Concrete at Early Ages, Paris, Vol. I, 137-143.

4.5.3 Temperature Effects

In engineering practice the correlation between the compressive strength of concrete and the mean ambient temperature is well known (Fig. 4.13). Systematic research on this topic dates back to the early thirties when Davis et al. [128] and Blanks [57] found that low initial curing temperatures resulted in higher ultimate strength. Often quoted tests of Klieger and many other experiments have confirmed this observation [48,126,299,275,359, 429,444,529,575,610]. Lehmann et al. [338], on the contrary, did not find such an effect. He explains that a low ultimate strength is only found if curing occurs under sealed conditions and not in the case of saturated curing. In agreement with Lehmann, Soroka [544] and Yudenfreund et al. [638] did not observe an increase in strength at low initial curing temperatures in the case of hydration under saturated conditions.

In line with numerous reports Odler et al. [420] found that curing at temperatures above 50°C results in a lower ultimate strength. For an explanation of this phenomenon Kjellsen [295] refers to earlier work by Verbeck et al. [602], who suggested that in the case of curing at high temperatures the hydration products would be formed more immediately surrounding the hydrating cement particles, resulting in a denser gel. This would have two effects, viz. a *geometrical* and a *physical* effect. Firstly, a less expanded gel volume will generate fewer contact points and smaller contact surfaces between hydrating particles. Secondly, the denser gel might result in a decrease of the rate of hydration due to lower diffusion rates of ions to and from the surface of the anhydrous cement core into the solution. Particularly the first mentioned effect can be interpreted as being in full agreement with Bentur's observation that hydration at higher temperatures causes an increase of the capillary porosity of the paste [41], as well as with later work of Kjellsen et al. [296,297].

Note that in the foregoing explanations the effect of temperature on strength development has been reduced to a geometrical, i.e. a *stereological problem*, viz. a mechanism of

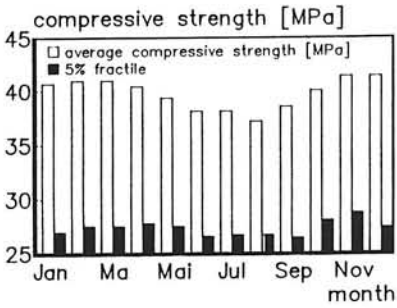

Fig. 4.13 Effect of seasonal temperature on strength of site concrete [444].

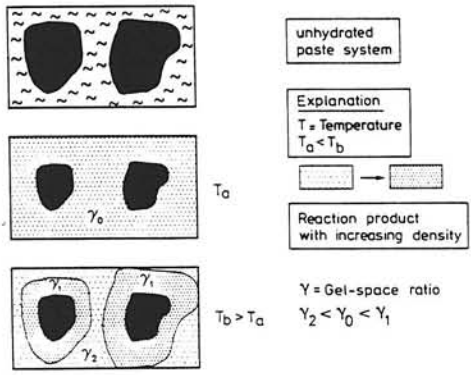

Fig. 4.14 Schematic representation of effect of curing temperature on structural development, i.e. intensity of merging [295].

reduced expansion, and hence a reduced interference between hydrating particles (Fig. 4.14). This geometry-oriented explanation offers interesting possibilities for mathematical modelling of the temperature effect on strength development. This subject will be studied in more detail in Chapters 6 and 8.

4.5.4 Water/Cement Ratio

The effect of the w/c ratio on strength has been expressed by Abrams in the classic Abrams' law, presented in the first decade of this century [1], viz.:

$$f = A * B^{-wcr} \tag{4.2}$$

in which f is the compressive strength and A and B are empirical constants. According to Graf [200] strength is inversely proportional to the cube of the w/c ratio. Grün et al. [216] point out that Graf's rule can be considered consistent with the colloidal strength concept according to which the interparticle attraction forces are inversely proportional to the cube of the interparticle distances. Since these interparticle distances are a linear function of the w/c ratio, Graf's rule seems to have a fundamental background.

The effect of the w/c ratio on the initial particle spacing, and hence on the intensity with which expanding particles can interfere, has also been mentioned by Henk [239] and Czernin [122]. They implicitly point to a *stereological* aspect of the effect of the w/c ratio on structural formation and strength development. It should be noted, however, that the effect of the w/c ratio is not only a stereological one. As Jambor [258] has pointed out, the w/c ratio also affects the character of hydration products and hence the strength properties of the gel.

4.5.5 Cement Composition

Major Cement Compounds

Since C_3S forms the greater part of cement, it is reasonable to expect that a relationship exists between the C_3S content and the strength of cement. Such a correlation was indeed found by Woods et al. [626] in 1932 already. From 3 days onward a linear correlation was found between strength and the C_3S content. For hydration periods exceeding 28 days a linear relation was found between strength and the amount of C_2S [627]. Woods further noted that changes in the oxide content of only a few percent might have a large influence on the magnitude and rate of strength development at ages up to six months.

For the determination of the contribution of the four major compounds to strength development several authors have carried out least square analyses [6,11,198]. From such an analysis, in which 228 cements and over 16,000 strength tests were involved, Alexander [11] concluded that the proportional contributions to strength of C_3S and C_3A depend on the stage of the hydration process. C_3A was found to operate by accelerating hydration rather than by changing the cementitious properties of the hydration products. Similar

results were obtained by Popovics [456,458]. The long term strength, on the contrary, was found to decrease with an increase of the C_3A content [419,458]. Jons et al. [273] suggest the latter phenomenon to be attributable to the high water needs of C_3A in the early stage of the hydration process, which would have a negative influence on the hydration of C_3S at later stages. The role of C_4AF has been found to be of less importance than that of C_3A [10,11].

Aldridge [6] submitted several New Zealand cements to a least square analysis. The cements considered were characterized by their Bogue composition. For cements from different works different least square coefficients were found. This points to a pronounced influence of minor oxides, i.e. alkalies, on the strength. *Obviously strength predictions based on the four major constituents can only be indicative!* Corrections seem to be inevitable for the effect of minor constituents.

Alkalies

In agreement with Aldridge [6], Knofel [301] also found that attempts to correlate the 28 day strength with the percentages in which the four major compounds are present in the cement suffer from the effect of the presence of alkalis. Up to about 3 days a positive effect due to alkalies was found, whereas for each percent of alkali expressed in K_2O equivalents the 28-day strength was found to decrease by about 10 MPa [425,426]. A change in the quality of the hydration products due to the presence of alkalies was suggested as a possible cause of this decrease. According to Locher [351] the lower ultimate strength of alkali-rich cements are caused by the fast hydration of C_3A in the presence of alkalies and the formation of a more porous structure.

Optimum Gypsum Content

Maximum strength values of cement pastes are reached for SO_3 contents ranging from 2.0 to 5.6% [319,357,448,542,544]. The optimum increases with increasing C_3A and alkali content [341,425] and varies (i.e. generally increases) with the specific surface of the cement [104,357,544]. According to Soroka [547] the effect of gypsum is generally a result of its effect on the rate of hydration. He also found, however, that for the same degree of hydration a higher SO_3 content resulted in a higher strength. The reason for this phenomenon could neither be related to differences in the pore structure of the paste (see Section 4.9.2), nor to differences in the density and the formation of micro flaws. This points to an effect on the *intrinsic* strength of the paste. Odler [419], on the contrary, seems to be able to fully explain the effect of SO_3 by its effect on *porosity*.

With respect to the influence of the specific surface of the cement on the optimum gypsum content, Iwasaki's postulation concerning the effect of the conversion of ettringite into monosulphate on the strength [256] should be considered. When discussing the effect of ettringite conversion in the matrix-aggregate interface he stated that *if* ettringite is involved in the interface structure and *if* the interface strength is a major factor in strength development, the conversion of ettringite to monosulphate might weaken the strength of the system. If Iwasaki's postulation is correct one can expect a more pronounced effect on

the proposed mechanism with increasing thickness of the ettringite layer[3]). As stated in Section 4.4.1, in the early stage of the hydration process ettringite layers are formed around hydrating cement grains. The amount of ettringite formed depends on the amount of added gypsum. The higher the gypsum content, the higher the amount of ettringite. From simple geometrical considerations it follows that the ettringite layer will be thicker the smaller the specific surface of the cement. With increasing thickness of the ettringite layer the effect of conversion of ettringite into monosulphate, which conversion is accompanied by a volume reduction of about 60% - will increase as well. The volume reduction of the ettringite layer might be expected to weaken the paste. This explains why the optimum gypsum content decreases with decreasing specific surface of the cement [504,547]. For a low specific surface the *critical thickness* of the ettringite layer, i.e. the layer thickness for which the weakening mechanism due to conversion of ettringite into monosulphate is activated, is reached for lower gypsum contents.

Similar considerations put forward by Iwasaki have been proposed by Jons et al. [274] when evaluating, among other things, the correlation between strength and porosity and the effect of volume changes associated with the conversion of ettringite into monosulphate on this correlation. Finally, reference is made to Schwiete et al. [521], who stated that it must be clarified whether the instability of the ettringite is a criterion for the diminution of the strengths and what the role of SO_3 might be in this respect.

It is obvious that foregoing explanations have to be totally reconsidered if the conversion of ettringite into monosulphate does not take place (see Section 4.3.1.1).

4.6 Paste Strength versus Strength of Concrete and Mortar

Paste strength cannot easily be related to mortar strength and particularly not to concrete strength [540]. The compressive strength of paste is generally about 30% higher than mortar strength and up to 50% higher than the strength of ordinary concrete [10,186]. Obviously the addition of rigid aggregate particles to the matrix weakens the material. Based on theoretical considerations Fagerlund [157] states that the strength of concrete and mortar can never be as high as that of pastes. Walz, however, found that under certain conditions, for example in the case of a mix with a low w/c ratio, the strength of concrete can exceed the strength of the paste [611]. Also the addition of silica fume to the cement can yield concrete strengths higher than the paste strength [527].

The observed increase in strength in the case of low w/c ratios and/or additional fines points to an improvement of the bond between the cement matrix and the aggregate. Since it is only variations in the w/c ratio and the addition of extra fines which significantly affect the spatial position of cement particles in the paste and also in the matrix-aggregate interface region, it is expected that the observed correlation between strength, on the one hand, and variations of these parameters, on the other, might have a *stereological* basis.

---

[3]) Reality is more complex than suggested in the geometric-oriented reasoning that is followed here. The mechanism described here can, therefore, only partly explain the existence of an optimum gypsum content (Aïtcin, 1992, privat communication).

Whether research carried out on the paste supports the suggestion that stereological considerations concerning the cement particle distribution in the matrix-aggregate interfacial zone are involved in the structural and strength development of mortar and concrete will be discussed in the next section.

4.7 Matrix-Aggregate Interfacial Phenomena

4.7.1 General

From straightforward stereological considerations it can easily be found that in ordinary concrete mixes, with aggregate percentages ranging from 75 to 80%, the average thickness of the paste layer between the aggregate particles, or ribbon thickness, varies between 50 and 200 μm. In the initial stage of the hydration process, i.e. immediately after mixing of the concrete, a quite significant "wall-effect" must be considered at the aggregate surface [511]. Such a wall effect is responsible for inhomogeneity of the microstructure and matrix properties over the thickness of the cement ribbons [27,123,158,637][4]). The need for research regarding this wall effect or "interface aspect" has been emphasized by several authors quoted in [377]. Diamond [140] has stated explicitly that the paste in concrete contains several inhomogeneities, including interfacial effects. It is also this paste that is actually found in practice. As such, the microstructure of the 'bulk' paste in concrete should be given more attention rather than the 'bulk' paste prepared in the laboratory.

4.7.2 Thickness of the Matrix-Aggregate Interface Layer

The thickness of this interface zone, or "zone d'aureole", depends on the fineness of the cement and the w/c ratio. An often adopted average value of the interface layer is 50 μm [140,323]. Scrivener et al. [527] and Zimbelmann [644] give interface thicknesses ranging from 0 to 40 μm and to 25 μm respectively, while others have mentioned thicknesses from 50 to 100 μm [202,389,423]. The thickness of the interface layer increases with increasing w/c ratio [368].

Contradictory information is found with respect to changes of the interface thickness with time. According to Maso [368] the thickness decreases with hardening time. A similar observation has been reported by Larbi et al. [324] for fly ash - Portland cement system. A reduction of the thickness of the interfacial zone was found from about 60 μm to less than 15 μm within one month hydration. Massaza et al. [370], on the contrary, stated that the thickness would remain constant in time.

For the indicated thicknesses of the interfacial zone the interface matrix forms about 15

---

[4]) Variation of paste properties over the thickness of a ribbon has been studied in more detail by Koenders in *Simulation of volume changes in hardening cement-based materials*, TU-Delft, 1997.

to 50% of the average thickness of the paste layer, whereas the remaining part consists of 'bulk' matrix. This emphasizes the need for increasing attention on interfacial aspects.

4.7.3 Structural and Morphological Aspects of the Interface Layer

Packing of Cement Particles and Porosity in the Interfacial Zone.
Poor packing of cement particles in the interfacial zone results in a high local w/c ratio. In ordinary concretes this poor packing will result in a high porosity of the interfacial zone [27,134,286,392,592] [5]). Min-Hong Zhang et al. [390] reports about a zone between 20 to 60 μm of high porosity. From an extensive literature survey, Conjeaud et al. [108] conclude that ll observations show an increase of the smaller particles near the surface. Over a thickness of 15 to 25 μm around the aggregate particles Zimbelmann [643] did not find any anhydrous cement. In a mature paste the porosity at the interface would, therefore, be relatively high, viz. 30 to 50%. The addition of ultra fines like silica fume was found to have only a small effect on the arrangement of the cement grains. It is merely the particle size distribution of the cement which determines the packing of the anhydrous cement grains in the interface zone during mixing [377]. This, in turn, implies that the extra fines concentrate in between the cement particles in the supposedly water-rich spaces. The foregoing is presented schematically in Fig. 4.15.

Interface Structure. Morphology and Microhardness
Several investigations have revealed a variable microhardness over the thickness of the interfacial zone. At the aggregate surface a small zone of about 2 to 3 μm thick with a high microhardness has been found [358]. This zone, also termed the "contact zone" [642], mainly consists of CH. Within this zone Diamond [140] distinguishes between a very thin layer, 0.5 μm thick, of CH and a so-called duplex layer, 1 μm thick, mainly consisting of short CSH fibers. A layer of CSH fibres adjacent to the CH layer has also been suggested by Hadley [221].

The contact zone is generally followed by a zone with lower microhardness. In Zimbelmann's terminology this zone is called the "intermediate layer", with a thickness of 2 to 10 μm [642]. The layer is built up of ettringite and CH crystals. Ettringite formation in the interfacial zone has been studied by Iwasaki et al. [256]. He postulates that if ettringite is involved in the interface structure and if the strength of the interface is a major factor in the development of the strength of mortar and concrete, the conversion of ettringite into monosulphate might weaken the system (see also Section 4.5.5).

The intermediate layer is followed by a "transition zone", ≈10 μm thick, with an increasing density and coarseness with increasing distance from the aggregate surface [642]. Large CH crystals penetrate from the contact layer through the intermediate and the transition layers into the matrix. The porosity of both the intermediate layer and the transition

---

[5]) In low water/cement ratio concretes, particularly in case silica fume is added to the paste, the porosity of the interfacial zone may not differ much from the bulk paste (Aïtcin, 1992, privat communication).

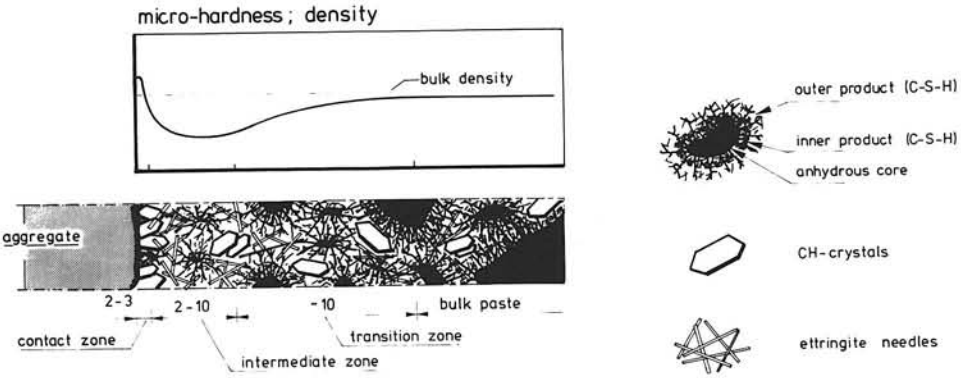

Fig. 4.15 Matrix-aggregate interface characteristics and development of microhardness. Schematic representation.

zone is generally significantly higher than the bulk porosity. The relatively higher porosity is associated with a lower microhardness [358].

An interface structure shown schematically in Fig. 4.15 seems to have no universal validity. The duplex film as suggested by Daimond, for example, has not been observed by other authors [370]. The addition of fly ash to the cement has appeared to be one of the reasons why a duplex layer is not formed [325]. Saito [512] did not find a zone with lower porosity and lower microhardness. A high microhardness in the interfacial zone has been reported by Popov [455]. Different results would originate from different chemical reactions in the interfacial regions as they occur when different types of aggregate are used.

It has been noted already that the existence of a layer with higher porosity can be explained by the loose packing of cement particles in the interfacial region. The fact that as the hydration process progresses a difference between bulk and interface density remains indicates that CSH seem to precipitate mostly quite close to the cement grain surfaces [141,580]. This indirectly obtained information supports the idea of the existence of a mechanism of concentric outward growth of hydrating particles as proposed by Granju et al. [205]. The concentric outward growth of hydrating particles constitutes one of the main cornerstones of the simulation model to be explained in Chapter 6.

Interfacial Bond. Physico-Chemical Aspects

Whether the bond between aggregate and cement matrix results from chemical reactions between the paste and the aggregate or results from mechanical interlocking is still not known [590]. Struble et al. [561] refers to the work of 8 authors who have suggested chemical bonds. The type of aggregate substantially influences the intensity of chemical surface reactions and hence the bond between aggregate and cement. Farran [158] found that the bond between cement paste and calcite or dolomite was better than with other aggregate types. Most researchers agree that carbonate aggregates are not inert but react with

the hydration products in the transition zone [394]. Between cement and siliceous aggregate no chemical bonding was observed [96].

4.7.4 Degree of Hydration in the Interfacial Zone

The concentration of small particles in the interfacial zone makes it plausible that the degree of hydration in this zone is higher than in the bulk paste. Fig. 4.16 shows the degree of hydration as a function of the distance from the aggregate surface as observed by Scrivener et al. [527]. The amount of unhydrated material in the bulk paste is significantly higher than adjacent to the aggregate surface. A degree of hydration in the zone close to the aggregate surface higher than in the bulk matrix has also been mentioned by Conjeaud et al. [108].

4.7.5 Matrix-Aggregate Interface Aspects of Strength Development

Interfacial Bond Strength. Absolute Values and Influencing Factors.
Interfacial bond strengths have been reported to range from 0.17 to 2.5 MPa [196] up to 3.5 to 10.5 MPa [9]. The wide range in bond strengths can be attributed to the influence of the w/c ratio, the size and type of the aggregate and the curing conditions. The relationship between bond strength and w/c ratio is similar to that between compressive strength and w/c ratio. With respect to the aggregate size the bond strength has been found to decrease with increasing aggregate size [9,249]. For different types of aggregate the bond strength has been found to vary by a factor 2 [134,534]. Drying of the relatively water-rich interface will cause a reduction of the bond strength.

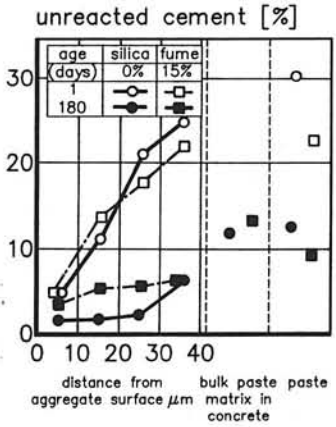

Fig. 4.16 Degree of hydration in the transition zone as a function of the distance from the aggregate surface. Paste with and without silica fume (after [527]).

Interfacial Bond Strength versus Strength of Paste and Concrete
In ordinary strength concretes the bond between paste and aggregate is generally considered to be the weakest link which dominates the strength of the composite [134,186,248, 642]. The total range within which the interface tensile strength could vary ranges from 40 to 90% of the tensile strength of the paste, depending on the rock type, surface roughness and w/c ratio [249]. According to Alexander [9] a linear relation exists between the bond strength and the concrete strength.

The weakest layer in the interfacial zone is the layer with high porosity and, consequently, a low microhardness [134,368]. A higher concrete strength can be obtained by reducing the porosity of this zone [370]. The addition of ultra fines like silica fume and flyash is found to be very effective in this respect [172,270,641]. The small particles are responsible for a better packing of solid material in the interface zone. Moreover, they act as nucleation centres which enhances the density of the matrix in the interfacial zone [270, 326,483,527].

Interface Phenomena. Summary
The higher microhardness in the immediate vicinity of the aggregate surface has a predominantly chemical origin, viz. the formation of CH crystals at the aggregate surface [27, 135,221]. *The higher porosity at some distance from the aggregate surface, on the other hand, has a more stereological origin, viz. the initially poor packing of cement particles due to the spatial constraints.*

In the framework of this study it is interesting to see that several authors have already pointed out the influence of the particle size distribution of the cement on the interface characteristics. In Chapter 8 it will be shown to what extent HYMOSTRUC is able to simulate the observed interface phenomena in so far as the stereological aspect is concerned.

4.8 Volumetric Considerations of Hydrating Pastes

It has been observed, particularly in low w/c ratio pastes, that in the early stages of hardening the bulk volume of the paste increases, whereas at later stages a volume reduction generally occurs [410,437,594]. For cement pastes with a w/c ratio of about 0.55 Steinour observed an expansion before the final set of 0.09...2.1% [556]. For low w/c ratio pastes the volume expansion might reach up to 2.7% [505]. Several authors have attributed this early increase in volume to the *formation of ettringite* [588]. However, if it were the formation of the ettringite *per se* that would be responsible for this increase in volume, a similar increase should also occur in a suspension hydrated specimen. Suspension tests carried out by Czernin [121] did not reveal such an increase.

According to Traetteberg et al. [594] the occurrence of *microcracking* in low water/solid ratio pastes would be responsible for the early expansion of samples. If this explanation were correct, the question rises as to what caused this microcracking. Cracking presupposes the existence of stresses, and stresses again presuppose the existence of deformations. So, before a cracking-induced expansion can occur, stresses and associated deformations must somehow have been created already. *Autogenous shrinkage* can be considered

as one of the possible causes for the occurrence of stresses. But also *expansion of hydrating particles under restraint conditions* can cause stresses and associated expansion [81].

Having considered the different possible mechanisms proposed for explaining early expansion of pastes we are inclined to follow Odler et al. [410] and believe that expansion of the hydrating sphere-like cement particles in a constraint state, rather than ettringite expansion or microcracking, is the main cause of early expansion in low w/c ratio specimen. In other words, the early volume increase has a predominantly *stereological* origin. As we see it, microcracking is much more a result than a cause of expansion.

4.9 Strength Laws. Macro Level

4.9.1 General

At macro or engineering levels several approaches are used to describe the development of strength with time or during the hydration process. Currently applied concepts are:

1. The porosity concept
2. The gel-space ratio concept
3. The degree of hydration concept
4. Maturity laws
5. Chemistry-oriented strength laws

The three concepts mentioned first are basically different from the last two concepts. Furthermore, since the porosity and the gel-space ratio are both functions of the degree of hydration, the first three concepts can be considered as closely related to each other. For fundamental research and attempts at bridging the gap between theory and practice the first of these concepts should be adopted.

The application of maturity laws is mainly restricted to the job site, albeit that a fruitful symbiosis of the basically different approaches is conceivable (see also [361]).

The chemistry-oriented, mainly empirical strength concepts will not be discussed in detail here. For information purposes, reference is made to Section 4.5.5 and the literature mentioned in that Section.

4.9.2 Strength-Porosity Concept (f/P-relationship)

In the last century BC it was Lucretius who stated: *"The more vacuum a thing contains within it, the more rapidly it yields"*. Abrams [1] argued from a different angle but came to a similar statement, viz.: *"The strongest cement pastes should be made without water"*. These statements point to the distinct relationship between strength and porosity of cement-based materials.

Since these early observations the relationship between porosity and strength has been emphasized by many authors [21,32,62,307,503,505,531]. Several authors hold the view

that not only porosity, but also the *pore size distribution*, the *pore shape* and the *orientation of the pores* with respect to stress are important factors which determine the mechanical behaviour of cement paste [40,62,260]. The assumed effect of the pore size distribution is substantiated by theoretical considerations in the field of fracture mechanics [291,363]. In this respect it should be noted that the presence of *macro-defects* (≈1 mm), which generally initiate fracturing of a material, exceeds the effect of porosity [291]. That porosity alone cannot adequately account for the development of paste properties has also been stated by Jambor [257]. Particularly for low porosity pastes the f/P relationship has turned out to fail [488].

In spite of the theoretical basis for an additional effect of the pore size distribution and pore shape on the f/P relationship, the experimental work by several authors did not confirm a significant influence of these factors [632,638]. On the other hand, there seems to be general agreement about the fact that the f/P relationship is predominantly governed by the *capillary porosity* of the cement paste [203,632]. Pores smaller than about 200 Å would hardly affect the strength [418].

Several authors have reviewed the strength-porosity equations which have been proposed over a period of almost 100 years [156,281,287,355,459]. Many of the proposed formulae are exponential functions (Fig. 4.17). For a large quantity of experimental data Hasselmann [232] found that a simple linear function would yield the best fit. Strong support for the strength-porosity concept comes from Odler et al., when explaining that both the effect of gypsum and of temperature on strength could be attributed to the effect of these parameters on the porosity [6,420].

Although many strength-porosity equations have turned out to predict the strength quite adequately, several authors have nevertheless pointed to a limited validity of this concept, since the majority of these equations do not allow for a possible effect of the pore size

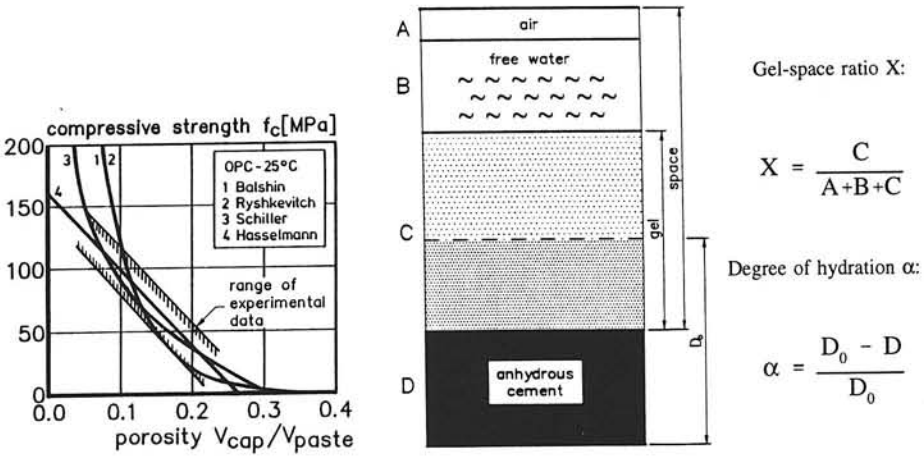

Fig. 4.17 Strength-porosity equations according to different authors [232].
Right: Degree of hydration and gel-space ratio - Schematic.

distribution or for any effect of the pore shape. Parcevaux [434] noticed many contradictions and Popovics [459] even stated that none of the current predictive methods for estimating the effect of porosity on concrete strength has been found to be good enough for practical use! Jons [274] points out that the f/P relationship is also affected by the chemical composition of the cement and the gypsum content. Kondo et al. [307], on the contrary, assumed the f/P relationship to be independent of the cement composition.

4.9.3 Gel-Space Ratio Concept

The "gel-space ratio concept" for the description of the strength was launched by Powers et al. [462] in the forties. The gel-space ratio X is defined as the quotient of the volume of the gel and the total volume of the paste *minus* the volume of the still unhydrated cement (Fig. 4.17). Between the compressive strength and the gel-space ratio a relationship was found of the form:

$$f = f_0 * X^3 \tag{4.3}$$

where f and f_0 are the cube compressive strength and the intrinsic strength of the paste, respectively. The intrinsic strength f_0, i.e. the strength of the capillary pore-free cement paste, varies from about 200 MPa for ordinary cement [355,506] up to 600 MPa for hot pressed cement pastes [506]. For the intrinsic strength of mortar a value of f_0 = 180...342 MPa is applicable with a mean value of 290 MPa and a standard deviation of 68 MPa [156].

The gel-space ratio concept and modifications of it have successfully been applied by Berger et al. [43], Beaudoin et al. [32] and many others. Also for the case of curing at elevated temperatures the concept has turned out to be applicable, albeit that in some cases (not in all cases! [420]) adjustment of the intrinsic strength had to be carried through [418]. Moreover, several authors have established the applicability of the gel-space ratio concept for the determination of tensile strength of cement [632,633]. In order to extend the validity of the concept, several modifications have been proposed. Karni [281] suggested that the volume of the gel should preferably be related to the overall volume of the paste (cement + water) minus the dry cement volume. Locher [355] points out that, as well as Powers' original definition of the gel-space ratio, the amount of unhydrated cement should be considered explicitly.

Popovics [459] and Fagerlund [157] have criticized the gel-space ratio concept on several points. Popovics argues that the concept has not been applied to concrete [6]), while Fagerlund even states that the gel-space ratio concept has never been a success. Fagerlund shows that the gel-space ratio concept can easily be rewritten into a strength-porosity relationship as proposed by Balshin [23] in 1949. This, in our opinion, can be considered as an argument in favour of the gel-space ratio concept rather than a point of criticism,

[6]) Note: The gel-space ratio concept has been applied for concrete indeed (See [361]).

since it illustrates that the gel-space ratio and porosity are mutually related quantities. This being so, it might be evident that all factors which have revealed to affect the f/P relationship, also affect the f/X relationship.

4.9.4 "Degree of Hydration" Concept

As early as 1928, Werner and Giertz-Hedstrom [612] found that the compressive strength could be related to the amount of hydrated cement. A few years later Woods [627] and Davis et al. [128] reported on a linear relationship between strength and the *amount of liberated heat.* Assuming a linear relationship between the amount of liberated heat and the degree of hydration their results implicitly reveal a linear relationship between strength f and degree of hydration α, i.e. a *f/α relationship.*

A linear relationship between strength and the *amount of chemically bound water* has been proposed by Eiger [149] in 1933 and Lea and Jones [336] in 1935, whereas Le Chatelier had already suggested a linear relationship between strength and *chemical shrinkage* in the first decade of this century (Geiker in [185]). Since both the amount of chemically bound water and chemical shrinkage can be considered as indicators of the degree of hydration, the observed correlation between these quantities and the strength can be judged as arguments in favour of the f/α relationship.

Since these early reports a linear f/α relationship has been reported by many authors [5, 81,156,176,185,262,287,334,338,362,387,422,430,440,530,565]. Fig. 4.18 shows an example of the f/α relationship based on data found by Taplin [574]. The w/c ratio, inserted as a parameter in this figure, turns out to significantly affect this relationship. This is quite evident, since a higher w/c ratio enhances the interparticle distances which consequently

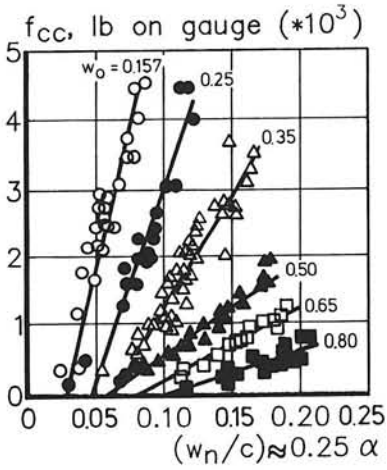

Fig. 4.18 Strength versus degree of hydration. Based on data by Taplin [574].

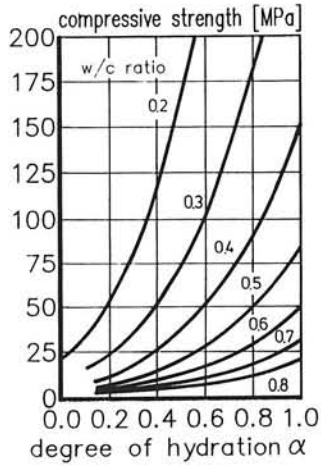

Fig. 4.19 Strength versus degree of hydration according to Locher [355].

also enhances the degree of hydration required for the production of sufficient material, i.e. hydration products, to bridge these distances.

Although the theoretical background of the effect of the w/c ratio is quite evident, it is nevertheless somewhat difficult to understand why the f/α relationship would be a linear one. From geometrical considerations a cubic or exponential relationship seems to be more plausible. A more than proportional growth in strength with increasing degree of hydration is shown in Fig. 4.19, presented by Locher [355] and is actually based on strength considerations put forward by Powers. A comparison of Fig. 4.18 and Fig. 4.19 explains why in the range of strengths which are of practical interest, i.e. from 10...60 MPa, the linear f/α relationship holds quite well.

A modified version of the degree-of-hydration concept has been proposed by Postaciogly [461], who inserted the thickness of the shell of hydrated cement as an extra parameter in the relationship between strength and degree of hydration. In this way the effect of the *fineness* of the cement on the strength-degree of the hydration relationship was assumed to be allowed for, at least in part.

Since both porosity and the gel-space ratio are direct functions of the degree of hydration, it is evident that factors affecting the f/P and f/X relationship also affect the f/α relationship. This in turn implies that strength is not a function of the degree of hydration alone [204,258,383,619]. The effect of the w/c ratio has already been demonstrated in Fig. 4.18. Several authors have pointed to the effect of the clinker composition on the f/α relationship [8]. Others have observed the effect of the curing temperature [409,575], which has been considered to point at the formation of different hydration products at different temperatures.

4.9.5 Maturity Laws

Maturity M(t) was originally defined as the integral of time and curing temperature, the latter measured from a certain datum temperature, generally below zero. In the pioneering stage of the utilization of the maturity concept the strength was considered to be a linear function of the logarithm of the maturity [517]. Poor f/M correlations reported by Klieger [299], Plowman [447], Al-Rawi [5] and more recently by Popovics [460] and Kjellsen [295], have inspired work on proposals for improvements and modifications of the original maturity concept [49,65,86,432]. Although these modifications have certainly contributed to the applicability of the concept in practice, they should still be judged as a predominantly, or better still, a fundamentally empirical approach. Because of its empirical character, several authors have emphasized that current maturity concepts basically fail to describe the effect of temperature history on strength [87,338,374,406].

4.9.6 Strength Laws. Discussion

Since the porosity and the gel-space ratio are both direct functions of the degree of hydration one can say that the porosity concept, gel-space ratio concept and the degree of hy-

dration concept for strength development are basically equivalent [156,281,355]. In all these concepts the w/c ratio turns out to be a most important parameter.

The role of the w/c ratio in strength development has been discussed explicitly by Granju and Maso [203,204]. They explain the development of strength as a process of increased merging of continuously expanding cement particles. Their concept allows for the fact that at higher w/c ratios, and thus for larger interparticle distances, merging of outer products of expanding particles will be less intensive, the degree of hydration being the same. For each w/c ratio one particular relationship between strength and degree of hydration exists.

A scenario put forward by Granju et al. offers interesting prospects for the mathematical modelling of structure and strength development. The development of strength has been reduced to a *geometrical problem*, viz. the determination of the number of contact points and magnitude of contact areas between expanding particles. It seems justified to expect that it is just the magnitude of the contact area and the formation of interparticle bonds in these areas which determine strength development.

In comparison with the aforementioned geometry-oriented strength concepts the maturity concept must be judged to be of a different order. It is a basically phenomenological approach which does not explicitly consider structural formation. Stating this, an exception must be made for the maturity concept as discussed by Powers [466] and Hansen [226]. In their concepts, however, the definition of maturity is identical to that of the degree of hydration. We thus arrive at the conclusion that the many definitions of maturity lead to confusion and make people less prepared to accept the concept, even when the limits of applicability are clearly defined. When applied within these limits of applicability maturity rules can be considered as valuable tools for quality control purposes on site. Having said this it must also be clear that because of its highly phenomenological character the maturity concept cannot serve as a basis for further fundamental research in the field of structural formation and strength development. For making progress in this area, research should concentrate on the relationship between strength and degree of hydration [21,295, 361].

4.10 Structural Formation and Strength Development. Summary and Discussion

Strength development is closely linked to structural formation. Thereby it appears relevant to distinguish between the structural formation as it occurs in a neat cement paste (bulk hydration) and in the close vicinity of the matrix-aggregate interface (interface hydration).

"Interparticle" Structural Formation

Immediately after their first contact with water, cement particles start to dissolve and form reaction products. Hydrating particles of some size, from about 3 μm onwards, can be considered as expanding centres, generally assumed to be spheres. Within the original grain boundaries the so-called inner product is formed, whereas outside these boundaries the outer product is formed. Cement particles smaller than 3 μm are considered to form only outer products. The reaction products produced by these small particles will precipitate and merge with the outer product of larger particles, thus allowing for extra ex-

pansion to the latter particles. As long as particles do not make contact, their mode of expansion appears to be concentric-wise, which supports the idea that the outer product has a more or less constant morphological structure, i.e. constant porosity and density, albeit not unconditionally identical to the morphology and density of the inner product. As soon as expanding particles make contact, merging of outer products takes place under conditions of increasing volume constraint which can be expected to lead to local densification of the gel. As the hydration process progresses the number of contact points will increase. At the same time the earlier formed contact points will change into contact areas. Densification of outer product of expanding particles and embedding of smaller particles in the outer shell of the large particles, i.e. increasingly intensive merging of reaction products, is most probably the reason, at least in part, why in later stages of the hydration process a distinct difference in chemical composition and density of inner and outer product gradually vanishes.

Paste Strength

Strength is developed due to the increasing number of contact points and, the increasing magnitude of the contact surface area between hydrating particles during the hydration process. Thinking in a scenario of expanding and merging particles implies that strength development has a distinct *stereological aspect*. The effect of the *w/c ratio* on strength development can easily be explained from a stereological point of view and is almost trivial. Moreover, there is also room to expect that *temperature effects* on strength development can be explained in stereological and geometrical terms, at least in part. In this respect reference is made to the observed increase in porosity when hydration occurs at elevated temperatures, which indicates less expansion of the hydrating cement particles and hence fewer contact points and smaller contact surfaces areas and hence lower strength.

The effect of the *chemical composition of the cement* on strength development can also partly be reduced to a geometrical problem, since it appears that the effect of the clinker composition on strength can be considered in terms of variations in the rate of hydration and of structural formation rather than in terms of dramatic changes in the physico-chemical structure of the cement paste. This fact reduces the need for chemistry-oriented, empirical formulae for the prediction of strength as proposed by, for example, Popovics [458]. It enhances, however, the need for investigating the effect of the chemical composition of the cement on the development of the pore structure of the paste and of the gel structure.

Interface Aspects

Differences between the structure of bulk paste, on the one hand, and interface paste, on the other, can be explained partly from a physico-chemical point of view and partly from a stereological standpoint. The stereological part refers to the "wall effect" as it occurs at the aggregate surface immediately after mixing of the cement with water and aggregate. Around the aggregate surface a water-rich zone forms which results in an interface layer with high porosity and a relatively low strength. The thickness of the interfacial zone has been reported to vary from 20 to 50 μm and even more, depending on the fineness of the cement and, above all, on the w/c ratio (see Chapter 7).

Strength

Strength can be expressed in terms of structural formation by relating strength to the degree of hydration or, alternatively, to quantities like porosity, gel-space ratio and chemical shrinkage, which can be described as functions of the degree of hydration. In these geometry-oriented descriptions of strength the role of the w/c ratio is a very important one. With the degree of hydration and the w/c ratio the geometrical constitution of a paste is largely defined. Not completely, however, since the effect of the fineness of the cement, curing temperature, chemical composition of the cement, gypsum content and recrystallization processes have turned out to limit the application of exclusively geometry-oriented strength concepts.

Considerations in View of Mathematical Modelling of Structure Development

Structural formation in cement-based materials exhibits a *physical*, a *chemical* and a *stereological* aspect. The presented literature survey on structural formation as well as some pilot calculations with respect to some colloidal phenomena like interparticle repulsion and attraction forces, have revealed that the gap between the colloidal micro level, or even molecular or atomic nano level, on the one hand, and the engineering or macro level, on the other, cannot be bridged without using *models*. If possible, these models should be consistent with well-established information that can be advanced by the three previously mentioned disciplines, i.e. physics, chemistry and stereology.

With respect to the stereological aspect the "unstable pore concept" as originally proposed by Powers et al. [462], and later adopted by Cranju et al. [205] for his concept of concentric outward growth of hydrating cement particles, are considered to be of major interest. One of the most important features of this concept is, that it enables, in essence, the computation of the number of contact points and magnitude of the contact area between expanding particles. The total contact area is postulated to be an important parameter in the development of strength. A second important feature of the unstable pore concept is, that the shell of reaction products which surrounds the anhydrous core of an hydrating particle is assumed to have a constant density. This will significantly simplify mathematical modelling of the diffusion-controlled stage of the hydration process since one can then stick to a constant value of the diffusion coefficient.

5 CEMENT HYDRATION AND FORMATION OF MICROSTRUCTURE
KINETICS AND RATE FORMULAE

5.1 Kinetics and Rate Formulae. An Introductory Survey

This chapter describes mathematical (kinetic) models currently used for describing and predicting reactions and processes involved in hydration and structure development in cement-water systems. The reaction considered is a heterogeneous reaction of the general form [192,509,612]:

$$\text{solid A} + \text{liquid B} = \text{solid C} \tag{5.1}$$

Several kinetic formulae for solid-liquid reactions have been proposed in the past. In this respect Glasstone's standard work "The theory of rate processes" can be mentioned. In his book Glasstone reviews a variety of mathematical expressions for different kinds of processes. Formulae are given in which effects of irregularities of the particle shape and impurities at the surface of the reactant are accounted for. With the proposed expressions trends can be shown and the influence of several parameters can be evaluated. The accuracy with which certain heterogeneous reactions can be calculated, however, has appeared not to be very high. A deviation of about 40 % between calculated and observed reaction rates is rather common and is considered a good result [192].

The complexity of heterogeneous reactions and the relative exactness of mathematical models and rate formulae has been discussed extensively by Hakvoort [224]. Unlike homogeneous reactions, i.e. liquid and gas reactions, heterogeneous reactions are much more complex because of particle size effects. In the case of cement hydration, the poly-mineral character of the reactant is another complicating factor with respect to the accuracy of mathematical modelling of reaction kinetics. For all these reasons one has to realize that the observed kinetics of heterogeneous reactions in poly-size and poly-mineral systems mirror an *average* or *combined* result of different reactions, processes and phenomena involved in the hydration process (see also Section 3.5).

Kinetic models for cement hydration can be subdivided in roughly four classes[1]). At first one can distinguish between models which describe *overall kinetics* and models which particularly focus on *particle kinetics*. A third class is formed by *hybrid kinetic models*. In this study emphasis has been placed on so-called *integrated kinetic models*. For the sake of completeness, and also because it is a remarkable new approach to the subject, we also have to mention the ideas put forward by Mehta [378]. Convinced of the complexity of

---

[1]) For other classifications of models see:

1. Garboczi et al. (1992). *Computer-based models of the microstructure and properties of cement-based materials*, in Proc. 9th Int. Congress on the Chemistry of Cement, New Delhi, Vol. VI, 3-15.
2. Jennings et al. (1996). *Modelling and Materials Science of Cement-Based Materials Part I: An Overview*, in The Modelling of Microstructure and Its Potential for Studying Transport Properties and Durability. Ed. Jennings et al., NATO ASI series, Vol. 304, 29-62.

modelling of poly-size and poly-mineral cement-water systems and hardening of pastes, and inspired by the work of Capra [85], he proposed to consider the potentialities of *holistic models.* A detailed discussion about the holistic approach would bring us beyond the scope of this thesis. Some comments, however, are summarized at the end of this paragraph.

Overall Kinetics

In overall kinetic models the effects of the particle size distribution and the poly-mineral character of the reaction are dealt with *implicitly.* With overall kinetic models nucleation and growth mechanisms, and also the effect of changes of ion concentrations in the liquid phase on the rate of reaction, can generally be described quite well. The effect of cement fineness can be accounted for by correction factors, i.e. adjustment of formula constants.

Particle Kinetics

In models based on particle kinetics the effect of the particle size distribution is *explicitly* accounted for. Particles are assumed to react separately throughout the reaction process. With these models one has the opportunity to allow for changes in rate controlling mechanisms according to which individual particles react. For subsequent particle sizes these changes can take place at different times [50,51,53]. Any interaction between hydrating particles which might affect the rate of hydration is ignored.

Hybrid Kinetics

In this study hybrid kinetics are used for models in which it is aimed to allow for the particular features of particle kinetics, and hence for the effect of the particle size distribution on the overall rate of hydration, as well as for both the state of water in the hydrating mass and the chemical composition of the cement. Effects of interactions between hydra ting cement particles, i.e. the formation of microstructure, on the rate of hydration are not dealt with *explicitly*, but can be considered phenomenologically by inserting correction factors.

Integrated Kinetics.

The term "integrated kinetics" is introduced here for models which *explicitly* account for the effect of particle interaction and formation of microstructure on the rate of hydration. Hence, integrated models must be considered as attempts to allow for the chemical, the physical *and* the stereological aspects of the hydration process. Accounting for mutual interactions between these three aspects in one model requires a huge calculation effort [496]. The rapid evolution of computer hardware, however, has cleared the way for interesting and promising developments in this field. Several computer-based models can already be categorized among these integrated models.

The difference between integrated kinetics and overall kinetics is that in integrated models interaction processes are modelled *explicitly*, whereas in overall-kinetic models these interactions are allowed for *implicitly.*

Integrated kinetic models also differ from the earlier mentioned *macro-models* (Chapter 1) in that integrated models refer to processes and interactions between individual pro-

cesses at *micro-* and *meso-level*, whereas macro-models must be considered to a large extent as *phenomenological* descriptions of chemical and physical processes as observed at the engineering or macro-level.

Holistic Models: Some commands.
A plea for a more comprehensive approach, i.e. for integrated models, in which allowance is made for all relevant aspects involved in hydration and structural formation, might be interpreted as a plea for a holistic approach as proposed by Mehta [378]. It is not the aim to discuss the features and background of the holistic approach of science here in detail. It is emphasized, however, that the comprehensive approach recommended in this thesis differs fundamentally from what is meant by the holistic approach to which Mehta referred. Mehta made his plea for a holistic approach in connection with his review of the microstructure-property relationships. After having quoted Capra, the physicist who can be regarded as the exponent of the holistic approach in the late eighties, Mehta explicitly stated:
"For dealing with complex systems it would help to keep abreast of developments in other disciplines. Recent advancements in theoretical physics occurred when the physicists changed their world view from reductionistic to holistic. That is instead of looking at the world as a machine made up of isolated and independent parts, the physicists now see the world as a web of interconnected and therefore interdependent relationships that are intrinsically dynamic. The more we know about the world of hardened cement paste and concrete, the more it appears to be a microcosm of the human world. Therefore, for research on hardened cement paste to be applicable to concrete practice, the reductionist approach to structure-property relationships must be replaced with a holistic approach".
The author fully agrees with Mehta when he emphasizes the need to keep oneself posted on achievements and developments in other disciplines. There is also full agreement with Capra, and with him with Mehta, when they emphasized that the nature of the whole always differs from the sum of its parts and that, as Mehta said, the world is more than a machine made up of isolated and independent parts, the starting point of the reductionist. There is no problem, therefore, to follow Mehta when he says that the reductionistic approach in science cannot offer us the final answers if we are to understand nature in depth. These points of agreement, however, do not mean that Mehta can also be followed when he concludes that for successful research and practical application of the results on structure-property relationships in hardening cement paste we must replace the reductionistic approach and turn to the holistic approach as outlined by Capra. Apart from the more principle points of disagreement concerning the holistic approach of science, of which a discussion would be beyond the scope of this thesis, the author is far from convinced that the possibilities of the reductionistic approach have yet been explored exhaustively. In this respect the potential of computer-based models as a powerful research tool should be borne in mind. As indicated in the foregoing, these models can be used for both analysis of complex mechanisms and interactions on micro-level scale and systematic evaluation of huge files of experimental data brought together from different disciplines. We are very much inclined to believe that stagnation in research and lack of understanding of micro-level features of cement-based systems is caused by the lack of flexibility, ability or maybe even willingness of scientists to cooperate with colleagues from other disciplines to investigate and solve complex, interdisciplinary phenomena rather than by a lack of information and knowledge about the constituent aspects of a certain problem on the intra-disciplinary level. Efforts aiming at bridging the gaps between the disciplines involved in the complex problem under consideration, including the gap between theory and practice, should, therefore, be given high priority. For successful attempts to bridge these gaps the potential of computer-based models to synthesize all information available in individual disciplines can hardly be overestimated. It is evident, that elaborating computer-based integrated models presupposes that information from different disciplines is available. In other words, the comprehensive approach presupposes and needs the reductionistic approach rather than the abandoning it.

5.2 Overall Kinetics

In this survey of overall kinetics two classes of rate equations can be distinguished. The first class refers to rate equations which mainly focus on nucleation and growth mechanisms. In the second class the overall rate of hydration is explicitly related to (changes in) the ion concentration in the liquid phase of the system.

For the present only isothermal reaction processes will be considered. Temperature effects will be dealt with separately in Section 5.6.

5.2.1 Review of Rate Equations

Classic formulae used for overall kinetics of cement-water and compound-water systems are the Avrami-Erofeev equation, the Kolmogoroff-Erofeev equation, the Johnson-Mehl equation and the Prout-Tompkins equation.

The Avrami-Erofeev equation describes nucleation and growth processes in an isothermally reacting system:

$$\alpha(t) = 1 - \exp[-(k_A.t)^n] \tag{5.2}$$

where $\alpha(t)$ is the degree of hydration at time t and k_A and n are experimentally obtained constants. With this formula an S-shaped reaction curve is described. Bombed [61] and Brown et al. *(Ibid. [71])* used the Avrami-Erofeev equation to describe hydration of C_3S, whereas Fierens et al. [168] applied this formula for the reactions in a C_3S+CaCl system. Reinhardt et al. [486] used the Avrami-Erofeev equation as the basis for computer-based predictions of temperature fields in hardening concrete structures. In many of these cases the results obtained using the Avrami-Erofeev equation turned out to be quite satisfactory.

The Kolmogoroff-Erofeev equation can be considered as a reshaped form of the Avrami-Erofeev equation, viz.:

$$\alpha(t) = 1 - \exp(-k_K.t^{\,n}) \tag{5.3}$$

where k_K and n are again empirical constants. From a comparison of eq. (5.3) with the Avrami-Kolmogoroff eq. (5.2) it can easily be seen that the equations are identical for $k_K=k_A^n$. The Kolmorogoff-Erofeev equation to the hydration processes has been discussed by, among others, Rumyantsev [509] and Brown et al. [71], whereas Vyrodov [608] has applied this equation for hydration of cement-based materials.

Another formula with which an S-shaped reaction curve is yielded is the Prout-Tompkins equation *(Ibid. [224])*:

$$\ln(\frac{\alpha}{1-\alpha}) = k.t + C \tag{5.4}$$

with k and C constants. For the model on which this equation is based it was assumed that during the reaction, nuclei branching takes place, resulting in a rapid increase in the number of the number of nuclei with time.

For hydration of tricalcium silicate Vollet et al. [606]) has used a formula similar to the Johnson-Mehl equation, viz:

$$J_\infty - J_t = (J_\infty - J_0) * \exp\left(\frac{-k^n . t^n}{n}\right) \tag{5.5}$$

where: J_0, J_t, J_∞ = scattering intensity values (SAXS) at time t, the extrapolated time=0 and corresponding to the apparent upper asymptote.
n = parameter, which is a function of the phase transformation determinant system.
k = empirical constant

From the good fit of experimental data for n≈2 Vollet concluded that gel growth was controlled by diffusion.

Greenberg and Chang [208], dealing with hydration of C_3S, proposed an equation with the concentrations of the anhydrous and dissolved C_3S as parameters:

$$\frac{-d(C_3S)}{dt} = k_1.O - k_2.(C_3S)_d.O \tag{5.6}$$

where: (C_3S) = concentration of anhydrous C_3S
$(C_3S)_d$ = concentration of reacted (dissolved) C_3S
O = outer surface area of the reactant
k_1, k_2 = reaction constants

Results obtained did not always correspond to the experimental data.

A similar equation has been proposed by Brunner & Tolloczko *(Ibid. [79])*:

$$\frac{-d(C_3S)}{dt} = k.O.[(C_3S)_s - (C_3S)_d] \tag{5.7}$$

with C_3S and O as in eq. (5.6), while k is a function proportional to the diffusion coefficient. $(C_3S)_s$ and $(C_3S)_d$ are the concentrations of dissolved C_3S on the interface of unhydrated C_3S and dissolved C_3S in the solution far from the unhydrated surface. The difference between eq. (5.6) and (5.7) refers to the diffusion function k. According to Greenberg et al. [208] results obtained using eq. (5.7) did not correspond to experimental data. He concluded that it would be necessary to take into consideration the thickness of the product layer around the anhydrous core through which diffusion actually takes place.

For ball-mill hydration of C_3S, Brunauer et al. [76] proposed:

$$\frac{-d(C_3S)_s}{dt} = k.(C_3S)^{\frac{2}{3}} \tag{5.8}$$

where (C_3S) is the concentration of C_3S and k is a rate constant (Note: In case of ball-mill hydration the hydration process occurs under constant stirring of a water rich cement-water system). With eq. (5.8) relatively good results were obtained. One of the reasons for a good fit of experimental data might be that in the case of ball-mill hydration the product layer is removed continuously from the surface of the anhydrous grain. Diffusion through a thickening layer of outer product, and hence a change of the rate determining mechanism, would thus not exist in this case.

5.2.2 Overall Kinetics. Discussion

The first major point of criticism concerning the application of the overall kinetics for cement and compound hydration refers to the role of the particle size distribution, which is not explicitly allowed for [51,53,302,303,570]. According to Bezjak [50] the Avrami-Erofeev equation may, therefore, not be used for a poly-size system. Comparison of theoretically obtained values with experimental data could even result in misleading interpretations concerning prevailing hydration mechanisms. In the light of Bezjak's remarks it might be questionable, for example, whether Vollet's conclusion, that a value for the factor n in the Johnson-Mehl equation of about 2 indicates that gel growth is controlled by diffusion, is correct. One should consider the possibility that the effect of the particle size distribution on the rate of hydration has substantially affected the overall rate of hydration and is partially responsible for a hydration effect incorrectly attributed to diffusion.

A second point of criticism refers to the fact that overall kinetics does not explicitly account for changes in rate determining mechanisms according to which individual particle fractions may hydrate simultaneously. It was Bezjak et al. who addressed this point in several papers [12,50-53]. Similar criticism came from Schlüssler [518]. He criticized the use of the Avrami-Kolmogoroff equation, since it would not suitably reflect the hydration process in different periods of hydration. Schlüssler also pointed to the effect of *particle interaction*, which is not considered explicitly in this equation at all.

With regard to kinetic equations in which the ion concentration outside the product layer is considered to be the predominant rate determining parameter, Kondo [307] critically suggests that the concentration at the interface of the anhydrous core of a reacting particle might be quite different from the concentration in the liquid phase. In other words, it is the concentration *gradient* in the product layer, and not merely the concentration in the liquid phase that should be considered in kinetic equations. Ignoring this fact might well result in misjudgment of the reaction mechanisms that occur.

Though we are dealing in this Section with overall kinetics and not with particle kinetics, it should be noted that some of the quoted equations can be categorized between overall and particle kinetics. The eqns. (5.6) and (5.7), which include the total particle surface of the anhydrous cores, require that the development of this surface during the hydration process is calculated. Implicit information is generated about the rate at which individual particles dissolve. Further it should be noted that, on the assumption of certain rate laws for the rate of penetration of the reaction front, particle kinetics can be derived from the overall hydration data. In this way the overall kinetics can be linked to particle

kinetics. In such a "backward approach", however, it is almost impossible to account for the earlier mentioned effect of changes in the rate determining processes occurring simultaneously in particles of different sizes.

5.3 Particle Kinetics

When dealing with particle kinetics it is convenient to distinguish between at least two types of reaction, i.e. two rate determining mechanisms, viz.:

1. *Phase-boundary reactions*
2. *Diffusion-controlled reactions*

5.3.1 Phase-Boundary Reactions

If the reaction in a poly-size system is a pure phase-boundary reaction, the overall rate of reaction is controlled by the rate of reaction at the particle surface and the development, i.e. decrease, of the surface area of the reactant. Moreover, changes in the ion concentration in the liquid phase during the reaction will influence the rate of reaction.

For a flat surface area of the reactant and a constant ion concentration in the liquid phase, the rate of reaction can be described using a first order equation (Fig. 5.1a):

$$\frac{d\alpha}{dt} = \frac{d\delta_{in}}{dt} = k \tag{5.9a}$$

where δ_{in} is the penetration depth of the reaction front and $\alpha=\delta_{in}/\delta_{max}$ is the degree of hydration. For the progress of the penetration depth with time it follows:

$$\delta_{in} = k.t \tag{5.9b}$$

The value of the rate constant k depends on the chemical composition of the reactant and the ion concentration in the liquid phase. It might be a function of the degree of hydration as well.

For a spherical particle with radius $r_0=x/2$ and penetration depth $\delta_{in}(t)$, the degree of hydration is given by (Fig. 5.1.b):

$$\alpha_{x;\delta_{in}} = 1 - [\ 1 - \frac{\delta_{in;x}(t)}{r_0}\ ]^3 \tag{5.10}$$

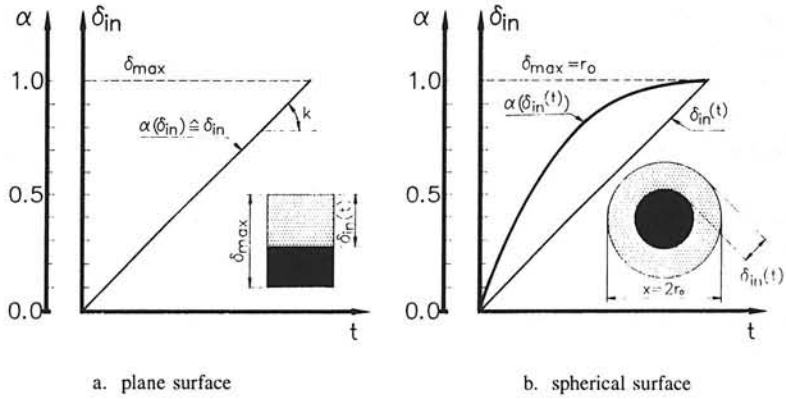

a. plane surface

b. spherical surface

Fig. 5.1 Schematic presentation of first order reactions.

For the penetration depth $\delta_{in;x}(t)$ it holds that (using rate equation (5.9b):

$$\delta_{in;x}(t) = k * t = r_0 * [\ 1 - (1 - \alpha_{x;\delta_{max}})^{\frac{1}{3}}] \tag{5.11}$$

With a constant rate of penetration $d\delta_{in;x}/dt=k$, the rate of hydration of the spherical particle x follows from:

$$\frac{d\alpha_x}{dt} = \frac{3.k}{r_0} * [\ 1 - \frac{k.t}{r_0}\ ]^2 \tag{5.12}$$

The rate of hydration of a spherical particle can be linked to the surface area $O_x(t)$ of the shrinking anhydrous core. For the magnitude of the decreasing surface area it holds that:

$$O_x(t) = 4.\pi * [\ r_0 - \delta_{in;x}(t)\ ]^2 \tag{5.13}$$

From eq. (5.11), (5.12) and (5.13) an expression can be deduced with which the rate of hydration of the spherical particle is written as a function of the surface area of the anhydrous core:

$$\frac{d\alpha_x}{dt} = \frac{3.k.O_x(t)}{4.\pi.r_0^3} \tag{5.14}$$

Attempts to relate the rate of hydration to the active surface area of the reactant dates back

to the late twenties. Maybe Werner [612] was the first who proposed a mathematical procedure to describe the rate of reaction as a function of the decreasing surface area of hydrating cement as early as 1928. In the absence of sufficient reliable information about both the hydration process itself and the hydration products that were formed, cement was considered to consist of chemically homogeneous particles, while the rate of the reaction front $d\delta_{in}/dt$ was assumed to be constant. On these assumptions the rate of hydration of a poly-size specimen could be calculated straightforwardly with the equation:

$$\frac{d\alpha}{dt} = K * O(t) \tag{5.15}$$

where K is a rate constant and O(t) the total surface area of anhydrous cement particles. Decades later expression (5.15), in combination with eqns (5.9b) and (5.13), has been discussed and applied by O'Connor et al. [407], Zur Strassen [645] and Halstead [225]. Both Werner and Zur Strassen commented that in their investigations the particle size distribution turned out to be a most important parameter in the overall rate of reaction.

The overall rate of hydration is proportional to the decreasing surface area of the anhydrous particles as long as the phase-boundary reaction is the rate controlling step. At low degrees of hydration this might be the case indeed. At later stages, however, when diffusion through an ever thickening product layer becomes increasingly important, the effect of the surface area upon the rate of hydration can become less pronounced [436].

5.3.2 Diffusion-controlled Reactions

As hydration proceeds, a gradually thickening shell of reaction products is formed around the anhydrous core. It is generally assumed that once a critical thickness of the shell is passed the reaction becomes diffusion-controlled. As early as 1925, Tammann [567] proposed an empirical formula for the rate of penetration of the reaction front for diffusion-controlled reactions, viz.:

$$\delta_{in}(t) = a * \log t + b \tag{5.16}$$

with a and b empirical constants. In a more fundamental approach the rate of penetration of a flat reaction front into a reactant can be related to the total thickness of δ of the product layer according to (Fig. 5.2):

$$\frac{d\delta_{in}}{dt} = \frac{k}{\delta_{in}} \tag{5.17}$$

in which k is a constant and is proportional to the diffusion constant. Integrating with respect to time t yields a parabolic rate formula for the total penetration depth, viz.:

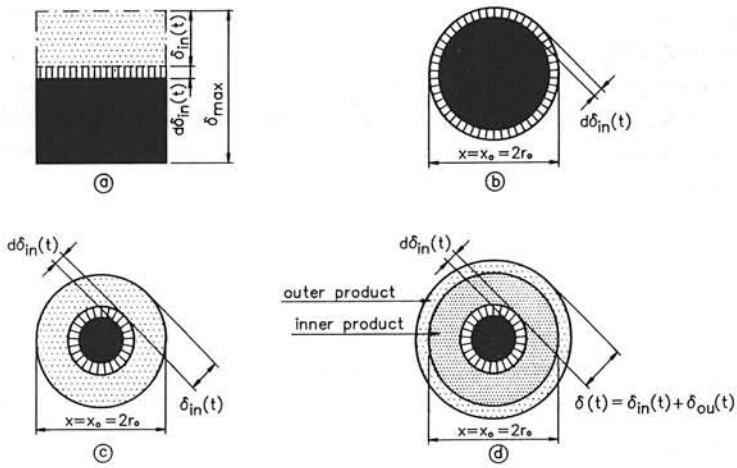

Fig. 5.2 Schematic presentation of hydrating particles.
a. Plane reactant surface area.
b. Jander [260]: spherical reactant surface / flat product layer
c. Ginstling-Brownshein [189]: spherical surface / spherical product layer
d. Carter [91]: spherical reactant surface / spheric product layer; inner and outer products

$$\delta_{in}^2 = 2.k.t \tag{5.18}$$

As early as 1927, Jander [260] derived an equation for the diffusion-controlled rate of hydration of a spherical particle. Neglecting the spherical shape of the product layer which surrounds the anhydrous core, he proposed the following expression (Fig. 5.2b):

$$[\ 1 - (1-\alpha_x)^{\frac{1}{3}}\ ]^N = \frac{2.k.t}{r_0^2} \tag{5.19}$$

In the original derivation Jander assumed a parabolic rate formula for the penetration depth, viz. N=2. In the case of linear kinetics eq. (5.11) is used. Jelenic et al. [264] applied the Jander equation for hydration of C_2S and β-C_2S. The best fit occurred when N=1.5 was used. The fit for N=1 and N=2 was also satisfactory. A modified form of the Jander equation is known as the Kingery equation:

$$[\ 1 - (1-\alpha_x)^{\frac{1}{3}}\ ] = K.t^{\frac{1}{2}} \tag{5.20}$$

The Kingery equation has been used by Oyefesobi [430] for the hydration of a cement type V-quartz system. For the rate constant K a value of $K=10^{-6}$/min was found, which is in reasonable agreement with values given by Kondo [306], viz.: $10^{-5}...10^{-8}$/min for hydrothermal lime-quartz reactions.

Plowman [446] used a modified Jander equation for the early hydration of a C_3A + C_4AF + gypsum system, viz.:

$$[\ 1 - (1-\alpha_x)^{\frac{1}{3}}\ ]^2 = \frac{2.k.t}{r_0^2} - C \qquad (5.21)$$

where k and C are empirical constants. From the good fit of experimental data Plowman concluded that diffusion through the hydration products should be the rate controlling step in the early stage (30 min) of hydration. Diffusion as the rate controlling mechanism in the early stage of hydration has also been suggested by Stein for the C_3A-gypsum system [551]. It should be noted that for the early diffusion mechanism Fick's *first* law of diffusion was assumed to be applicable.

In these equations the shape of the product layer which surrounds the anhydrous core was assumed to be flat instead of spherical. Consequently, good results and correct interpretations can only be expected in the very early stage of reaction when the product layer is still very thin. A formula in which the diffusion through a spherical diffusion layer is considered has been derived by Ginstling and Brownshtein [189]. In its original form their formula was (see [224]) (Fig. 5.2c):

$$[\ 1 - \frac{2\ \alpha_x}{3}\ ] - (1 - \alpha_x)^{\frac{2}{3}} = K.t \qquad (5.22)$$

where K is a constant depending on the concentration difference over the product layer, the diffusion coefficient D and the original particle radius r_0.

Kondo et al. [307] has reshaped this formula in order to simplify comparison with the original Jander formula. In its reshaped form, the result is:

$$[1 - (1-\alpha_x)^{\frac{1}{3}}\ ]^2 - \frac{2}{3}\ [1 - (1-\alpha_x)^{\frac{1}{3}}\ ]^3 = \frac{2.D.C.t}{a.r_0^2} \qquad (5.23)$$

where "a" is a reaction constant.

Carter [91] proposed an equation in which the ratio ν of the volume of the reaction product relative to that of the dissolved part of the reactant is also considered. His equation is (Fig. 5.2d):

$$[1 + (\nu-1).\alpha_x]^{\frac{2}{3}} + (\nu-1) * (1-\alpha_x)^{\frac{2}{3}} - \nu = K.t \qquad (5.24)$$

The effect of diffusion through the outer product on the rate of hydration has been emphasized by Taplin on several occasions. As early as 1959 he suggested that particularly at later stages diffusion through the outer product causes a decrease of the rate of hydration and would even become the rate controlling step. A modified form of the expression Taplin proposed for the hydration of spherical C_2S particles runs as follows *(Ibid. [307])* (eq. 5.25):

$$\frac{1}{D_i n}.[1-(1-\alpha_x)^{\frac{2}{3}}-\frac{2.\alpha_x}{3}]+\frac{1}{D_{ou}}.(\nu-1).\{1+\frac{2}{3}.(\nu-1).\alpha_x-[1+(\nu-1).\alpha_x]^{\frac{2}{3}}\} = \frac{2.C.t}{a.r_0^2} \qquad (5.25)$$

where D_{in} and D_{ou} are the diffusion coefficients of the inner and outer product, respectively. For $D_{in}=D_{ou}$ Carter's formula is used. For $D_{in}=D_{ou}$ and $\nu=1$ this formula corresponds with the equation of Ginstling and Brounshtein.

Diffusion through a product layer consisting of inner and outer product has also been investigated by Tsumura [596]. He used the Jander equation for the diffusion controlled part ($\alpha>\approx 20\%$) of C_4AF hydration:

$$[1 - (1-\alpha_x)^{\frac{1}{3}}]^2 = \frac{2.D.t}{r_0^2.\nu^2} \qquad (5.26)$$

where ν is the volume ratio of the reaction product and the dissolved material. The diffusion coefficient D was found to be dependent on the penetration thickness δ_{in} of the reaction front according to:

$$D = 0.16 * (\delta_{in})^{-3} * \nu^2 \qquad [\mu m^2/h] \qquad (5.27)$$

Kondo et al. [307], after summarizing and discussing several rate equations proposed prior to 1968, suggested a more sophisticated model for the hydration of C_3S. In accordance with Taplin's work he also distinguished between diffusion through inner and outer products. He further considered diffusion through a gradually dissolving intermediate layer or protective barrier (Fig. 5.3). During the hydration process, the rate determining mechanisms change from diffusion through the vanishing protective barrier (acceleration stage) via diffusion through the inner product (early deceleration stage) to diffusion through both the inner and outer product (late deceleration stage). For details of the formulae pertaining to this model, reference is made to the original paper [307]. Here it is only remarked that in the late deceleration stage (stage V) Fick's *second* law of diffusion was adopted:

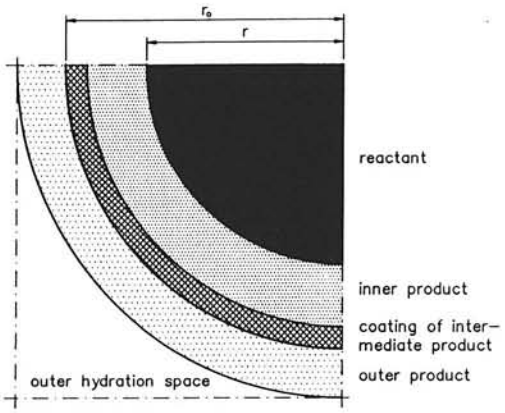

Fig. 5.3 Conceptional view of hydrating C_3S particle. (After Kondo et al. [307]).

$$\frac{\partial C(r,t)}{\partial t} = \frac{1}{r^2}.\frac{\partial}{\partial r}(D.r^2.\frac{\partial C}{\partial r}) \tag{5.28}$$

in which formula the diffusion coefficient D(r,C,T) was considered not to be constant. With increasing degree of hydration the diffusion coefficient would continuously decrease. Furthermore according to Kondo the overall reaction could be approximated by the empirical Jander equation for N>2 (generally N=2.5..2.8).

5.3.3 Particle Kinetics. Discussion

As long as a phase-boundary reaction is the rate controlling step it is obvious, that besides the rate of penetration of the reaction front the particle size distribution of the cement is of paramount importance for the resulting overall rate of hydration. Apart from the *particle size distribution* the *particle shape* will also affect the resulting rate of hydration. Note that cement particles are generally considered as spheres. Assuming spherical particles substantially simplifies mathematical modelling. As outlined in Chapter 2, however, there is no doubt that the assumption of spherical particles must be considered as a simplification of reality. A simplification, which inevitably gives rise to misinterpretations of observed hydration data. This also holds for the diffusion controlled particle kinetics, where diffusion coefficients deduced from hydration data implicitly mirror the effect of the particle shape.

With regard to the diffusion-controlled particle kinetics it should furthermore be noted that among the models considered so far Kondo's model is the most sophisticated one. Several authors, however, have criticized parts of Kondo's model. Taplin [573] pointed to the effect of particle size distribution, which was not explicitly accounted for in Kondo's

model. According to Stein [553] nucleation and growth phenomena were not properly dealt with, whereas Pommersheim [453] pointed to some incorrectnesses in the formulae. When reviewing the literature since Kondo's publication, however, it is obvious that in spite of these critical but correct remarks, his "multi-diffusion layer approach" has certainly stimulated researchers to work in a similar direction as he did.

5.4 Hybrid Kinetic Models

In this Section kinetic models are dealt with which explicitly allow for particle kinetics and the particle size distribution of the cement and, additionally, for one or more other relevant influencing factors, like the chemical composition of the cement and the state of water in the hydrating mass. In this context, attention will be paid to the ideas put forward by Taplin, Knudsen, Bezjak et al., Pommersheim et al., Röhling, Roth and Parrott, respectively.

5.4.1 Effect of Particle Size Distribution on the Overall Rate of Hydration

Early PSD-Considerations. Work by Taplin
The effect of the particle size distribution on the overall kinetics of a poly-size powder has been investigated by Taplin [573] by using linear kinetics for particle hydration, i.e. the penetration depth δ_{in} was considered to be *independent* of the particle radius R. From numerical evaluations it was concluded that, particularly at later stages of the reaction, the effect of the particle size distribution is generally about as great in comparison with a mono-size system as is a change from a linear to a parabolic reaction mechanism.

Considerations and Models proposed by Knudsen
Inspired by the work of Taplin, Knudsen [302] has formed models which show the particle size distribution to be of major significance for the overall rate of hydration. In 1980 he reported on the results of sensitivity studies, in which the effect of particle kinetics on the overall rate of hydration was investigated. The overall rate of hydration was calculated using the formula:

$$\alpha(t) = \int_0^\infty \alpha_x(t,x/2) * W(x)\, dx \qquad (5.29)$$

where: $\alpha_x(t,x) = \{(k.t)/(x/2)\}^n$, with n either 1 or 2 and k = a constant
$W(x)$ = cement mass per fraction

Knudsen concluded that the overall rate of hydration was virtually insensitive to the form of the kinetics of the single particles (n=1 or 2). The effect of the particle size distribution dominated the effect of the penetration law of individual particles.

In 1984 Knudsen [303] launched his "dispersion model". The influence on the rate of hydration of the small fractions (=0...15% by weight) was not considered in this model. The particle size distribution was represented by a simple expression, viz.:

$$W(r) = \frac{1}{r_0} * e^{-\frac{r}{r_0}} \tag{5.30}$$

where r_0 is a constant, depending on the fineness of the cement. For the rate of hydration of a single particle it was initially proposed:

$$\alpha(r,t) = e^{-\frac{r}{(k.t)^n}} \tag{5.31}$$

with n=1 for linear and n=1/2 for parabolic kinetics. In the final form of the dispersion model the linear and parabolic kinetics were written as:

$$t = t_0 + t_1.A \quad \text{(linear kinetics)} \tag{5.32a}$$

and

$$t = t_0 + t_2.A^2 \quad \text{(parabolic kinetics)} \tag{5.32b}$$

where: $A = \alpha/(1-\alpha)$
t_0 = time accounting for the dormant stage
$t_1 = r_0/k_1$, parameter referring to linear kinetics
$t_2 = r_0^2/k_2$, parameter referring to parabolic kinetics

Good results can be obtained with a combined formula such as:

$$t = t_0 + t_1.A + t_2.A^2 \tag{5.33}$$

Hydration processes could be described quite well with this formula up to a degree of hydration of about 70%. A change from linear to parabolic kinetics appeared to come too late to have any practical implication.

Bezjak [54], in a reaction on Knudsen's dispersion model, has attempted to generalize this model. For that purpose he utilized a particle size distribution as proposed by Aveejev [20]. Good results were obtained. This, as Bezjak argued, would not mean that the dispersion model could fully substitute earlier proposed mathematical models. In these models, to be discussed in the following Section, simultaneous contributions to the overall rate and overall degree of hydration of different rate determining processes are considered explicitly, which is not the case in Knudsen's dispersion model.

Considerations and Models put forward by Bezjak et al.
In several publications Bezjak has emphasized the change in rate determining mechanisms

that occur *simultaneously* in particles of different size [51-54]. Subsequently, nucleation and growth, phase-boundary reactions and diffusion through product layers are considered as rate controlling mechanisms [52]. The change from one mechanism to another takes place when a particle has reached a certain critical degree of reaction. For different particle sizes these critical degrees of reaction are reached at different times. The overall rate of hydration is the overall result of simultaneously operative processes and mechanisms.

It should be noted that, in line with the earlier quoted work by Taplin [578] and Tsumura [596], Bezjak's parameter studies have also indicated that diffusion through the outer product may *not* be neglected [51]. The effect of the outer product on the rate of hydration was accounted for with a modified Jander equation, viz.:

$$[\ (1+v.\alpha_x)^{\frac{1}{3}} - (1-\alpha_x)^{\frac{1}{3}}\ ]^2 = \frac{k_3.t}{r_0^2} \qquad (5.34)$$

For more detailed considerations concerning the change-over from a phase-boundary reaction to a diffusion controlled mechanism, see Section 6.5.2.2.

Mathematical Models put forward by Pommersheim

Interesting and stimulating work on mathematical modelling of cement compounds was carried out by Pommersheim et al. [450-454]. In 1980 he reported on a mathematical model for C_3S hydration. Similar to Kondo's model diffusion through an ever-thickening product layer was considered to be of paramount importance. The product layer was assumed to consist of an inner and outer product and a gradually disappearing intermediate or middle layer (see Fig. 5.4). The rate of hydration of individual particles was considered to be *independent* of their position in the system. It was concluded that at first, before formation of any middle layer has occurred, the combined effects of the chemical reactions at the particle surface and diffusion in the initially thin inner hydrate dominated the

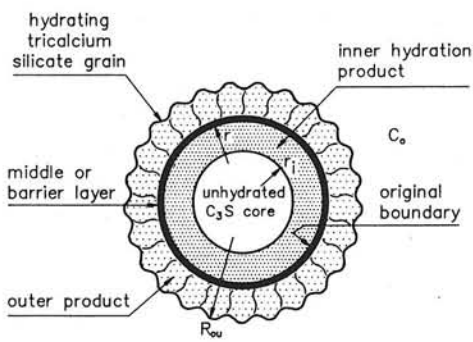

Fig. 5.4 Conceptional model for hydration of C_3S. (Pommersheim et al. [451]).

rate of hydration. During the induction period and the beginning of the acceleration period the resistance of the middle layer became predominant. In later stages the dominant resistance became diffusion through the outer hydrate layer. Pommersheim finally observed that in view of recent conceptional models (see [133,443]), in which the middle layer was layer was considered to follow the reaction front, his model could easily be modified to account for this phenomenon.

With Pommersheim and Frohnsdorff as co-authors, Brown et al. [72] has presented a more detailed model for C_3S hydration. The approach earlier proposed by Pommersheim is still quite obvious in this model. From his model Brown concluded that in the acceleration period CSH-formation was controlled by interfacial processes at the particle surface, whereas in the deceleration period the reaction products were formed in a diffusion controlled process.

For C_3A hydration of a mono-size sample Pommersheim et al. [454] considered three steps in the hydration process, viz. *a)* diffusion through the hexagonal barrier layer, *b)* dissolution and film diffusion through the mass transfer layer surrounding the barrier layer and *c)* crystallization after film diffusion through the boundary layer outside the particle. From curve fitting analyses of experimental data Pommersheim concluded that pore diffusion through the barrier layer, dissolution of this layer and crystallization phenomena were all contributing resistances in the proposed model, although diffusion through the barrier formed by the reaction products was considered to be the rate controlling step.

In another publication Pommersheim [453] draw particular attention to the effect of the particle size distribution on the kinetics of cement. Mathematical models based on average or mean sized particles to represent the distribution - and the author agrees with that statement - were said to be incorrect, since *no particle is really representative*. In line with Bezjak he also pointed to different, simultaneously occurring rate controlling processes. New in his model was the allowance for "dead particles", i.e. totally hydrated particles, which do not further contribute to the rate of hydration.

Mathematical Model proposed by Röhling

An approach close to that of Pommersheim and Bezjak is followed by Röhling [499]. In the early stage of hydration a phase-boundary reaction is considered with a rate of penetration of the reaction front according to:

$$\delta_{in;x}(t) = (k_1.t)^{k_2} \tag{5.35}$$

where $\delta_{in;x}(t)$ is the penetration depth at time t, whereas k_1 and k_2 are empirical constants. The rate of hydration of a spherical particle is obtained after inserting eq. (5.35) in eq. (5.10):

$$\frac{d\alpha_x}{dt} = \frac{3.k_1.k_2.(1-\alpha_x)^{\frac{2}{3}}}{\frac{x}{2}} * [\ \frac{x}{2} * \{\ 1 - (1-\alpha_x)^{\frac{1}{3}}\ \}\ ]^{\frac{k_2-1}{k_2}} \tag{5.36}$$

For the diffusion controlled stage of the hydration process Fick's *first* law of diffusion was applied. A concentration coefficient C_w was introduced in order to account for the amount of free water relative to the total volume of free water and the inner and outer products:

$$C_w(\alpha) = 1 - \frac{\nu.\alpha.\rho_{ce}^{-1}}{\omega_0+\alpha.\rho_{ce}^{-1}} \tag{5.37}$$

with ν the ratio between the volume of the reaction products and the reactant. For the rate of penetration of the reaction front in the diffusion phase it was assumed:

$$\frac{\delta_{in;x}}{dt} = D\ .\ \frac{C_w(\alpha)}{\delta(t)} \tag{5.38}$$

where D [$\mu m^2/h$] is the diffusion coefficient. With (5.38) and (5.10) it follows for the rate of hydration of a single particle x:

$$\frac{d\alpha_x}{dt} = \frac{3.D}{(\frac{x}{2})^2} * \frac{C_w(\alpha).(1-\alpha_x)^{\frac{2}{3}}}{[1-(1-\alpha_x)^{\frac{1}{3}}]} \tag{5.39}$$

The constants k_1 and k_2 and the diffusion coefficient D must be determined experimentally. The *overall degree* and *overall rate* of hydration is obtained by adding up the contributions to these quantities of the individual particle fractions.

5.4.2 Relative Humidity and Gel-Space Ratio as Rate Determining Factors

Effect of Relative Humidity

As suggested by Röhling the state of water in the hydrating mass must be considered as a factor of paramount importance. A significant effect of changes in the state of water in the hydrating system on the rate of hydration has also been emphasized by Knudsen [304]. From experimental data he concluded that, particularly at later stages adsorption processes in the pore system might become the rate controlling mechanism.

Thermodynamic considerations teach us that the state of water is linked to the relative humidity in the pore system. It is reasonable, therefore, that the rate of hydration can also

be considered in connection with the relative humidity. According to Parrott et al. [438] the effect of the relative humidity on the rate of reaction could be allowed for using a reduction coefficient β_{RH}:

$$\beta_{RH} = \left[\frac{RH - 0.55}{0.45} \right]^4 \qquad \text{for } RH > 0.55 \tag{5.40a}$$

$$\beta_{RH} = 0 \qquad \text{for } RH \leq 0.55 \tag{5.40b}$$

Because of the power 4 in eq. (5.40a) the rate of hydration will be almost zero when the relative humidity drops down to about 70%.

The effect of the relative humidity (RH) has also been considered by Jonassen [271]. Based on earlier work by Bažant, who, in turn, had based his approach on ideas put forward by Powers, Jonasson proposed a reduction coefficient β_{RH} as follows:

$$\beta_{RH} = \frac{1}{1 + \left[3.5 * \left(1 - \frac{RH}{100}\right) \right]^4} \tag{5.41}$$

The reduction factors according to eq. (5.40) and eq. (5.41) are shown in Fig. 5.5. In most practical situations the RH in the pore system will not drop below 85% (Powers: 90%). The figure shows that a small decrease of the RH can result in a significant reduction of the rate of hydration.

Recently Ho et al. [244] discussed the effect of the relative humidity on cement hydration in connection with the consequences for the quality of the concrete. From experimen-

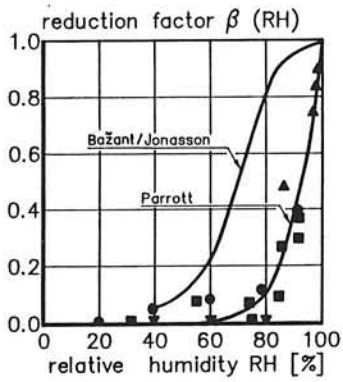

Fig. 5.5 Effect of relative humidity on the rate of hydration according to different authors. Note: Effect of carbonation not considered explicitly.

tal work it was concluded that at humidity levels below 80% hydration becomes negligible and so the quality of concrete. This value is in good agreement with the values indicated in Fig. 5.5. The practical consequence of this is that in arid areas concrete surfaces should be protected against early drying to avoid a dramatic decrease in strength.

Effect of Gel-Space Ratio

According to Verbeck [601] the relative rate of hydration is a function of the gel-space ratio $X(\alpha)$ discussed in Section 4.9.3. The relationship between these two quantities is shown in Fig. 5.6a for two w/c ratios. A correlation between the relative rate of hydration and the gel-space ratio is quite reasonable since the gel-space ratio can be considered as the pendant of the water concentration factor C_w proposed by Röhling (Section 5.4.1). The relationship between the two quantities is illustrated in Fig. 5.6b. A good correlation between the water concentration factor and the rate of hydration inevitably implies an equally good correlation between the rate of hydration and the gel-space ratio. Note that in both cases the established correlations have a distinct phenomenological character.

5.4.3 Kinetic Models allowing for Chemical Composition of the Cement

In the foregoing Sections emphasis was placed mainly on particle and overall kinetics. Only minor attention was given to the effect of the chemical composition of the cement on the rate of hydration. From the discussion, or controversy, about hydration mechanisms, viz. hydration at equal fractional rates of independent hydration in Section 3.5, it is obvi-

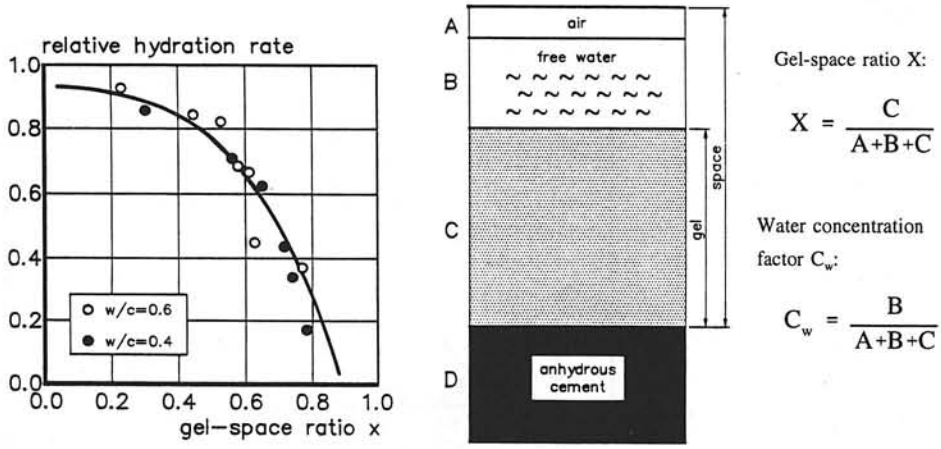

Fig. 5.6 *a)* Relative rate of hydration as a function of the gel-space ratio according to Verbeck [601].

b) Gel-space ratio $X(\alpha)$ and water concentration factor C_w - schematic.

ous that the chemical composition of the cement should be allowed for in kinetic models in one way or another. In this respect the work of Roth and Parrott will be considered.

Roth: Mathematical Procedure for Predicting Adiabatic Hydration Curves
Interesting and practically orientated investigations on the effect of both the clinker composition of the cement and the gypsum content on the rate of hydration have been carried out by Roth [504]. A simple formula was proposed, with which adiabatic hydration curves could be approximated quite accurately for hydration times exceeding 1.5 days. In his formula, viz.:

$$Q(t) = 100 + (a.t^{-1} + b)^{-1} \tag{5.42}$$

Q(t) is the heat of hydration liberated at time t, whereas a and b are constants depending on the clinker composition, gypsum content and cement fineness. The benefit of a simple formula with only two constants lies in its applicability for practical purposes. One should bear in mind, however, that behind the simplicity of this expression most complex processes and mechanisms are operative, which are still waiting for explicit modelling. The final result in the form of eq. (5.42) cannot, therefore, be considered as a *model* in the proper sense of the word, but should be judged as a phenomenological *calculation procedure*.

Parrott: "Multi-Compound Model"
An approach which comprises more elements so as to make it a real model has been followed by Parrott et al. [436]. He proposed to consider the overall rate of hydration of cement as the result of the individual rates of hydration of the cement compounds. These compounds are assumed to react independently from each other (Section 3.5.2). In the model both nucleation and growth mechanisms and diffusion through hydration products were considered as rate controlling steps.

The main input for Parrott's model consists of the hydration curves of individual compounds. For these hydration curves Parrott used curves fitting the average of hydration curves presented in the literature. Fig. 5.7, taken from [435], shows that in individual cases compound hydration may significantly deviate from the fitted curves. In this respect one should bear in mind that the mean or "design hydration curve" for, for example, alite (Fig. 5.7a) is expected to represent a wide range of w/c ratios (from ω_0=0.35 to 0.65), of fineness of the cement and curing conditions (paste hydration as well as ball-mill hydration). Using hydration curves for differently cured specimen for the determination of representative design curves can only be justified in the light of the practical goal to achieve workable predictive methods, but deserves critical appraisal from the materials science point of view. Parrott's approach must therefore be judged as a straightforward and certainly welcome attempt to make progress in a very complicated field rather than a step forward in understanding mechanisms which do or may occur in a hydrating and hardening system. Parrott's observation that in a substantial number of cases measured hydration curves could be approximated with a coefficient of variation of about 10% does not eliminate this point of reluctance.

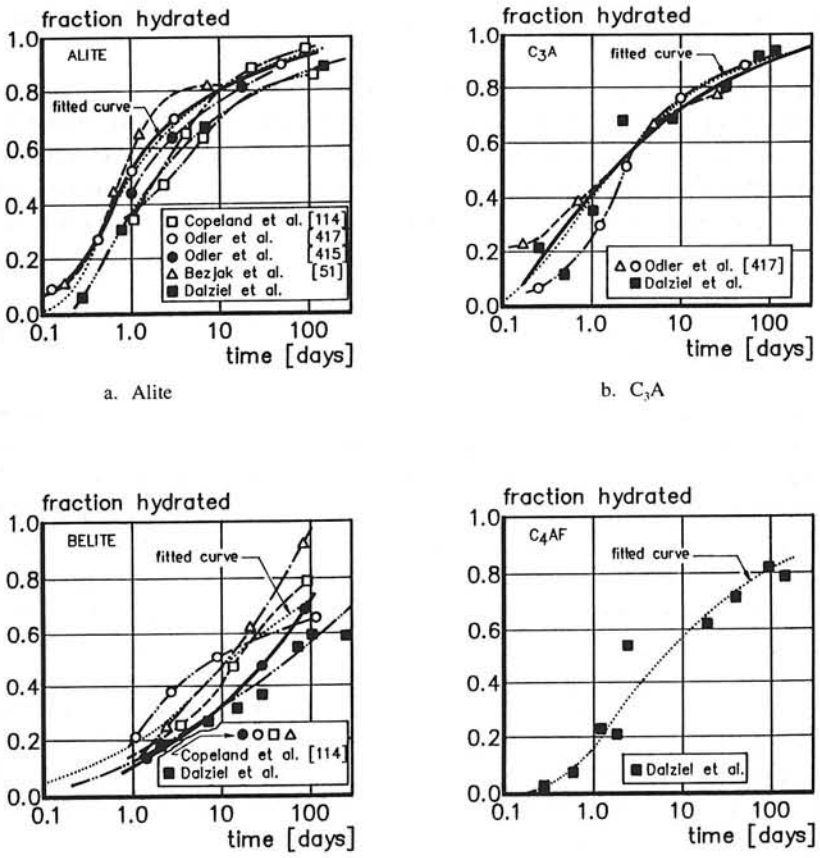

Fig. 5.7 Hydration curves of individual constituents with mathematically determined mean curves (from Parrott et al. [435]).

5.4.4 Overall, Particle and Hybrid Kinetic Models. Intermediate Evaluation

In the mathematical kinetic models discussed so far nucleation and growth, phase-boundary reactions and diffusion processes were considered, as well as effects of the particle size distribution, the relative humidity and the chemical composition of the cement.

With respect to the effect of particle kinetics on the overall rate of hydration it should be noted that several authors seem to be able to reach satisfactory approximations of experimental data using both Avrami's equation and the Jander equation [168,264]. This is remarkable since the Avrami equation refers to a nucleation and growth mechanism, whereas the Jander equation only refers to diffusion controlled processes!

The majority of mathematical models for cement hydration are based on the assumption

of hydration at equal fractional rates. An exception is Parrott's multi-compound model. The fact that good results can be obtained with such fundamentally different models - models which even exclude each other - is a strong argument in favour of Taplins's statement that agreement between theoretical and experimental data does not necessarily prove the correctness of a model, but merely fails to eliminate it as a possible model [572].

Although the *rate* of hydration of individual compounds may differ quite substantially, it has been suggested that the rate determining *mechanisms* operative at different times are basically the same for each compound [596,635]. This would imply that, in essence, mathematical models proposed for, for example, hydration of C_3S, can also be applied successfully for other compounds. In this respect it should be noted that comparable hydration mechanisms of cement compounds do not necessarily imply that the composite cement hydrates according to these mechanisms as well. Hydration of C_3S, for example, exhibits some particular differences compared with cement hydration [266,294,538].

With respect to conclusions drawn from comparisons of experimentally and mathematically obtained data Bezjak [53] has noted that recent observations of so-called "Hadley grains" [26,468], the difference in diffusion coefficients of individual product layers [267] and the possible existence of membranes between hydration layers [144], call for an increase of parameters that should be considered in mathematical models. Similar statements have been put forward by Pommersheim et al. [454]. One should be careful, however, when increasing the number of model parameters. Models with more than three free parameters might be strong in being able to fit almost any hydration curve, but become increasingly weak in proving the correctness of the assumed hydration mechanisms!

Several aspects that might have a more or less significant effect on the rate of hydration have not been explicitly dealt with in the foregoing. Some of these aspects are expected to be quite important in view of either hydration kinetics or formation of structure. Relevant aspects are the following.

1. Early Flocculation and Particle Agglomeration

Early flocculation and agglomeration of cement particles has been observed by several authors (Section 4.2.1.3). According to Schlüssler [518] mathematical kinetic models should account for this aspect. In this respect recent observations by Odler et al. [421] are of interest. With increasing hydration time the number of particles in a cement-water system was found to decrease. In Chapter 7 this aspect will be covered in more detail.

2. Particle Interaction

It is obvious that particle interaction is a prerequisite for strength development. A possible effect of particle interaction on the rate of hydration has been suggested by Taplin [572]. Pommersheim et al. [450,451] presumed an effect of particle interaction since at later stages of hydration the diffusion coefficient turned out to decrease. This decrease was attributed to the merging of the outer product of adjacent particles. The merging process as such, however, was not modelled. Schlüssler [518] pointed to the interaction of very small and large particles and stated that the effect of this interaction cannot be sub-ordinated to the principle of some law of evolution. In other words, this effect should be modelled *explicitly*.

3. Formation of Structure

One could state that models, in which diffusion through a thickening product layer is considered as a rate determining step, implicitly allow for the effect of structural formation on the rate of hydration. This interpretation, however, does not cover what is generally understood by structural formation. Structure development is the formation of a porous matrix built up of expanding particles which come in contact with each other at several points. The merging of the outer products of expanding particles has been discussed by Taplin [573] and Pommersheim et al. [450] in view of a possible effect on the rate of hydration. Granju et al. [205] referred to merging mechanisms in connection with strength development of cement paste. Explicit modelling of structural formation and its influence on the rate of hydration, however, is still lacking.

4. Effect of Gypsum and Additives

Much experimental work has been carried out in the past to investigate the effect of gypsum and additives on the rate of hydration and strength development. Models for cement hydration proposed so far, however, do not explicitly account for these effects.

5.5 Integrated Kinetic Models

As stated in Section 5.1 integrated kinetic models allow for the interaction between the progress of the hydration process, on the one hand, and structural formation, on the other. In Section 5.1 it has further been stated that several computer-based simulation models can be considered as integrated models. At least those models indeed simulate the interactions between chemical and physical processes and account for stereological aspects of hydration and structural formation as well.

5.5.1 Concepts put Forward by Frohnsdorf et al. and Jennings [2])

Probably Frohnsdorf et al. [178] were the first to point to computer simulations as one of the most promising approaches for future work on modelling of hydration processes. He proposed a simulation model with which he could predict the development of, among other things, the progress of the hydration process, the porosity and the composition of the aqueous phase as a function of the cement composition, the particle size distribution and the w/c ratio. Although Frohnsdorf had to admit that because of the complexity of the hydration process his model could not be considered as realistic at all points, he could never-

[2]) After the first edition of this thesis was published a large number of extremely interesting papers and reports on numerical modelling have been published by Garboczi and Bentz. Their work will not be discussed in detail here. The simulation model developed by these researchers would fall within the definition of integrated models as adopted in this book. For a review of modelling activities in the last decade reference is made to the proceedings of the NATO-Modelling workshop mentioned in footnote [1]) in Section 5.1 (See also PREFACE TO THE SECOND EDITION).

theless show that his simulation model was able to account for a number of aspects of cement hydration and structural formation which were not covered in traditional analytical models. Anyhow, his preliminary results can be judged as an illustration of the vast potential of computer-based models.

More recently the potential of computer-aided simulations of hydration processes and structural formation has been discussed comprehensively by Jennings [268]. Though his publication was mainly conceptual and no results were shown, the advantages of simulation models outlined by Jennings, and earlier by Frohnsdorff, are most interesting and certainly realistic.

5.5.2 Preliminary Delft Studies

5.5.2.1 General

It is along the lines put forward by Frohnsdorf and Jennings that computer simulations for cement hydration and structural formation were carried out at the Delft University of Technology. These Delft studies actually started in 1984, and were inspired by the work by Taplin [570,572], Kondo et al. [307], Knudsen [302,303], Pommersheim et al. [451, 452] and Bezjak et al. [50,53]. Several statements by Sereda et al. [532], Krokosky [315], Greene [209] and Polak et al. [449] on the presumed, but until then not quantified, correlation between the contact area between expanding cement particles and the development of material properties have also constituted a great challenge to investigate and quantify the presumed correlations.

In view of investigations regarding the possibilities of quantification of the contact area between hydrating particles and the presumed correlation between contact area and material properties due attention must be given to the stereological aspect of hydration processes and structural formation. A proposal for a mathematical determination of the contact area has been elaborated in a computer-based model called "HYDRASIM", the acronym for HYDRAtion SIMulation. This model has been described extensively by Berlage [46] and is to be considered as the predecessor of the simulation model that will be presented in detail in Chapter 6. Some particular features and results of these preliminary Delft studies will be discussed in the following Sub-Sections.

5.5.2.2 Stereological Aspects of Hydration and Formation of Structure

Particle Spacing in Cement-Water Systems

An investigation of the stereological aspect of cement hydration and structure formation starts with the determination of the centre-to-centre particle spacing in the cement-water system. For reasons mentioned in Chapter 2 the particle size distribution will be described using the Rosin-Rammler equation (see also eq. (2.1)):

$$G(x) = 1 - \exp(-b.x^{n}) \qquad [g] \qquad (5.43)$$

where G(x) is the under-size weight of particles ≤x μm. By definition the constants n and b are so determined that $G(x \rightarrow \infty)=1$ g. On the assumption of equal centre-to-centre distances between particles which belong to the particle fraction F_x, the particle spacing L_x in a cement-water system using a w/c ratio ω_0 can be calculated according to:

$$L_x = \frac{\text{(volume paste)-(volume cement >x)}}{\text{number of particles in fraction } F_x}$$

or:

$$L_x = \frac{\left[\frac{G(\infty)}{\rho_{ce}} + \rho_0.G(\infty)\right] - \frac{G(\infty)-G(x-1)}{\rho_{ce}}}{N_x} \qquad (5.44)$$

where:

$N_x = W_x / (v_x.\rho_{ce})$ = number of particles x in fraction F_x
$W_x = dG(x)/dx$ = mass of cement per fraction F_x
$v_x = (1/6).\pi.x^3$ = volume of a particle with diameter x.
ρ_{ce} = specific mass of cement [g/cm^3]

For a fine, normal and coarse cement the centre-to-centre spacings in a cement-water system with ω_0=0.4 are shown in Fig. 5.8. The effect of the w/c ratio on the interparticle spacing is given in Fig. 5.9. In a system with ω_0=0.4 the interparticle spacing of small

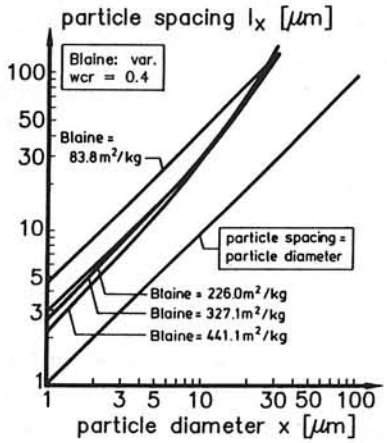

Fig. 5.8 Interparticle spacing as a function of cement fineness (Blaine). ω_0=0.4.

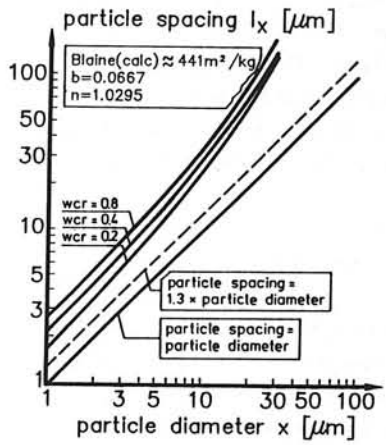

Fig. 5.9 Interparticle spacing as a function of w/c ratio. Blaine≈550 m^2/kg.

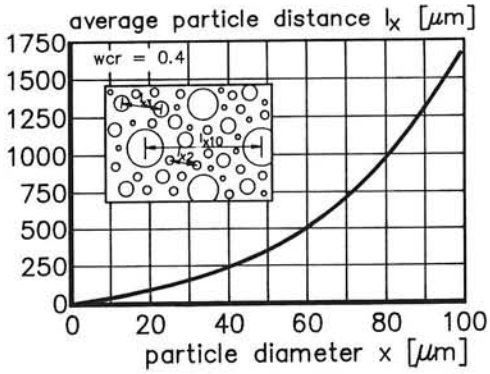

Fig. 5.10 2D-representation of particle spacing in poly-size specimen. Paste: ω_0=0.4.

particles, say x≤3 μm, varies from 7 μm for Blaine=441 m^2/kg up to 13 μm for Blaine = 84 m^2/kg. The interparticle spacing of particles ≤1 μm varies from 2 to 5 μm for the aforementioned Blaine values. A two dimensional sketch of the particle distances is shown in Fig. 5.10. In foregoing considerations a stable dispersion has been assumed, i.e. bleeding effects were ignored.

From Figures 5.8 and 5.9 it can easily be deduced that on the assumption of a ratio between the volume of reaction products and the reactant ν≈2.2, the outer product of larger ger particles will merge with smaller particles. With HYDRASIM, particle growth and the formation of interparticle contact area are calculated in a step-wise procedure. The thickness of the product layer around the anhydrous core of a cement particle *and* the contact area reached at the end of each time step constitute the input for the calculation of a hydration increment in the subsequent time step. In HYDRASIM the rate of hydration in each time step was calculated according to a modified Carter equation, in which the diffusion resistance of the outer product was also taken into account. Either first, second or third order kinetics for the penetration rate of the reaction front were considered [46].

Determination of Contact Area

For the determination of the interparticle contact area concessions had to be made with respect to the assumed spherical shape of the expanding particles. If one would stick to the spherical shape of particles, even for the hydrating and expanding particles, one would, due to stereological and granular constraints, only be able to calculate the *number of contact points* between expanding particles, but not a contact area. In HYDRASIM the following solution was chosen to solve this geometrical problem (see Fig. 5.11). A basic assumption was that, in the first instance, the expanding particles would preserve their spherical shape. On expansion a particle with an initial diameter x will encounter particles <x. The encountered particles are assumed to be pushed to the periphery of the outer shell which surrounds particle x. When being pushed to the periphery these particles will in turn encounter other small particles, which will also be pushed in an outward direction, albeit

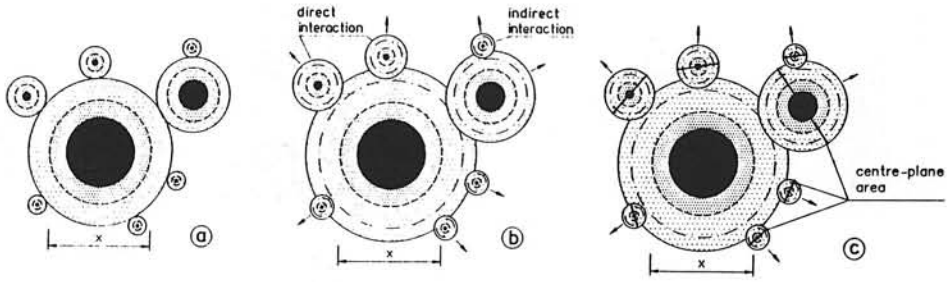

a. Expansion and Expulsion b. Embedding of particles c. Contact area - schematic

Fig. 5.11 Schematic representation of particle interaction and particle expulsion in HYDRASIM (Preliminary Delft studies [46]).
a: situation after expansion of central particle and expulsion.
b: Encapsulation mechanism: position of particles if no ex-pulsion of particles occurs.
c: Contact area: schematic.

indirectly this time (Fig. 5.11b). The indirectly encountered particles can in turn also encounter some small particles, etc. The agglomeration of the central particle x and the directly and indirectly encountered particles is indicated as a *free cluster* C_x. The number of particles encountered and pushed in an outward direction in a time step Δt depends on the momentary composition of the *reduced paste*. The reduced paste is defined as the paste fraction that consists of the water left for hydration (free capillary water) *plus* the free particles and free clusters with central particles with a diameter <x μm.

The contact area belonging to one single cluster C_x is now defined as the sum of centre-planes of all directly and indirectly encountered particles (Fig. 5.11c). The contact area in the hydrating system is found by adding up the centre-plane areas of all free clusters.

5.5.2.3 Effect of Particle Interaction on Rate of Hydration

For quantification of the effect of particle interaction on the rate of hydration several options were considered.

1. Water Withdrawal Mechanism
As a first option the encountered and still hydrating particles were considered to withdraw water, i.e. OH^- ions, from the water diffusing to the anhydrous core of a central particle (Fig. 5.12a). An overall reduction factor for the rate of hydration of the system was defined as the quotient of the total contact area of the whole system and the total outer surface of the free clusters. In this concept the rate of hydration of the expelled particles - if still hydrating - was assumed *not* to be reduced due to partial engulfment by the outer shell of the central particles.

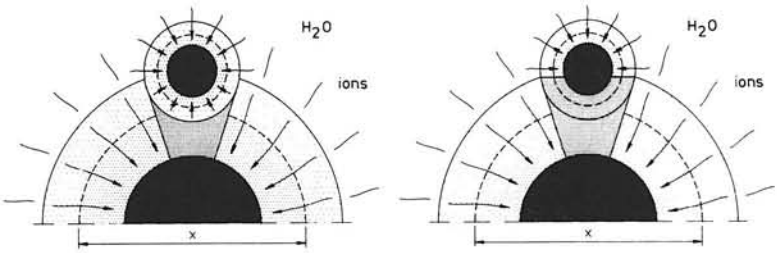

a. Water withdrawal mechanism

b. Complete shielding

Fig. 5.12 Rate reduction mechanisms caused by particle interaction [46].

2. Complete Shielding
Water and ions diffusing in the direction of the anhydrous core of the central particle are stopped by the expelled particles located at the periphery of the outer shell of the centre particle (Fig. 5.12b). The suggested shielding mechanism is considered conservative, since the outer product of the expelled particles will in essence be able to transport water to the central particle.

5.5.2.4 Parameter Studies carried out using HYDRASIM

The main aim of the preliminary studies was to investigate the effect of the contact area on the rate of hydration and to check whether a distinct correlation existed between the total contact area and the strength. The effect of the adopted particle kinetics (first, second and third order) on the overall rate of hydration was investigated as well. In order to check our assumptions experimental data published by Keienburg [287] and Knudsen [302] has been used as a reference. A summary of the most relevant results will be presented. For details, reference should be made to the original report [46].

5.5.2.4a Conclusions with respect to the Rate of Hydration

Order of Kinetics
The order of the particle kinetics, viz. first order kinetics (phase-boundary reaction), second order kinetics (diffusion process) or third order kinetics ($d\alpha/dt$=constant), substantially influences the overall kinetics. To fit the experimental data of Knudsen a first order reaction proved to be the best fit, whereas for a good fit of some of Keienburg's data a second order reaction turned out to give the best results.

Effect of Particle Size Distribution
A comparison of the calculated degree of hydration and experimental data revealed that

the effect of the particle size distribution on the rate of overall hydration could be predicted quite accurately. Reversely, and in agreement with the literature on this point, it was found that the particle size distribution significantly influenced the overall rate of hydration.

Diffusion-controlled Reactions
In case diffusion through the product layer around the anhydrous core is the rate controlling step, the exact form of the diffusion equation turned out not to influence the final results significantly. This is in accordance with Knudsen [302].

Effect of Particle Interaction on the Rate of Hydration
Contrary to what was expected, a significant reduction of the rate of hydration due to the formation of contact area between expanding particles could not be established. It was observed, however, that for a firm statement on the relevance of particle interaction on the rate of hydration more research would be required [46].

5.5.2.4b Correlation between Contact Area and Strength Development

Relationship between Contact Area and Degree of Hydration
The simulation model revealed a more or less linear relationship between the degree of hydration and the total contact area (Fig. 5.13). This is an interesting result in view of the well-known linear relationship between degree of hydration and strength (Section 4.9.4). The assumed (linear) relationship between contact area and strength development thus seems to exist.

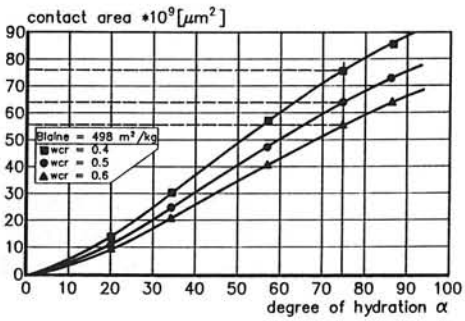

Calculated contact area for α=77%			Abram's Law: $f_c = A * B^{-\omega_0}$	
wcr	Contact Area [μm^2]		f_c	Coeff. of Abram's Law
ω_0	Abs. $*10^9$	rel. %	%	
0.4	≈78.0	100	100	A = 200
0.5	≈65.5	84	84	B = 5.72
0.6	≈57.0	73	70	predicted

Fig. 5.13 Correlation *Strength - Total Contact Area* for different w/c ratios found in preliminary Delft studies (after [46]).

Effect of WCR on the Relationship between Total Contact Area and Strength
It is well-known that the relationship between strength f and degree of hydration α strongly depends on the w/c ratio (Section 4.9.4). Consequently, curves representing the f/α-relationship have to be established for mixes with different w/c ratios. With the calculated contact area, however, the effect of the w/c ratio is accounted for implicitly. It could be expected, therefore, that the relationship between contact area and strength will be more or less *independent* of the w/c ratio. In order to check this assumption the contact area has area has been calculated for different w/c ratios, viz. ω_0=0.4, 0.5 and 0.6. It was found that the relative *decrease* of contact area with *increasing* w/c ratio corresponds to a decrease in strength in the same way as might be expected from the Abrams' law quoted in Section 4.5.4 (see Fig. 5.13). This result seems to substantiate the idea that the contact area might be considered as an important, and probably unambiguous strength parameter!

5.5.2.5 Preliminary Delft Studies: General Discussion, Evaluation and Outlook

The ability of HYDRASIM to model the progress of the hydration process quite accurately, and the ability to quantify the correlation between the contact area and strength development are two reasons to assume that the basic idea behind the model is well-founded. Agreement between experimental results and theoretical predictions, however, are not sufficient to conclude to the correctness of a model. Several assumptions made in the preliminary studies certainly require critical evaluation.

The first and maybe most important point of criticism refers to the assumed mechanism of outward directed expulsion of particles by expanding central particles. That such a mechanism occurs must be considered as *incompatible* with a number of generally accepted features on structural formation (see Section 4.4). An argument in favour of the mechanism could be that it inherently presupposes constancy of the density of the reaction product, i.e. of the gel. A constant density of hydration products throughout the hydration process has been proposed by several authors (see Section 4.4), and is also one of the axioms in the interesting work of Granju et al. [205]. Some expansion mechanisms put forward to explain early volumetric changes in hydrating pastes (see Section 4.8) can also be considered as in agreement, or at any rate not in contradiction with the expulsion concept. Nevertheless there remain several serious points of criticism. A more realistic assumption would be that all particles have a fixed position in the hydrating system and become engulfed, wholly or in part, by the outer product of expanding particles. Such an engulfment or embedding mechanism will be elaborated in detail in Chapter 6.

A second point of criticism, associated with the point just raised, concerns the assumption that particles, even the small ones, keep their geometrical identity. As discussed in Chapter 4 the small particles, i.e. particles with diameter <3 μm, completely dissolve and hence do not preserve their original shape. Consequently, the centre-plane areas of small particles may not be considered to contribute to the development of the total contact area in the system in a similar way as the centre-plane areas of large particles do. Chapter 6 shows that there still exists an effect of the small particles on the development of contact area, but only in an *indirect* manner.

In addition to these points there are several aspects which have not been considered at all in the preliminary studies. Some of these aspects will be briefly mentioned here.

Change of rate determining processes
Bezjak's [51,53] statement, that particles belonging to different fractions might react according to different mechanisms at the same time, was not accounted for. Furthermore, a change of rate determining processes in the hydrating system *as a whole*, i.e. a change from a phase-boundary reaction to a diffusion controlled mechanism for *all particles at the same time*, was not considered.

Cement composition
The effect of cement composition on the rate of hydration, i.e. on the rate constants, was not considered. Also the effect of gypsum still has to be mathematically modelled.

State of water
The effect of water shortage during the hydration process was not investigated exhaustively. In view of recent work by Knudsen [304] and Parrott et al. [438] this point should be given more attention.

Interface aspects
In the preliminary Delft studies only *bulk* hydration was considered. As discussed in Chapter 4, matrix-aggregate interface studies have revealed that bulk or paste hydration is only partly representative of hydration in actual concrete. At the aggregate surface a kind of "wall effect" occurs, which can not easily be simulated using HYDRASIM.

The challenging results obtained in the preliminary Delft studies, on the one hand, and the shortcomings of HYDRASIM, on the other, have formed the basis for the development of a more comprehensive to be presented in Chapter 6.

5.6 Temperature Dependency of Rate Processes

5.6.1 General

The kinetic formulae discussed so far referred to isothermal reactions. Since the simulation of adiabatic processes is also envisaged, the effect of the reaction temperature on the rate of hydration must also be considered.

The rate of most chemical and physical reactions increase with increasing reaction temperature. A well-known rule of thumb says that with an increase of the reaction temperature by 10°C the rate of reaction increases by a factor of 2. This rule has been applied several times and it must be admitted that the results were not always bad [477,518]. Many experiments, however, have revealed that the rate factor is not a constant, but varies with the type of cement, the reaction temperature itself and the degree of hydration.

The effect of temperature on the rate of hydration is, in essence, very complicated. The

major reasons for the complexity of the subject are:

- the poly-mineral character of cement;
- the fact that different reaction mechanisms occur simultaneously;
- the effect of temperature on morphology and structure of the reaction products.

As discussed in Chapter 3, the rate of reaction of different constituents differs. Moreover, the morphology of the reaction products differ for different constituents and is also affected by the reaction temperature (Section 4.3.2). The morphology and the thickness of the shell of hydration products which surrounds an anhydrous core in turn determine the moment at which the hydration mechanism changes from a predominantly boundary reaction to a diffusion controlled reaction. As stated by Bezjak, this moment can in principle be different for different particle sizes [51]. The *temperature sensitivity* of a boundary reaction is known to be higher than that of a diffusion controlled reaction [41,192]. Consequently a change of rate determining mechanism will imply a change of temperature sensitivity of the hydrating system.

With regard to the diffusion controlled reaction one might have to differentiate between diffusion of ions through the pore water in the gel and diffusion of ions through a solid mass, or consider a mixture of these two possible mechanisms. For these two diffusion mechanisms a different temperature sensitivity may hold. Since the boundary and diffusion mechanisms can occur simultaneously, it is obvious that the temperature dependency of the reaction processes as observed on macro-scale is, in fact, the "net" result of the temperature dependency of individual processes and mechanisms. Parameters with which the temperature dependency is generally described must therefore be indicated as "apparent quantities". Parameters currently utilized are:

1. *The temperature sensitivity factor "g" of the cement;*
2. *Activation energy E;*
3. *κ-value of the cement.*

These parameters will be discussed in more detail in the following.

5.6.2 Temperature Parameters

5.6.2.1 Temperature Sensitivity Factor "g"

The "g-factor concept", or "g-concept", is based on the rule of thumb mentioned above. This rule in turn originates in a proposal by Van 't Hoff to allow for the effect of temperature on the rate of chemical reactions. Based on Van 't Hoff's proposal, Rastrup [477] proposed an expression of the form (see Fig. 5.14):

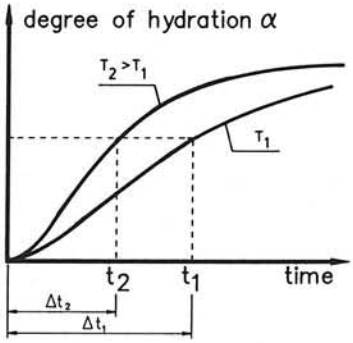

Rastrup

$$\Delta t_1 = 2^{\frac{T_2-T_1}{\gamma \cdot 10}} * \Delta t_2$$

$$\gamma = \frac{T_2-T_1}{10} * \frac{\ln 2}{\ln \frac{t_1}{t_2}} \qquad (5.45)$$

Fig. 5.14 Relationship between rates of reaction at different temperatures. *Left:* Diagrammatical representation. *Right:* Relationship applied by Rastrup

$$\frac{\Delta t_1}{\Delta t_2} = g^{\frac{T_2-T_1}{\gamma \cdot 10}} \qquad (5.46)$$

where: $\Delta t_1, \Delta t_2$ = period of time needed for an arbitrary increase of the reaction at temperatures T_1 and T_2, respectively [°C].
g = rate factor. Original proposal: g=2
γ = experimentally obtained correction factor.

In Rastrup's original paper the factor γ was taken as unity. In a later publication Rastrup [478] reported on γ-values ranging from 0.9 to 1.8. This means that for doubling the rate of reaction the temperature has to be increased between 9 to 18°C. The higher values were generally found for higher degrees of hydration. Rastrup deduced these values from hydration data published by Lerch et al. [603]. The γ-values were determined using a re-shaped form of eq. (5.46) as indicated in the insert of Fig. 5.14 (eq. (5.45)). Similar results were obtained by Kristulovic [313]. The latter author also found that the temperature sensitivity of the cement was most pronounced in the temperature range 30...35°C and for intermediate values of the degree of hydration, i.e. $0.2<\alpha<0.6$, the latter range depending on the prevailing temperature range.

Note that instead of the factor γ, the factor "g" can also be taken as the variable parameter. With γ taken as unity it holds that (Fig. 5.14):

$$g(T,\alpha) = \left(\frac{\Delta t_2}{\Delta t_1}\right)^{\frac{10}{T_1-T_2}} = e^{\frac{10}{T_1-T_2} * \ln\frac{\Delta t_2}{\Delta t_1}} \qquad (5.47)$$

An expression of the same form was used by the author [66], albeit that a different proce-

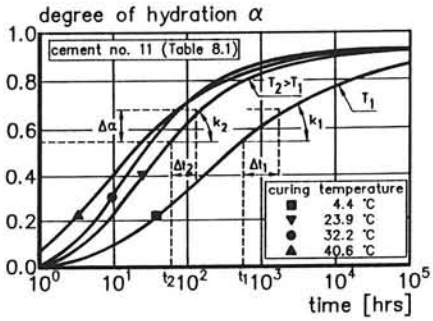

Fig. 5.15 Degree of hydration at different temperatures. Experimental data from [603].

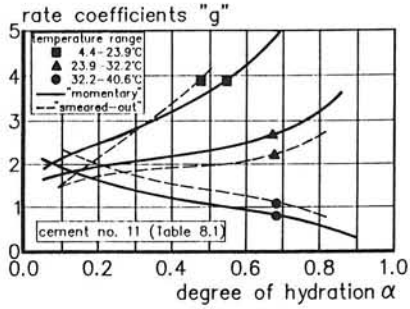

Fig. 5.16 "g"-values according to eq. (5.47) ("smeared-out") and eq. (5.48) ("momentary values").

dure was used for the determination of the g-values. The difference is illustrated in Fig. 5.15. The g-values now refer to the time increments Δt_i required for an *incremental* increase of the degree of hydration $\Delta\alpha$ and determined by the expression:

$$g(T,\alpha) = \left(\frac{K_1}{K_2}\right)^{\frac{10}{T_1-T_2}} = e^{\frac{10}{T_1-T_2}\cdot\ln\frac{K_1}{K_2}} \tag{5.48}$$

where K_1 and K_2 represent the momentary rates of hydration $\Delta\alpha/\Delta t_i$ (i=1,2) at temperature T_1 and T_2, respectively. The latter approach is considered to give more detailed information about the temperature dependency of the process in subsequent time steps as compared with Rastrup's "smeared-out approach".

From the hydration curves presented in Fig. 5.15, the g-values have been calculated according to eq. (5.47) and (5.48). The results are shown in Fig. 5.16. From this figure it is obvious that both equations generate g-values which vary with the degree of hydration and the reaction temperature. This is in agreement with the observations of Zacedatelev [639].

The Rastrup-approach has been modified significantly by Solovyanchik et al. to allow for changes in the rate controlling mechanisms [543]. Solovyanchik's approach is interesting because of his explicit allowance for the effect of temperature on the viscosity of water and the resulting effect on the rate of diffusion of water through the porous mass.

5.6.2.2 Activation Energy Concept

The activation energy E is one of the factors in the well-known Arrhenius equation used for quantification of temperature effects on rate processes [17]:

$$K(\theta) = A * e^{-\frac{E}{R.\theta}} \tag{5.49}$$

where: $K(\theta)$ = the rate factor
E = activation energy [J/mol]
Θ = absolute temperature [K]
R = gas constant = 8.31 [J/mol.K]
A = "collision number" or "frequency factor"

This expression was first launched by Arrhenius to quantify the influence of temperature on the inversion of sucrose. Assumptions on which the equation is based are [192]]:

1. *Equilibrium between inert and active molecules of the reactant;*
2. *Only active molecules are able to take part in the inversion process.*

With respect to the applicability of eq. (5.49) it was Arrhenius himself who noted that different rate functions had been found [17]. Nevertheless, Glasstone et al. [192] is quite positive with regard to the applicability of the Arrhenius function for a wide range of chemical reactions and physical, i.e. diffusion controlled, processes. The quantities A and E appeared to have an almost constant value provided that the temperature range from which they are deduced is not too wide.

Glasstone emphasized that the activation energy E is an *experimentally* obtained quantity. As indicated already at the beginning of this Section such experimentally obtained values are in fact the net result of the temperature dependency of several simultaneously occurring processes. From macro-level measurements it is, therefore, very difficult, if not impossible, to deduce the temperature dependency of individual processes. In this respect it is remarked that, according to Glasstone, the calculated and observed absolute values of diffusion rates can differ by more than 100%. It is obvious that deviations in reaction rates and diffusion coefficients of this order of magnitude will substantially affect attempts to bridge the gap between micro- and macro-level simulation models. On the other hand, it is information of this kind that brings us to accept simplifications and deviations from reality and to apply "apparent" temperature coefficients.

Analogous to the procedures for the determination of the g-values, the values of the apparent activation energy AE can be calculated as "smeared-out" values and "momentary" values. viz. (see also Fig. 5.15):

"smeared-out": $$AE(\theta,\alpha) = - \{(R.\theta_1.\theta_2)/(\theta_2-\theta_1)\} * \ln(t_2/t_1) \tag{5.50}$$

"momentary": $$AE(\theta,\alpha) = - \{(R.\theta_1.\theta_2)/(\theta_2-\theta_1)\} * \ln(K_1/K_2) \tag{5.51}$$

Results are shown in Fig. 5.17. It appears that similarly to the g-values the AE-values also depend on both the actual reaction temperature and the degree of hydration. A decrease of the activation energy in the temperature range from 32.2 to 40.6°C with increasing degree

of hydration is in agreement with trends mentioned by Copeland et al. [114], whereas an increase in AE-values with increasing degree of hydration as found to apply for the reactions in the low temperature range are in agreement with data of Brunauer et al. [78]. The AE-values presented in Table 5.1 further illustrate the wide range in which these values have been found by several authors. The wide scatter is predominantly attributable to a distinct effect of the reaction temperature on the morphology and structure of the reaction products (also [578]). A mathematical expression which describes the activation energy as a function of both the actual curing temperature and the degree of hydration is presented in Chapter 6.

5.6.2.3 Rate Concept proposed by Röhling

According to Röhling [499] the effect of temperature on the rate of reaction could be described with a rate factor $\kappa(T,\alpha)$, which relates the rate of reaction $\partial\alpha/\partial t$ at a temperature $T \neq 20°C$ to the rate of reaction at $T=20°C$. The following expression was proposed:

$$\kappa(T,\alpha) = \frac{(\partial\alpha/\partial t)_T}{(\partial\alpha/\partial t)_{20}} \tag{5.52}$$

Values of the rate factor $\kappa(T,\alpha)$ are shown in Fig. 5.18. The temperature dependency of the rate factor and its dependency on the degree of hydration are quite convincing. The κ-approach, although most interesting from the practical engineering point of view, will not be considered further in this review.

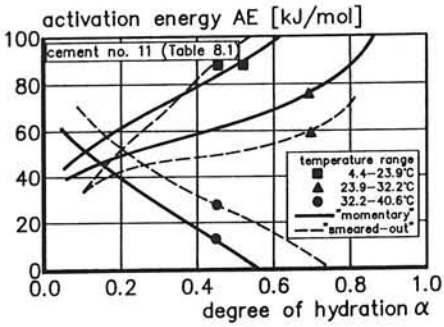

Fig. 5.17 Apparent activation energy according to eq. 5.50 ("smeared-out values") and eq. 5.51 ("momentary values").

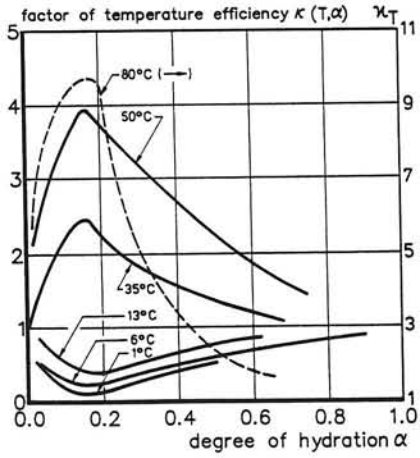

Fig. 5.18 κ-values as proposed by Röhling [499].

Table 5.1 Activation Energy. Summary of literature data

Author	ref.	year	C_3S	C_2S	C_3A	C_4AF	PC	BFS	Comment
Glasstone	[192]	1941	---	---	---	---	---	---	AE=15 kJ/mol for simple ions in aqueous solution
Schwiete et al.	[520]	1960	9	7.5	---	---	---	---	Temperature range 20-60°C
van Bemst	[38]	1960	---	---	---	---	---	---	Temp. range 4-40°C. Also negative temperature coefficients
Taplin	[570]	1960	≈42	75	---	---	42	---	AE-C_2S. At first very high values, then rapid decrease
				8	---	---	---	---	*Ibid. Brunauer*
Taplin	[571]	1960	---	---	---	---	<42	---	
Kondo et al.	[307]	1962	---	---	---	---	70	---	*Ibid. Halstead et al.*, Diss. of coll. Si.-powder
			---	---	---	---	33-77	---	*Ibid. Greenberg*, Diss. of coll. Si.-powder
			---	---	---	---	---	---	*Ibid. Kondo*, quartz-lime; AE=60 → 52 kJ/mol
			---	---	---	38	---	---	*Ibid. Tanaka*, (1966)
									Ibid. Layden, MgO: AE=67 kJ/mol, often >42 kJ/mol
Lawrence	[330]	1966	---	---	38-40	---	---	---	$C_3A+CaCl_2$; w/s ratio=10
Lawrence	[330]	1966	---	---	---	---	38±2	---	Temperature range 15-45°C
			---	---	---	---	33-22	---	*Ibid. Copeland et al.* t=3 → 7d; T=25°C
Tenoutasse	[585]	1967	---	---	50	---	---		$C_3A+CaSO_4.2H_2O$; w/s=1.2; Temp. range 20-40°C
			---	---	55-61	---	---	---	$C_3A+CaCl_2$; w/s=1.2; Acc. to Arrhenius and experimentally
Taplin	[572]	1968	31	50	---	---	---	---	Alite: 36-41 kJ/mol; MgO: 75 kJ/mol
Copeland	[114]	1968	41-26	---	---	---	---	---	Degree of hydration: α=0.6.....0.7
			---	56-31	---	---	---	---	Degree of hydration: α=0.4; belite resp. β-C_2S
Brunauer et al.	[77]	1973	---	---	---	---	20-32	---	Range 5-50°C; w/c=0.2-0.3; α=0.3.....0.6
			---	---	---	---	38-47	---	Range 5-50°C; α=0.4.....0.6
Courtault et al.	[116]	1977	---	---	---	---	46	50	BFS with 80% slag
Regourd et al.	[482]	1980	---	---	---	---	47	56	C_3S=73%, C_3A=4%, Temp. range 20-80°C
			---	---	---	---	42	---	C_3S=62%, C_3A=12%, $CaSO_4$=3.9%, Temp. range 20-80°C
			---	---	---	---	42	---	C_3S=62%, C_3A=12%, $CaSO_4$=5.6%, Temp. range 20-80°C
Roy	[507]	1982	---	---	---	---	44	49	Regourd: same order of magnitude
Fierens et al.	[167]	1982	50-49	---	---	---	---	---	w/s=0.6, Temperature range 5-45°C
Wu et al.	[628]	1983	---	---	---	---	44	49	According to method proposed by Knudsen (1980)
Byfors	[84]	1984	---	---	---	---	34	---	*Ibid. Pedersen*. For T<20°C: AE=3.5+1.47*(20-T) kJ/mol
Brown	[72]	1985	54-155	---	---	---	---	---	*Ibid. Kondo et al.* (1969), acceleration period
			21	---	---	---	---	---	*Ibid. Fujii et al.* (1974), post-acceleration period
Vollet et al.	[606]	1986	37	---	---	---	---	---	w/s=0.5, Temperature range 22-65°C

5.6.2.4 Relationship between g-Factor and AE-Values

The three approaches discussed are comparable in the sense that they all generate "apparent" values. When these values are deduced from the same sets of experimental data, they can easily be expressed in terms of each other. For the relationship between the temperature sensitivity factor g and the activation energy AE it holds that:

$$AE = \frac{\theta_1 * \theta_2}{10 * R} * \ln g \tag{5.53}$$

In the temperature range from 273 K to 313 K the activation energy varies from 62 ln g to 81 ln g kJ/mol. For g=2 the activation energy varies from 42 to 56 kJ/mol. For g-values from 1.3 to 2.5 the activation energy varies from 17 to 70 kJ/mol. These values are in good agreement with those of Table 5.1.

5.6.3 Temperature Effects. Discussion

The different concepts proposed to allow for the effect of temperature on the rate of hydration all have in common that they predict a *positive* effect of the temperature on the rate of hydration. It has been observed several times, however, that an increase of the reaction temperature has resulted in a *decrease* of the rate of reaction. Negative temperature coefficients have been observed for hydrating C_3A+gypsum pastes [396], aluminates [146], C_3S pastes [38,41], high alumina cements [82,493] and Portland cement pastes [45]. Negative temperature coefficients are particularly found in the temperature range from 4°C to 20°C [41,146]. They have been attributed to the formation of reaction products with different morphology and structure when formed at different temperatures. Hydration at low temperatures would promote the formation of products with a more open structure. This would allow boundary reactions to take place over a longer period of time in favour of diffusion controlled reactions. Since boundary reactions are more temperature sensitive than diffusion controlled reactions the low temperature pastes may hydrate faster over a longer period of time.

Apart from being elucidating, the explanation of the temperature related changes in morphology and structural formation and the associated effects of these changes on the rate of hydration, also demonstrates the complexity of the subject. The explanation further implies - and this is considered to be of major importance in view of mathematical modelling of the hydration process! - that:

"the rate of hydration cannot be considered and investigated separately from morphological considerations or without allowance for formation of microstructure".

With regard to the values of the activation energy given in Table 5.1 it is noted that these values must be considered too high to promote diffusion controlled processes [192,585].

Although it must be borne in mind that it is very difficult to conclude from observed overall phenomena which mechanism has been at work at a certain stage of the hydration process, there is certainly room to assume that phase-boundary reactions dominate the kinetics over quite a period of time, particularly in the low temperature ranges. This point will be considered in more detail in Chapters 6 and 7.

5.7 Models for Kinetics. Summary and Concluding Remarks

Towards Computer-Based Integrated Models

The kinetics of a poly-size and poly-mineral cement-water system exhibit granular, stereological, chemical and physical aspects. The multi-disciplinary character of processes and mechanisms involved in hydration and structural formation is the most complex factor in mathematical modelling of the reaction kinetics. It is almost self-evident, therefore, that kinetic models proposed so far are one-sided oriented to only a limited number of aspects involved. It is well-understood that models which only allow for a limited number of aspects, and hence of relevant parameters, may well predict the overall kinetics in terms of heat evolution, but fail, wholly or in part, in predicting structural formation. As an example models can be mentioned which exclusively focus on reaction kinetics of individual particles but do not allow for any effect of the formation of interparticle contacts in relevant processes and mechanisms in the hydration process. Ignoring the latter processes and mechanisms may give rise to misinterpretations of experimental data. Disregarding the actual shape of cement particles can be another source of misjudgment, for example concerning the penetration rates of reaction fronts in hydrating particles. Pronounced temperature effects also significantly contribute to the complexity of the subject. Finally it is remarked that current hydration models do not cater for the effect of pressure on the rate of hydration explicitly. The latter effects are expected to affect the hydration process significantly [81,625] and should, therefore, be considered in mathematical models if misinterpretations of the actual operating mechanisms and processes are to be avoided.

Comprehensive and consistent modelling of cement-based systems requires rigorous systematization of available knowledge on hydration processes and mechanisms of structure development and, subsequently, a well-considered synthesis of this knowledge in more or less complex algorithms. Allowance for the many non-linearities and discontinuities in prevailing processes and mechanisms as well as the complex interactions between these processes and mechanisms is, in essence, possible to a great extent by the use of computer-based models. These computer-based models enable the step-by-step evaluation and description of the relevant processes and mechanisms. In this way they can account for huge files of information pertaining to particular phases and aspects of the hydration process. Comprehensive models which allow explicitly for the effect of the formation of interparticle contacts, and hence of structural formation, on the rate of hydration have been termed integrated models. The potentialities of computer-based integrated models will be further discussed and elaborated in the subsequent chapters.

PART II

HYMOSTRUC

Computer Simulation of Hydration and Formation of Structure of Hardening Cement-Based Materials

Theoretical Part

Model Features

Determination of Model Parameters / Reliability and Predictability

6 HYMOSTRUC: SIMULATION MODEL FOR CEMENT HYDRATION AND FORMATION OF STRUCTURE

Theoretical part

6.1 General

In the preliminary Delft studies, presented in Section 5.5.2, the first steps were undertaken to quantify the development of the interparticle contact area and the effect of particle interaction on the rate of hydration. Moreover, a possible correlation between the interparticle contact area and strength development was investigated. The mathematical analyses were carried out using a simulation program called HYDRASIM, of which some particular features were discussed in Section 5.5.2.5. In that Section the development of a more comprehensive simulation model was mentioned. In the latter model the major shortcomings of HYDRASIM will be obviated. The model is called HYMOSTRUC, the acronym for HYdration, MOrphology and STRUCture formation. *Morphological aspects* of the hydration process, for example the effect of temperature on the characteristics of the reaction products - hardly addressed in HYDRASIM - will be given more attention, while the formation of microstructure will be treated more realistically. Also stereological aspects of paste-aggregate interface hydration will be dealt with. Changes in rate determining mechanisms will be allowed for as well. A temperature module is proposed, with which the effect of curing temperature on the rate of hydration, structure formation and strength development are also accounted for.

Structure of Chapter 6
In the Sections 6.2 and 6.3 stereological aspects of HYMOSTRUC are dealt with. Section 6.4 presents an algorithm which describes the interaction between hydrating and expanding particles. Several factors which influence the rate of hydration are discussed in Sections 6.5 to 6.7.

6.2 Stereological Aspects. "Cell" Definition

6.2.1 Particle Size Distribution

Just as in the preliminary Delft studies, the cumulative particle size distribution of the cement is described using the Rosin-Rammler [1]) function (see Section 5.5.2.2, eq. (5.43)):

$$G(x) = 1 - \exp(-bx^n) \qquad [g] \qquad (x \text{ in } \mu m) \tag{6.1}$$

[1]) Instead of the Rosin-Rammler distribution the actual particle size distribution can be used. The adoption of the R-R function, however, allows easy comparison with literature data and simplifies the mathematical evaluations to be outlined in the following Sections.

with constants b (b>0) and n so that $G(x \rightarrow \infty)=1$ g. The maximum particle size x_{max} is defined as the particle with no more than 0.01 g oversize weight:

$$G(x_{max}) = 0.99 \text{ g}$$

or:

$$x_{max} = e^{\left[\frac{1}{n} * \ln \frac{\ln 0.01}{-b}\right]} \tag{6.2}$$

For the minimum particle size $x=x_{min}$ a realistic value is taken, depending on the fineness of the cement (see Section 2.3). Disregarding particles $x<x_{min}$ as well as particles $x>x_{max}$ requires a correction factor in order to establish the physical consistency of eq. (6.1). The correction factor γ follows from:

$$\gamma = \frac{G(x=\infty)}{G(x_{max})-G(x_{min})} = \frac{1}{G(x_{max})-G(x_{min})} \tag{6.3}$$

For the majority of particle size distributions this correction factor does not exceed a value of $\gamma=1.02$.

The cement mass W(x) of the fraction F_x is obtained by differentiating eq. (6.1) with respect to x:

$$W(x) = \gamma * b * n * x^{n-1} * e^{-bx^n} \qquad [g] \tag{6.4}$$

For the volume V_x of all cement particles in fraction F_x it holds that:

$$V_x = \frac{W(x)}{\rho_{ce}} \qquad [cm^3] \tag{6.5}$$

where ρ_{ce} [g/cm^3] is the specific mass of the cement.

The number of particles N_x in fraction F_x is found by dividing the volume V_x of fraction F_x by the volume of a single particle v_x (N_x per gram of cement):

$$N_x = \frac{V_x}{v_x} = \frac{\gamma * b * n * x^{n-1} * e^{(-bx^n)}}{\frac{\pi * x^3}{6} * \rho_{ce} * 10^{-12}} \tag{6.6}$$

In the following Sections the correction factor γ will not be mentioned explicitly. In calculations, however, this factor has been used consistently.

6.2.2 Specific Surface

For the surface area O_x of a spherical particle with diameter x it holds that (x in μm):

$$O_x = \pi * x^2 \qquad [\mu m^2] \qquad (6.7)$$

The total surface area of all particles of fraction F_x follows from:

$$O_{F_x} = N_x * O_x \qquad [\mu m^2] \qquad (6.8)$$

For the total particle surface area of all particles with diameter $x_{min} \leq x \leq x_m$ it holds that:

$$O_{\leq x_m} = \sum_{i=1}^{m} N_{x_i} * O_{x_i} \qquad [\mu m^2] \qquad (6.9)$$

The specific surface SS of a cement is obtained using eq. (6.9) for $x_m = x_{max}$.

6.2.3 Paste Characteristics

For the *specific mass* ρ_{pa} of a paste with a w/c=ω_0 it holds that (air content ignored):

$$\rho_{pa} = \frac{\rho_{ce} * (1 + \omega_0)}{1 + \frac{\rho_{ce}}{\rho_w} * \omega_0} \qquad [g/cm^3] \qquad (6.10)$$

The *(volumetric) paste density* ζ_{pa} is defined as the cement volume relative to the volume of the fresh paste:

$$\zeta_{pa} = \frac{G(\infty)}{\rho_{ce} * V_{pa}}$$

where: $$V_{pa} = G(\infty) * [1/\rho_{ce} + \omega_0/\rho_w] \qquad [cm^3] \qquad (6.11)$$

With $G(\infty)$=1 g and ρ_w=1 g/cm^3 it follows:

$$\zeta_{pa} = [1 + \rho_{ce}/\rho_w * \omega_0]^{-1} \qquad [--] \qquad (6.12)$$

Fig. 6.1 shows the volumetric paste density as a function of the w/c ratio.

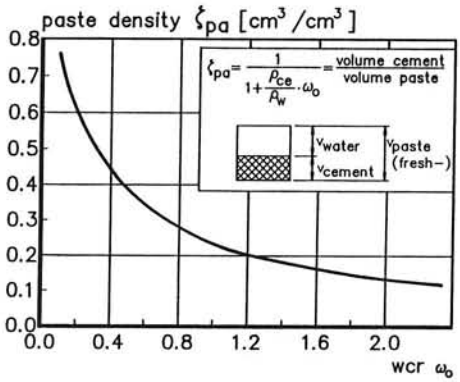

Fig. 6.1 Volumetric paste density ζ_{pa} as a function of the w/c ratio.
Note: The curve in this figure refers to fresh paste!

6.2.4 Cell Definition. Cell Volume and Particle Spacing

The mean spacing L_x between particles belonging to fraction F_x in a mix with w/c ratio ω_0 can be estimated by assuming that the particles under discussion are situated in the centre of a cube-shaped *"cell"*. For a cell the following definition holds:

"Cell definition"
A cell "I_x^c" is defined as a cubic space in which the largest cement particle has a diameter x, and further consists of $1/N_x$ times the original water volume and of $1/N_x$ times the volume of all particles with diameter smaller than that of particle x.

$$I_x^c = (V_w + V_{\leq x}) * N_x^{-1} \qquad [cm^3] \qquad (6.13)$$

where: V_w = initial water volume = $[\omega_0 * G(\infty)]/\rho_w$ [cm³]
$V_{\leq x} = G(x)/\rho_{ce}$ = cement volume of particles ≤x [cm³]
ρ_w, ρ_{ce} = specific mass [g/cm³]

The mean centre-to-centre particle spacing L_x [μm] is assumed to be equal to the rib size S_x of the cubic cell I_x^c (for detailed considerations, see [560]):

$$L_x = S_x = [I_x^c * 10^{12}]^{1/3} \qquad [\mu m] \qquad (6.14)$$

Since the cell volume I_x^c is a function of both the w/c ratio and the particle size distribution, the particle spacing L_x is a function of these parameters as well. For an indication of the particle spacing, reference is made to Figures 5.8 and 5.9. These figures clearly demonstrate that even in the case of low w/c ratios the particle spacing L_x of particles belon-

ging to fraction F_x substantially exceeds the particle diameter x. Indicative values of the rib size S_x, i.e. the particle spacing L_x, can be read off from Fig. 6.4.

6.2.5 Cell Density

Analogous to the volumetric paste density ζ_{pa} a *volumetric cell density* ζ_x is defined:

$$\zeta_x = \frac{\text{volume cement in cel } I_x^c}{\text{cel volume } I_x^c}$$

Using eq. (6.6) and eq. (6.13) it is found:

$$\zeta_x = \frac{\dfrac{G(x)}{\rho_{ce} * N_x}}{[\omega_0 * \dfrac{G(\infty)}{\rho_w} + \dfrac{G(x)}{\rho_{ce}}] * \dfrac{1}{N_x}}$$

or:

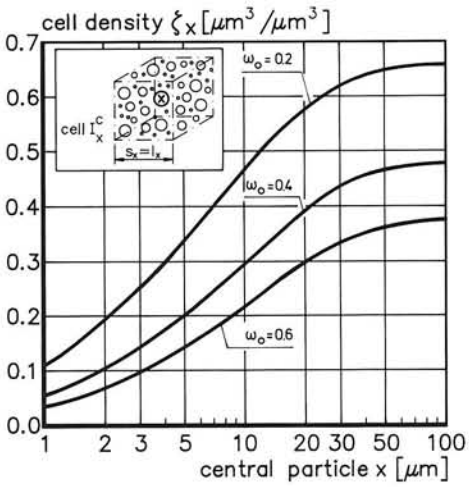

Fig. 6.2 Cell density ζ_x as a function of central particle x. ω_0 as parameter. Blaine≈350 m^2/kg.

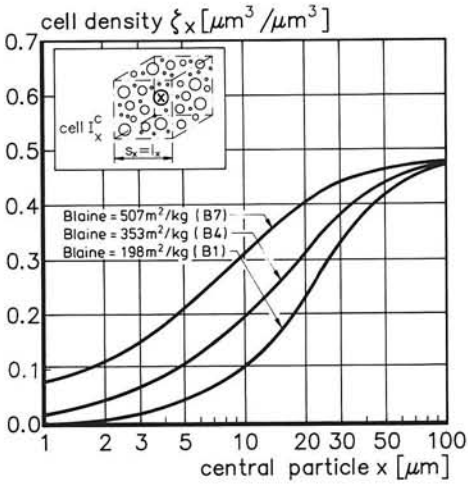

Fig. 6.3 Cell density ζ_x for different fineness of the cement as a function of the size of the central particle x. ω=0.4.

$$\zeta_x = \frac{1}{1 + \omega_0 * \frac{\rho_{ce}}{\rho_w} * \frac{G(\infty)}{G(x)}}$$

For $G(\infty)=1$ g and $\rho_w=1$ g/cm^3 it follows:

$$\zeta_x = \zeta_x(\omega_0,x) = \frac{1}{1 + \omega_0 * \frac{\rho_{ce}}{G(x)}} \qquad [--] \qquad (6.15)$$

For $x \rightarrow \infty$ the cell density ζ_x changes into the paste density ζ_{pa} (eq. (6.12)).

In view of further mathematical evaluations it is convenient to consider the cell density as a function of the cube root of the cell volume, viz.:

$$\zeta_x = \zeta_x\{S_x\} = \zeta_x\{ (I_x^c)^{\frac{1}{3}} \} \qquad (6.16)$$

Since the rib size S_x is a function of both the w/c ratio and the particle size distribution (Section 6.2.4), it is worth considering the effect of these two parameters on the cell density $\zeta_x\{S_x\}$. For a cement of moderate fineness (Blaine=350 m^2/kg) Fig. 6.2 shows the cell density for different w/c ratios. Fig. 6.3 shows the effect of the cement fineness on the cell density for ω_0=0.4.

As will be shown later on, the cell density is an important and helpful quantity for explaining the effects of particle interactions on both the rate of hydration and structure formation. Furthermore, to give a better understanding of matrix-aggregate interface phenomena the cell concept will be very useful.

6.3 The Spherical Cell

6.3.1 Smeared-out and Discrete Cell Density

For the determination of centre-to-centre spacing L_x particles with diameter x are assumed to be located in the centre of fictitious cubes I_x^c with rib size S_x. For such a cell we define a volumetric cell density ζ_x. The thus defined cell density is a "smeared out" quantity. The *actual* presence of the cement in the cell, however, has a *discrete* character. It is either 100%, viz. within the boundary of the cement particle, or 0%, viz. in the liquid phase.

In Fig. 6.4 a schematic representation is given of the cement density over a centre plane of a cubic cell. Going from the periphery of the spherical central particle in a radial direction, the local cement density is at first zero and then gradually increases until the smeared-out value of the cell density ζ_x is reached.

6.3.2 Shell Density. Volumetric Considerations and Conversion Factor

From Fig. 6.4 it is obvious that for calculating the *average shell density*, i.e. the amount of cement in the *shell* which surrounds a central particle, one has to find a solution for changing from the *spherical* shape of both the central particle x and the surrounding shell to the *cubic* shape of the earlier defined cell I_x^c. The most convenient way to solve this spatial problem is to convert the cubic cell into a spherical one of *a) equivalent volume* and *b) equivalent average cell density* as the corresponding cubic cell.

Ad a): Spherical versus Cubic Cell. Volumetric Conversion Factor
The first requirement which should be fulfilled when changing from the cubic to the spherical cell shape is:

$$V_{cube} = V_{sphere}$$

For a cube with a rib "s" and a sphere with radius "y" it holds that:

$$s^3 = 4/3 * \pi * y^3$$

It follows:

$$s = \left(\frac{4.\pi}{3}\right)^{\frac{1}{3}} * y = \chi * y \qquad (6.17)$$

where χ is a *stereometric conversion factor*. Similarly the radius Y_x of a spherical cell I_x^s

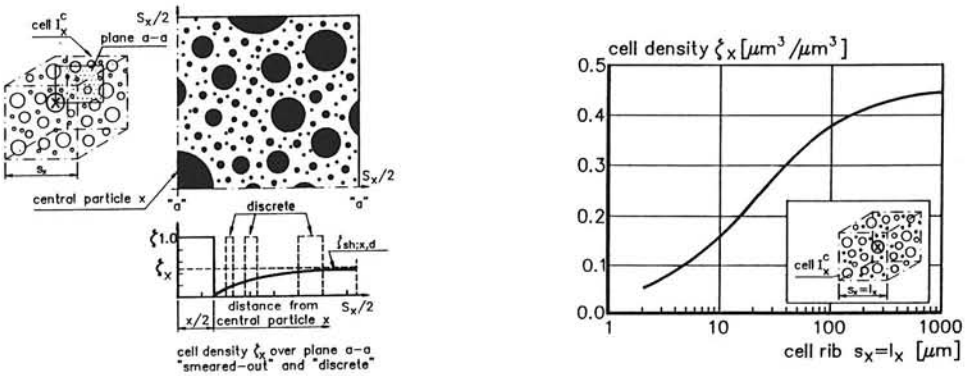

Fig. 6.4 Left: Schematic representation of the cell density as a function of the distance from the outer surface of a spherical central particle.
Right: Cell density as a function of rib size of the cell; Blaine≈350 m^2/kg.

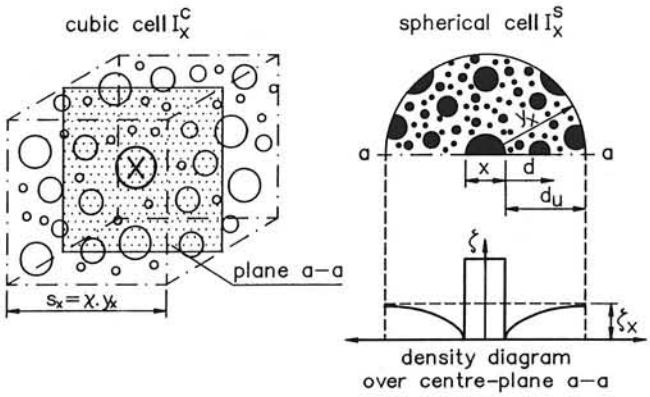

Fig. 6.5 Conversion of cubic to spherical cell geometry: schematic.

with the same volume I_x^c of a cubic cell with ribs S_x can be calculated according to (see also Fig. 6.5):

$$S_x = \chi * Y_x \tag{6.18}$$

Ad b: Shell Density

With respect to the second criterion, i.e. equal densities of cubic and spherical cells, the reasoning is as follows. With increasing thickness d of the spherical shell around the central particle x, the amount of cement in the shell, or shell density, increases. It is assumed that the *true average shell density*, indicated as $\zeta_{sh;x,d}$, can be approximated by $\zeta^*_{sh;x,d}$, viz:

$$\zeta^*_{sh;x,d} \approx \zeta(s) = \zeta(\chi * d) \tag{6.19}$$

For a shell thickness d=0 the average shell density is zero as well. In the ultimate case, when the outer surface of the spherical shell coincides with the outer surface of the spherical cell I_x^s, i.e. when $d_u = Y_x - (x/2)$, the shell density would be (see also Fig. 6.5):

$$\zeta^*_{sh;x,d_u} = \zeta(s) = \zeta(\chi * d_u) = \zeta(\chi * (Y_x - \frac{x}{2})) \tag{6.20}$$

For the *exact* value of the shell density in this ultimate case it holds by definition (see also Section 6.2.5) that:

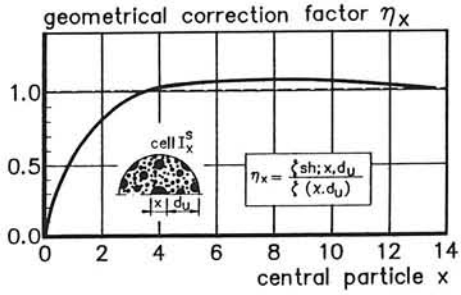

Fig. 6.6 Geometrical correction factor η_x for determination of the shell density in a spherical shell as a function of the central particle size x. Blaine=350 m^2/kg. ω_0=0.4.

$$\zeta_{sh;x,d_u} = \frac{\text{cement volume in spherical shell with thickness } d_u}{\text{total shell volume}}$$

$$\zeta_{sh;x,d_u} = \frac{\zeta_x * I_x^c - v_x}{I_x^c - v_x} \tag{6.21}$$

By equating the expressions (6.20) and (6.21) a correction factor η_x is obtained. The shell density according to eq. (6.20) has to be multiplied by η_x in order to establish volumetric consistency. The correction factor η_x is defined straightforwardly as:

$$\eta_x = \frac{\zeta_{sh;x,d_u}}{\zeta^*_{sh;x,d_u}}$$

or:

$$\eta_x = \frac{\zeta_x * I_x^c - v_x}{I_x^c - v_x} * \frac{1}{\zeta^*_{sh;x,d_u}} \tag{6.22}$$

For the density of a shell with an arbitrary shell thickness d it follows:

$$\zeta_{sh;x,d} = \eta_x * \zeta^*_{sh;x,d} \tag{6.23}$$

In Fig. 6.6 the value of η_x is given as a function of the diameter of the central particle x.

The figure refers to a cement with Blaine=350 m^2/kg and ω_0=0.4. It can be been that the correction factor η_x reaches substantial values for small particles only, i.e. deviates substantially from unity. The small particles, however, hardly affect the development of hydration and structure formation of the system as a whole. It can, therefore, be concluded that the proposed description of the variation in shell density with increasing distance from a particle surface is accurate enough for the given goal.

The introduction of the shell density concept allows to calculate the amount of cement met by the outer products of a hydrating and expanding central particle and, moreover, to calculate the effect of particle interaction on the rate of hydration. This interaction mechanism will be the subject of the next Section.

6.4 Interaction Mechanisms

6.4.1 Introductory Remarks and Basic Assumptions

6.4.1.1 Spatial Distribution of Particles.

For quantification of the interaction between hydrating particles, assumptions have to be made concerning the spatial distribution of the cement particles in the water-cement system. In the foregoing a homogeneous distribution was assumed. Particles of the same size were assumed to be located at equal distances from each other. This approach has significantly simplified the determination of the amount of cement found in a fictitious shell around an arbitrary cement particle x. It can be argued, however, that in reality the particles are located more randomly in the system and that a probabilistic approach would be more suitable to characterize the stereological distribution of the particles in the system. This would also be a more realistic starting point for simulating the development of a microstructure during the hydration process.

Aforementioned arguments are certainly valid and have been the reason for a more detailed investigation on this point[2]). Main emphasize in these investigations was on the consequences of a full probabilistic approach, i.e. explicit allowance for the random distribution of the particles in the system, for the required computation time. The computation time largely depends on the *number* of particles that has to be considered. In this respect one should bear in mind that when a random distribution of the cement particles is considered, each particle of the poly-size cement powder has a unique position relative to its neighbour particles. Consequently, also the interaction with neighbour particles during hydration and structure development is unique and so the effect of the interaction on the rate of hydration of individual particles. Accounting for different rates of hydration of individual particles would result in computation times up to over 1,000 hours for a simulati-

[2]) "Some considerations on the consequences of adopted particle distributions in cement-water systems in view of required computation times of simulation models", Van Breugel, K., Delft, 1991, 8 p. (internal note).

on of 28-days hydration of a sample of moderate fineness[2]) (Note: year 1991; AT+co-processor). These computation times could be reduced substantially by ignoring the hydration of the smaller fractions, since in these fraction, although representing only a relatively small amount of a cement sample, a very large number of particles is accommodated. Ignoring the smaller fractions, however, adversely affects the reliability and consistency of the simulation model.

Foregoing considerations have made us deciding for a straightforward concept of a homogeneous distribution of the cement particles in the paste. As mentioned already, a homogeneous particle distribution is adequate for computing the *amount* of cement present in a fictitious shell around an arbitrary cement particle x. Anticipating on the derivations in subsequent Sections it is emphasized here, that in considerations concerning the degree of hydration of the cement that is present in this fictitious shell, this cement is considered to consist of particles with diameters in the range from 1 to (x-1) μm. In this way it is still possible to simulate that *also* particles of approximately the same size directly interfere with each other during the hydration process.

The adopted procedure, whereby at first a homogeneous distribution if the cement particles is considered for the determination of the amount of cement in a fictitious shell around a certain central particle, and, subsequently, a more probabilistic-oriented, i.e. statistical, approach is followed for both the characterization of the degree of hydration of the cement present in this shell and for the determination of the physical interaction between the central particle and adjacent particles in this shell, is called a "pseudo-probabilistic approach".

In the second, probabilistic-oriented part of the calculations the position of the particles in the paste is *not* defined explicitly. A consequence of this is that the number of particles involved in the interaction process must be counted carefully on penalty of counting them more than once. This has lead to the concept of *"free"* and *"embedded"* particles as outlined in more detail in Section 6.4.3.

6.4.1.2 Basic Assumptions

In order to obtain a workable mathematical model for the physical interaction between hydrating particles four basic assumptions are made.

1. *Particles belonging to the same fraction hydrate at the same rate.*
   Comment: It is obvious that a small particle which is completely surrounded in the liquid phase will hydrate in a different way, and probably at a different rate, than a particle of the same size but located close to the surface of a large particle. As explained in the foregoing Section, however, accounting for different rates of hydration of individual particles of the same fraction would increase the calculation effort tremendously, since each particle has a unique position in the system and hence a unique environment that determines its rate of hydration.

2. *For isothermal curing the ratio* ν *between the volume of the gel and that of the reactant is assumed to be a constant throughout the hydration process.*
   Comment: A constant value of the parameter ν in mathematical modelling has also been used, in the absence of reliable experimental data, by Pommersheim [452]. For indicative values of ν reference is made to Section 4.4.3.3.
   As suggested with the formulation of this second basic assumption, *non-isothermal* effects will be considered differently, i.e. with a temperature dependent value of the ratio under consideration. A proposal for a temperature-dependent value of ν, i.e. $\nu=\nu(T)$, reference is made in Section 6.6.

3. *Reaction products precipitate in the close vicinity of the cement particles from which they are formed.*
   Comment: The reaction products are assumed to build up a gel of constant density. This assumption is based on the "unstable pore concept" suggested by Powers [462] and also adopted by Granju et al. [205] (Section 4.4.5.2).

4. *The development of internal stresses associated with formation of microstructure is not considered explicitly.*
   Comment: Chemical shrinkage is considered to cause internal stresses and microcracking [625]. Both hydration under pressure and the process of microcracking might affect the rate of hydration. The effect of these processes are partly allowed for implicitly in the value of the independent model parameters to be discussed in detail in Chapter 8.

With these basic assumptions the framework has been established within which the simulation model will be developed. To avoid confusion it will be emphasized here that these basic assumptions refer to a *model*, and should not be interpreted as conclusions with regard to the far more complex reality of hydrating poly-mineral and poly-size two-phase systems!

6.4.2 "Particle Expansion" during Hydration

To explain the interaction mechanism that occurs around a hydrating particle x, the progress of the hydration process and associated expansion of the particle x will be followed. An arbitrary stage in the hydration process is shown diagrammatically in Fig. 6.7. In this stage, i.e. at time $t=t_j$, the degree of hydration of particle x is $\alpha_{x,j}$. For the corresponding *penetration depth* $\delta_{in;x,j}$ of the reaction front it holds that:

$$\delta_{in;x,j} = (\frac{x}{2}) * [1-\{1-\alpha_{x,j}\}^{1/3}] \tag{6.24}$$

The volume of the outer product $v_{ou;x,j}$ that corresponds to the degree of hydration $\alpha_{x,j}$ follows from:

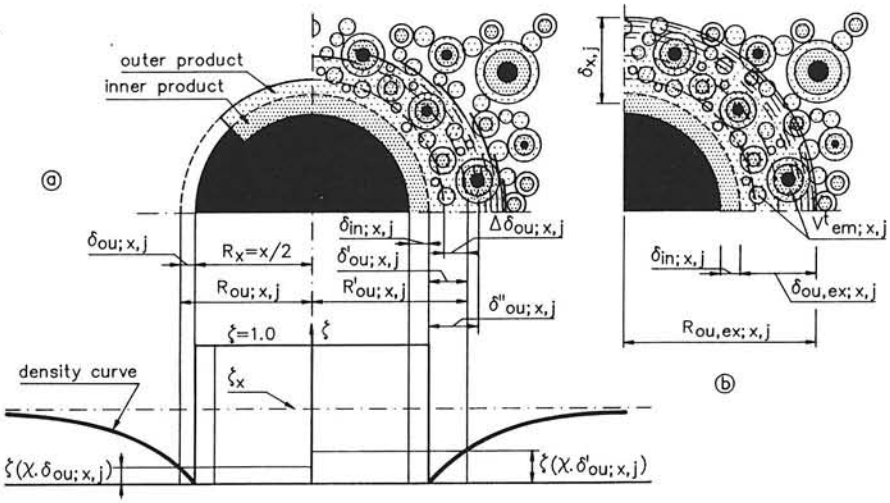

Fig. 6.7 Interaction mechanism for expanding particles.
a. Left: free expansion. Right: particle embedding; several steps.
b. Expansion, affected by embedding of small particles; final stage.

$$v_{ou;x,j} = (v-1) * \alpha_{x,j} * v_x \tag{6.25}$$

Absence of cement in the shell surrounding particle x would lead to free expansion of this particle. As a result, the outer radius $R_{ou;x,j}$ of the expanding central particle would be:

$$R_{ou;x,j} = \left[\frac{v_{ou;x,j}}{\frac{4\pi}{3}} + \left(\frac{x}{2}\right)^3\right]^{1/3} \tag{6.26}$$

For the thickness $\delta_{ou;x,j}$ of the outer shell it follows (see Fig. 6.7a):

$$\delta_{ou;x,j} = R_{ou;x,j} - \frac{x}{2} \tag{6.27}$$

In reality the outer shell is partly filled with embedded cement particles. The volume of the cement in the outer shell with thickness $\delta_{ou;x,j}$, which volume is called the *directly embedded cement volume* $v_{em;x,j}$, can be determined by multiplying the shell volume $v_{ou;x,j}$ with the shell density factor according to eq. (6.19) and eq. (6.23) (η_x ignored):

$$v_{em;x,j} = \zeta(\chi.\delta_{ou;x,j}) * v_{ou;x,j} \tag{6.28}$$

This directly embedded cement volume is built up of particles smaller than x μm and is partly hydrated. In the partly hydrated state the volume of the directly embedded cement at time $t=t_j$ can be calculated using (see Fig. 6.7b):

$$v_{em;x,j,\alpha} = v_{em;x,j} * (1-\alpha_{<x,j}) + v_{em,x,j} * \alpha_{<x,j} * \nu$$

or:

$$v_{em;x,j,\alpha} = v_{em;x,j} * \{(1 + (\nu-1) * \alpha_{<x,j}\}$$

The embedded and partly hydrated cement volume accounts for an *additional* expansion of the outer shell of particle x. For the total volume of the additionally expanded outer shell it follows:

$$v'_{ou;x,j} = v_{ou;x,j} + v_{em;x,j,\alpha}$$

The outer radius $R'_{ou;x,j}$ of the extra expanded outer shell is now:

$$R'_{ou;x,j} = \left[\frac{v'_{ou;x,j}}{\frac{4\pi}{3}} + \left(\frac{x}{2}\right)^3\right]^{1/3}$$

For the new thickness of the outer shell it follows:

$$\delta'_{ou;x,j} = R'_{ou;x,j} - \frac{x}{2}$$

With the extra increase of the shell thickness, viz.:

$$\Delta\delta_{ou;x,j} = \delta'_{ou;x,j} - \delta_{ou;x,j}$$

the amount of embedded cement will increase as well. The amount of cement found in the shell with a thickness $\Delta\delta_{ou;x,j}$ is called *indirectly embedded cement volume*. The total of directly and indirectly embedded cement volumes can be calculated in a way analogous to the calculation of the directly embedded cement volume. From comparison with (6.28) it follows:

$$v'_{em;x,j} = \zeta(\chi.\delta'_{ou;x,j}) * v'_{ou;x,j}$$

Since $\delta'_{ou;x,j} > \delta_{ou;x,j}$, the value of $\zeta(\chi.\delta'_{ou;x,j})$ will be slightly higher than the value of $\zeta(\chi.\delta_{ou;x,j})$ (bottom part of Fig. 6.7a). Consequently, the total volume of embedded cement will increase. The extra embedded cement in turn causes another extra increase of the outer shell, etc. This expansion mechanism, which is inherent in the spatial composition of the hydrating system, on the one hand, and to the adopted constancy of the volume ratio ν between reaction products and reactant, on the other, finally results in the following geometrical series:

$$v^{n}_{ou;x,j} = V_{ou;x,j} + [1 + \zeta(\chi.\delta^{n}_{ou;x,j}) * \{ 1 + (\nu-1) * \alpha_{<x,j} \}^{1} +$$

$$+ \zeta(\chi.\delta^{n}_{ou;x,j}) * \zeta(\chi.\delta^{n-1}_{ou;x,j}) * \{ 1 + (\nu-1) * \alpha_{<x,j} \}^{2} +$$

$$+ \zeta(\chi.\delta^{n}_{ou;x,j}) * \zeta(\chi.\delta^{n-1}_{ou;x,j}) * \zeta(\chi.\delta^{n-2}_{ou;x,j}) * \{ 1 + (\nu-1) * \alpha_{<x,j} \}^{3} +$$

$$+ \ldots\ldots\ldots\ldots\ldots\ldots\ldots\ldots\ldots\ldots\ldots\ldots\ldots\ldots\ldots\ldots]$$

Unfortunately the geometrical ratio of this series is not a constant. In most cases, however, and certainly at the start of the hydration process, the directly embedded cement volume is much larger than the indirectly embedded cement volume. It can, therefore, be assumed that for the calculation of the indirectly embedded cement volume the shell density $\zeta(\chi.\delta_{ou;x,j})$, which belongs to the initial outer volume $v_{ou;x,j}$ of particle x, can be adopted. Under this condition the geometrical ratio of the series becomes:

$$r = \zeta(\chi.\delta_{ou;x,j}) * \{ 1 + (\nu-1) * \alpha_{<x,j} \}$$

For the *volume of the expanded outer shell*, $v_{ou;ex;x,j}$, it then follows:

$$v_{ou,ex;x,j} = \frac{v_{ou;x,j}}{1 - \zeta(\chi.\delta_{ou;x,j}) * \{ 1 + (\nu-1) * \alpha_{<x,j} \}} \qquad (6.29)$$

For the outer radius of the expanded outer shell we obtain (Fig. 6.7b):

$$R_{ou,ex;x,j} = [\frac{V_{ou,ex;x,j}}{\frac{4.\pi}{3}} + (\frac{x}{2})^3]^{1/3} \tag{6.30}$$

while for the thickness of the expanded outer shell it holds that:

$$\delta_{ou,ex;x,j} = R_{ou,ex;x,j} - \frac{x}{2} \tag{6.31}$$

With eq. (6.24) and eq. (6.31) the total thickness $\delta_{x,j}$ of the shell which surrounds the shrinking anhydrous core is:

$$\delta_{x,j} = \delta_{in;x,j} + \delta_{ou,ex;x,j} \tag{6.32}$$

For the total embedded cement volume $v^t_{em;x,j}$, i.e. the sum of directly and indirectly embedded, partly hydrated, cement volume it follows:

$$v^t_{em;x,j} = v_{ou,ex;x,j} - v_{ou;x,j} \tag{6.33}$$

This embedded cement, consisting of particles with a diameter smaller than x, is hydrated up to a degree $\alpha_{\leq x,j}$. For the original volume of embedded cement, i.e. the cement volume in its anhydrous state, $v^0_{em;x,j}$, it holds that:

$$v^0_{em;x,j} = \frac{v^t_{em;x,j}}{1 + (\nu-1) * \alpha_{\leq x,j}} \tag{6.34}$$

Indicative values

Indicative values for the volume of the embedded cement will be given in Chapter 7 (see Fig. 7.4). For orientation: for a particle with diameter x=16 μm and a volume of 2,144 μm^3, hydrating in a system with a w/c ratio of 0.4 the maximum amount of directly and indirectly embedded, partly hydrated cement has been calculated at about 1,000 μm^3.

6.4.3 Embedded and Free Particles

With increasing degree of hydration more particles become embedded in the expanding outer shells of large particles. Hence, the number of hydrating "free clusters" decreases with time. The number of free particles $N_{x;fr}$, i.e. free clusters with a central particle x,

consists of the original number of particles N_x of fraction F_x *minus* the particles of this fraction embedded in the outer shells of particles larger than x µm. For the determination of $N_{x;fr}$ the following procedure is proposed.

The number of particles embedded in the expanded outer shell of a particle z>x can be calculated with the help of the quantity $\lambda_{z,j}$, defined as the ratio between the embedded cement volume $v^0_{em;z,j}$ and the cement volume of all particles smaller than particle z at time t_j ("Embedded/Free ratio"):

$$\lambda_{z,j} = \frac{v^0_{em;z,j}}{\frac{G(z-1)}{\rho_{ce}}} \tag{6.35}$$

The number of particles $n_{em,x;z,j}$ with particle diameter x embedded in the outer shell of particle z>x at time t_j follows from:

$$n_{em,x;z,j} = \lambda_{z,j} \cdot N_x \tag{6.36}$$

with N_x according to eq. (6.6). For the number of particles $\Delta N_{em,x;z,j}$, belonging to fraction F_x and embedded in the outer shells of the free particles of fraction F_z, it holds that:

$$\Delta N_{em,x;z,j} = n_{em,x;z,j} \cdot N_{z;fr} \tag{6.37}$$

where $N_{z;fr}$ is the number of free particles in fraction F_z. This number is known from preceding calculation steps. For the number of particles with diameter x embedded in the outer shells of all free particles z>x it holds that:

$$N_{em,x;j} = \sum_{z=x+1}^{x_{max}} \Delta N_{em,x;z,j} \tag{6.38}$$

The number of free particles or free clusters $N_{x;fr;j}$ in fraction F_x with central particle x at time t_j is found by subtracting the sum of embedded particles $N_{em,x;j}$ from the initial number of free particles N_x:

$$N_{x;fr,j} = N_x - N_{em,x;j} \tag{6.39}$$

6.4.4 Embedded Centre-plane Area and Contact Area

The cement volume embedded in the outer shell of particle x consists, by definition, of particles with diameter smaller than x μm. As discussed in Section 5.4.2 the small particles, say $x \leq x_{dis} \approx 3$ μm, completely dissolve and hence lose their geometrical identity. These particles only contribute to an extra outward growth of the outer shell of the central particle. Larger particles, with diameters up to x μm, can be either fully of partly embedded in the outer shell of particle x. For particles with a diameter exceeding the thickness of the outer shell $\delta_{ou,ex;x}$, it is only possible that these are partly embedded. It is assumed that the larger embedded particles, and in particular the particles with a diameter exceeding the thickness of the outer shell, are able to bridge the interparticle distances between adjacent expanding particles and hence determine the strength of the cement paste. This concept is diagrammatically shown in Fig. 6.8. Within the boundaries of this concept it can be expected that the total centre-plane area of particles which bridge the interparticle distances will show a more or less distinct correlation with strength.

For the determination of the embedded centre-plane area we proceed as follows. The centre-plane area a_x of an arbitrary spherical particle x can easily be related to its surface area O_x since it holds that:

$$a_x = \frac{O_x}{4} \tag{6.40a}$$

Analogously it follows for the accumulated centre-plane area of all particles smaller that particle x:

$$A_{\leq x} = \frac{O_{\leq x}}{4} \tag{6.40b}$$

where $O_{\leq x}$ is the total particle surface area according to eq. (6.9). The *embedded centre-plane area* $a_{em;x,j}$ of particles smaller than x μm, which are embedded in the outer shell of particle x at time t_j can be calculated by multiplying the total centre-plane area A with the earlier discussed quantity $\lambda_{x,j}$ according to eq. (6.35). Thus:

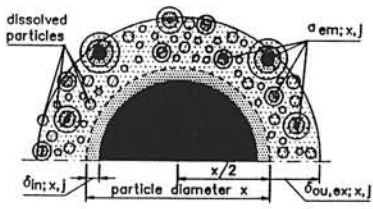

Fig. 6.8 Definition and formation of contact area; conceptual.

$$a_{em;x,j} = \lambda_{x,j} * A_{<x} \tag{6.41}$$

For the embedded centre-plane area of particles in the range $x_{dis}<x_i<x$ it follows:

$$a_{em;x_{dis}\rightarrow x,j} = \lambda_{x,j} * [A_{<x} - A_{\leq x_{dis}}] \tag{6.42}$$

The total centre-plane area $\Delta A_{em;x,j}$ in the outer shells of all free particles of fraction F_x is obtained using:

$$\Delta A_{em;x,j} = a_{em;x,j} \cdot N_{x;fr,j} \tag{6.43}$$

For the total embedded centre-plane area $A_{em;j}$ of the hydrating system as a whole at time t_j it holds that:

$$A_{em;j} = \sum_{x=x_{dis}}^{x_{max}} \Delta A_{em;x,j} \qquad [\mu m^2/g \text{ cement}] \tag{6.44a}$$

When disregarding the contribution to the embedded centre-plane area of particles smaller than x_{dis} it alternatively holds that:

$$A_{em;>x_{dis},j} = \sum_{x=(x_{dis}+1)}^{x_{max}} \Delta A_{em;x,j} \qquad [\mu m^2/g \text{ cement}] \tag{6.44b}$$

6.5 Rate of Hydration

In the foregoing Sections the stereological aspect of hydration has been dealt with. It was shown how expanding particles will embed smaller particles, the latter either fully or partly hydrated. In this Section the rate of hydration will be discussed. Particular attention will be given to the effect of particle interaction on the rate of hydration.

6.5.1 Particle Shape Effect

6.5.1.1 Particle Shape Effect in case of Phase-Boundary Reaction

In the early stage of the hydration process the reaction is generally assumed to be a phase-boundary reaction (Section 5.3). For an arbitrary penetration formula $\delta_{in}(t)=k.t$, the

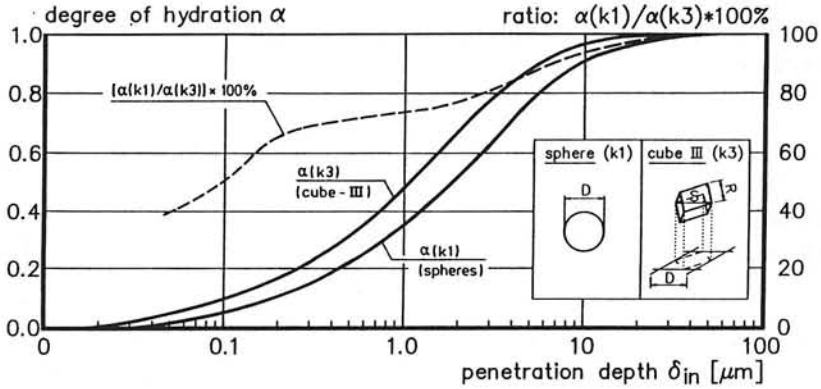

Fig. 6.9 Effect of particle shape on the rate of hydration for equal depths of penetration.

(overall) rate of hydration will increase with increasing surface/volume ratio. Spherical particles have the lowest possible surface/volume ratio and will, therefore, exhibit a slower rate of hydration than cube-shaped particles, which have a pronounced higher surface/volume ratio (see also Section 2.3). The effect of the particle shape on the rate of hydration is shown in Fig. 6.9. Two cement samples are considered, consisting of spherical and cubic particles, respectively. The Rosin-Rammler distribution for both samples is the same. The rate of hydration is shown as a function of the penetration depth δ_{in}. It is evident that for the same penetration depth the sample made up of cubic particles hydrates faster than the sample made up of spherical particles.

Although there is a distinct effect of the surface/volume ratio, i.e. of the particle shape, on the rate of hydration, this effect will not be investigated in more detail here. A major reason for disregarding this effect is mainly a practical one. Since in the majority of current hydration models particles are considered to be spherical, changing to an other particle shape would make it less easy to compare mathematically obtained results with those obtained with other models and with the published data. Moreover, since a major aim of this study is to investigate the effect of particle interactions on the rate of hydration and the relationship between particle interaction and strength development, it is not very important which particle shape we consider. A pronounced effect of the particle granulometry, however, should certainly be born in mind.

6.5.1.2 Particle Shape Effect in case of Diffusion-controlled Reaction

Diffusion processes considered by Jander, Ginstling-Brownshtein, Carter, Kondo, Taplin, Pommersheim and many others all refer to *spherical* particles. In Section 2.3 it has been shown that the assumption of sphere-shaped particles is as arbitrary as the assumption of cubic particles. From a comparison of calculated particle surfaces with nitrogen adsorption

surfaces it was concluded that the cube-shape is probably even more realistic than the spherical shape [3]).

When considering hydration of cube shaped particles, particular attention must be given to the progress of the hydration process at the edges and corners of the particle. Although there appears to be some preference for the reaction to start at these points, hydrating particles of some size do not lose there original particle shape. On the contrary; hydrating particles have turned out to preserve their original shape throughout the hydration process (Section 4.4.2). Probably more important is that the shape of the reaction front was not found to differ significantly from the original particle shape. The only explanation for congruency between the reaction front and the original particle shape is that the rate of penetration is virtually *independent* of the particle shape. *Consequently it has been considered justified to proceed with a simple concept of diffusion through a thickening shell without making allowance for a possible effect of the shape of the shell, i.e. diffusion through a flat diffusion layer!*

Further with respect to the shape of the diffusion layer, viz. either a spherical shape or a flat layer, it is noted that it will be very difficult to conclude from a comparison of theoretical and experimental data which concept is correct. A couple of arguments can be given to inderpin this statement.

a. At first we have to realize that a possible effect of the spherical shape of a hydrating particle will become relevant no sooner than in a situation where the ratio between the original particle radius and the radius of the shrinking anhydrous core has reached a substantial value. This situation will be reached rather soon for the very small particles. Those small fractions, however, only form a minor part of the hydrating cement volume and will, therefore, not substantially influence the overall rate of hydration.
b. Secondly, the predominant amount of particles belongs to the fractions be tween 10 to 50 μm. For a representative particle of 30 μm, hydrated by 60%, the penetration depth is only 4 μm. So, in fact the shell of the reactant that has actually reacted is relatively small. It is obvious that the larger the particles, the less pronounced any possible effect of the shape of the diffusion layer on the rate of hydration will be. Small particles, i.e. particles which have almost completely hydrated, might hydrate faster because of a higher ion concentration at the anhydrous surface. But, for the same reason as mentioned under a, the rate of hydration of the almost hydrated particles will hardly affect the overall rate of hydration. This makes it very difficult to determine the actual rate of hydration of particles in the final stage of hydration (see also Daimon [124]).
c. Thirdly, with increasing degree of hydration, merging of expanding particles might significantly affect the overall rate of hydration. This merging effect, if not explicitly considered in a kinetic model, can lead to incorrect conclusions with respect to any assumed effect of the particle shape on the rate of hydration.
d. Finally it is noted that comparative calculations, in which both flat and curved, i.e. spherical, diffusion layers were considered, did not generate more consistent information for one of the two alternatives considered.

---

[3]) The actual shape of cement particles will depend significantly on the grindability of the clinker.

For aforementioned reasons, but particularly with reference to the observation of preservation of the particle shape throughout the hydration process, the diffusion layer surrounding the hydrating particles will be considered flat and the diffusion resistance will be correlated merely with the total thickness δ of the diffusion layer.

6.5.2 Rate of Penetration

6.5.2.1 Basic Rate Equation

For the determination of an incremental increase of the penetration depth $\Delta\delta_{in;x,j+1}$ of particle x during a time increment $\Delta t_{j+1} = t_{j+1} - t_j$ a penetration formula is proposed, which in its basic form is as follows:

$$\Delta\delta_{in;x,j+1} = \{\Delta\delta_{in;x,j+1}\}_0 * \Omega_1(x,\alpha_{x,j}) \qquad [\mu m/h] \qquad (6.45a)$$

with:

$$\{\Delta\delta_{in;x,j+1}\}_0 = \frac{K_i(\alpha_j) * F_1(.) * (F_2(.))^{\lambda} * \Omega_2(.) * \Omega_3(.)}{\{(\delta_{x,j})^{\lambda}\}^{\beta_1}} \cdot \Delta t_{j+1} \qquad (6.45b)$$

where:

K_i = rate constant, depending on the rate-controlling mechanism, cement composition and degree of hydration.
$i = 0$ in case of phase-boundary reaction [$\mu m/h$].
$i = 1$ in case of diffusion-controlled reaction [$\mu m^2/h$]

$F_1(.)=F_1(T,\alpha,C_3S)$ = "net" temperature function, accounting for the effect of the curing temperature on the rate of processes;

$F_2(.)=F_2(T,\alpha,C_3S)$ = temperature function, accounting for effect of curing temperature on morphology and formation of structure. Operative only in diffusion stage;

$\Omega_1(x,\alpha_{x,j})$ = reduction or *partition factor*, accounting for water withdrawal effects as occurring for a particle with diameter x (see Section 6.5.4);

$\Omega_2(\alpha_j)$ = reduction factor, accounting for water shortage in the pore system (overall effect);

$\Omega_3(\alpha_j)$ = reduction factor, accounting for reduction of the *amount* of water in the hydrating mass (overall effect).

λ = factor, depending on the rate-controlling mechanism
$\lambda = 0$ for phase-boundary reaction
$\lambda = 1$ for diffusion-controlled reaction.

β_1 = a constant, to be determined from suitable tests.

$\delta_{x,j}$ = total thickness of product layer [μm] of particle with diameter x at the end of time step Δt_j.

Particular features of the rate constant K_i will be discussed in the Sections 6.5.2.2 and 6.6.3.3. The reduction factors $\Omega_1(.)$, $\Omega_2(.)$ and $\Omega_3(.)$ are discussed in Sections 6.5.4.2, 6.5.5, 6.5.6 and 6.5.7, respectively, whereas the temperature functions $F_1(.)$ and $F_2(.)$ are discussed in Section 6.6.

6.5.2.2 Basic Rate Factors K_0 and K_1 and Transition Thickness δ_{tr}

The change from a phase-boundary to a diffusion-controlled reaction would occur at an overall degree of hydration $\alpha \approx 0.2$ [50,596]. Depending on the fineness of the cement the corresponding penetration depth is then about 2...3 µm. For this value of the penetration depth the degree of hydration of individual particles will differ quite significantly. Small particles will be fully hydrated already, whereas large particles are hydrated by only a few percent. It would not be correct, therefore, to relate the change from phase-boundary reactions to diffusion-controlled reactions to a fixed value of the degree of hydration that is applicable *irrespective* of the particle size. Instead of a transition value of the degree of hydration it is proposed to correlate the moment of the change from one rate-controlling mechanism to another to the thickness of the diffusion layer, i.e. to a *"transition thickness* δ_{tr}". It is further assumed that this change takes place gradually. This assumption can be allowed for by equalizing the rates of hydration, i.e. the rates of penetration, for both the phase-boundary reaction and the diffusion reaction at the moment when the thickness of the product shell has reached the transition thickness. Fig. 6.10 shows the situation at the transition point diagrammatically. The required equal rates of penetration directly prior and after the transition point determine a relationship between the rate constants K_0 and K_1 of eq. (6.45b). Thus:

$$\frac{\{\Delta\delta_{in;x,j+1}\}_0}{\Delta t_{j+1}} = \frac{K_0 * F_1(.) * (F_1(.))^{\lambda=0} * \Omega_2(.) * \Omega_3(.)}{\{(\delta_{x,j})^{\lambda=0}\}^{\beta_1}} = \frac{K_1 * F_1(.) * (F_2(.))^{\lambda=1} * \Omega_2(.) * (\Omega_3(.)}{\{(\delta_{x,j})^{\lambda=1}\}^{\beta_1}}$$

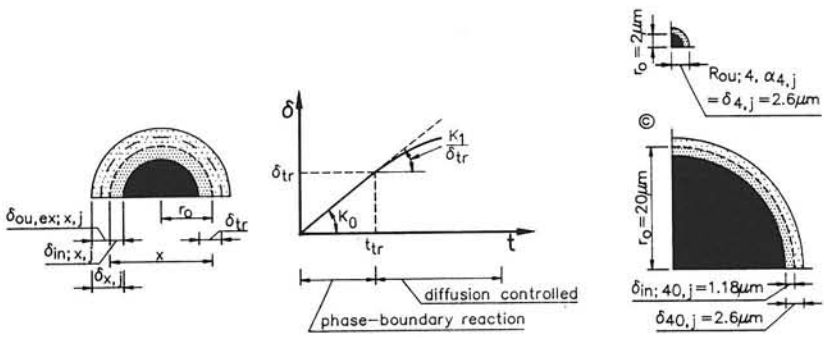

Fig. 6.10 Change of rate controlling processes; schematic presentation.

At the transition point, when $\delta_{x,j}=\delta_{tr}$, then (for $F_1(.)=1$):

$$K_1 = K_0 * \{\delta_{tr}\}^{\beta_1} \tag{6.46}$$

Transition Thickness. Tentative Values

An indication of the magnitude of the transition thickness δ_{tr}, and hence of the ratio K_1/K_0, can be deduced from data presented by Bezjak et al. [51,53] and Alujevic et al. [12]. According to Bezjak [53] the phase boundary reaction would be the rate controlling mechanism for small particles with radius up to $r_0 \approx 2\mu m$. For particles with radius $r_0 > 20$ μm diffusion soon becomes the rate ntrolling step. Disregarding any embedding of particles in the outer shells of particles with a radius $r_0=2$ μm, the outer radius of these particles at an arbitrary degree of hydration $\alpha_{x,j}$ would be:

$$R_{ou;x,\alpha_{x,j}} = r_0 * \{ 1 + (\nu - 1) * \alpha_{x,j} \}^{1/3} \tag{6.47}$$

For $r_0=2$ μm, $\nu=2.2$ and $\alpha_{x,j}=1$ we get (see also Fig. 6.10c):

$$R_{ou;x,\alpha_{x,j}} = 2.6 \ \mu m$$

An interpretation of the foregoing could be that for a thickness of the product layer $\delta_{x,j}=2.6$ μm the reaction changes from a phase-boundary reaction to a diffusion controlled reaction. Hence, the transition thickness would be $\delta_{tr}=2.6$ μm. For larger particles, say $r_0=20$ μm, the penetration depth $\delta_{in;x}$ that corresponds to a transition thickness $\delta_{tr}=2.6$ μm would only be about $2.6/\nu=1.18$ μm (Fig. 6.10c). The degree of hydration would then be:

$$\alpha_x = 1 - [1 - (\frac{\delta_{in;x}}{r_0})]^3 \tag{6.48}$$

With $r_0=x/2=20$ μm and $\delta_{in;x}=1.18$ μm the degree of hydration at which the change of rate-controlling mechanisms would take place is $\alpha_{x=40}(\delta_{in}=1.18)=0.167$. We thus see that, as suggested previously (Section 6.5.1.2), that for large particles diffusion will become the rate controlling step at a much lower degree of hydration than for small particles.

According to Alujevic, investigating a hydrating CaO-quartz system, the ratio K_1/K_0 ranges from 1.76 to 3.26. Similar investigations, carried out by Bezjak et al. with Portland cement pastes, revealed a K_1/K_0 ratio between 2.35 and 3.43. From eq. (6.46) it follows that for $\beta_1=1$ these K_1/K_0 ratios can be interpreted as transition thicknesses δ_{tr} [μm]. These values are in good agreement with the value $\delta_{tr}=2.6$ μm derived from Bezjak's data.

These considerations undeniably show distinct trends regarding the transition thickness of the diffusion layer. When quantifying the transition thickness δ_{tr} (Chapter 8) values in

the range from 1.5 to 4 μm can be expected.

It should be noted that the results obtained by Alujevic and Bezjak have shown, that with an increase of the degree of hydration the ratio K_1/K_0 increases as well. A possible interpretation of this result is, that during the hydration process diffusion through the outer shell becomes increasingly difficult, i.e. merging of outer products of mutually interfering particles becomes of paramount importance.

Furthermore it should be noted that the degree of hydration, i.e. the depth of penetration, at which the change of rate-controlling mechanisms takes place roughly coincides with the stage in the hydration process in which the ion concentration in the liquid phase significantly changes (see also Section 3.6).

6.5.3 Degree of Hydration. Particle -, Cell - and Overall Hydration

In Section 6.4.2 it has been shown that the thickness $\delta_{x,j}$ of the shell which surrounds an arbitrary particle x is determined by the *degree of hydration of particle x*, viz. $\alpha_{x,j}$, and the volume of embedded material. The latter volume depends on the shell density and the degree of hydration of the embedded cement, i.e. the degree of hydration $\alpha_{<x,j}$ of particles smaller than particle x. This is in fact the *degree of hydration reached in a cell* I_{x-1}.

Degree of Hydration. Particle Level

The increase of the degree of hydration $\Delta\alpha_{x,j}$ of particle x that corresponds to an increase of the penetration depth $\Delta\delta_{x,j}$ during Δt_j follows from:

$$\Delta\alpha_{x,j} = \left[1 - \frac{2.\delta_{x,j-1}}{x} \right]^3 - \left[1 - \frac{2.(\delta_{x,j-1} + \Delta\delta_{x,j})}{x} \right]^3 \tag{6.49}$$

For the degree of hydration of particle x, i.e. fraction F_x, at time t_j it holds that:

$$\alpha_{x,j} = \sum_{i=1}^{j} \Delta\alpha_{x,i} \tag{6.50}$$

Degree of Hydration. Cell Level

The degree of hydration of a cell I_x follows from adding up the hydrated cement volume in fractions $F_z<F_x$ and dividing this sum by the original amount of cement G(x-1) (see also Fig. 6.11):

$$\alpha_{\leq x,j} = \frac{1}{G(x-1)} \sum_{z=x_{min}}^{x-1} \alpha_{z,j} * W(z) \tag{6.51a}$$

with W(z) according to eq. (6.4).

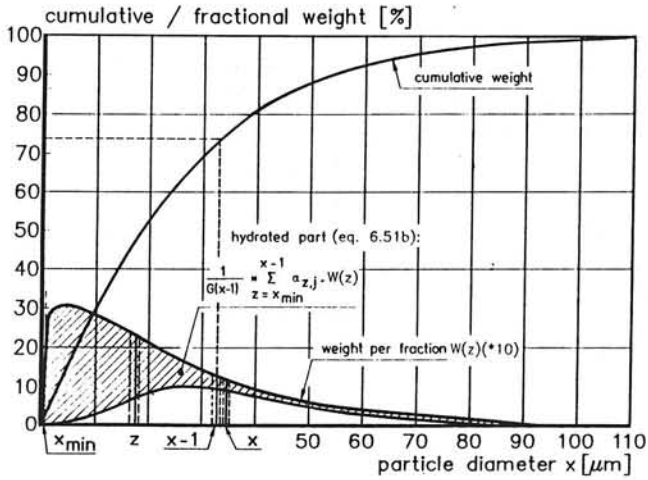

Fig. 6.11 Degree of hydration of an arbitrary cell I_x. Diagrammatical representation.

Degree of Hydration. Overall Hydration

The overall degree of hydration α_j at time t_j can be considered as a special case of cell hydration and can, therefore, be calculated using the expression (6.51a) for $x=x_{max}$. The expression is shown in the insert of Fig. 6.11, denoted as eq. (6.51b).

6.5.4 Effects of Particle Interaction on the Rate of Penetration

The consequence of the embedding of particles in the outer shell of a hydrating central particle on the rate of penetration is *two-fold*. Firstly, extra expansion of the outer shell will cause a decrease of the diffusion rate. Secondly, water withdrawal will occur due to the presence of incompletely hydrated particles in the outer shell of the central particle considered. Both effects will be discussed in the next two Sections.

6.5.4.1 Increased Shell Expansion

Initially the extra thickening of the outer shell occurs as discussed in Section 6.4.2. This extra expansion implies a higher diffusion resistance for ions or particles moving to and from the anhydrous core of the central particle and an associated decrease of the rate of penetration. The effect of extra shell expansion due to particle embedding will be discussed in detail in Section 7.3.3.

6.5.4.2 Water Withdrawal by Embedded Particles: Reduction Factor $\Omega_1(x,a_{x,j})$

The second factor refers to the hydration of embedded and still incompletely hydrated particles. A consequence of the first basic assumption made in Section 6.4.1, viz. the assumption of an equal degree of hydration of particles which belong to the same fraction, is that the embedded and still hydrating particles will withdraw a certain amount of the water needed for further hydration of the central particle. The resulting decrease of the rate of penetration of the reaction front in particle x is accounted for with the reduction factor $\Omega_1=\Omega_{em;x,\alpha}$ (see eq. 6.45a). For the determination of the reduction factor $\Omega_1(.)$ the following reasoning is proposed (see also Fig. 6.12).

Let us consider the progress of the hydration process in the time increment Δt_{j+1}. As a first step the increase in the penetration depth $\{\Delta\delta_{in;x,j+1}\}_0$ is calculated according to eq. (6.45b). For the corresponding amount of cement $\{\Delta v_{x,j+1}\}_0$ that would hydrate it holds that:

$$\{\Delta v_{x,j+1}\}_0 = \frac{4.\pi}{3} * [\{\frac{x}{2} - \delta_{in;x,j}\}^3 - \{\frac{x}{2} - (\delta_{in;x,j} + \{\Delta\delta_{in;x,j+1}\}_0)\}^3]$$

For hydration of the cement volume $\{\Delta v_{x,j+1}\}_0$ an amount of water $\{\Delta w_{x,j+1}\}_0$ is needed for which it roughly holds that (see Section 4.4):

$$\{\Delta w_{x,j+1}\}_0 = 0.4 * \{\Delta v_{x,j+1}\}_0 * \frac{\rho_{ce}}{\rho_w} \tag{6.52}$$

Due to water withdrawal by hydrating embedded particles the amount of water available for hydration of the central particle x will be $\Delta w_{x,j+1}<\{\Delta w_{x,j+1}\}_0$. For a first approximation of the ratio of the amounts of water used up for further hydration of particle x during Δt_{j+1} on the one hand, and for hydration of the embedded particles, on the other, the ratio is considered applicable during the preceding time step Δt_j. For the amount of water needed for an increase of the degree of hydration $\Delta\alpha_{x,j}$ of particle x during Δt_j it holds that:

$$\Delta w_{x,j} = 0.4 * \Delta\alpha_{x,j} * (v_x * \frac{\rho_{ce}}{\rho_w}) \tag{6.52a}$$

The amount of water that was required for further hydration of the embedded particles in time step Δt_j follows from (Fig. 6.12b):

$$\Delta w_{em;x,j} = 0.4 * \{v^0_{em;x,j} * \frac{\rho_{ce}}{\rho_w}\} * [\alpha_{\leq x-1,j} - \alpha_{\leq x-1,j-1}] \tag{6.53}$$

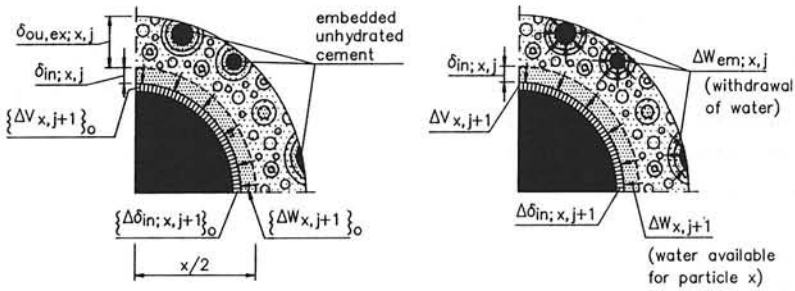

a. No water withdrawal

b. Water withdrawal considered

Fig. 6.12 Effect of embedded particles on the rate of hydration. Water withdrawal, schematic view.

with: $v^0_{em;x,j}$ = embedded particle volume according to eq. (6.34)

$\alpha_{\leq x-1,j}$, $\alpha_{\leq x-1,j-1}$ = degree of hydration of particles ≤(x-1), calculated according to eq. (6.51a)

The first approximation for the reduction or *partition factor* $\Omega_1=\Omega_{em;x,j}$ (or: $\Omega_1(x,\alpha_{x,j})$) to be considered in the time step Δt_{j+1} is defined now as follows:

$$\Omega_{em;x,j} = \frac{\Delta w_{x,j}}{\Delta w_{x,j} + \Delta w_{em;x,j}} \tag{6.54}$$

with $\Delta w_{x,j}$ and $\Delta w_{em;x,j}$ according to eqns. (6.52a) and (6.53), respectively. The real increase of the penetration depth $\Delta\delta_{in;x,j+1}$ is approximated by:

$$\Delta\delta_{in;x,j+1} = \Omega_{em;x,j} * \{\Delta\delta_{in;x,j+1}\}_0 \tag{6.55}$$

With the thus calculated approximated increase of the penetration depth the amounts of water needed for hydration of the central particle x, viz. $\Delta w_{x;j+1}$, and of the embedded particles, viz. $\Delta w_{em;x,j}$, during the time step Δt_{j+1} can be recalculated now. The sum of these amounts

$$\{\Delta w_{x,j+1}\}^*_0 = \Delta w_{x,j+1} + \Delta w_{em;x,j} \tag{6.56}$$

will generally differ from the amount of water with which we started, viz. $\{\Delta w_{x,j+1}\}_0$, calculated according to eq. (6.52). In an iterative calculation procedure the difference between these two amounts:

$$\Delta\Delta w_{x,j+1} = \{\Delta w_{x,j+1}\}_0 - \{\Delta w_{x,j+1}\}_0^* \tag{6.57}$$

is minimized down to a value of less than 1%. During this calculation procedure the partition factor $\Omega_l(.)$ iteratively reaches its final value, i.e. the value for the time step and particle size considered. At the end of the iteration procedure the resulting increase of the penetration depth $\Delta\delta_{in;x,j+1}$ and the corresponding amount of hydrated cement of the particle, i.e. $\Delta v_{x,j+1}$, can be calculated.

6.5.5 Effect of Water Shortage in the Pore System

It has been commented in Section 5.4.1 (Röhling) and 5.4.2 already, that the availability of water in the pore system of a hydrating mass can be of paramount importance when considering the rate of hydration. In this section a mechanism is proposed that caters for the effect of water shortage in the pore system on the rate of reaction. For that purpose we start with a schematization of the pore size distribution.

6.5.5.1 Porosity and Pore Size Distribution

As discussed in Section 4.5 the pore system consists of narrow gel pores of a diameter up to about 20 Å and wider capillary pores. With increasing degree of hydration the pore volume decreases, mainly at the cost of the volume of the larger pores (Section 4.4.4.3). The water available for hydration accumulates in the smaller pore regions. A typical result of porosity and pore size measurements is shown in Fig. 6.13a. In a plot of the pore volume against the logarithm of the pore size it appears that the slope of those parts of the curves which represents the pore size distribution of the *capillary pores*, are more or less independent of the pore volume. This will turn out to be an interesting feature for mathematical modelling of the effect of the water shortage on the rate of hydration.

As commented in Section 4.4.4.2 already the measurement of porosity and pore sizes and the interpretations of these measurements are generally based on the assumption of a *cylindrical* pore shape. Since kinetic models for hydration of poly-size cement-water systems are generally based on hydration of spherical particles, one has to expect it to be very difficult to find a consistent explanation for the formation of cylindrical pores. To be consistent, if we stick to concentric outward growth of hydrating spherical particles, a pore system consisting of cylindrical pores could *never* be formed (see also Young in [637]). The geometrical inconsistency touched upon here will not be dealt with in detail in this study. We will restrict ourselfs to a phenomenological approach to the effect that a straightforward mathematical expression is proposed, which relates the porosity and pore size distribution, on the one hand, with the degree of hydration, on the other.

In view of mathematical manipulations the capillary pore volume of all pores with diameter $\leq\phi$ will be approximated by a simple expression (see Fig. 6.13b):

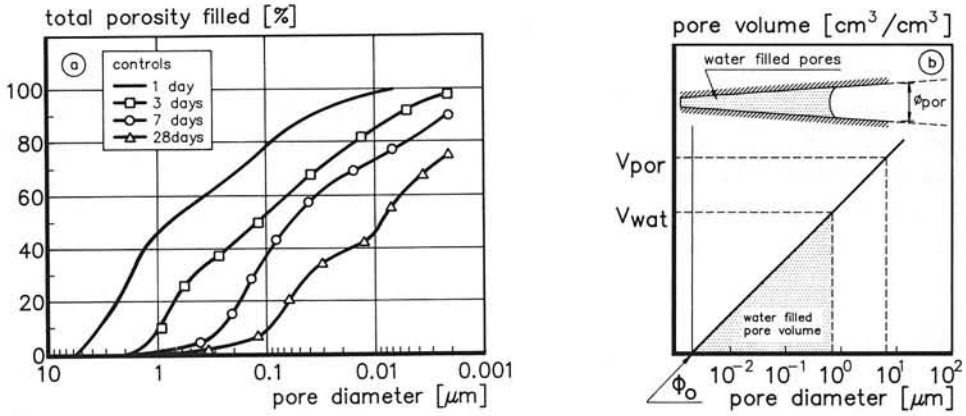

Fig. 6.13 Pore size distribution.
a. Experimental data from Whiting et al. [614];
b. Schematized pore size distribution; diagrammatical explanation of proposed water shortage mechanism.

$$V_{\leq\phi} = a * (\ln \frac{\phi}{\phi_0})^n \triangleq a.V * (\ln \frac{\phi}{\phi_0})^n \tag{6.58}$$

where $\phi/_0\phi$ is the relative pore diameter, V a volumetric unit, ϕ_0 the size of the smallest capillary pore, a and n are constants which depend on type and fineness of the cement and the w/c ratio. A straight line in the log-plot of the porosity against pore diameter is obtained for n=1, leading to the expression:

$$V_{\leq\phi} = a.V * (\ln \frac{\phi}{\phi_0}) \tag{6.58a}$$

The pore volume formed by pores smaller than $\phi=\phi_0=0.002$ μm, i.e. the gel porosity, is not included in the pore volume $V_{\leq\phi}$. Assuming, firstly, a fixed value for the smallest pore ϕ_0 that will always remain filled with water and, secondly, a constant slope of the curve that represents the pore size distribution, the constant a can easily be calculated from only a few experimentally obtained porosity values.

6.5.5.2 Maximum Pore Size ϕ_{max}

The maximum pore size in the pore system at time t_j, i.e. $\phi_{max,j}$, can be obtained by equating eq. (6.58) with the total pore volume as calculated on the basis of volumetric considerations. For the porosity at an arbitrary degree of hydration α it holds that:

$$V_{por}(\alpha) = V_{cap}(\alpha) + V_{chsh}(\alpha) \qquad [cm^3/cm^3] \qquad (6.59)$$

with $V_{cap}(\alpha)$ the amount of capillary water at a degree of hydration α, whereas $V_{chsh}(\alpha)$ represents the chemical or "Le Chatelier" shrinkage. The amount of capillary water left when a degree of hydration α is reached follows from:

$$V_{cap}(\alpha) = V_w^0 - 0.4 * \alpha * \frac{\rho_{ce}}{\rho_w + \rho_{ce}.\omega_0} . V \qquad [cm^3/cm^3] \qquad (6.60)$$

where V_w^0 is the initial water volume in the paste. This volume can easily be found with the help of the earlier defined paste density factor ζ_{pa} (eq. (6.12)). For this initial volume in 1 cm^3 paste it holds by definition that:

$$V_w^0 = 1 - V_{ce} = 1 - \zeta_{pa}$$

$$V_w^0 = \frac{\rho_{ce}\ \omega_0}{\rho_w + \rho_{ce}.\omega_0} . V \qquad [cm^3/cm^3] \qquad (6.61)$$

Eq. (6.61) inserted in eq. (6.60) yields the volume of the capillary water:

$$V_{cap}(\alpha) = \frac{\rho_{ce}}{\rho_w + \rho_{ce}\ \omega_0} * (\omega_0 - 0.4\ \alpha) . V \qquad [cm^3/cm^3] \qquad (6.62)$$

For the determination of the pore volume caused by chemical shrinkage it is assumed that this volume corresponds to about 25% of the volume of the chemically bound water (see Section 3.4.2). The chemically bound water is estimated at 25% of the weight of the reacted cement. For the chemical shrinkage it thus follows:

$$V_{chsh}(\alpha) = 0.25 * 0.25 * \alpha * \frac{\rho_{ce}}{\rho_w + \rho_{ce}.\omega_0} . V \qquad [cm^3/cm^3] \qquad (6.63)$$

With the equations (6.59), (6.62) and (6.63) we arrive at:

$$V_{por}(\alpha) = \frac{\rho_{ce}}{\rho_w + \rho_{ce}\ \omega_0} * (\omega_0 - 0.3375\ \alpha) . V \qquad [cm^3/cm^3] \qquad (6.64a)$$

The pore volume in cm^3/g can simply be obtained by dividing the value of $V_{por}(\alpha)$ according to (6.64a) by the specific mass of the paste ρ_{pa} as given by eq. (6.10). This results in:

$$V_{por}(\alpha) = \frac{1}{\rho_w\,(1 + \omega_0)} * (\omega_0 - 0.3375\ \alpha)\ .\ V \qquad [cm^3/g] \qquad (6.64b)$$

The maximum pore size $\phi_{por;\alpha}$ can now be found if we equalize eq. (6.64a) with eq. (6.58a). It holds that:

$$\phi_{por}(\alpha) = \phi_{max}(\alpha) = \phi_0 * \exp\left\{ \frac{V_{por}(\alpha)}{a} \right\} \qquad [\mu m] \qquad (6.65)$$

6.5.5.3 State of Water in Pore System. Reduction Factor $\Omega_2(\alpha_j)$

During the hydration process the capillary pores are gradually emptied until a thermodynamic equilibrium is reached. This state of equilibrium depends on the relative humidity in the pore system, the pore size distribution and the pore size. In any intermediate stage of equilibrium the pore system will be filled partly with water and partly with water vapour. Depending on the vapour pressure, i.e. the relative humidity, the walls of the empty pores will be covered with a thin layer of water (see Section 4.4.3 and 4.4.5). According to Hagymassy et al. [223] the average thickness of the adsorption layer decreases steeply from a six mono-molecular layer at RH=100% to a three mono-molecular layer at RH=80%. A further decrease of the relative humidity results in a gradual decrease of the layer thickness until a thickness of about 1 mono-molecular layer is reached at RH=20% (see Fig. 6.14). If, in line with Powers and Jonassen (see Section 5.4.2), it is assumed that in many practical cases the relative humidity in the pore system does not drop below values of 85 to 90%, it can be concluded that at the pore wall an adsorption layer of some thickness will remain [4]). The water in this adsorption layer is assumed to be less easy to mobilize for further hydration.

In view of these considerations the capillary water will be sub-divided into *free capillary water* V_{fr} and *adsorbed water* V_{ad} (see also Fig. 6.15):

$$V_{cap} = V_{fr} + V_{ad} \qquad (6.66)$$

For the determination of the volume of the adsorption layer with thickness Γ the pore wall area A_{por} of all pores in the range from ϕ_0 to ϕ_{max} has to be determined. The free capillary water will be located in the "remaining pore space", i.e. in the pore space made up of pores which are narrowed by the adsorption layer. The largest pore completely filled with

---

[4]) In low water/cement ratio concretes, like high strength concretes, the relative humidity in pore system can decrease below 85% (See, for example, V. Baroghel Bouny (1996), in Proc. RILEM-seminar *Béton: du Matèriau à la Structure*, Arles (Fr), and E.A.B. Koenders (1997) in *Simulation of volume changes in hardening cement-based materials*, PhD-Thesis, TU-Delft).

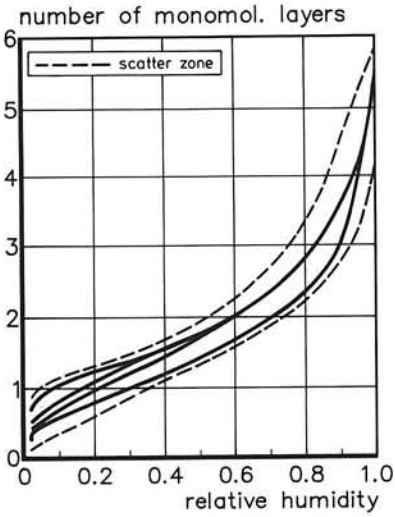

Fig. 6.14 Thickness of adsorption layer as function of the relative humidity. (after Hagymassy [223]).

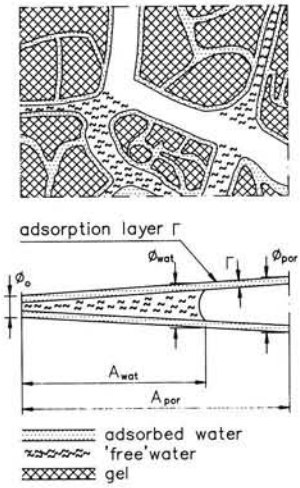

Fig. 6.15 Schematic view of state of water in pore system.

water, ϕ_{wat}, determines the pore wall area A_{wat} that is in contact with free water, i.e. with water that is available for further hydration. It is now assumed that *the fact that a certain amount of the cement matrix is not in direct contact with free water will, in some way, affect the rate of hydration of the system as a whole*. By saying "in some way" one should think in terms of longer distances over which ions involved in the reaction process have to travel from the bulk liquid phase to the anhydrous cement and visa versa.

To account for the assumed phenomenon a reduction factor $\Omega_2(\alpha)$ is proposed as follows (see also Fig. 6.15):

$$\Omega_2(\alpha) = \frac{A_{wat}(\alpha)}{A_{por}(\alpha)} \tag{6.67}$$

in which $A_{por}(\alpha)$ and $A_{wat}(\alpha)$ are the total pore wall area and of the wall area of the pores which are completely filled at a degree of hydration $\alpha=\alpha_j$, respectively.

6.5.5.4 Total Capillary Pore Wall Area $A_{por}(\alpha)$

From the pore volume $V_{\leq\phi}$ according to eq. (6.58a) the pore volume per pore fraction F_ϕ can be found by differentiating this equation with respect to ϕ.

$$dV_\phi = \frac{a.V}{\phi}\, d\phi \tag{6.68}$$

Assuming a cylindrical pore shape, the total pore length l_ϕ of all pores with diameter ϕ µm can be calculated using the equation:

$$dV_\phi = \frac{\pi\, \phi^2}{4} * dl_\phi \tag{6.69}$$

With eq. (6.68) in eq. (6.69) it follows for the pore length dl_ϕ of pores with diameter ϕ:

$$dl_\phi = \frac{4\ a.V}{\pi\ \phi^3}\, d\phi \tag{6.70}$$

The pore wall area ΔA_ϕ of pores with diameter ϕ follows from:

$$dA_\phi = (\pi * \phi) * dl_\phi = \frac{4\ a.V}{\phi^2}\, d\phi \tag{6.71}$$

The total pore wall area A_{por} is found by integrating eq. (6.71) between the boundaries ϕ_0+1 and ϕ_{por}:

$$A_{por} = \int_{\phi_0+1}^{\phi_{por}} \frac{4\ a.V}{\phi^2}\, d\phi$$

For the total pore wall at a degree of hydration α it follows:

$$A_{por}(\alpha) = -\ 4 * a.V * \{\ \phi_{por;\alpha}^{-1} - \phi_0^{-1}\ \} \quad [\mu m^2] \tag{6.72}$$

Note that $A_{por}(\alpha)$ is the total pore wall area [μm^2] per unit of volume V.

6.5.5.5 Wet Pore Wall Area $A_{wat}(\alpha)$. Reduction Factor $\Omega_2(\alpha)$

In cases where the pore walls are covered with a water layer of thickness Γ, a "narrowed pore system" remains in which the free capillary water is accommodated. For the reduced space $\Delta V_{red;\phi}$ that is available per pore fraction F_ϕ to accommodate free capillary water it follows that (see Fig. 6.15):

$$dV_{red;\phi} = \frac{\pi * (\phi - 2\,\Gamma)^2}{4} * dl_\phi \tag{6.73}$$

With l_ϕ according to eq. (6.70) inserted in eq. (6.73) we obtain:

$$dV_{red;\phi} = a.V * \frac{(\phi - 2\,\Gamma)^2}{\phi^3}\, d\phi$$

Integrating with respect to ϕ we obtain the total reduced pore volume:

$$V_{red;\phi} = \int \{a.V * \frac{(\phi - 2\,\Gamma)^2}{\phi^3}\}\, d\phi$$

$$V_{red;\phi} = a.V * [\ \ln \phi + \frac{4\,\Gamma}{\phi} - \frac{2\,\Gamma^2}{\phi^2}\ ] + C \tag{6.74}$$

The constant C can be determined from the requirement that for $\phi=\phi_0$ the volume $V_{red;\phi}$ is zero. After choosing the layer thickness Γ, the constant C is the only remaining unknown quantity and can thus be determined. It follows that:

$$C(\Gamma,\phi_0) = -\ a.V * [\ \ln \phi_0 + \frac{4\,\Gamma}{\phi_0} - \frac{2\,\Gamma^2}{\phi_0^2}\ ] \tag{6.75}$$

With eq. (6.74) the volume is given in which free capillary water can be accommodated. The largest pore still completely filled with water, ϕ_{wat}, can be obtained by equalizing $V_{red;\phi}$ (eq. (6.74)) with the volume of free capillary water V_{fr}. The latter volume must in turn be obtained from the expression (6.66), viz. (in reshaped form):

$$V_{fr} = V_{cap} - V_{ad}$$

In this expression the value of the free capillary water V_{cap} is a known quantity (via eq. (6.62)), whereas the volume of the adsorbed water layer V_{ad} is still to be determined. For the determination of the volume of this water layer the reasoning is as follows: For the cross-sectional surface of an adsorbed cylindrical water layer with thickness Γ and outer diameter d it holds that:

$$O_{ad;\Gamma,\phi} = \frac{\pi * \phi^2}{4} - \frac{\pi * (\phi - 2\ \Gamma)^2}{4}$$

For the water volume adsorbed at the pores walls of fraction F_ϕ we obtain (with pore length dl_ϕ according to eq. (6.70)):

$$dV_{ad;\phi} = O_{ad;\Gamma,\phi} * dl_\phi = \frac{4 * a.V * (\Gamma * \phi - \Gamma^2)}{\phi^3}\ d\phi$$

Integrating between ϕ_0 and ϕ_{por} yields the volume of the ad-sorbed water layer:

$$V_{ad} = \int_{\phi_0}^{\phi_{por}} 4 * a.V * \frac{(\Gamma * \phi - \Gamma^2)}{\phi^3}\ d\phi$$

For the amount of adsorbed water at a degree of hydration α it follows:

$$V_{ad}(\alpha) = 4 * a.V * [- \frac{\Gamma}{\phi} + \frac{\Gamma^2}{2\ \phi^2}]_{\phi_0}^{\phi_{por;\alpha}} \tag{6.76}$$

where $\phi_{por}(\alpha)=\phi_{max}(\alpha)$ is the maximum pore size according to eq. (6.65). Inserting eq. (6.62) and (6.76) in equation (6.66) yields the free capillary water $V_{fr}(\alpha)$. The largest pore completely filled with water, $\phi_{wat;\alpha}$, can now be determined in a way similar to the calculation of the $\phi_{por}(\alpha)$, i.e. with an expression similar to eq. (6.65):

$$\phi_{wat;\alpha} = \phi_0 * \exp\ [\frac{(V_{fr}(\alpha)\ )}{a}] \quad [\mu m] \tag{6.77}$$

The effectively wetted pore wall area is determined by the largest filled pore $\phi_{wat;\alpha}$. For this area it can be derived (analogously to expression (6.72)):

$$A_{wat}(\alpha) = -\ 4 * a.V * \{\ \phi_{wat;\alpha}^{-1} - \phi_0^{-1}\ \} \quad [\mu m^2] \tag{6.78}$$

For the reduction factor $\Omega_2(\alpha)$ (eq. (6.67)) defined previously it follows:

$$\Omega_2(\alpha) = \frac{A_{wat}(\alpha)}{A_{por}(\alpha)} = \frac{-\ 4 * a.V * \{\ \phi_{wat;\alpha}^{-1} - \phi_0^{-1}\ \}}{-\ 4 * a.V * \{\ \phi_{por;\alpha}^{-1} - \phi_0^{-1}\ \}}$$

or

$$\Omega_2(\alpha) = \frac{\phi_{wat;\alpha} - \phi_0}{\phi_{por;\alpha} - \phi_0} * \frac{\phi_{por;\alpha}}{\phi_{wat;\alpha}} \tag{6.79}$$

Note that the form of the expression (6.79) does not change when the thickness of the adsorbed layer changes. Neither will its form change when the pore size distribution is described with a more sophisticated expression, i.e. with a coefficient n in eq. (6.58) taken unequal to 1.

6.5.5.6 Reduction Factor $\Omega_2(\alpha)$. Indicative Values

For a pore size distribution according to eq. (6.58), with ϕ_0=0.002 μm and a=36 10^9 μm^3, the reduction factor $\Omega_2(\alpha)$ has been determined as a function of the degree of hydration for different w/c ratios and different values of the thickness of the adsorption layer Γ.

The effect of the w/c ratio is shown in Fig. 6.16 for Γ=0. We see a very steep decrease of the $\Omega_2(\alpha)$-value when the degree of hydration approaches its ultimate value. For w/c ratios exceeding about 0.4 the effect of the w/c ratio is negligible for degrees of hydration in the practical range.

The effect of a remaining adsorption layer on the pore walls is shown in Fig. 6.17. For ω_0=0.2 and 0.4 the reduction factor $\Omega_2(\alpha)$ is given for an alternative with a dry pore wall, i.e. Γ=0, and for a one, a two and a three mono-molecular thick layer, i.e. Γ≈3, 6 and 9 Å, respectively. From the course of the theoretical $\Omega_2(\alpha)$-curves it can be concluded that the assumed phenomenon of gradual emptying of the larger pores can significantly affect the rate of hydration mainly in the final stage of the hydration process.

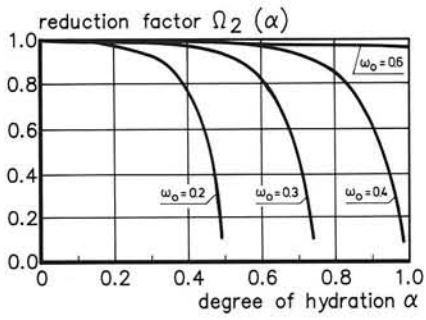

Fig. 6.16 Reduction factor $\Omega_2(\alpha)$ as function of the degree of hydration for different w/c ratios.
Adsorption layer Γ=0.

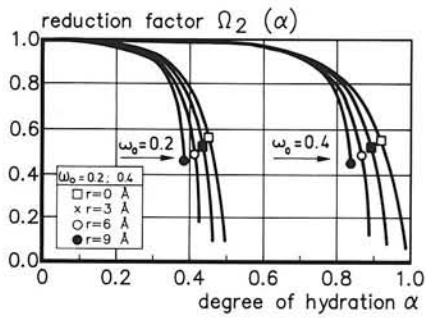

Fig. 6.17 Reduction factor $\Omega_2(\alpha)$ as a function of the degree of hydration.
Thickness of the adsorption layer as parameter. ω_0=0.2 and 0.4.

Note that Figs. 6.16 and 6.17 refer to hydration under sealed conditions. Ingress of additional water from outside would change the slope of the curves. The majority of practical curing conditions in actual structural elements, however, can be considered identical to sealed conditions.

6.5.6 Effect of Decrease of Water Content. Reduction Factor $\Omega_3(\alpha)$

6.5.6.1 General

As the hydration process progresses, the *amount of water* involved in the reaction with cement decreases. The reduction of the amount of water in the hydrating paste is considered to cause a decrease in the rate of hydration (Sections 5.4.1 and 5.4.2). In Section 5.4.1 Röhling [498] has been quoted, who proposed to allow for the effect of this phenomenon with a "water concentration factor C_w", represented by eq. (5.37). The factor C_w is diagrammatically shown in Fig. 6.18 as a function of the degree of hydration for different values of the w/c ratio. With the introduction of this water concentration factor Röhling has been able to simulate the effect of the water reduction fairly satisfactorily.

The promising results obtained with Röhling's phenomenological approach constitute a challenge for further research in this direction in order to clarify the physical background of this factor. In this respect the considerations laid down in the preceding Section should be referred to. It was assumed there that the rate of hydration is a function of the effectively wetted pore wall area relative to the total pore wall area. We saw that only at high degrees of hydration such a rate reduction mechanism could result in a substantial reduction of the overall rate of hydration. Fig. 6.18, however, suggests a significant reduction of the rate of hydration at relatively low values of the degree of hydration. Obviously the rate

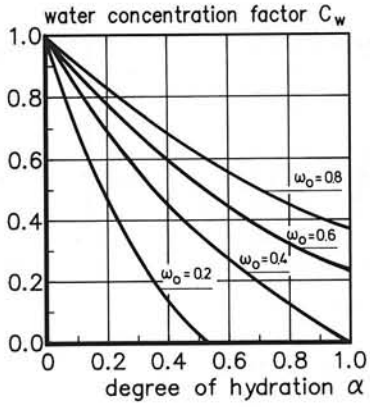

Fig. 6.18 Water concentration factor C_w (eq. 5.37) to allow for water shortage in the paste (deduced from [498]).

of hydration does not only depend on the *availability* of water immediately at the pore wall surfaces, but also on the total *amount* of water in the pore system. This conclusion makes it essential to consider a point not discussed so far, namely that of the ion concentration in the pore water and the effect of it on the rate of hydration.

6.5.6.2 Pore Water Chemistry and Rate of Reaction. Some Considerations

As discussed in Section 3.6 the ion concentration in the liquid phase exhibits significant changes during the hydration process. Nevertheless, in mathematical simulation models for cement hydration this concentration has been considered constant throughout the duration of the hydration process [498]. This simplification substantially eases mathematical modelling of the concentration-related aspect of the hydration process. Even the assumption of a constant ion concentration in the liquid phase, however, gives rise to interesting considerations with respect to the rate of hydration if the *reduction of the amount of pore water* is taken into account.

On condition of *a)* a flat surface of the reactant, *b)* a constant concentration difference over the thickness of the product layer and *c)* a constant value to the diffusion coefficient, the rate of penetration dy/dt of the reaction front can be described according to (see Fig. 6.19):

$$dy/dt = A * dC/dr \tag{6.80}$$

where:

$dC/dr = (C_0 - C_1)/\delta(t)$;

C_0, C_1 = ion concentration in the pore water and at the surface of the reactant, respectively;

$\delta(t)$ = total thickness of the product layer at time t;

A = a constant.

Let us focus now on the ion concentration in the pore water, and in particular on the Ca^{++} concentration. A basic principle in reaction kinetics says that in the case of a constant ion concentration the rate of reaction is also constant. This principle, although not unconditionally applicable for diffusion controlled reactions, has nevertheless been considered to have some relevance for the effect of the ion concentration in the pore water on the rate of reaction. The constancy of the ion concentration implies a balance between the amount of ions that are going from the anhydrous surface into the solution and the amount of ions used for the formation of new hydration products. A balance which holds also when due to progress of the hydration process the amount of water in the pore system available to accommodate the Ca^{++} ions decreases.

The balance between supply and precipitation of ions, i.e of the reaction products, without noticeable fluctuations in the ion concentration in the pore water in later stages can easily be expressed in formulae. For this purpose we consider the dissolution of a certain amount of cement, $\Delta v_{ce;j}$, during an increment of time Δt_j. Part of the Ca^{++} ions involved in the dissolution process are used up for the formation of inner products. The remaining Ca^{++}

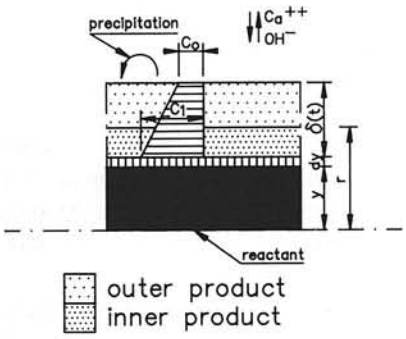

Fig. 6.19 Diffusion controlled reaction: diagrammatical representation.

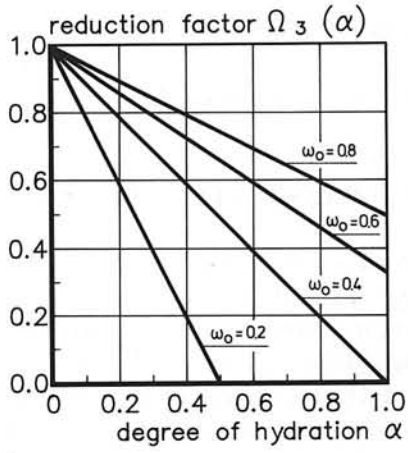

Fig. 6.20 Reduction factor $\Omega_3(\alpha)$ for water reduction in hydrating mass (eq. (6.85)).

ions pass through the diffusion layer and go partly into solution and partly form outer products. The amount of water available to accommodate the Ca^{++} ions at time t_j is

$$v_{w;j} = \frac{\omega_0 * G_\infty - 0.4 * \alpha_j * G_\infty}{\rho_w} = \frac{\omega_0 - 0.4 * \alpha_j}{\rho_w} \tag{6.81}$$

A constant ion concentration C_0 in the pore water requires correlations between the amount of cement dissolved in the time step Δt_j, the amount of reaction products formed in this time step and the (decreasing) amount of water available to accommodate the ions. For the correlation between the ion concentration $(C_0)_j$ and the amount of cement $\Delta v_{ce;j}$ dissolved in time step Δt_j is given by:

$$(C_0)_j \div \frac{\Delta v_{ce;j}}{v_{w;j}} \tag{6.82}$$

For the initial concentration reached in the first increment of time $\Delta t_{j=1}$ it holds analogously:

$$(C_0)_{j=1} \div \frac{\Delta v_{ce;j=1}}{\omega_0 * \frac{G_\infty}{\rho_w}} \tag{6.83}$$

where G_∞=1 g and ρ_w=1 g/cm^3. The assumed constancy of the ion concentration requires that $(C_0)_j=(C_0)_{j=1}$. Equalizing eqns. (6.82) and (6.83) and with $v_{w;j}$ according to (6.81) results in:

$$\Delta v_{ce;j} = \Omega_3(\alpha) * \Delta v_{ce;j=1} \tag{6.84}$$

in which $\Omega_3(\alpha)$ is the reduction factor which accounts for the water shortage:

$$\Omega_3(\alpha) = \frac{\omega_0 - 0.4\ \alpha_j}{\omega_0} \tag{6.85}$$

A diagrammatical representation of the reduction factor $\Omega_3(\alpha)$ is shown in Fig. 6.20. The curves for $\Omega_3(\alpha)$ appear to be quite similar to the curves for the water concentration factor C_w proposed by Röhling as shown in Fig. 6.18. From the good agreement between $\Omega_3(\alpha)$ and C_w we may *not* unconditionally conclude to the correctness of the way in which the effect of a decreasing water content in the pore system on the rate of hydration is modelled. The remarkable semblance of the curves in Fig. 6.18 and 6.20, however, make us prepared, for the time being, to accept the outlined approach.

It has been noted already at the beginning of this Section that, unlike as assumed in the derivation of eq. (6.85), the ion concentration in the liquid phase is not a constant, but changes during the hydration process. These changes are most remarkable in the stage when the reaction mechanism changes from a boundary reaction into a diffusion controlled reaction. The coincidence of the change from one reaction mechanism to another with the significant change in ion concentration makes it hard to decide whether the change in ion concentration is the *cause* or the *result* of the change in reaction mechanisms. Undoubtedly the two phenomena are interrelated, but reliable modelling of this interrelationship was considered to be beyond our current ability. As far as mathematical modelling is concerned the coincidence of these two phenomena will inevitably affect the absolute values for the transition thickness δ_{tr} and the coefficient β_1, which values have to be determined from experimental hydration data. Since the values of these parameters also reflect the effect of phenomena not explicitly considered it would be better to consider them as "apparent" values.

Critical Remarks

In the foregoing the effect of the decrease of the amount of water on the rate of hydration has been discussed in connection with presumed associated effects on the ion concentration in the liquid phase. The very subject, viz. the effect of the amount of water and asso-

ciated changes (or absence of changes) of the ion concentration in the liquid phase, has been discussed in literature by several authors but, unfortunately, with divergent conclusions. This makes us reluctant to make firm statements as to whether the described phenomenon has a major impact on the progress of the reaction process. More comprehensive research on this point is badly required. As noticed in the foregoing already, the decreasing ion concentration in the liquid phase with progress of the hydration process and the resulting, i.e. associated, effects on the rate of reaction is one of the items that should be given more attention in further investigations. Moreover, the formation of interparticle contact surfaces and the associated decrease of the surface of the reactant that is in contact with the liquid phase (shielding effect: see Section 5.5.2.3) is still to be considered as another phenomenon that might affect the rate of the reaction in the same direction as aforementioned phenomena may do. These facts, i.e. the occurrence of several simultaneously operating mechanisms, should be born in mind when interpreting the results of the evaluation program in Chapter 8, where the model parameters K_0, δ_{tr} and β_1 are established.

6.5.7 Water Shortage Effects. A Comparison of Different Concepts

6.5.7.1 General

In Section 5.4.2 two expressions have been quoted, one of Parrott (eq. (5.40)), and one of Jonasson (eq. (5.41)), which relate the rate of hydration to the relative humidity. In order to allow for the effect of the decreasing amount of water on the rate of hydration Röhling introduced the water concentration factor C_w, which was expressed as a direct function of the degree of hydration (eq. 5.37). In HYMOSTRUC water shortage effects are accounted for by two reduction factors, viz. $\Omega_2(\alpha)$ and $\Omega_3(\alpha)$. Both factors are expressed, either directly or indirectly, as functions of the degree of hydration α (eq. (6.79) and eq. (6.85)). It would be useful to know to what extent the different approaches for allowing for water shortage effects quantitatively agree with, or deviate from each other. In the following Sections the different concepts will be compared with each other for a cement paste with w/c ratio ω_0=0.4.

6.5.7.2 Water Shortage Concepts. HYMOSTRUC versus Röhling

In Section 6.5.6 the variation of the water concentration factor C_w has already been compared with the reduction factor Ω_3. An integral comparison of the C_w-concept and the approach followed in HYMOSTRUC requires a comparison of the C_w-values with the product $\Omega_{23}=\Omega_2*\Omega_3$. The latter quantity Ω_{23} can easily be obtained from data presented in Fig. 6.17 and 6.20. Fig. 6.21 shows the C_w-curve together with two Ω_{23}-curves as a function of the degree of hydration. One Ω_{23}-curve is based on Ω_2-values determined without making allowance for water adsorption at the empty pore walls (Γ=0 Å), whereas for the second curve a two mono-molecular adsorption layer is considered (Γ=6 Å). From a theoretical

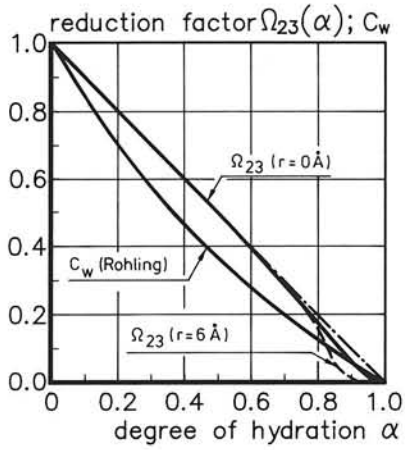

Fig. 6.21 Reduction factors C_w (Röhling) and $\Omega_{23}(\alpha)$ (HYMOSTRUC) allowing for water shortage in the paste. ω_0=0.4.

point of view the second Ω_{23}-α curve should be considered as the most realistic of the two. The curves presented in Fig. 6.21 show that the theoretically determined reduction factor $\Omega_{23}(\alpha)$ is in good accordance with the phenomenological reduction factor C_w found by Röhling.

6.5.7.3 Water Shortage Concepts [5]).

In order to compare the reduction factors β(RH) as proposed by Parrott and Jonassen (see Section 5.4.2) with the reduction factor $\Omega_{23}(\alpha)$ in HYMOSTRUC these two factors have to be expressed as functions of similar parameters. This implies that a relationship can be established between the relative humidity RH in the pore system and the degree of hydration α. In order to find this relationship we have to enter into the field of thermodynamics. The state of water and relative humidity in the pore system of a cement paste has been investigated thoroughly by, among others, Setzer [533]. In the present study the state of water in the pore system has been investigated with the help of a simple formula which was also used by Grün and Grün [216]. According to these authors the relationship between the relative humidity in the pore system and the maximum pore size completely filled with water could be described using the expression:

[5]) Koenders has elaborated the basic thoughts addressed in this section in more detail. The aim of his work was to model the volume changes of cement paste and concrete associated with self-desiccation processes. Koenders, E.A.B. (1997) *Simulation of volume changes in hardening cement-based materials*, Thesis, Delft.

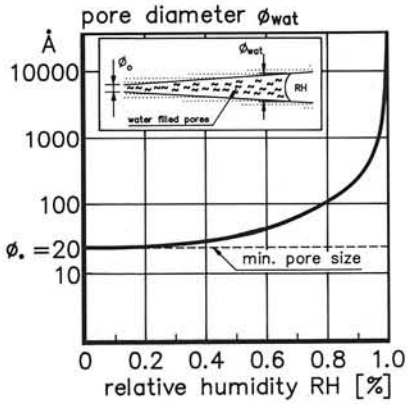

Fig. 6.22 Maximum pore ϕ_{wat} of complete water-filled pores as a function of Relative Humidity according to eq. (6.86).

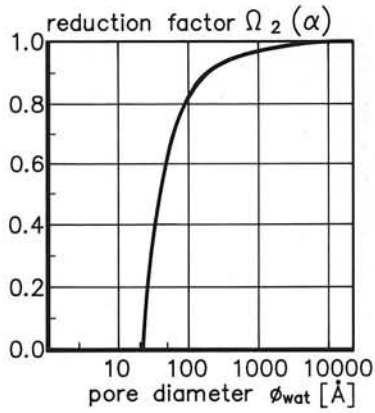

Fig. 6.23 Reduction factor $\Omega_2(\alpha)$ as a function of the maximum pore $\phi_{wat;\alpha}$ which is completely filled with water (eq. (6.79)).

$$RH = \frac{P_K}{P_0} = e^{-\frac{2.\sigma}{R.T.\gamma_w.\frac{\phi_{wat}}{2}}} \tag{6.86}$$

where:

P_0 = atmospheric pressure
P_K = water vapour pressure in pore system
R = $4.9\ 10^3$ [cm/K] = gas constant of water vapour
T = absolute temperature [K]
γ_w = specific mass of water
σ = surface tension of water: normally 72 dyne/cm (1 dyne = 10^{-5} N)
ϕ_{wat} = diameter of maximum pore filled with water

With σ in N/m, R in m/K, T in K, γ_w in N/m^3 and ϕ_{wat} in m, the relative humidity RH can be calculated as a function of the pore size ϕ_{wat}. Results are given in Fig. 6.22. In Fig. 6.23 the reduction factor $\Omega_2(\alpha)$ (eq. (6.79) for ω_0=0.4) is expressed as a function of the maximum filled pore size $\phi_{wat;\alpha}$. The information given in Fig. 6.22 and 6.23 is sufficient to express the reduction factor $\Omega_2(\alpha)$ as a function of the relative humidity RH in the pore system, simply by eliminating the factor ϕ_{wat} (Fig. 6.24). In Fig. 6.17 the reduction factor $\Omega_2(\alpha)$ was expressed as a function of the degree of hydration α. Combining the information given in Figs. 6.17 and 6.24, i.e. eliminating the reduction factor $\Omega_2(\alpha)$, results in the relationship between the degree of hydration α and relative humidity RH. For the particular paste, with a ω_0=0.4 and cured under sealed conditions, the RH-α relationship is presented in Fig. 6.25.

With the relationship between the degree of hydration and the relative humidity being known for the paste, the reduction factor $\Omega_{23}(\alpha)$ presented in Fig. 6.21 as a function of the

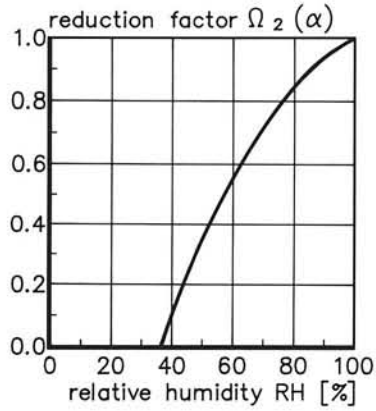

Fig. 6.24 Reduction factor $\Omega_2(\alpha)$ as a function of the relative humidity RH in the pore system. Sealed curing. ω_0=0.4. (Deduced from Figs. 6.22 and 6.23).

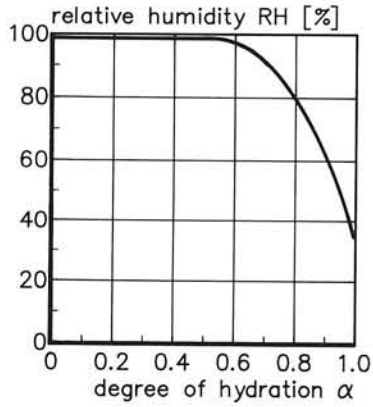

Fig. 6.25 Relative humidity RH in pore system as a function of the degree of hyhydration. Sealed curing. ω_0=0.4. (Deduced from Figs. 6.17 and Fig. 6.24).

degree of hydration α, can now be expressed as a function of the relative humidity RH, which enables comparison of the reduction factors, i.e. β_{RH}-values, proposed by Parrott and Jonasson with the Ω_{23}-values. The β_{23}-RH curves and the Ω_{23}-RH curves are presented together in Fig. 6.26. From the good agreement between both the curve proposed by Parrott and the inserted experimental data on the one hand and the Ω_{23}-RH curve on the other hand, it seems justified to conclude that the reduction factor $\Omega_{23}(\alpha)$ can be expected to cover the water shortage effects quite reliably.

Since, in our opinion, the physical relationship between the rate of hydration and the

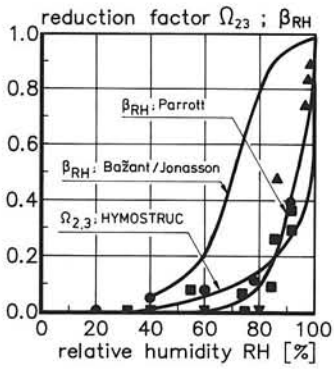

Fig. 6.26 Comparison of reduction factors which account for water shortage and water distribution effects on the rate of hydration as proposed by different authors.

relative humidity is not clear, we are inclined to state that *it is the state of water, i.e. the distribution and the amount of water in the pore system, which determines the overall rate of reaction, whereas the relative humidity is merely a parameter with which the state of water in the pore system is described.*

It is noted that the foregoing comparison of the Ω_{23}-concept with the concepts proposed by Jonasson and Parrott refer to a paste with ω_0=0.4, cured under sealed conditions.

Sealed curing conditions can be considered as representative of the majority of practical situations of concrete curing. In the case of saturated curing, water supply from outside will affect the Ω_{23}-values, particularly in later stages of the hydration process. Depending on the size of the specimen the pore system will remain completely filled with water, resulting in a constant value of Ω_2, viz. $\Omega_2(\alpha)=1$. A continues supply of water will also result in a less rapidly descending Ω_3-α curve and in a smaller reduction of the rate of hydration. It should be noted that in the case of a specimen of some size complete saturation may not be achieved, at least not in the early stage of hydration, because of the slow ingress of water into the pore system [212].

6.6 Temperature Effects

6.6.1 General

In Section 4.4 and 5.6 it has been commented that the curing temperature does not merely affect the rate of the reaction, but also the morphology and structure of the reaction products. In HYMOSTRUC we intend to model the effect of the reaction temperature on morphology and structural formation explicitly. Hence, we are obliged to find a way to separate the "net" temperature effect on the rate of chemical and physical reactions and processes from the morphology- and structure-related component of the temperature effect.

For the determination of the "net" temperature effect, to be described with the temperature function $F_1(.)$, the well-documented isothermal tests of Lerch et al. [342] have been evaluated in detail. Attempts were made to define the apparent activation energy as a function of the reaction temperature, the degree of hydration and the cement composition. For the morphology and structure related component of the temperature effect, to be accounted for using the temperature function $F_2(.)$, the experimental results of Bentur et al. [41] were evaluated.

6.6.2 Net Temperature Effect. Determination of Apparent Activation Energy

6.6.2.1 Isothermal Tests carried out by Lerch and Ford

Analysis of Test Results

Lerch et al. [342] carried out isothermal tests on pastes made with cement types I, II, III, and IV. The chemical composition (Bogue) and Blaine values of the individual cements are given in Table 8.1 of Chapter 8. The average values of the cement composition and

Blaine values per cement type are indicated in this table as well. For the individual cements, measurements of the isothermal heat of hydration were taken at four different temperatures, viz. 4.4°C, 23.9°C, 32.2°C and 40.6°C. By dividing the measured heat of hydration by the calculated maximum heat of hydration at complete hydration (see Section 3.3), the degree of hydration is obtained. Fig. 6.27 shows a typical example of thus determined hydration curves (solid curves). Actually these curves are approximations of calculated discrete hydration values with curves of the shape:

$$\alpha(T_i,t) = \exp\ [\ -a(T_i) * t^{b(T_i)}\ ] \tag{6.87}$$

where the index i refers to the individual hydration curves pertaining to the different curing temperatures. The coefficients $a(T_i)$ and $b(T_i)$ follow from least square analyses. For the majority of analyses regression coefficients ranged from 0.97 to 0.995.

The activation energy can now be calculated according to eq. (5.53). For the hydration data shown in Fig. 6.27 the AE-values are presented in Fig. 6.28 (solid lines). Three temperature ranges were considered, i.e. the 4.4°C - 23.9°C , the 23.9°C - 32.3°C and the 32.3°C - 40.6°C range. Note that, particularly in the later stages of the hydration process, the AE-values are inclined to diverge quite significantly. This particularly holds for those areas where the hydration curves presented in Fig. 6.27 approach or even intersect each other. In the latter case even negative values of the activation energy are found. In Section 5.4 we have seen that the reason for intersection of the hydration curves lies in the temperature dependency of the morphology and structure of the reaction products. A practical and straightforward way to overcome this morphology and structure related anomaly in the AE-values is achieved by a slight adjustment of the hydration curves so that intersections no longer occur in the practical range of hydration values. The adjusted hydration curves are shown in Fig. 6.27 with dashed lines. The AE-values calculated from the adjusted curves are shown in Fig. 6.28, again with dashed lines.

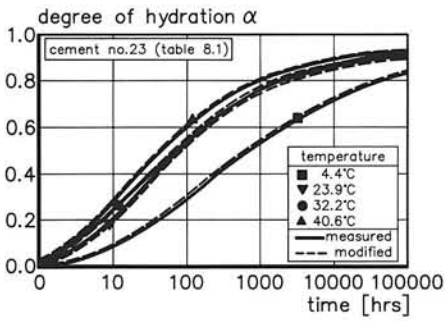

Fig. 6.27 Degree of hydration deduced from heat of hydration data (cond. cal.) (Based on data of Lerch et al. [342]).

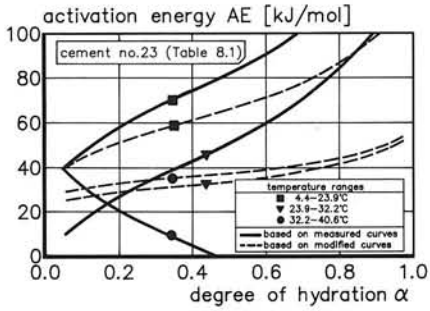

Fig. 6.28 Activation energy calculated from hydration data of Fig. 6.27.

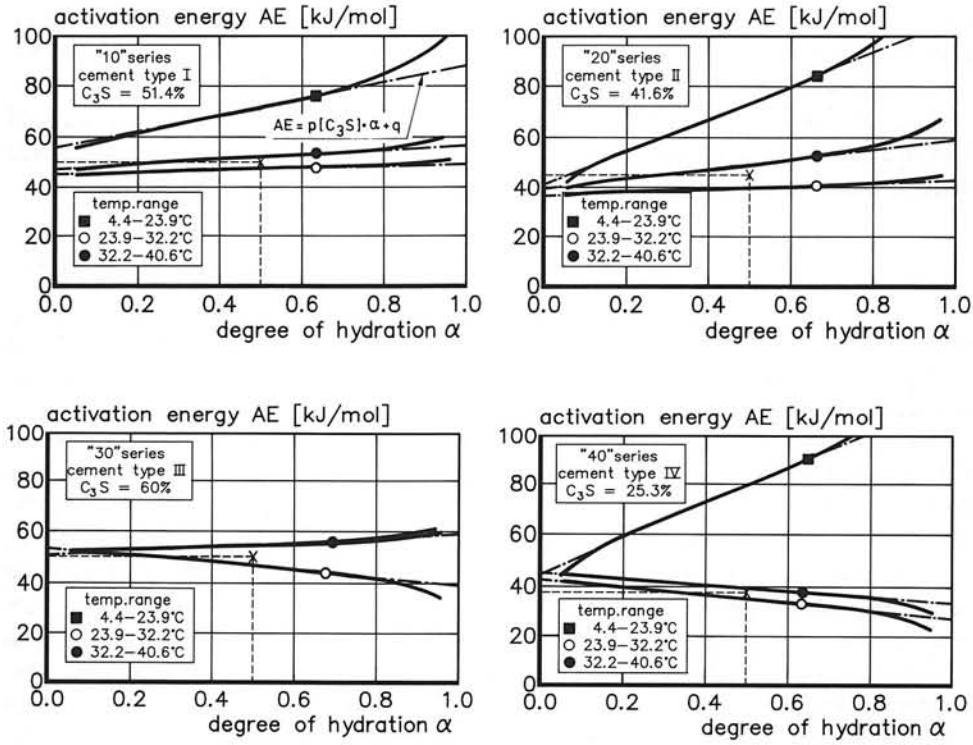

Fig. 6.29 Apparent activation energy as a function of degree of hydration for different temperature ranges. The curves represent mean values obtained for different types of cement (cement types: see Table 8.1).

All the cements indicated in Table 8.1 have been subjected to the procedure outlined above. For each type of cement the mean AE-values for the different temperature ranges are shown in Fig. 6.29a-d. The figures show a pronounced dependence of the activation energy on both the reaction temperature and the degree of hydration. It is obvious that for temperatures above about 20°C the dependence on these two parameters is much less than below this temperature.

Interpretation of the Analysis. Proposal for AE-Function

For a mathematical formalization of the information presented in Fig. 6.29 the procedure has been as follows.

For temperatures in the *high temperature range*, i.e. above 20°C, the activation energy is assumed to remain constant throughout the hydration process. The representative value of this constant activation energy is arbitrarily taken as the value at a degree of hydration α=0.5 falling just between the curves for the two higher temperature ranges (see Fig. 6.29). The thus determined AE-values are indicated in Fig. 6.30a with squares as a function of the mean value of the C_3S content of the type of the particular cement. Curve a,

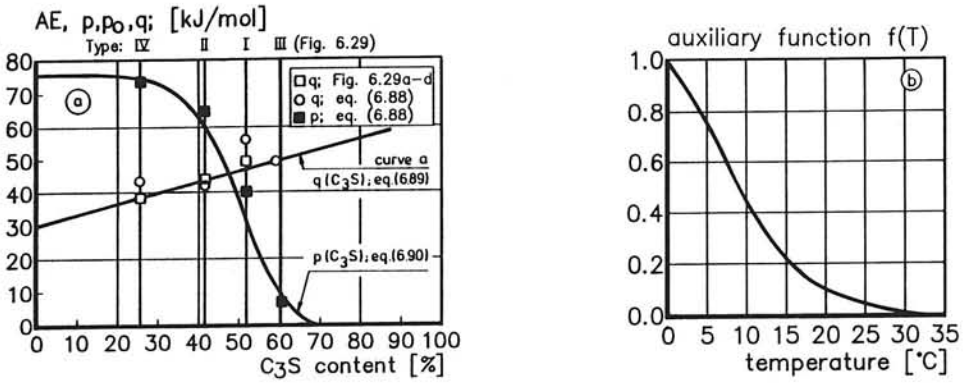

a. Formula constants p(.) and q(.)

b. Auxiliary function f(T)

Fig. 6.30 Constants p and q and auxiliary function to allow for temperature effects
Left: Constants p(.) and q(.) of expression (6.88) as a function of the mean C_3S content of the cement (deduced from test data by Lerch et al. [342].
Right: Auxiliary function f(T), proposed to establish continuity in the course of the activation energy when going from low to high temperatures.

which approximates the discretely indicated squares, shows that in the temperature range under consideration the activation energy slightly increases with increasing C_3S content.

In order to quantify the activation energy in the *low temperature range*, i.e. below 20°C, the mean AE-α curves of the four types of cement are initially approximated with linear functions of the form (see Fig. 6.29):

$$AE = p(.) * f(T) * \alpha + q(.) \qquad [kJ/mol] \qquad (6.88)$$

where p(.) and q(.) are constants of which the values are assumed to depend on the chemical composition of the cement. The function f(T) is an auxiliary function to be discussed later on. The values for p(.) and q(.), found by curve fitting, are shown in Fig. 6.30a as a function of the mean C_3S content. Fig. 6.30a shows that the q-values in eq. (6.88), denoted with open circles, which in essence represent the AE-values for α=0, do not differ very much from the AE-values found in the high temperature range which are approximated with curve a. In *both* cases a slight but distinct increase of these AE-values with increasing C_3S content is observed. It was decided, therefore, to describe the correlation between both the q- and AE-values, on the one hand, and the C_3S content, on the other, with one single linear function, viz.:

$$q(C_3S) = 0.33 * (C_3S\%) + 30 \qquad [kJ/mol] \qquad (6.89)$$

The p-values shown in Fig. 6.30a, indicated with full squares, can be correlated with the C_3S content using an expression of the form:

$$p(C_3S) = p_0 * e^{-m * (C_3S\%)^n} \qquad (6.90)$$

where m and n are constants to be obtained by curve fitting. With p_0=76 kJ/mol (see Fig. 6.30a for C_3S=0%) a regression coefficient of 0.99 was obtained for m=2.52 10^{-11} and n=6.15.

In order to allow for the change of the variable value of the activation energy in the low temperature range to the constant value in the high temperature range, a dimensionless auxiliary function f(T) is introduced. This function f(T) has to decrease gradually from f(T)=1 for T=0°C to f(T)=0 for T≈20°C. A function that suits this requirement is an exponential function of the form (see Fig. 6.30b):

$$f(T) = e^{-0.025 * T^{\frac{1}{2}}} \qquad (6.91)$$

Inserting the expressions (6.89), (6.90) and (6.91) in eq. (6.88) results in the final expression for the apparent activation energy AE [kJ/mol], viz.:

$$AE\{T,\alpha,C_3S\} = p_0 * \alpha * e^{-[m*(C_3S\%)^n + 0.025*T^{1.5}]} + 0.33*(C_3S\%) + 30 \qquad (6.92)$$

with values for p_0, m and n as mentioned in the foregoing. In Fig. 6.31 the apparent acti-

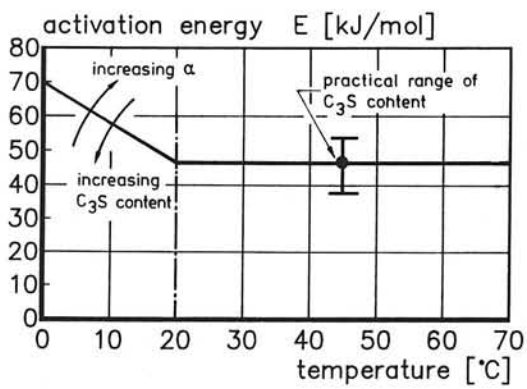

Fig. 6.31 Apparent activation energy as function of reaction temperature with indication of the influence of the C_3S content of the cement and the degree of hydration.

vation energy is expressed as a function of the reaction temperature. The influence of the C_3S content and the degree of hydration on the activation energy is indicated qualitatively.

The variation of the activation energy as presented in Fig. 6.31 shows similarity with the values mentioned by Freiesleben et al. [174], viz.:

$$AE(T) = 33.5 \text{ kJ/mol} \qquad \text{for } T > 20°C \tag{6.93a}$$

$$AE(T) = 33.5 + (20 - T) \text{ kJ/mol} \qquad \text{for } T \leq 20°C \tag{6.93b}$$

In these values the effect of the degree of hydration and the cement composition, or the C_3S content, has not been considered. From the evaluation of the experimental data of Lerch and Ford it must be concluded, however, that the latter factors may have a pronounced effect on the activation energy. A quite significant effect of these factors on the rate constants has also been reported by Röhling [500] and the author [66].

6.6.2.2 Temperature Function $F_1(T)$. Implementation in HYMOSTRUC [6])

The effect of the curing temperature T on the rate of penetration of the reaction front in an individual cement particle is accounted for with the Arrhenius function $F_1(T,a,C_3S)$ (see also Section 5.6.2.2, eq. (5.49)):

$$F_1(T,\alpha,C_3S) = A * e^{-\frac{AE(T,\alpha,C_3S)}{R*(273+T)}} \tag{6.94}$$

where R is the gas constant (8.31 10^3 kJ/mol.K), A is a constant and AE the activation energy according to eq. (6.92). In view of the determination of the constant A, the temperature T=20°C is defined as a reference temperature with a *neutral* temperature effect, i.e. $F_1(T_{20})=1$. For the constant A it follows:

$$A = e^{\frac{AE(T_{20})}{R*(273+20)}} \tag{6.95}$$

with $AE(T_{20})$ computed according to eq. (6.92).

---

[6]) In the commercial versions of HYMOSTRUC (HYMOSTRUC 2.0, 2.1 and 3.1), the first term of the right hand part of equation (6.92) is ignored when dealing with isothermal hydration processes. This in order to obviate numerical inconsistancies caused by approximative character of the auxiliary function f(T) (eq. (6.91)).

6.6.3 Morphology and Structure Related Temperature Effects on Reaction Rate

6.6.3.1 General Considerations

In order to account for the effect of temperature-induced morphological and structural changes a temperature function $F_2(T)$ has to be introduced. In the absence of detailed and directly applicable information on this subject it must be admitted that the reliability of the proposed function will be limited.

For quantification of $F_2(T)$, the experimentally obtained porosity data of Bentur et al. [41] has been evaluated. He reported on the effect of the curing temperature on the capillary porosity of C_3S pastes. The pastes, with ω_0=0.4, hydrated under sealed conditions at 4°C, 25°C and 65°C. The higher the temperature, the higher the capillary porosity, the degree of hydration being the same. This result can be interpreted as a decrease of the ratio ν between the volume of the reaction products and the reactant. The consequences of a decrease of the factor ν on the rate of reaction is twofold:

1. With decreasing value of ν the *thickness* of the product layer *decreases*. A thinner layer implies a lower diffusion resistance and hence an *increase* in the rate of reaction.
2. With decreasing value of ν the *density* of the product layer *increases*. This enhances the diffusion resistance of the product layer and will hence cause a *decrease* in the rate of reaction.

In the following, a proposal for quantification of these two contradictory effects is considered.

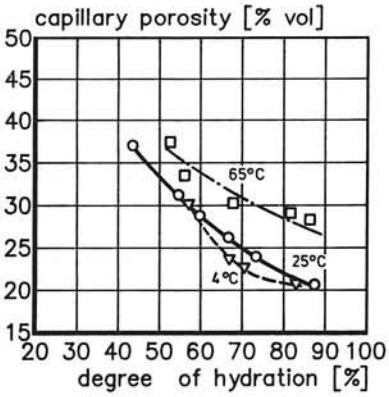

Fig. 6.32a Capillary porosity curves for C_3S pastes as a function of the degree of hydration. Temperature as parameter. (Tests of Bentur et al. [41])

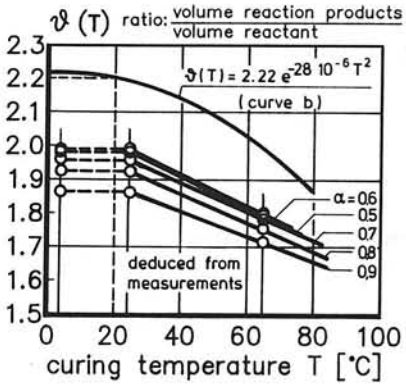

Fig. 6.32b ν-factor as a function of temperature. *Circles*: values deduced from experimental data [41].
Curve b: proposed ν(T)-function.

6.6.3.2 Determination of ν-Factor as a Function of Curing Temperature

Porosity measurements on the C_3S-pastes carried out by Bentur et al. [41] have revealed a distinct increase of the capillary porosity in the temperature range from 25°C to 65°C, whereas hardly any effect on the porosity was observed in the range from 4°C to 25°C (Fig. 6.32a). From the porosity data in Fig. 6.32a a temperature dependent ν-factor can be deduced with the help of the straightforward equation:

$$V_{por}^{cap} = \frac{\omega_0}{\rho_w} - \frac{\alpha}{\rho_s} * (\nu(T)-1) \tag{6.96a}$$

or:

$$\nu(T) = [\frac{\omega_0}{\rho_w} - V_{por}^{cap}] * \frac{\rho_s}{\alpha} - 1 \tag{6.96b}$$

where V_{por}^{cap} is the capillary porosity given in Fig. 6.32a and ρ_w and ρ_s the specific mass of water and of the C_3S, respectively. With ρ_s=3.1 g/cm^3 and ω_0=0.4, the $\nu(T_{25})$-factor was found to decrease slightly from about 2.0 to 1.85 with an increase of the degree of hydration from α=0.5 to 0.9. For the same increase in the degree of hydration the $\nu(T_{65})$-factor was found to decrease from about 1.80 to 1.70. The values are shown diagrammatically in Fig. 6.32b. This data gives an *indication* of the temperature dependency of the ν-factor. The absolute value of the calculated ν-factor, however, is substantially lower than the often mentioned value of ν=2.2. In line with what is currently used for the value of the ν-factor, but also allowing for the trends in the temperature dependency of the ν-factor as deduced from Bentur's experiments, a ν-T relationship is proposed as shown in Fig. 6.32b, curve b[7]). The corresponding mathematical expression is given by:

$$\nu(T) = 2.2 * e^{-28\ 10^{-6} \cdot T^2} \tag{6.97}$$

In this expression the temperature T, in essence, refers to an *isothermal* temperature regime. When dealing with a *variable* curing temperature, as is the case in the vast majority of all problems in engineering practice, the actual temperature history should be allowed for in one way or another. Ignoring the *temperature history* would seriously undermine the mathematical procedure for the determination of the embedded cement volume as outlined in Section 6.4.2. To solve this problem it is proposed to replace the momentary curing temperature T in eq. (6.97) by a "weighted temperature $\bar{T}$", i.e. the mean temperature in the *hydration domain*, to be calculated according to:

---

[7]) In case of more precise investigations of the volume changes of hardening pastes and concretes, and of modelling of these changes, the adoption of a ν-value of 2.2 would jeopardise the mass balance in the hardening system. In those studies more accurate ν-values have to be considered.

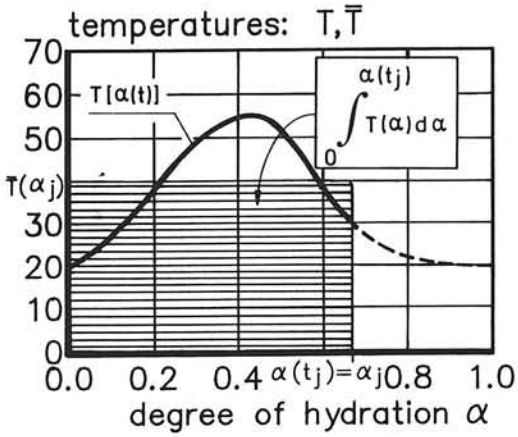

Fig. 6.33 Weighted temperature $\bar{T}$, defined as the mean temperature in the hydration domain (eq. (6.98)).

$$\bar{T}_j = \frac{1}{\alpha_j} * \int_0^{\alpha_j} T(\alpha)\ d(\alpha) \triangleq \frac{1}{\alpha_j} * \sum_{i=1}^{j} T_i * \Delta\alpha_i \tag{6.98}$$

The concept of a weighted temperature $\bar{T}$ is diagrammatically shown in Fig. 6.33.

6.6.3.3 Temperature function $F_2(T)$. Implementation in HYMOSTRUC

It is assumed that in the diffusion stage of a hydration process temperature-induced densification of the diffusion layer allows for a reduction of the rate of penetration according to:

$$F_2(T) = \left(\frac{\nu(\bar{T})}{\nu_{20}} \right)^{\beta_2} \tag{6.99}$$

with $\nu_{20}=\nu(T_{20})$ and β_2 a constant to be derived from adequate experimental data or has to determined by curve fitting as will be discussed in Chapter 8.

It is obvious that allowance for a temperature function $F_2(T)\neq 1$ will have a bearing on the considerations with respect to the transition thickness δ_{tr} as outlined in Section 6.5.2.2. When following the procedure for the determination of δ_{tr} as described in the latter section, the situation at the transition point will now lead to the expression (disregarding $\Omega_1(.)$, $\Omega_2(.)$, $\Omega_3(.)$ and $F_1(.)$, i.e. giving them the value 1):

$$K_0 * \Delta t = K_1 * \frac{\left(\frac{\nu_{tr}(\bar{T})}{\nu_{20}}\right)^{\beta_2}}{(\delta_{tr}(\bar{T}))^{\beta_1}} * \Delta t \tag{6.100}$$

where $\nu_{tr}(\bar{T})$ is the ν-factor at the moment when the transition thickness $\delta_{tr}(\bar{T})$ is reached. It is assumed now that due to temperature-induced densification of the product layer the transition thickness will decrease according to:

$$\delta_{tr}(\bar{T}) = \delta_{tr,20} * \left(\frac{\nu(\bar{T})}{\nu_{20}}\right)^{\beta_2} \tag{6.101}$$

Inserting eq. (6.101) in eq. (6.100) yields the following expression for K_1:

$$K_1 = K_0 * \frac{\left\{\delta_{tr,20} * \left(\frac{\nu(\bar{T})}{\nu_{20}}\right)^{\beta_2}\right\}^{\beta_1}}{\left(\frac{\nu_{tr}(\bar{T})}{\nu_{20}}\right)^{\beta_2}} \tag{6.102}$$

For a rate factor K_1 according to eq. (6.102) continuity has been established in the rate of penetration at the transition point, *irrespective* of the value of the ν-factor and, moreover, *irrespective* of the coefficients β_1 and β_2.

Insertion of eqns. (6.99) and (6.102) in eqns. (6.45a,b) results in the final form of the rate equation, viz.:

$$\frac{\Delta\delta_{in;x,j+1}}{\Delta t_{j+1}} = K_0 * F_1(.) * \Omega_1(.) * \Omega_2(.) * \Omega_3(.) * \left[\left(\frac{\nu(\bar{T}_j)}{\nu_{tr}(\bar{T}_j)}\right)^{\beta_2} * \left\{\left(\frac{\nu(\bar{T}_j)}{\nu_{20}}\right)^{\beta_2} * \frac{\delta_{tr,20}}{\delta_{x,j}}\right\}^{\beta_1}\right]^{\lambda} \tag{6.103}$$

with $F_1(.)=F_1(T_j,\alpha_j,C_3S)$, $\Omega_1(.)=\Omega_1(x,\alpha_{x,j})$, $\Omega_2(.)=\Omega_2(\alpha_j)$ and $\Omega_3(.)=\Omega_3(\alpha_j)$. It is clear that in this form the rate equation has lost its transparency. In Chapter 7, where the most relevant features of HYMOSTRUC are discussed, it will be endeavoured to regain its transparency by showing the impact of the individual factors and parameters on the rate of hydration.

6.6.4 Temperature Rise in Adiabatic Tests

In case of non-isothermal, adiabatic experiments the temperature rise ΔT_j reached at time t_j of the sample is calculated according to [66]:

$$\Delta T_j = \frac{\alpha_j \cdot Q^{max} \cdot G_c}{\rho_c \cdot c_c} \tag{6.104}$$

where:

Q^{max}	= maximum heat of hydration	[kJ/kg]	(see Section 3.3.2)
G_c	= cement content in the mix	[kg/m^3]	
ρ_c	= specific mass of the sample	[kg/m^3]	
c_c	= specific heat of the sample	[kJ/kg.K]	

The specific heat of the sample is, in essence, not a constant but depends on the degree of hydration and the temperature of the sample. In [66] the following expression for the specific heat has been worked out:

$$c_c = \frac{1}{\rho_c} * [\ G_c.\alpha_j.c_{cef} + G_c.(1-\alpha_j).c_{ce} + G_a.c_a + G_w.c_w\ ] \tag{6.105}$$

where:

G_a, G_w	= amount by weight of aggregate and water	[kg/m^3]
c_a, c_{ce}, c_w	= specific heat of aggregate, cement and water	[kJ/kg.K]
c_{cef}	= fictitious specific heat of the hydrated part of cement	[kJ/kg.K]

For the fictitious specific heat of the hydrated cement it would hold [66]:

$$c_{cef} = 0.0084\ T_j + 0.339 \qquad [kJ/kg.K] \tag{6.106}$$

with T_j the actual temperature of the sample at time t_j.

6.7 Chemical Composition of the Cement as Rate Controlling Factor

6.7.1 General Considerations

In Section 5.4.3 Parrott's "Multi-compound model", based on the assumption of independent hydration of the individual constituents, has been briefly discussed. In that section, and earlier in Section 3.5, it was shown that the assumption of independent hydration is certainly questionable. On the other hand, it is quite obvious that the chemical composition of the cement does have a pronounced effect on the rate of hydration. And so has the amount of gypsum that is added to the cement. Therefore, and certainly inspired by Parrott's work, attempts were made to establish a link between Parrott's independent hydration concept and the approach followed in HYMOSTRUC. As discussed until now, HYMOSTRUC is based on the "Equal Fractional Rates" concept, which, in essence, excludes Parrott's concept (see also Section 3.5.3). Nevertheless we are convinced of the need, and also of the possibility, of some kind of symbiosis of these two concepts. The possibility of

such a symbiosis will be briefly discussed in the next section.

6.7.2 Model Parameters K_0 and δ_{tr} as a Function of the Cement Composition

In Section 6.6.3.3 the final form was established of the rate equation according to which the rate of penetration of the reaction front in individual cement particles can be determined. In this equation the values of the factors $F_1(T,\alpha,C_3S)$, $\Omega_1(x,\alpha_x)$, $\Omega_2(\alpha)$ and $\Omega_3(\alpha)$, as well their development during the hydration process, are, at least for the time being, assumed to be completely predetermined by the w/c ratio, the particle size distribution of the cement and the curing temperature. Any effect of the cement composition on the rate of hydration was only considered in the temperature function $F_1(T,\alpha,C_3S)$.

Apart from these factors, the rate equation (6.103) comprises four *independent model parameters*, of which the values are still open to further investigation, viz. the basic rate factor K_0, the transition thickness $\delta_{tr,20}$ (in short: δ_{tr}) and the two coefficients β_1 and β_2. It would be most interesting if these parameters could be written as functions of the cement composition. If that were possible, these parameters could be considered as links between the equal fractional rate concept on which the stereological part of HYMOSTRUC is based, and some of the particular features of Parrott's independent hydration concept. The possible dependence of the four independent model parameters on the cement composition will be investigated quantitatively in Chapter 8. Some preliminary qualitative remarks concerning a possible correlation between both the K_0- and δ_{tr}-value and the cement composition will already be made in the next sections.

Basic Rate Factor K_0

In the discussion in Section 3.5 on this topic, as well as in Parrott's independent hydration model, it has been shown that in the early stage of the hydration process the rate of hydration is dominated by the hydration of C_3S and C_3A. In HYMOSTRUC the rate of hydration in the early stage depends predominantly on the basic rate factor K_0. It can be expected, therefore, that a more or less distinct correlation will exist between, at least, the C_3S content - generally the largest portion of the cement - and the basic rate factor K_0.

Transition Thickness δ_{tr}

The transition thickness δ_{tr} determines the change-over from a phase-boundary reaction into a diffusion-controlled reaction. At which thickness of this layer this change takes place depends on the resistance experienced by ions to pass this layer. The diffusion resistance in turn depends on the structure and porosity of both the product layer (gel porosity) and of the hardened cement paste as a whole (capillary porosity). Since the cement composition does affect the structure and porosity of the reaction (gel) products and the cement paste (Section 4.4), a correlation has to be expected between the transition thickness and the cement composition. The nature of this correlation is hard to predict. In this respect it should be borne in mind that it is not quite clear until now whether *diffusion of ions and reaction products through the product layer or diffusion of water in the capillary pore system* is the dominant rate controlling step (see Section 5.6).

6.8 HYMOSTRUC - Theoretical Part. Summary

Basic Rate Equation

In this chapter the theoretical background of a simulation model for hydration and structure formation of Portland cement-based materials has been described, called HYMOSTRUC. In a systematic calculation procedure HYMOSTRUC determines the increase of the overall degree of hydration by adding up the contributions to this quantity of the individual particle fractions. These contributions are determined from the progress of the reaction front in individual cement particles.

For the rate of penetration of the reaction front in a cement particle a rate equation is proposed in which the rate-reducing effect of structure formation, i.e. of the interaction between hydrating and expanding particles, is explicitly accounted for. This rate equation, viz. (see Section 6.6.3.3, eq. (6.103)):

$$\frac{\Delta\delta_{in;x,j+1}}{\Delta t_{j+1}} = K_0 * F_1(.) * \Omega_1(.) * \Omega_2(.) * \Omega_3(.) * \left[\left(\frac{\nu(\bar{T}_j)}{\nu_{tr}(\bar{T}_j)}\right)^{\beta_2} * \left\{ \left(\frac{\nu(\bar{T}_j)}{\nu_{20}}\right)^{\beta_2} * \frac{\delta_{tr,20}}{\delta_{x,j}} \right\}^{\beta_1} \right]^{\lambda}$$

comprises five factors, viz. the first five of the right-hand part of the equation preceding the term in straight brackets, which determine the rate of penetration in the "phase-boundary stage" of the reaction, and the term in straight brackets, which becomes operative only in the diffusion stage of the reaction, viz. when $\lambda=1$.

Effect of State of Water

The factors $\Omega_1(.)=\Omega_1(x,\alpha_{x,j})$, $\Omega_2(.)=\Omega_2(\alpha_j)$ and $\Omega_3(.)=\Omega_3(\alpha_j)$ account for different phenomena related to the momentary *state of water* in the paste. The factor $\Omega_1(x,\alpha_{x,j})$ allows for the effect of water withdrawal by small particles which are embedded in the outer shell of larger particles. This so-called water withdrawal mechanism causes a reduction of the rate of reaction of the large particles. The value of $\Omega_1(.)$ changes during the hydration process and is unique for each individual particle. The factors $\Omega_2(\alpha_j)$ and $\Omega_3(\alpha_j)$ account for the effect of the *distribution* and the *amount* of water in the pore system, respectively. They describe an "overall effect", i.e. are independent of the particle size.

Effect of Curing Temperature

The effect of the curing temperature on the rate of penetration is accounted for using a "net" temperature function $F_1(T_j,\alpha_j,C_3S)$. The value of $F_1(.)$ depends on the overall degree of hydration α and the actual curing temperature T. The $F_1(.)$-values were also found to depend on the C_3S content of the cement.

Apart from the "net" temperature function $F_1(.)$ the rate of hydration was considered to be affected by temperature-related changes of the morphology and structure of the reaction products. In order to allow for these effects the ratio between the volume of the reaction products and the original volume of the reactant, i.e. $\nu(\bar{T})$, was assumed to be a function

of the "weighted temperature $\bar{T}$", being the mean temperature in the hydration domain (Section 6.6.3.2). This ratio determines the thickness and density of the product layer and, implicitly, the diffusion resistance of this layer.

Independent Model Parameters
The rate equation (6.103) contains *four independent model parameters*, i.e. the basic rate factor K_0, the transition thickness δ_{tr} and the coefficients β_1 and β_2. The values of these parameters have to be determined from an evaluation of adequate experimental data. For the time being it is assumed that these parameters will exhibit a more or less distinct correlation with the chemical composition of the cement. These correlations will be investigated in Chapter 8.

6.9 HYMOSTRUC: Condensed Flow Chart

In a condensed flow chart presented on the next three pages the structure of the simulation program has been summarized. The input consists of the phase composition of the cement or, if available, the clinker compound composition, the particle size distribution of the cement, the w/c ratio and the specific weight of the cement. This input is evaluated in two auxiliary programs called "CEMENT" and "GRAIN", respectively. Additional input data concerning the mix composition is called for when entering the MAIN PROGRAM. After evaluation of all the input data the values of the independent model parameters are chosen. In case HYMOSTRUC is used for practical, predictive purposes the *default values* of the independent model parameters are used. These default values will be determined in Chapter 8. When HYMOSTRUC is used for pure research purposes the model parameters can also be inserted manually.

The subsequent calculation steps according to which HYMOSTRUC operates can easily be followed now from the flow chart. The output generated by HYMOSTRUC consists of the overall degree of hydration $\alpha(t)$, the penetration depth $\delta_{in;x}(t)$ and degree of hydration of in $\alpha_x(t)$ of individual particles x, the volume of embedded cement at particle level and for the system as a whole (i.e. per gram cement or per cm^3 paste), the embedded centre-plane area, again at particle level and for the system as a whole, and the (adiabatic) temperature of the mix T(t). Additional modules provide us with information about the degree of hydration and porosity in the matrix-aggregate interfacial zone.

The modular structure of the program and the step-wise calculation procedure give the program a high degree of flexibility. Additional modules can easily be inserted without jeopardizing the main numerical algorithms.

As was aimed at, the simulation program can be run in a PC-environment. The program is written in PASCAL, version 6.0. For more details about the program reference is made to section 11.9.

HYMOSTRUC - Condensed flow chart

INPUT

* mineral composition of the cement

* particle size distribution of the cement
* specific weight of cement ρ_{ce}
* w/c ratio

CEMENT (Auxiliary program)

Determination of:
* Clinker composition (according to Bogue)
* Max. heat of hydration Q^{max} (eq. 3.2) [1)]

[1)] Eq. (3.2) with q_1.....q_6 according to Bogue [12] in Table 3.1, except that for q_3 = 1,350J/g is adopted

GRAIN (Auxiliary program)

Determination of:
* R-R coefficients n and b (eq. 6.1)
* Max. particle size x_{max} (eq. 6.2)
* Mass per fraction W(x) (eq. 6.4)
* Number of particles N_x/fraction (eq. 6.6)
* "Cell" characterics:
  - cell volume l_x (eq. 6.13)
  - cell rib S_x = particle spacing L_x (eq. 6.14)
  - cell density ζ_x (eq. 6.15)

MAIN PROGRAM

INPUT

Mix composition:
* amount of aggregate and sand
* air content

---

* initial mix temperature T_0

Independent model parameters (K_0, δ_{tr}, β_1, β_2)

A If applied for engineering, predictive purpose, HYMOSTRUC operates with default values as determined in chapter 8 (par. 8.7)

B If applied for research purposes, independent model parameters can also be inserted manually

Initiation of the simulation procedure:

j = time step counter; starting with j = 0, then j = 1, 2, 3, ...
t_{max} = simulation period; default value is 1,000 hrs
$\Delta t_{j=0}$ = time increment: default value, depending on fineness of the cement
m = index, indicating minimum particle not completely hydrated; $m_{j=0}$=1
u = index, indicating maximum particle size: $x_u = x_{max}$ (determined in **GRAIN**)
i = particle counter (in x_i, with i = u, ..., m)
λ = 0 (starting with boundary reaction)
$\Omega_1(.)$, $\Omega_2(.)$, $\Omega_3(.)$ = initial values: 1
$F_1(T_0, C_3S)$ = temperature function (eq. 6.94)
$v(T)$ = volumetric ratio gel/reactant (eq. 6.97)

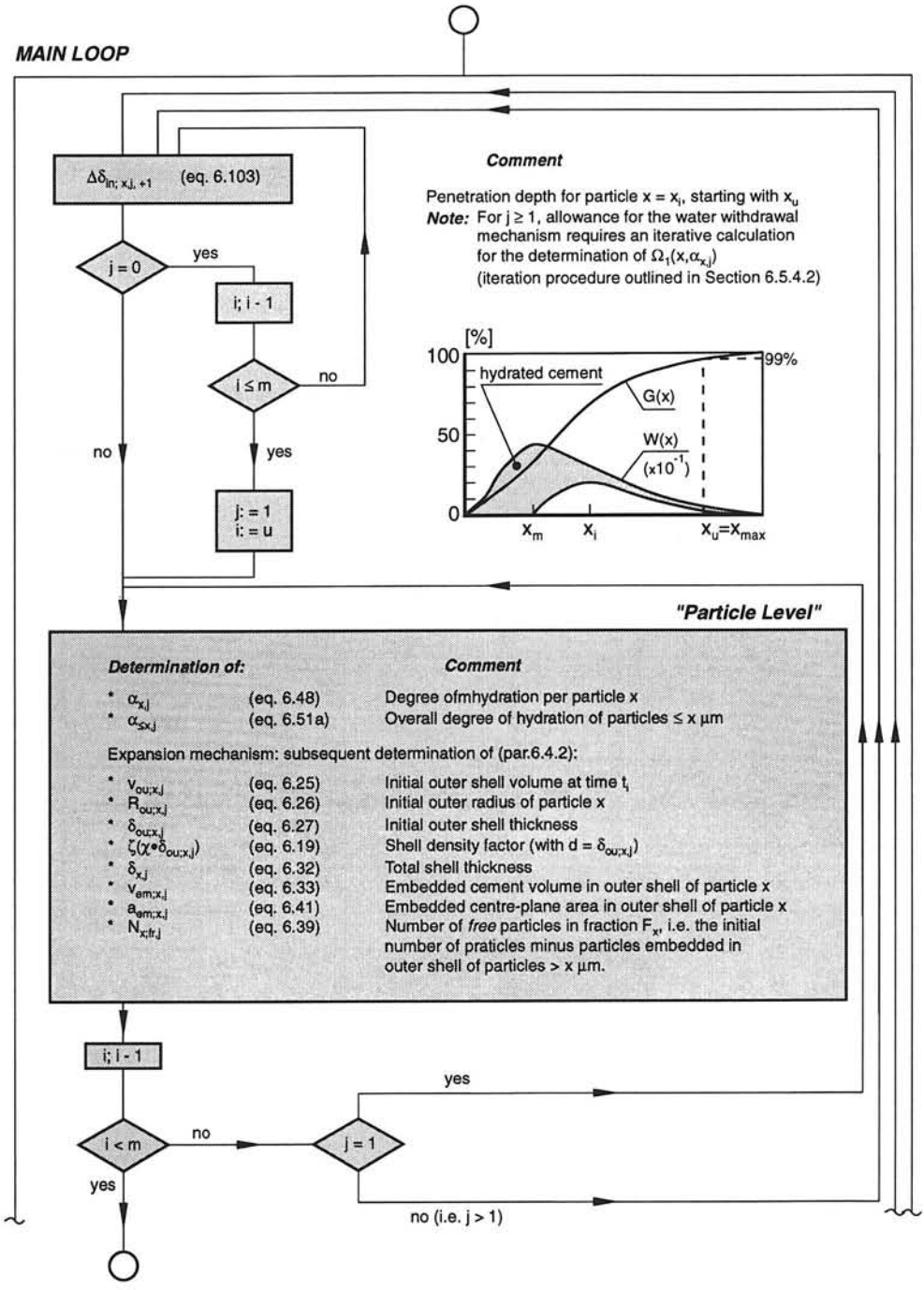
MAIN LOOP
$\Delta\delta_{in;x,j,+1}$ (eq. 6.103)
j = 0
yes
i; i - 1
i ≤ m
no
yes
no
j: = 1
i: = u
Comment
Penetration depth for particle x = x_i, starting with x_u
Note: For j ≥ 1, allowance for the water withdrawal mechanism requires an iterative calculation for the determination of $\Omega_1(x,\alpha_{x,j})$
(iteration procedure outlined in Section 6.5.4.2)
[%]
100
50
0
hydrated cement
G(x)
W(x)
(x10^{-1})
99%
x_m
x_i
x_u=x_{max}
"Particle Level"
Determination of:
Comment
• $\alpha_{x,j}$ (eq. 6.48) Degree ofmhydration per particle x
• $\alpha_{\leq x,j}$ (eq. 6.51a) Overall degree of hydration of particles ≤ x µm
Expansion mechanism: subsequent determination of (par.6.4.2):
• $v_{ou;x,j}$ (eq. 6.25) Initial outer shell volume at time t_i
• $R_{ou;x,j}$ (eq. 6.26) Initial outer radius of particle x
• $\delta_{ou;x,j}$ (eq. 6.27) Initial outer shell thickness
• $\zeta(\chi \bullet \delta_{ou;x,j})$ (eq. 6.19) Shell density factor (with d = $\delta_{ou;x,j}$)
• $\delta_{x,j}$ (eq. 6.32) Total shell thickness
• $v_{em;x,j}$ (eq. 6.33) Embedded cement volume in outer shell of particle x
• $a_{em;x,j}$ (eq. 6.41) Embedded centre-plane area in outer shell of particle x
• $N_{x;fr,j}$ (eq. 6.39) Number of free particles in fraction F_x, i.e. the initial number of praticles minus particles embedded in outer shell of particles > x µm.
i; i - 1
i < m
no
j = 1
yes
yes
no (i.e. j > 1)

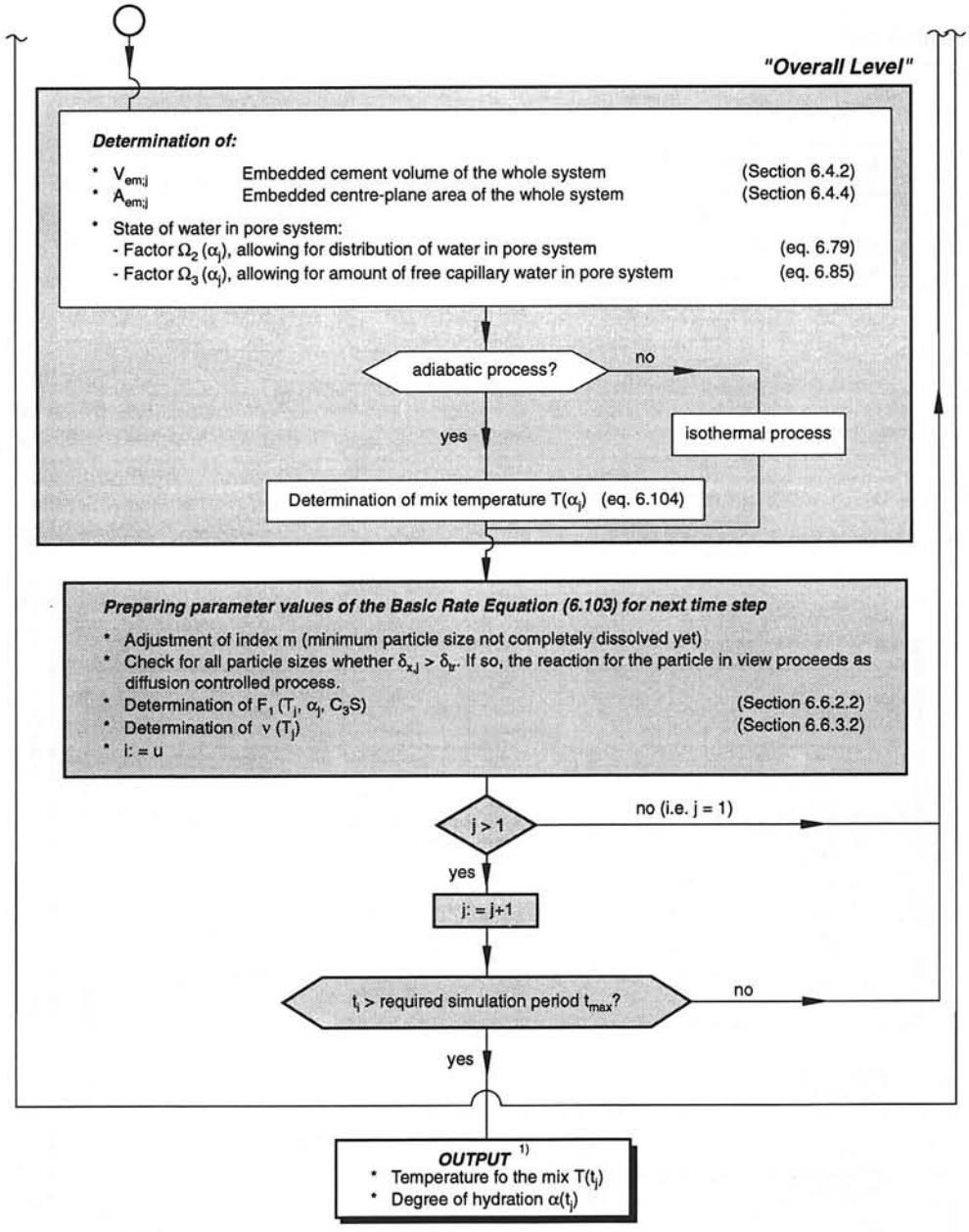

[1] If used for research purposes, information can be called for regarding embedded cement volume, embedded centre-plane area, penetration depths and thickness of the product layer of individual particles.

7 HYMOSTRUC: MODEL FEATURES

7.1 General

Since HYMOSTRUC includes several unconventional parameters and mechanisms, such as *embedded cement volume* and *embedded centre-plane area*, a *water withdrawal mechanism* and a non-traditional procedure for the quantification of the effect of *water shortage* on the rate of hydration, it is necessary to check the reliability, consistency and workability of these parameters and mechanisms. Particularly the emphasis placed on the stereological aspect of both the hydration process and structural formation needs critical appraisal. This chapter therefore discusses the main model parameters and characteristics. The suggested correlation between strength development and the increase of the embedded cement volume, i.e. the embedded centre-plane area, are dealt with. Attention is also given to the ability of HYMOSTRUC to give information about stereological aspects of hydration and structural formation in the matrix-aggregate interface zone. Some particular model features will be checked quantitatively by comparing data generated with HYMOSTRUC with the published data.

All calculations considered in this chapter have been carried out with a reduced form of the rate eq. (6.103), viz.:

$$\frac{\Delta\delta_{in;x,j+1}}{\Delta t_{j+1}} = K_0 * \Omega_1(.) * \Omega_2(.) * \Omega_3(.) * [\frac{\delta_{tr}}{\delta_{x,j}}]^{\lambda} \tag{7.1}$$

For the basic rate factor K_0 and the transition thickness δ_{tr} arbitrary values are taken. The time scales in most of the figures to be presented are, therefore, only indicative. Unless stated otherwise, the parameters $F_1(.)$, $F_2(.)$, β_1 and β_2 were taken as unity.

7.2 Clustering of Particles: Reduction of the Number of Free Particles

As outlined in Section 6.4 an expanding central particle will accommodate smaller particles in its outer shell. The resulting agglomeration of a central particle and embedded particles is called a cluster. During the hydration process the number of clusters will decrease at the cost of the number of small particles. Not only small particles but even small clusters, for example clusters with central particle x=3 μm and with no more than a couple of smaller particles in their outer shell, can be embedded in the outer shell of larger particles. In conclusion one can say, that as the hydration process progresses a shift from a large number of small clusters to a smaller number of large clusters takes place. This conclusion can be substantiated with experimental data recently published by Odler et al. [421]. For an ordinary Portland cement paste, ω_0=0.3 and Blaine=300 m^2/kg, Odler observed a change of the number of particles with a certain outer diameter during the hydration process. Fig. 7.1 shows the observed particle size distributions in a hydrating paste for t=0,

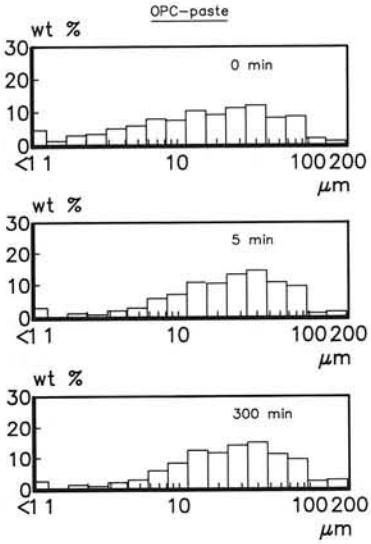

Fig. 7.1 Changes in particle size distribution in a hydrating paste as observed by Odler et al. [421].

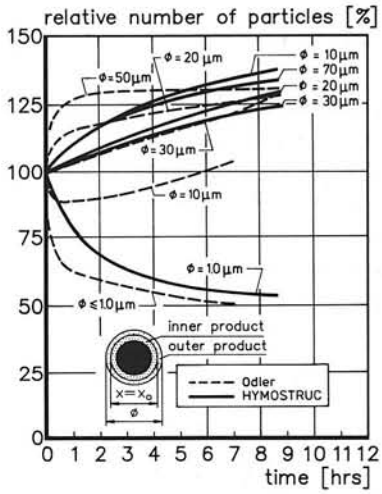

Fig. 7.2 Proportional changes in particle size distribution. Experimental (Odler et al. [421]) and according to HYMOSTRUC.

5 and 300 minutes respectively. In Fig. 7.2, deduced from Fig. 7.1, the proportional changes in particle distributions are given for particles with diameters x<1, x=10, 20 and 30 μm (dashed curves). For a cement with Blaine=350 m^2/kg HYMOSTRUC predicts a proportional change of the number of particles, or clusters, with outer diameters x=1, 10, 20, 30 and 70 μm as indicated with the solid curves in Fig. 7.2. The calculations refer to a paste with ω_0=0.5. Comparison of results is nevertheless assumed applicable, since we are interested in consistency of trends rather than in absolute values of the changes.

In view of the experimental error that has to be considered when counting the particles in a hydrating system, on the one hand, and the simplifications in HYMOSTRUC, on the other, it can be concluded that the experimental and theoretical data show at least the same trends. This warrants the conclusion that the concept of particle embedding as considered and modelled in HYMOSTRUC is not in contradiction with experimental results.

7.3 Rate of Hydration

7.3.1 Particle Hydration versus Overall Hydration

For a paste manufactured with a cement of moderate fineness, i.e. Blaine=353 m^2/kg (B4-cement, see Table 8.2), and ω_0=0.5, the calculated overall degree of hydration is shown in Fig. 7.3a. Fig. 7.3b shows the degree of hydration of six individual particles.

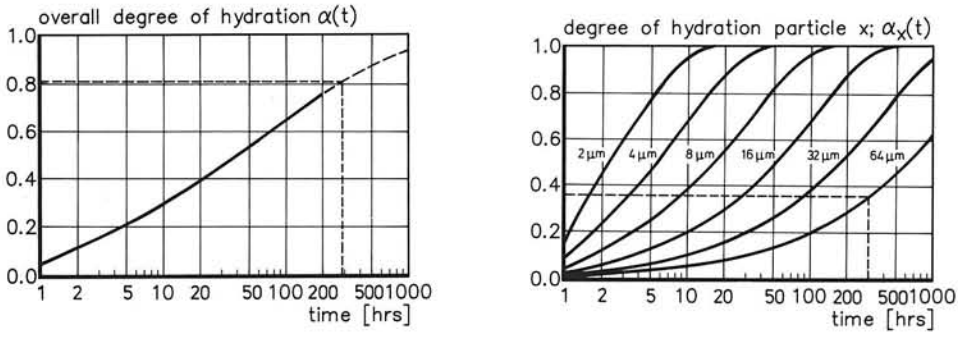

a. Overall hydration

b. Particle hydration

Fig. 7.3 Calculated degree of hydration for a B4-cement (Table 8.2)

From the curves presented in Fig. 7.3b the penetration thickness $\delta_{in;x}$ of the individual particles can be calculated using eq. (6.48). It was found that at t=100 hrs the penetration depths for particles x=8 μm and x=64 μm are 2.76 μm and 2.11 μm, respectively. So, the rate of penetration turns out to *decrease* with *increasing* particle diameter. The reason for this is two-fold. Firstly there is a *geometrical effect*, due to which the increase of the volume of the reaction products relative to the original volume of the reactant will result in a *smaller* increase of the thickness of the diffusion layer, the more curved the reaction surface. Secondly, and inherent in the first reason but certainly of greater importance: *the smaller* the outward growth of the diffusion layer (first reason), *the smaller* the amount of embedded cement and the associated *extra* expansion of the outer shell. A thin diffusion layer in turn will result in a relatively high penetration rate of the small particles.

7.3.2 Embedding of Particles and Shell Expansion

For a cement paste made with B4-cement (Table 8.2), ω_0=0.5, Fig. 7.4 shows the amount of cement embedded in the outer shell of particles with diameters x=2, 4, 8, 16, 32 and 64 μm as a function of time. The embedded cement in the outer shell of large particles can result in a significant increase of the thickness of the outer shell. This is illustrated in Fig. 7.5, where the increase of the shell thickness is shown as a function of the particle diameter at various times. It appears that during the first 50 hours of the hydration process the effect of the particle size on shell growth is not very significant. At later stages, however, when the amount of embedded cement in the outer shell further increases, the shell thickness increases significantly. This increase is greater the larger the particle diameter.

For the particles x=16 μm and x=64 μm Fig. 7.6 shows the penetration depth $\delta_{in;x,t}$ and the total shell thickness $\delta_{x,t}$ (according eq. (6.32)) as a function of time. The shell thick-

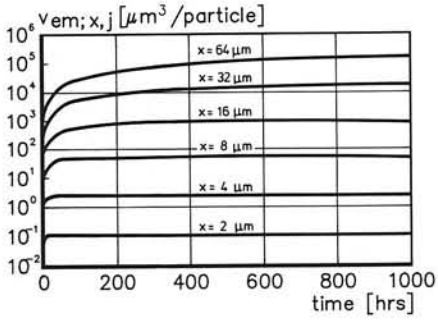

Fig. 7.4 Embedded cement volume $v_{em;x,j}$ in outer shells of hydrating particles. Paste: ω_0=0.5, B4-cement (Table 8.2).

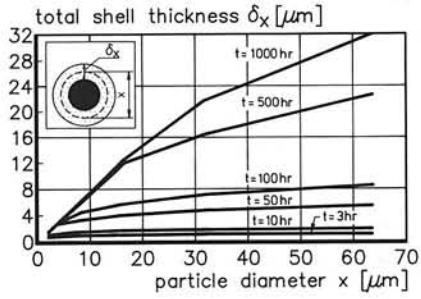

Fig. 7.5 Shell thickness δ_x as a function of the particle diameter. Paste: ω_0=0.5, B4-cement (Table 8.2).

ness that would develop if no extra expansion of the outer shell due to particle embedding had been considered is indicated with dashed lines.

It is to be expected that particularly for large particles the extra growth of the shell due to particle embedding will significantly affect the rate of hydration. Ignoring the extra increase of the effective thickness of the diffusion layer will result in misinterpretations with respect to the hydration mechanisms which might have occurred at different stages of the hydration process and hence to incorrect values of rate parameters such as diffusion coefficients.

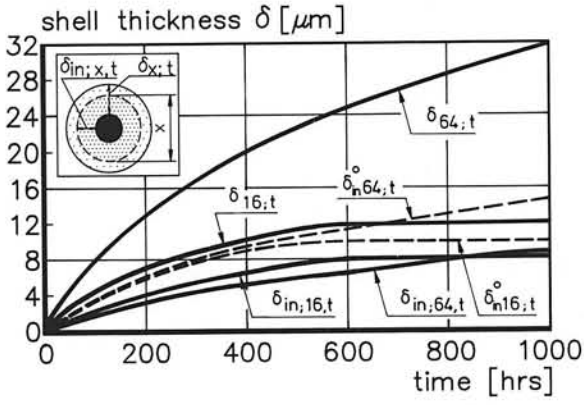

Fig. 7.6 Development of penetration depth and shell thickness as a function of time. Particles x=16 μm and 64 μm. Paste: B4-cement (Table 8.2). ω_0=0.5.
Note: $\delta^0_{in;x,t}$ = penetration depth if no particle embedding would occur (dashed lines).

7.3.3 Effects of Embedding of Particles on the Rate of Hydration

7.3.3.1 Shell Expansion and Water Withdrawal caused by Embedded Particles

The effect of particle embedding in the outer shells of hydrating particles on the rate of hydration is shown in Fig. 7.7. Calculations refer to paste hydration of the B4-cement (Table 8.2) with ω_0=0.4. No allowance is made for water shortage effects ($\Omega_2(.)= \Omega_3(.)=1$).
Curve I of Fig. 7.7 represents the rate of hydration without taking into account embedding of particles and associated expansion of the outer shell.
Curve II represents the rate of hydration in the case where extra shell expansion due to particle embedding is accounted for. Water withdrawal is still neglected, i.e. the partition factor $\Omega_1(.)$ in eq. (7.1) is taken as unity.
Curve III shows further reduction of the rate of hydration due to water withdrawal by the embedded particles, i.e. $\Omega_1(x,\alpha_x)\neq 1$, for $x_{min}<x<x_{max}$.

As the hydration process progresses the effect of water withdrawal becomes increasingly important. For the cement considered, the withdrawal effect results in a reduction of the degree of hydration of up to 10% after 28 days hydration. More details about the water withdrawal mechanism and the partition factor $\Omega_1(.)$ are given in Section 7.3.3.3.

7.3.3.2 Influence of Water/Cement Ratio on the Effect of Embedded Particles

It is to be expected that the lower the water/cement ratio, and hence the smaller the initial particle spacing, the more pronounced the effect of particle embedding and water withdrawal on the rate of hydration will be. In order to check this assumption calculations were carried out with $\Omega_1(.)\neq 1$ and $\Omega_2(.)=\Omega_3(.)=1$ for different w/c ratios. Results of the calculations are shown in Fig. 7.8, where the degree of hydration is given as a function of

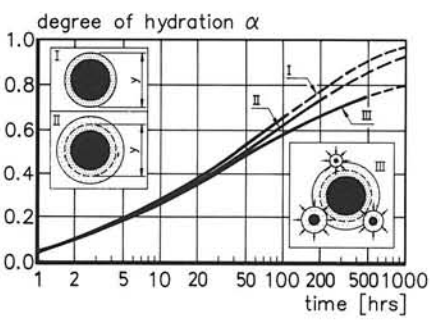

Fig. 7.7 Effect of particle embedding on the rate of hydration.
B4-cement (Table 8.2).
ω_0=0.4; $\Omega_1(.)\neq 1$; $\Omega_2(.)=\Omega_3(.)=1$

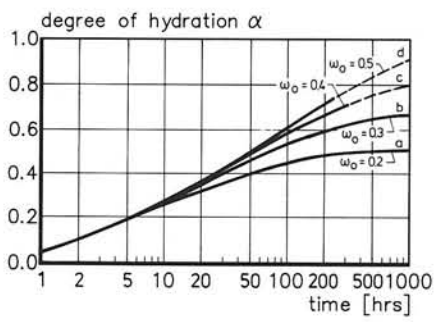

Fig. 7.8 Effect of water/cement ratio on the rate of hydration.
B4-cement (Table 8.2).
ω_0=variable; $\Omega_1(.)\neq 1$; $\Omega_2(.)=\Omega_3(.)=1$

time for ω_0=0.2, 0.3, 0.4 and 0.5, i.e. curve a, b, c and d, respectively.

From the coincidence of the curves a, b, c and d in the early stage of the hydration process it can be concluded that any effect of the w/c ratio on the rate of hydration at this stage can be attributed to neither particle embedding and associated shell expansion, nor to water withdrawal.

7.3.3.3 Water Withdrawal Mechanism: The Partition Factor $\Omega_1(.)$

In effect, the partition factor $\Omega_1(x,\alpha_x)$ divides the amount of water available for the hydration of a cluster of particles with central particle x into two parts. One part is calculated to be available for further hydration of the embedded particles and the remaining part for hydration of the central particle. A partition factor $\Omega_1(x,\alpha_x)=1$ means that no water withdrawal occurs, i.e. all the available water is used for further hydration of the central particle. A partition factor $\Omega_1(x,\alpha_x)=0$ means that all the available water is used up for further hydration of the embedded particles.

It is to be expected that for small particles, which hardly accommodate any cement in their outer shell, the partition factor will be close to 1. For large particles, however, which accommodate a substantial amount of cement in their outer shells particularly during the later stages of the hydration process, the partition factor can significantly decrease. This can be made plausible by comparing the volume of the embedded cement with the volume of the anhydrous core of a central particle. Let us consider, for example, particle x_{64} after 300 hrs hydration (Note: x_{64} = particle with diameter x=64 μm). As shown in Fig. 7.4, the amount of embedded cement at that time is about 100,000 μm^3. The degree of hydration of the *embedded cement* $\alpha_{\leq 63,300}$, i.e. of the cement in the fractions with particles x≤63 μm, can be deduced from Fig. 7.9. For t=300 hrs it holds that $\alpha_{\leq 63,300}$=0.8. This means that the amount of *unhydrated* cement present in the outer shell of particle x_{64} is (1-0.8)*100,000= 20,000 μm^3. In Fig. 7.3b it was found that at t=300 hrs particle x_{64} is approximately 35% hydrated. The volume of remaining anhydrous core of this central particle is about 89,000

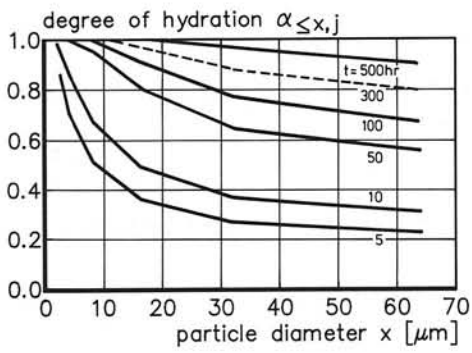

Fig. 7.9 Degree of hydration $\alpha_{<x,j}$ of fractions $\leq F_x$ for different hydration times. Paste: B4-cement (Table 8.2). ω_0=0.5.

μm^3 (=(1-0.65)*$^1/_6$.π.64^3). Since the 20,000 μm^3 of the anhydrous embedded cement is built up of particles x≤64 μm and will, therefore, exhibit a relatively large anhydrous surface area, perhaps even larger than the anhydrous surface area of the central particle, is to be expected that a major part of the water available for hydration will be used up for hydration of the embedded particles.

For a paste manufactured with the B4-cement, ω_0=0.4, the variation of the partition factor $\Omega_1(x,\alpha_x)$ is shown in Fig. 7.10a as a function of time t for particles x_{20}, x_{40} and x_{110}. The overall degree of hydration $\alpha(t)$ is indicated as well. The expected trends are quite distinct. Hydration of small particles is only slightly affected by water withdrawal effects; for particles $x<x_{20}$ it holds that: $0.84<\Omega_1(20,\alpha_{20})<1$. For larger particles the partition factor drops down to 0.64 at t≈500 h. Later on, when hydration of the embedded particles approaches completion, more water will become available for hydration of the central particle and the value of the partition factors increases again.

The lower the w/c ratio the more pronounced the effect of particle embedding and water withdrawal on the rate of hydration of the central particle will be. Fig. 7.10b shows the partition factors for particles x_{20}, x_{40} and x_{110} of a paste with the same B4-cement, but now with ω_0=0.2. It appears that the hydration of large particles will completely stop due to water withdrawal by the smaller embedded particles.

A water withdrawal mechanism as introduced here can contribute to the explanation of the observation, that even after many years of hydration the penetration depth of large cement particles is much less than the hydration depth of smaller particles (Section 3.8.2).

7.3.4 Water Shortage Effects: The Reduction Factor $\Omega_{23}(\alpha)$

The effect of the decrease of the amount of water in the pore system that is available to take part in the hydration process is allowed for with the water shortage factor $\Omega_{23}(\alpha)$=

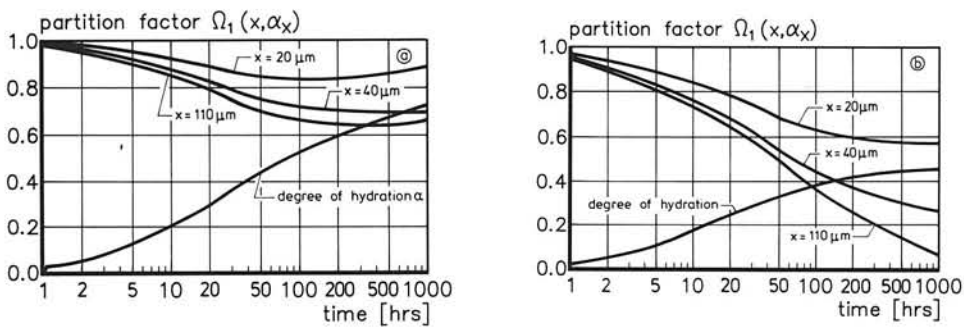

a. w/c ratio = 0.4

b. w/c ratio = 0.2

Fig. 7.10 Partition factor $\Omega_1(x,\alpha_x)$, accounting for water withdrawal by embedded cement. Paste: B4-cement (Table 8.2).

$\Omega_2(\alpha)*\Omega_3(\alpha)$. The reliability and accuracy of the water shortage factor $\Omega_{23}(\alpha)$ has been investigated by comparing the water shortage effects as predicted by HYMOSTRUC using experimental data published by Taplin [569]. Fig. 7.11 shows the amount of non-evaporable water Wn(t) of pastes made with different w/c ratios. In the absence of details concerning the chemical composition and particle size distribution of the cement it was assumed that *a)* the maximum amount of non-evaporable water would amount to $\hat{W}n=0.22$ g/g and *b)* the cement used was of moderate fineness with R-R coefficients as indicated in the legend of Fig. 11b. From the measured Wn- and assumed $\hat{W}n$-values the degree of hydration can be obtained by dividing these two quantities. The resulting hydration curves are shown in Fig. 7.11b with discrete points. The theoretical curves obtained with HYMOSTRUC are inserted in Fig. 7.11b with solid lines. The theoretical curves were obtained using a basic rate factor $K_0=0.03$ μm/h and a transition thickness $\delta_{tr}=3.0$ μm. The absolute values of these parameters, however, are not so important in this example, since we are mainly interested in the potential of HYMOSTRUC to predict the effect of the state of water in the hydrating mass on the rate of hydration. As far as this point is concerned, it can be concluded from Fig. 7.11b that the proposed reduction factor $\Omega_{23}(\alpha)$, in combination with the previously discussed water withdrawal factor $\Omega_1(x,\alpha_x)$, accounts for the effect of the decreasing amount of water on the rate of hydration quite satisfactorily.

With regard to the reliability of the measured degree of hydration reference should be made to the accuracy considerations in Section 3.4.2. It was outlined there that the coefficient of variation for the degree of hydration determined on the basis of non-evaporable water considerations can amount to about 7%. In the light of this value the deviations between the predicted and measured hydration data of Fig. 7.11b do not give rise to any further improvement or re-evaluation of HYMOSTRUC. Only in the very early stage of the hydration process the differences between measured and predicted values are relatively large. That stage of the hydration process, however, is of less importance as far as the de-

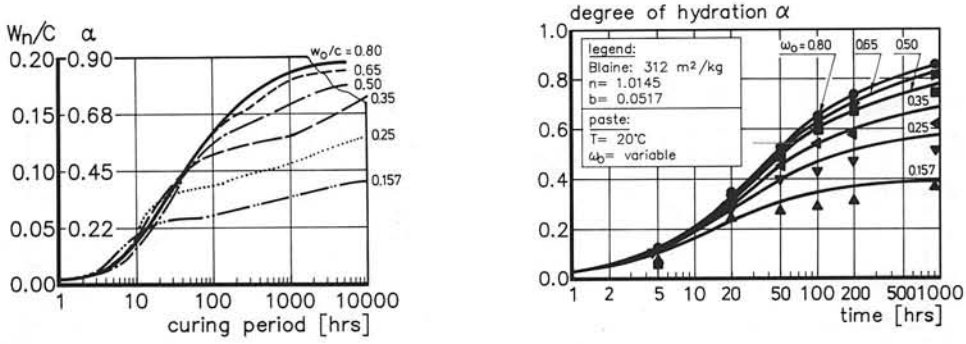

a. Data of Taplin [569]

b. HYMOSTRUC simulations

Fig. 7.11 Effect of water/cement ratio on the hydration process.
a. Non-evaporable water data for different water/cement ratios.
b. Comparison of measured and predicted degree of hydration.

velopment of the majority of engineering properties is concerned. Deviations in that stage are, therefore, of little concern in view of practical application of the simulation model.

7.3.5 Rate of Penetration

7.3.5.1 Basic Rate Factor K_0

As will be shown later in Chapter 8, the values of the basic rate factor K_0 vary in the range from 0.02 to 0.06 μm/h. For a paste made with a cement of moderate fineness and ω_0=0.4, the effect of the K_0-values in the range from 0.02 to 0.038 μm/h on the rate of hydration is shown in Fig. 7.12. In these calculations water shortage effects and the water withdrawal mechanism were not considered. For the transition thickness δ_{tr} an arbitrary value of 2 μm has been used.

7.3.5.2 Development of Rate of Penetration with Elapse of Time

The basic rate factor K_0 determines the rate of penetration as long as there are no mechanisms operative which cause a reduction of this rate. Rate reductions will be caused by water withdrawal mechanisms, water shortage effects and, when the reaction becomes diffusion-controlled, by the diffusion resistance of the product layer. For a paste made with a cement of moderate fineness, ω_0=0.65, Fig. 7.13a shows the development of the rate of penetration as a function of time for particles x=4, 8, 16 and 64 μm. The rate of penetration of large particles is substantially less than that of smaller particles (see also Section 7.3.1). A distinct drop of the rate of penetration occurs when the reaction changes from a boundary reaction to a diffusion controlled process. As indicated in the figure, the mo-

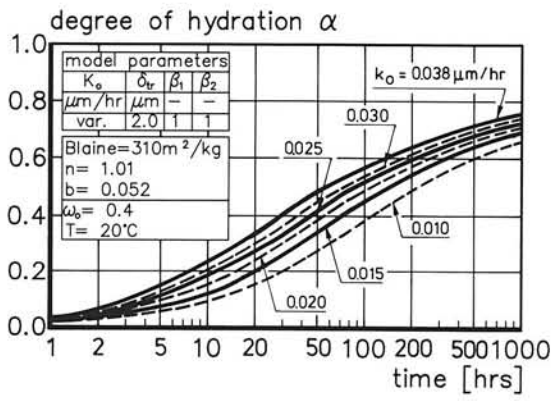

Fig. 7.12 Effect of basic rate factor K_0 on the rate of hydration. B4-cement (Table 8.2). Blaine=360 m^2/kg; ω_0=0.5.

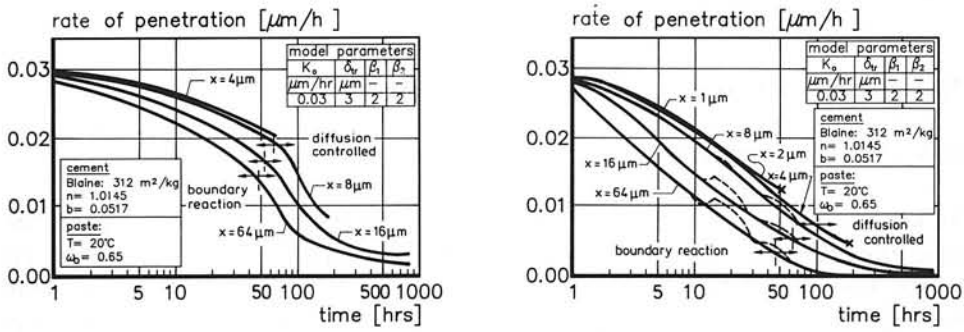

a. w/c ratio = 0.65

b. w/c ratio = 0.25

Fig. 7.13 Rate of penetration as a function of time.

ment at which this change occurs depends on the particle diameter. This is in agreement with Bezjak, according to whom different mechanisms can occur simultaneously in particles of a different size.

In Fig. 7.13b the rate of penetration is shown for particles hydrating in a paste with ω_0=0.25. As expected, the rate of penetration decreases much more rapidly than in the paste with ω_0=0.65. Particular attention must be given to the dashed curves, which represent the data which were actually generated by HYMOSTRUC. These dashed curves reveal the combined effect of the water withdrawal mechanism as it is considered in HYMOSTRUC and one of the main postulations of our model, viz. that particles of the same size hydrate at the same speed. The latter postulation implies that small particles, for example x=1 μm, which become embedded in the outer shell of a large particle, say x=64 μm, hydrate as fast as the particles which are not embedded. As soon as the embedded small particles are hydrated completely, they will no longer withdraw water from the large central particle. Consequently the amount of water available for hydration of the central particles increases, which results in an increase of the rate of penetration of these particles. It should be noted that the effect as it is shown by the dashed lines exaggerates the actual situation a little bit because of the rather large time steps that were chosen. With smaller time steps smoothly ondulating curves are obtained. It further appears that the rate of penetration of large particles has almost dropped to zero after about 150 hrs, while at that time particles of a diameter x=8 μm still hydrate, albeit at a low rate of penetration.

7.3.6 Effect of Transition Thickness δ_{tr} on the Course of the Hydration Curve

In Section 6.5.2.2 it was tentatively concluded that reasonable values for the transition thickness δ_{tr}, at which the boundary reaction changes into a diffusion-controlled reaction, might vary between 2 to 4 μm. For the B4-cement paste (Table 8.2) with ω_0=0.5 the cal-

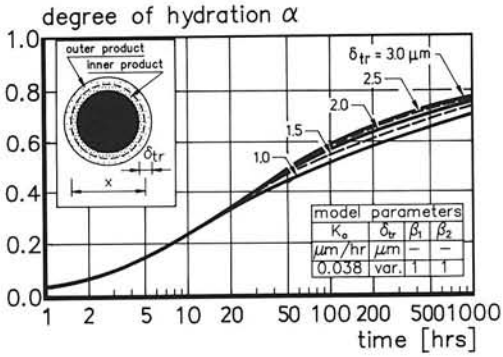

Fig. 7.14 Effect of the transition thickness δ_{tr} on the course of the hydration curve. B4-cement (Table 8.2). Blaine≈360 m^2/kg. ω_0=0.5.

culated effect of variations in the transition thickness from 1.0 to 3.0 μm on the course of the hydration curve is shown in Fig. 7.14. The higher the transition thickness the later the process becomes diffusion controlled.

7.4 Strength Considerations

7.4.1 General

As outlined in Section 4.4.5, the strength of a cement-based material should somehow be a function of the contact area or the number of contact points between expanding cement particles. In Section 6.4 it has already been suggested, that either the total *amount of embedded cement* $v^0_{em;j}$ (eq. (6.34)), or the total *embedded centre-plane area* $A_{em;j}$ (eq. (6.44)) could be considered as a measure of the contact area or the number of inter-particle contact points. Knowing, from both practice and previous publications, that in many cases strength can be described as a linear function of the degree of hydration, it might be worthwhile to investigate the relationship between the embedded cement volume and the embedded centre-plane area on the one hand, and the degree of hydration, on the other.

When investigating the relationship between these quantities the following items will be considered explicitly:

- *The effect of the w/c ratio on strength and particle embedding;*
- *The most effective particle fractions in view of particle embedding;*
- *Fracture modes: inter- and intra-particle fracture.*

The effect of the slope of the particle size distribution on both strength development and particle embedding will be discussed in Section 8.3.2.2.

7.4.2 Amount of Embedded Cement and Strength Development

This section discusses the effectiveness of individual particles to generate contact points and contact areas with other particles. Subsequently the embedded particle volume and the embedded centre-plane area are considered. The calculations refer to the previously mentioned B4-cement (Table 8.2).

7.4.2.1 Embedded Cement Volume

For different values of the w/c ratio Fig. 7.15 shows the increase of the total embedded cement $v^0_{em;j}(\alpha)$ as a function of the degree of hydration. The effect of the w/c ratio is quite pronounced, particularly for low w/c-ratio samples. For ω_0=0.5 Fig. 7.16 shows the volume of the embedded cement for individual particle fractions as a function of time. Initially the smaller fractions are most effective in accommodating cement particles in their outer shell. With elapse of time, however, the fractions with larger particles become increasingly important in this respect. It further appears that after a peak is reached the embedded cement volume decreases. The reason for this is that with elapse of time an increasing number of free particles belonging to a certain fraction F_x, i.e. free clusters with a central particle x, become embedded in the outer shells of larger particles. In this way the number of free particles in fraction F_x decreases. After some time the decrease of the embedded cement volume associated with the decrease of the free particles in fraction F_x can exceed the increase in the embedded cement volume associated with progressive hydration of the remaining free particles of the fraction considered. Hence, a net decrease of the embedded cement volume per fraction can occur as indicated in Fig. 7.16.

If the amount of embedded cement is indeed an important parameter in strength development, the tendencies shown in this figure are at any rate in agreement with the findings of those authors, who found that larger particles become effective at later stages of the hydration process (see Section 4.5.2).

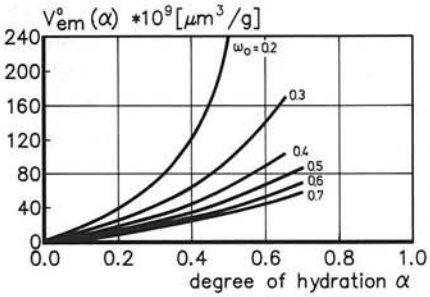

Fig. 7.15 Embedded cement volume as function of degree of hydration.
Paste: B4-cement (Table 8.2). ω_0=var.

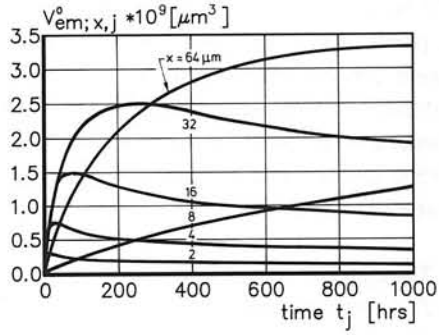

Fig. 7.16 Embedded cement volume per fraction as a function of time. Paste made of B4-cement (Table 8.2). ω_0=0.5.

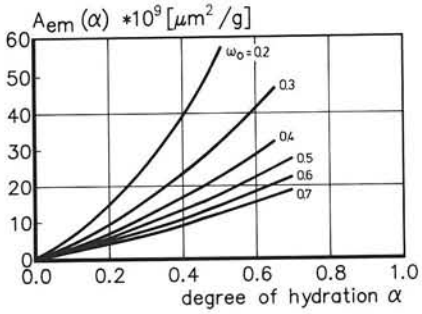

Fig. 7.17 Embedded centre-plane area $\Delta A_{em;x}$ per fraction as a function of the degree of hydration. Paste: B4-cement (Table 8.2). ω_0=variable.

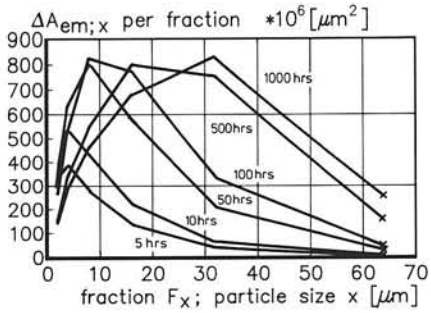

Fig. 7.18 Embedded centre-plane area $\Delta A_{em;x}$ per fraction as a function of the particle size.
Paste: B4-cement (Table 8.2); ω_0=0.5

7.4.2.2 Embedded Centre-Plane Area or Contact Surface Area

Considering the B4-cement again Fig. 7.17 shows the centre-plane area $A_{em;j}(\alpha)$ as a function of the degree of hydration for various water/cement ratios. The trends turn out to be are similar to those in Fig. 7.15. The relationship with the degree of hydration, however, is now almost linear. Similar results were obtained in the preliminary Delft studies using the simulation program HYDRASIM (Fig. 5.13).

In Fig. 7.18 the embedded contact area $\Delta A_{em;x}$ per fraction is shown as a function of the particle size. Only the embedded contact areas of the free particles in the fractions are considered. Time is inserted as a parameter. The figure shows that with elapse of time the major contributions to the contact area subsequently come from fractions with higher particle diameters. This phenomenon is similar to the one discussed above for the embedded cement volume and can be considered as consistent with experimental results showing that larger particles become more effective at later ages. It further appears that over a long period of time, i.e. from 50 to 1,000 hrs, the major contributions to the embedded centre-plane area come from the fractions between 10 and 30 μm. This might explain why the fractions between 10 and 30 μm are of major importance in view of strength development (see also Section 4.5.2).

7.4.3 Embedded Cement and Strength Development. Effect of Water/Cement Ratio

Several experiment-based procedures have been described in the literature which relate the strength f of cement paste to the degree of hydration α, and for different w/c ratios. The results of two such procedures are diagrammatically shown in Fig. 7.19. Fig. 7.19a, presented by Locher [355] shows the f/α relationships based on a proposal by Powers (see al-

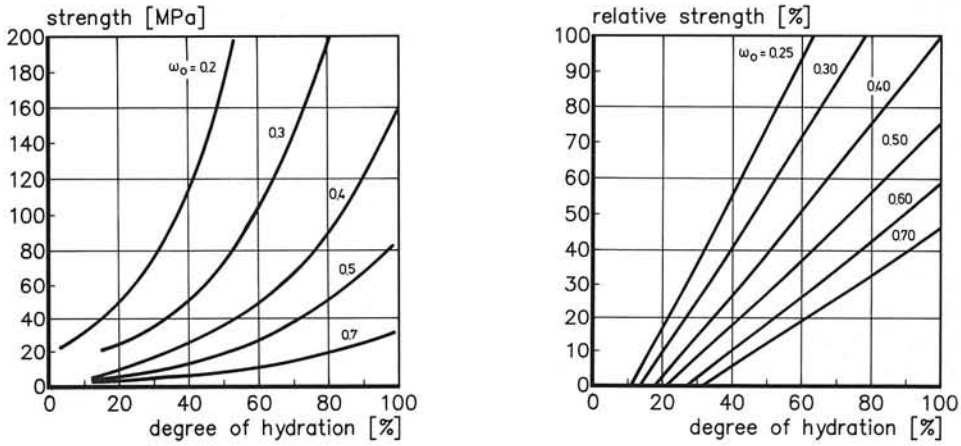

a. Paste strength (after Powers)

b. Relative strength (after Fagerlund)

Fig. 7.19 Strength as a function of the degree of hydration for different w/c ratios.
a. Paste strength according to a proposal of Powers *(Ibid [355])*.
b. Relative increase of strength according to Fagerlund [156].

so Fig. 4.19), whereas Fig. 7.19b shows the relative strength as a function of the degree of hydration after a proposal of Fagerlund [156]. Taking the ultimate strengths of the paste with ω_0=0.4 as a reference, i.e. at 100%, both figures can be transferred into dimensionless diagrams, in which the proportional strength is expressed as a function of the degree of hydration for variable w/c ratios. The thus obtained curves are shown in Figures 7.20 and 7.21 with dashed-dotted and dashed curves, respectively, for ω_0=0.3, 0.4 and 0.7. In a similar way Figures 7.15 and 7.17, representing the embedded cement volume and the embedded centre-plane or contact area, can be transferred into diagrams which show the proportional increase of the indicated quantities as a function of the degree of hydration. Bearing in mind that we actually want to check whether either the amount of embedded cement or the embedded centre-plane area can be considered as a strength parameter, it is reasonable to consider the amount of embedded cement and embedded centre-plane area *per unity of paste (by volume)*, i.e. v_{em}^{pa} and A_{em}^{pa}, instead of *per gram cement*. In this way the influence of the w/c ratio on the amount of embedded cement and the embedded centre-plane area is accounted for implicitly.

In the dimensionless form the development of the embedded cement volume v_{em}^{pa} and the embedded centre-plane area A_{em}^{pa} can be compared with the proportional increase in strength as proposed by Powers and Fagerlund. The curves indicating the proportional increase in the embedded cement volume and the embedded centre-plane area are shown in

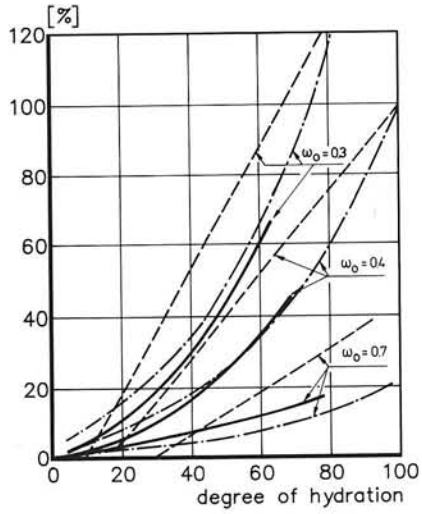

——— relative embedded cement volume
-.-.-.- relative strength after Powers (Fig. 7.19a)
- - - - rel. strength after Fagerlund (Fig. 7.19b)

Fig. 7.20 Relative increase in strength and of embedded cement volume $v_{cm}^{pa}(\alpha)$.

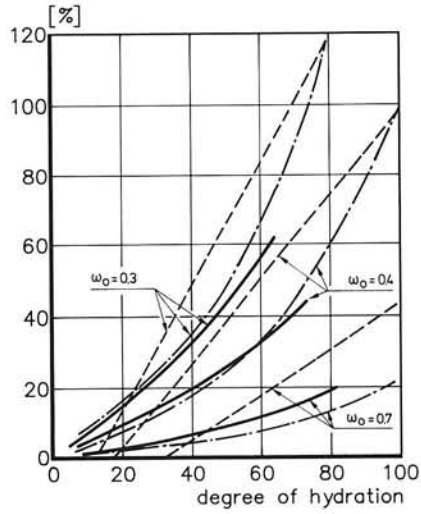

——— relative embedded centre-plane area
-.-.-.- relative strength after Powers (Fig. 7.19a)
- - - - rel. strength after Fagerlund (Fig. 7.19b)

Fig. 7.21 Relative increase in strength and embedded centre-plane area $A_{cm}^{pa}(\alpha)$.

Figs. 7.20 and 7.21, respectively, with solid lines. From the comparison of the experiment-based curves and the theoretical curves generated using HYMOSTRUC it can be concluded that the trends of the different curves are quite similar. This observation can be interpreted cautiously as an argument in favour of the presumed correlation between strength development, on the one hand, and the increase of the amount of embedded cement and embedded centre-plane area, on the other. This subject will be covered in more detail in Section 8.6.2.

7.4.4 Interparticle versus Transparticle Fracturing

An interesting feature of HYMOSTRUC in view of strength considerations is the option to quantify the physical interaction between expanding particles. In Section 4.4.5.2 reference has been made to experimental results which revealed that as the hydration process proceeds, the fracture mode changed from interparticle to transparticle. Both fracture modes are shown diagrammatically in Fig. 7.22. Obviously there is a moment, i.e. a degree of hydration, beyond which the strength of the contact points and contact surfaces between adjacent particles exceeds the strength of the shell of hydration products that surrounds the anhydrous core of a cement grain. For a particle x this moment is determined by the ratio between

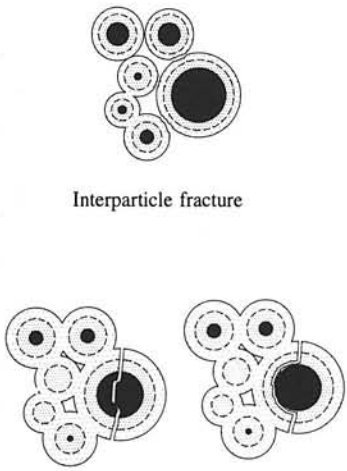

Fig. 7.22 Interparticle versus transparticle fracture mode. (schematic representation)

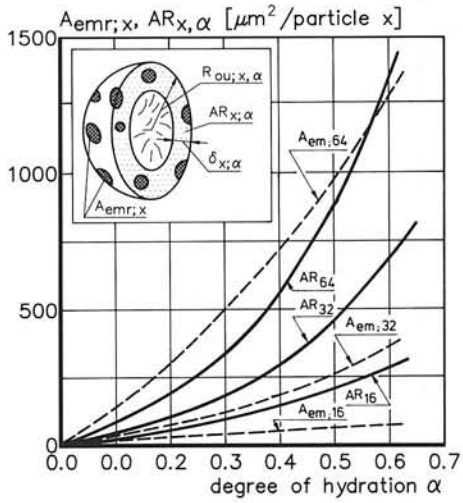

Fig. 7.23 Reduced embedded centre-plane area $A_{emr,\alpha}$ versus ring area $AR_{x;\alpha}$ of the central particles.

the surface area $AR_{x,\alpha}$ of a ring with outer radius $R_{ou;x,\alpha}$ and thickness $\delta_{x,\alpha}$, viz. (see Fig. 7.23):

$$AR_{x;\alpha} = \pi * [\ R^2_{ou;x,\alpha} - (R_{ou;x,\alpha} - \delta_{x;\alpha})^2\ ] \tag{7.2}$$

on the one hand, and 50% of the total embedded centre-plane area of the particle considered, on the other. With regard to the embedded centre-plane area it seems plausible to assume that those particles which are most effective in interparticle load transfer are those where the diameter exceeds the thickness of the outer shell of a central particle. The centre-plane area that remains after subtraction of the contribution of the embedded particles with diameters smaller than the outer shell thickness is called the "reduced embedded centre-plane area $A_{emr;x}$". For several particle sizes the ring area $AR_{x,\alpha}$ and the reduced embedded centre-plane area are shown in Fig. 7.23 as a function of the overall degree of hydration. It turns out that for small particles the ring area always exceeds the reduced embedded centre-plane area. For large particles the reduced embedded centre-plane area approaches or can even exceed the ring area of the shell which surrounds the anhydrous core. These particles are considered to be susceptible to the transparticle fracture mode.

7.5 Interface Phenomena

7.5.1 Potentialities of HYMOSTRUC for Quantitative Analyses of "Wall Effects"

Due to wall effects at the matrix-aggregate interface the average volumetric paste density in the interface region will be lower than the *average paste density* ζ_{pa} $[\mu m^3/\mu m^3]$ according to eq. (6.12). Section 6.2.5 has made us familiar with this phenomenon in a conceptual way already (Fig. 6.4). In that paragraph the *cell density* ζ_x $[\mu m^3/\mu m^3]$, was introduced, being the relative amount of cement in a cubic cell with rib size S_x. It can be stated alternatively, that with increasing distance y from the aggregate surface the average paste density will increase in the same way as the average cell density increases with increasing rib size S_x of a cubic cell I_x^c. Obviously HYMOSTRUC is able to quantify wall effects as outlined. The potential of HYMOSTRUC to do so for any arbitrary granular material will be checked now by investigating the wall effect as it occurs in an ordinary concrete mix at the wall of a moulding. In this case it is the spatial distribution of the aggregate particles that is subjected to the wall effect. For this quantitative verification the experimental work by Sadouki [511] will be used.

According to Sadouki the thickness of the zone over which the relative amount of aggregate increases from zero at the wall surface of a moulding to its bulk value is equal to approximately half the diameter of the largest aggregate particle. To check whether HYMOSTRUC is able to predict this distance over which the wall effect occurs accurately, the particle size distribution of the aggregate and the aggregate volume concentration in a concrete mix must be known. For the particle size distribution of the aggregate the Fuller distribution is assumed (Fig. 7.24a):

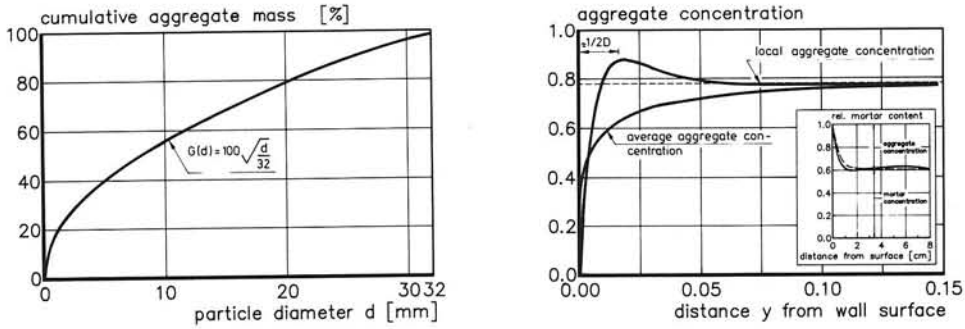

a. Fuller curve for aggregate

b. Average and local relative aggregate volume

Fig. 7.24 Wall effect as predicted by HYMOSTRUC.
a. Fuller curve of the particle size distribution of the aggregate
b. Average and local relative aggregate volume near wall surface.
Insert: Measurements by Sadouki [511].

$$G(d) = 100 \left(\frac{d}{D}\right)^{1/2} \qquad [\%] \qquad (7.3)$$

where d [m] and D [m] are the intermediate and maximum size of the aggregate particles. Analogously to the definitions for the cement cell I_x and the cell density ζ_x as discussed in Section 6.2 an aggregate cell $I_{a;d}$ and a cell density $\zeta_{a;d}$ can be defined. In formula form:

$$I_{a;d} = \frac{\pi * d^3 * \left(\frac{d}{D}\right)^{1/2} * \left[C * \left(\frac{1}{\rho_{ce}} + \frac{\omega_0}{\rho_w}\right) + V_a * \frac{G(d)}{100} \right]}{3 * V_a} \qquad [m] \qquad (7.4)$$

and:

$$\zeta_{a;d} = \frac{1}{1 + \frac{V_{ma}}{V_a} * \left(\frac{D}{d}\right)^{1/2}} \qquad [m^3/m^3] \qquad (7.5)$$

where: V_{ma} = volume of the matrix = $C*\{(1/\rho_{ce})+(\omega_0/\rho_w)\}$ [m^3]
C = amount of cement in the mix [kg]
V_a = aggregate volume [m^3]
ρ_{ce}, ρ_w = specific mass of cement and water, respectively. [kg/m^3]

For the rib size $S_{a;d}$ of a cubic aggregate cell it holds that (see also eq. (6.17)):

$$S_{a;d} = (I_{a;d})^{1/3} \qquad (7.6)$$

For an ordinary concrete mix with C=300 kg/m^3 and a w/c ratio ω_0=0.4, Fig. 7.24b shows the average value of the relative amount of aggregate as a function of the rib size of the cell, i.e. as a function of the distance from a wall surface.

For numerical evaluations it is convenient to approximate the average relative amount of aggregate by a mathematical expression of the form:

$$\zeta(y) = \zeta_a * \left[1 - e^{-\frac{y}{y_0}} \right] \qquad (7.7)$$

where ζ_a is the bulk value of the average relative amount of aggregate (eq. (7.5) for d=D), y a length parameter and y_0 a constant. From the approximate curve for the average relative amount of aggregate the *local* relative amount of aggregate $\zeta_a^L(y)$ can be deduced by differentiating eq. (7.7) with respect to y. It follows:

$$\zeta_a^L(y) = \frac{d\zeta_a(y)}{dy} = \zeta_a * [\ 1 - (1-\frac{y}{y_0}) * e^{-\frac{y}{y_0}}\ ] \tag{7.8}$$

The graphical representation of the local relative amount of cement in Fig. 7.24b shows that the thickness of the zone with pronounced variations in the amount of aggregate is about 15 mm, which is half the diameter of the largest aggregate diameter D=32 mm. This result is in full agreement with the data reported by Sadouki. It seems justified, therefore, to conclude that HYMOSTRUC describes the density variations at the wall surface quite accurately. This presents a good basis for the applicability of HYMOSTRUC for analyses of variations of the paste density at the matrix-aggregate interface.

7.5.2 Paste Density at the Matrix-Aggregate Interfacial Zone

Analogous to the procedure outlined in the foregoing section, the variations in the average and local paste densities near matrix-aggregate interface surfaces have been investigated. The calculations refer to a paste made with a coarse, an intermediate and a fine cement, viz. the B1-, B4- and B7-cements of which the particle size distributions are given in Table 8.2. For all pastes it holds that ω_0=0.4. The results of density calculations are given in Fig. 7.25. Fig. 7.25b shows that the thickness of the zone with local densities less than the bulk density varies from about 30 μm for the fine cement to 50 μm and even 120 μm for the intermediate and coarse cement respectively. These results are in good agreement with the literature data as discussed in Section 4.7.2.

Note that, other than in the case of the aggregate-wall interface zone where the thickness of the interface zone is about half the diameter of the largest aggregate particle, the

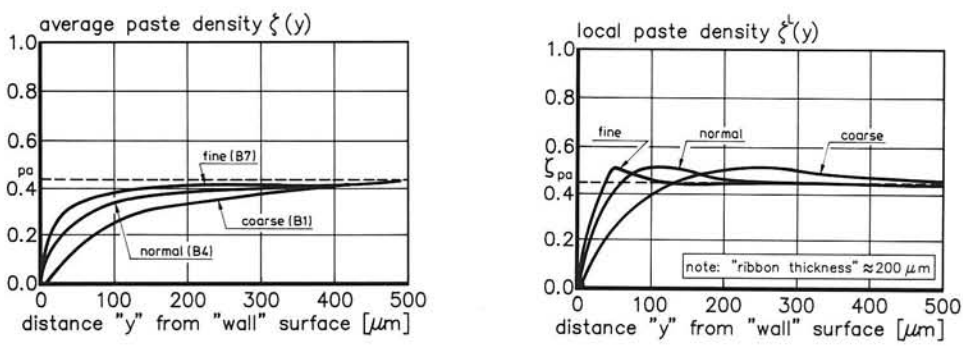

a. Average paste density

b. Local paste density

Fig. 7.25 Effect of cement fineness on average and local paste density in matrix-aggregate interface zone. Coarse, intermediate and fine cement. Cement: Table 8.2; ω_0=0.4.

matrix-aggregate interface zone is *thicker* than half the diameter of the largest cement particle. Fig. 7.25b suggests the thickness of the matrix-aggregate to be equal to the whole diameter of the largest cement particle rather than to half the diameter. The relatively large thickness of the interface zone can easily be understood when bearing in mind that the interface thickness is *not* only determined by the particle size distribution of the granular material, but *also* by the amount of the granular material in the system. The relative amount of the aggregate in an ordinary concrete mix varies in the range from 0.75 to 0.8, whereas the relative amount of cement in an ordinary paste, i.e. the paste density, varies from 0.35 to 0.45 (see also Fig. 6.1). Since the particle spacing, and hence the thickness of the interface, is about inversely proportional to the volume concentration of the granular component in the system, the wider interface zone in the case of a cement paste relative to the width of the matrix-aggregate interface zone is considered reasonable.

With respect to the reliability of the foregoing considerations concerning the interface thickness, and in view of the transfer of the generated quantitative information about pastes to mortars and concrete mixes, one should bear in mind that the ribbon thickness of the cement paste in an ordinary mortar and concrete mix varies between 50 and 200 μm (Section 4.7.1). It is obvious that allowance for the actual ribbon thickness affects the quantitative values, particularly for the coarse cements.

7.5.3 Hydration in the Interfacial Zone

Since the amount of cement in the matrix-aggregate interface zone mainly consists of small particles, it is to be expected that the degree of hydration in that region is significantly higher than in the bulk paste. For a paste with a B4-cement (Table 8.2) with ω_0=0.4, the calculated degree of hydration is shown in Fig. 7.26a as a function of the distance from the aggregate surface for various time durations. Hydration of the cement in a

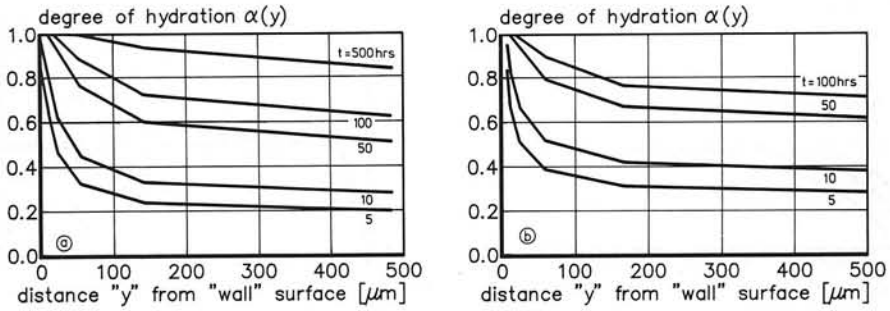

a. Medium fineness: Blaine=353 m^2/g

b. Fine cement: Blaine=507 m^2/g

Fig. 7.26 Degree of hydration as a function of the distance to the aggregate surface. Paste: ω_0=0.4.

50 μm thick interface zone is almost complete after 100 hrs, whereas the degree of hydration in the bulk paste is only about 60% complete at that time. The trends generated with HYMOSTRUC are in good agreement with observations of Zimbelmann [642], Diamond [141] and Scrivener et al. [527] (see also Section 4.7.4).

In the foregoing calculations the effect of the relatively high w/c ratio in the interface zone on the rate of hydration is allowed for in the sense that due to the high inter-particle spacing in the water-rich interfacial zone no or hardly any effect of particle embedding, and hence of extra growth of the diffusion barriers and water withdrawal mechanisms, will occur.

Since the amount of cement in the interfacial zone is relatively small, the high degree of hydration of the interface cement does not imply a dense, and hence a strong product. For example, since the average paste density in a 50 μm thick interface zone is not higher than about $\zeta_{y=50}$=0.26, whereas the bulk paste density ζ_{pa}=0.45, the density of the cement paste in the interface region at full hydration must be expected to be about 58% of the ultimate density in the bulk paste (=0.26/0.45 * 100%). The high porosity of the interfacial zone as predicted with HYMOSTRUC is in agreement with interface considerations put forward by Barnes [27] and Tognon [593].

A more detailed picture of the variation of the porosity over the thickness of the interface zone is shown in Fig. 7.27. Fig. 7.27a shows results of porosity measurements by Scrivener et al. [527]. In Fig. 7.27b the relative decrease of the porosity with increasing distance of the aggregate surface is shown for both the data of Scrivener and theoretical data generated with HYMOSTRUC. The theoretical data refers to a paste made with a cement of moderate fineness, Blaine=312 m^2/kg and ω_0=0.4 (Tests of Danielsson [127]; for details, see Section 8.4.1). When comparing the measured and calculated porosities it must

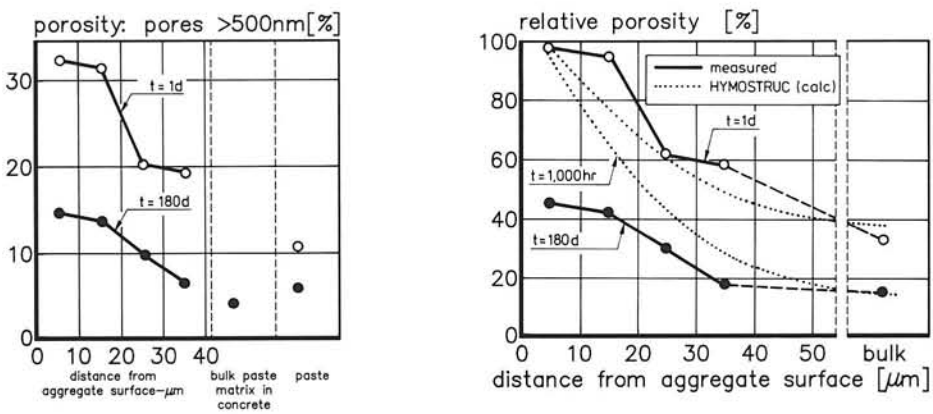

a. Measured porosity

b. Measured versus calculated porosity

Fig. 7.27 Variation of porosity over the interface thickness.

a. Measured porosity (Scrivener et al. [527]).

b. Calculated porosity. Input data taken from [127] (see Section 8.4.1).

be borne in mind that in the porosity calculations the hydration products are assumed to precipitate in the vicinity of the cement grains from which they are formed. From the discussion on hydration mechanisms in the Sections 4.4 and 4.10 this assumption seems to be valid, particularly for the CSH-gel. CH-crystals, or other morphological CH-modifications, however, should be considered to form preferably in the water-rich interfacial zone. The latter aspect is not accounted for in HYMOSTRUC and is one of the reasons for the differences between measured and calculated porosities. The good agreement, however, between the measured and calculated distances over which the porosity decreases seems to provide evidence of a significant influence of stereological phenomena in the matrix-aggregate interfacial zone.

7.5.4 Strength Considerations in view of Interface Phenomena. Discussion

As discussed in Section 4.7, the strength and hardness of the cement paste in the matrix-aggregate interface zone exhibit a pronounced correlation with the porosity in this zone. Zones with low microhardness, i.e. low densities, have been observed by Lyubimova et al. [358]. Alexander et al. [9] found that the matrix-aggregate bond strength is less that the bond strength in the bulk paste. According to Hsu [249] the matrix-aggregate bond strength is about 41 to 91% of the tensile strength of the plane matrix. Massaza [369] reports on microhardness in some zones in the interface region of about half the microhardness of the bulk paste. Similar results have been reported by Detriche [134]. Many of these findings have been attributed to stereological interface phenomena. The phenomena can be simulated with HYMOSTRUC quite reliably.

From Fig. 7.25 as well as from a comparison of Figures 7.26a and 7.26b, it is obvious that both the paste density and the degree of hydration of the cement in the interface zone will be higher the finer the cement. Consequently the porosity of the interface zone will be less the finer the cement. There is stereologic evidence, therefore, for densification of the interface zone due to the addition of extra fines like silica fume and fine fly ashes. For details on this topic reference is made to literature [393,324] and Section 4.7.

8 NUMERICAL EVALUATION PROGRAM FOR THE DETERMINATION OF MODEL PARAMETERS

Accuracy Considerations and Predictability

8.1 General

In the foregoing chapter some characteristic model features and the relative influence of several rate determining factors of HYMOSTRUC were discussed qualitatively. This chapter deals with the quantification of the four independent model parameters of eq. (6.103), which determine the rate of penetration in individual cement particles, viz. the basic rate factor K_0, the transition thickness δ_{tr} and the coefficients β_1 and β_2. For this purpose an evaluation program was executed in which experimentally obtained hydration and strength data published in the literature, as well as the results of a modest experimental program carried out for this particular project, were analyzed using HYMOSTRUC. The literature data were selected so as to cover a widest spectrum of cement compositions, particle size distributions, w/c ratios and curing conditions.

When investigating the magnitude of the model parameters it must be borne in mind that the basic rate factor K_0 is, in essence, a function of the chemical composition of the cement. The transition thickness δ_{tr} in turn refers to the thickness of the product layer at which the boundary reaction changes into a diffusion controlled process. The coefficient β_1 determines the diffusion law which is operative, whereas the factor β_2 refers to the morphology-related effect of the reaction temperature on the rate of hydration.

8.2 Effect of Chemical Composition of the Cement on Model Parameters

8.2.1 Tests of Lerch and Ford

From the excellently documented 'Long-time Studies' of Lerch and Ford [342] on cement performance in concrete, which studies comprise 27 different cements, 17 cements were chosen for investigating the dependence of both the basic rate factor K_0 and the transition thickness δ_{tr} on the chemical composition of the cement. The clinker composition and fineness of these cements is given in Table 8.1, together with their potential heats of hydration at complete hydration. For the particle size distribution of the cements reference is made to the original paper [342]. For the indicated cements, heat of hydration data is on the basis of sealed pastes (ω_0=0.4). Heat data was obtained by conduction calorimetry for pastes cured at 24.9°C for hydration times of up to 72 hours and by the heat of solution method for pastes cured at 21.1°C for curing periods of up to 1 year. The heat of solution data was corrected for the temperature difference between the latter tests and the conduction calorimetry tests in order to make them mutually comparable. The degree of hydration was obtained by dividing the measured heat of hydration by the potential heat of hydration at complete hydration Q^{max} as indicated in Table 8.1. The independent model pa-

Table 8.1 Cement characteristics and heat of hydration data for different cements published by Lerch et al. [342]. Model parameters K_0, δ_{tr}, β_1 and β_2 in last four columns.

Calculated compound composition (Bogue [1])					Sp. surf. Blaine	Q^{max} Calc.[2])	Heat of hydration [J/g] Cond. cal. / Heat of sol.					Model parameter K_0	δ_{tr}	β_1	β_2
No.	C_3S	C_2S	C_3A	C_4AF	m^2/kg	J/g	12 h	1d	3d	7d	28d	µm/h	µm	--	--
						Portland cement Type I									
11	50.0	22.0	12.1	7.2	344	505	122	165	262	339	394	0.035	8.0	1	1
12	45.0	28.0	12.6	7.3	328	497	103	151	242	348	417	0.035	12.0	1	1
13	50.0	26.0	10.1	6.5	343	475	116	152	212	269	349	0.035	4.0	1	1
15	64.5	10.0	12.1	12.1	324	544	171	216	298	366	452	0.050	7.0	1	1
16	53.5	21.0	7.5	10.7	326	466	130	162	252	332	382	0.045	8.0	1	1
17	52.0	32.0	10.4	9.3	399	493	126	165	255	332	427	0.045	10.0	1	1
18	44.5	28.0	13.2	6.8	327	497	130	174	255	340	418	0.040	12.0	1	1
av.	51.4	22.6	11.1	7.9	341	497						0.041	8.7	1	1
						Portland cement Type II									
21	40.0	41.0	6.4	9.7	289	442	91	121	191	255	332	0.030	5.0	1	1
22	41.5	33.5	6.6	11.7	307	428	88	117	183	262	359	0.025	10.0	1	1
23	51.0	24.0	3.7	16.6	331	436	97	136	194	229	346	0.025	6.0	1	1
25	34.0	39.0	4.7	14.9	329	394	111	141	197	255	307	0.040	5.0	1	1
av.	41.6	34.4	5.4	13.2	309	420						0.030	6.5	1	1
						Portland cement Type III									
31	56.0	17.0	10.8	6.4	580	494	180	221	339	400	447	0.035	10.0	1	1
33	60.0	13.0	10.4	7.7	527	499	198	242	327	385	425	0.055	5.0	1	1
34	64.0	10.5	5.7	10.1	497	460	173	207	288	352	404	0.050	7.0	1	1
av.	60.0	13.5	8.9	8.1	535	484						0.047	7.3	1	1
						Portland cement Type IV									
41	20.0	51.0	4.5	15.2	368	353	100	126	188	218	275	0.040	6.0	1	1
42	27.0	55.0	3.5	8.2	350	353	81	116	155	176	248	0.025	2.0	1	1
43	25.0	48.0	6.2	13.8	385	384	93	119	192	247	301	0.030	6.0	1	1
av.	24.0	51.5	4.9	11.6	368	363						0.032	4.7	1	1

[1]) Bogue composition, not corrected for minor oxides (see [342])
[2]) Calculation on basis of Bogue composition (eq. 3.2)

rameters of HYMOSTRUC were now determined so as to obtain a good fit of the measured hydration data with the theoretical hydration curves. The results are shown in the last four columns of Table 8.1.

In Fig. 8.1 the mean K_0-values as determined for each type of cement are expressed as a function of the average C_3S content of the different cement types (mean values denoted with a, b, c and d).

Knowing that C_2S becomes active in the later stages of the hydration process, it has been assumed that there may exist some correlation between the transition thickness δ_{tr} and the C_2S content. In order to check this assumption, the calculated δ_{tr}-values are expressed as a function of the C_2S content in Fig. 8.2. Both Fig. 8.1 and Fig. 8.2 will be discussed in more detail in Section 8.2.3.

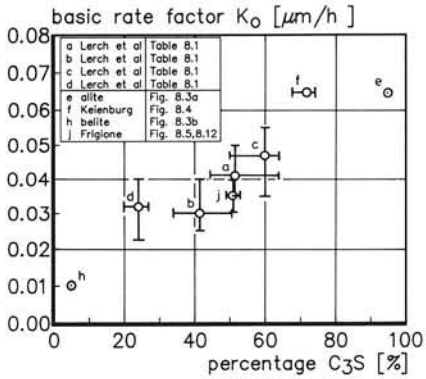

Fig. 8.1 Basic rate factor K_0 as a function of the C_3S content in Portland cement.

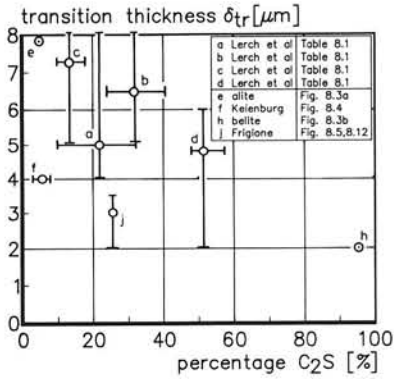

Fig. 8.2 Transition thickness δ_{tr} as a function of the C_2S content in Portland cement.

8.2.2 Model Parameters for Alite and Belite Hydration

For a further check of the assumed correlation between the C_3S and C_2S contents, on the one hand, and K_0- and δ_{tr}-values, on the other, the latter parameters were investigated for alite and belite hydration. For this purpose the alite and belite samples are considered as fictitious cements with C_3S contents of 95% and 5%, respectively. Hydration of alite and belite was assumed to proceed as indicated with the discrete points in Fig. 8.3a and Fig. 8.3b, representing the mean hydration curves as determined by Parrott [435] and discussed previously in Section 5.4.3. Note that these mean curves are obtained from a curve fit analyses of experimental data obtained for samples made with different w/c ratios and different particle size distributions, while both sealed and saturated curing conditions were involved. The data must, therefore, be considered as indicative only. In view of mathematical evaluations of this data using HYMOSTRUC it has been assumed that the data referred to alite and belite samples of moderate fineness, i.e. Blaine=350 m^2/kg, made with ω_0=0.4 and cured under sealed conditions at 20°C.

For the alite a good fit of the hydration data was obtained for K_0=0.065 μm/h, whereas the transition thickness would exceed 10 μm. To fit the belite hydration data a K_0-value was required of about 0.01 μm/h and a transition thickness of about 2 μm. The K_0 and δ_{tr}-values are inserted in the figures 8.1 and 8.2.

8.2.3 Chemical Clinker Composition. Discussion

Basic Rate Factor K_0

From the plot in Fig. 8.1 of the K_0-values against the C_3S content as established for the Type I, II, III, and IV cements, a distinct tendency of increasing K_0-values with increasing

C_3S content is quite obvious. The scatter in the results must be attributed to the effects of compound interaction, of gypsum and of minor compounds, which effects are not accounted for in HYMOSTRUC explicitly.

The dependence of the K_0-value on the C_3S content is further substantiated by inserting the K_0-values for alite and belite in Fig. 8.1. The observed relationship between K_0 and C_3S content can be used as a reference for further analysis of other cements.

Transition Thickness δ_{tr}

The test results of Lerch et al. [342] suggest a slight correlation between the transition thickness and the C_2S content of the cement (Fig. 8.2). Insertion of the transition thicknesses for alite and belite appear to substantiate the validity of this correlation.

Most of the test data analysed so far can be approximated fairly accurately for transition thicknesses exceeding 4.5 μm. At that time the degree of hydration generally exceeded 40...60%. Obviously a boundary reaction takes up quite a long period of time. This finding is in good agreement with the majority of the data on the apparent activation energies, which are generally found to be much too high for diffusion controlled reactions (Section 5.6), suggesting that the phase-boundary reaction is the rate controlling mechanisms up to about the beginning of the *late period*, i.e. at a degree of hydration of about 40% to 50% (for late period, see also Table 3.5).

Beta-Coefficients β_1 *and* β_2

Since in the foregoing analyses the phase-boundary reaction turned out to be the predominant rate controlling mechanism, the exact value of the β-coefficients - which refer to the diffusion controlled stage - could not be determined. The fact that they are taken as unity does not, however, exclude the possibility of values different from 1, for example 1.5 or 2. The weak, or even absence of a distinct correlation between the β-coefficients and the

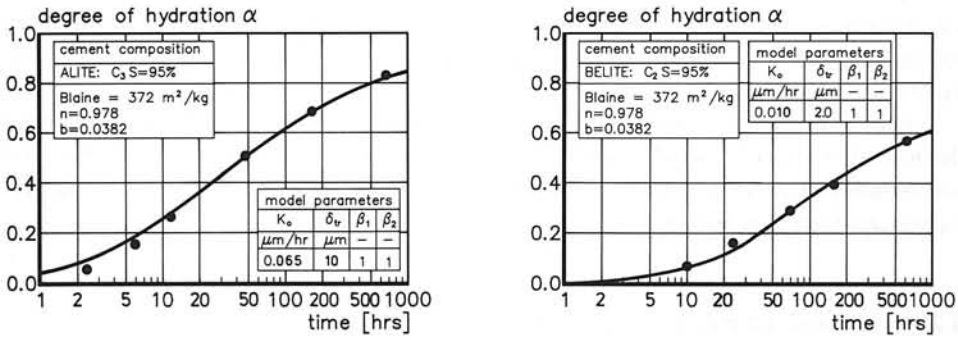

a. alite b. belite

Fig. 8.3 Alite (a) and belite (b) hydration curves according to different authors and approximations obtained with HYMOSTRUC.

chemical composition of the cement and the implications thereof for the reliability of the model will be dealt with in more detail in Section 8.7.

8.3 Effect Cement Fineness and Particle Size Distribution on Model Parameters

8.3.1 Tests of Keienburg

As discussed in Section 8.1 the model parameters should, in essence, be independent of the fineness of the cement, i.e. of the particle size distribution. In order to check this proposition, experimental data of Keienburg [287] has been used. For three different types of cement Keienburg investigated the effect of the cement fineness on the rate of hydration and strength development. Hydration data was obtained from mortar samples, manufactured with ω_0=0.5 and cured at 20°C under saturated conditions. The degree of hydration was obtained by dividing the measured non-evaporable water content by the maximum amount of chemically bound water calculated from the Bogue composition of the cement.

For each cement Keienburg investigated 7 fineness classes with Blaine values, ranging from less than 200 m^2/kg up to 500 m^2/kg. With the particular aim to check whether HYMOSTRUC would yield reliable results in the case of extreme finenesses three fineness classes were considered, viz. the coarsest, the intermediate and the finest cement, and this for each of the three types of cement. The chemical composition and particle size distribution of the cements are given in Table 8.2.

Results of the analyses are shown diagrammatically in Fig. 8.4. In the legends the mo-

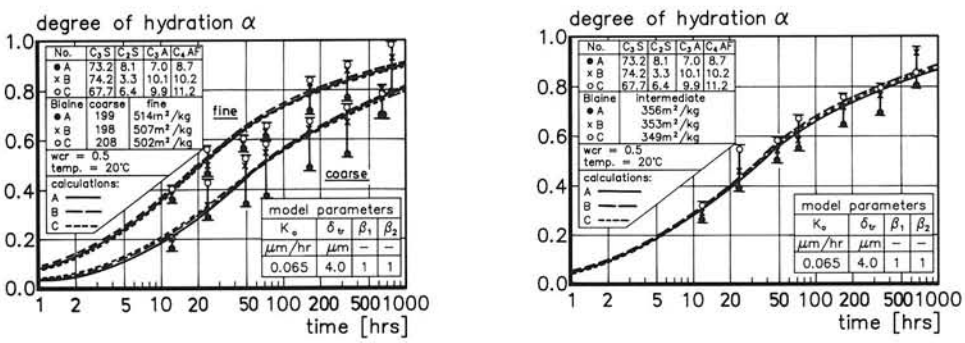

Fine and coarse cements

Cement of medium fineness

Fig. 8.4 Effect of cement fineness on the rate of hydration in mortar. Sealed curing.
- Experimental hydration data [287], indicated with discrete points and vertical bars.
- Approximations with HYMOSTRUC presented with solid and dashed curves.

Table 8.2 Chemical composition and particle size distribution of cements investigated by Keienburg [287].

Chemical composition				
Cement no.	C_3S [%]	C_2S [%]	C_3A [%]	C_4AF [%]
A	73.23	8.14	7.04	8.67
B	74.23	3.30	10.11	10.23
C	67.70	6.42	9.85	11.17

Particle size distribution - cumulative weight									
Particle size [mm]	Cement no. A1	A4	A7	B1	B4	B7	C1	C4	C7
125.0	0.978	0.994	0.993	0.990	0.998	0.998	0.970	0.999	0.995
100.0	0.932	0.989	0.989	0.991	0.994	0.994	0.900	0.996	0.992
80.0	0.895	0.984	0.986	0.919	0.990	0.992	0.844	0.994	0.989
63.0	0.845	0.977	0.974	0.861	0.975	0.984	0.768	0.982	0.984
50.0	0.772	0.895	0.942	0.719	0.909	0.947	0.634	0.909	0.959
40.0	0.630	0.838	0.907	0.628	0.846	0.914	0.579	0.837	0.894
32.0	0.550	0.770	0.855	0.534	0.777	0.873	0.509	0.757	0.855
20.0	0.377	0.599	0.717	0.373	0.604	0.735	0.367	0.579	0.709
12.5	0.224	0.416	0.549	0.225	0.421	0.585	0.238	0.399	0.550
8.0	0.125	0.283	0.414	0.133	0.277	0.437	0.146	0.265	0.408
5.0	0.057	0.183	0.304	0.070	0.177	0.315	0.081	0.169	0.289
2.5	0.016	0.060	0.148	0.016	0.062	0.181	0.022	0.052	0.146
Blaine [m^2/kg]:	200	356	515	198	353	507	208	349	502
(calc. [287] :	147	314	553	151	320	629	167	294	549)

del parameters of HYMOSTRUC are indicated. It appears that a satisfactory approximation of the experimental data is possible with only one set of independent model parame-- ters, Obviously, and in line with what was expected, the model parameters are independent of the particle size distribution of the cement.

It is further noted that the K_0- and δ_{tr}- values are in good agreement with those indicated in Fig. 8.1 and 8.2, albeit that the K_0-value is relatively high and the δ_{tr}-value relatively low. A high value of K_0 implies a relatively high degree of hydration. Also Keienburg has pointed to the high degrees of hydration in his tests. After an evaluation of his tests he concluded, however, that there was little scope to doubt the measurements. Bearing in mind that in Keienburg's tests hydration of the mortar samples took place under saturated conditions, which must have resulted in higher hydration values, and that, moreover, hydration in mortar is said to proceed more rapidly than in neat pastes (Section 3.8.3), the relatively high degree of hydration in these tests appears to be partly explained.

8.3.2 Effect of the Particle Size Distribution

8.3.2.1 Tests of Frigione et al.

Frigione et al. [176] investigated the effect of the shape of the particle size distribution on the rate of hydration. Four cement samples were manufactured with n-values of the R-R distribution ranging from 1.15, 1.50, 2.14 to 3.31. In all cases Blaine surfaces were about 320 m^2/kg. The Bogue composition of the cement are given in the legend of Fig. 8.5. Gypsum content ($CaSO_4.2H_2O$) is 6%. Hydration of neat pastes, ω_0=0.4, took place under sealed conditions at 20±1°C.

Fig. 8.5 shows the measured degree of hydration (non-evaporable water, D-drying), together with theoretical values obtained using HYMOSTRUC. The values of the model parameters for which the best fit for the individual tests was obtained are also given. Comparison of the mean values of K_0 and δ_{tr} with those of Fig. 8.1 and 8.2 reveals that the K_0-values seem to follow the correlation between K_0 and C_3S content as found in earlier tests, whereas the δ_{tr}-C_2S correlation is rather weak.

For a good fit it was necessary to adopt a β_2-coefficient larger than 1, indicating that diffusion through the product shell was of paramount importance in these tests. One might wonder why in these tests, which are fairly well comparable with those carried out by Lerch et al., diffusion turns out to be so important. One of the reasons could be a difference in alkali content, which is not accounted for in HYMOSTRUC. Furthermore it must be born in mind that the measured degree of hydration is a function of the measuring method, including pre-treatment of the samples, and of the laboratory assistant. It is known from previous studies that these factors might affect the final results quite substantially (Chapter 2). In Section 8.4.2 this topic will be addressed again.

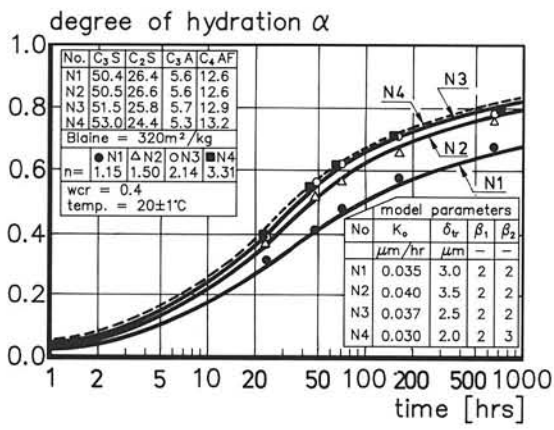

Fig. 8.5 Effect of slope of the particle size distribution (n-values of R-R-curves) on the rate of hydration. Sealed curing of pastes [176]. Experimental data shown with discrete points. Approximations by HYMOSTRUC indicated with solid lines.

Table 8.3 Characteristics of cements investigated by Locher et al. [353].

Series	Cement no.	Blaine m^2/kg	n	d' [1] µm	Clinker composition after Bogue [%] C_3S	C_2S	C_3A	C_4AF
	20	261	1.05	28				
"20"	21	257	2.1	17				
	22	257	1.39	23				
	23	242	0.78	41				
	30	343	1.01	20				
"30"	31	363	3.15	10	≈62%	≈15%	≈12%	≈10%
	32	354	1.93	13				
	33	363	1.11	17	Note:			
					Clinker composition dependent on			
	40	453	1.06	13	the particle size of the cement.			
"40"	41	440	2.93	9	Above percentages are mean values			
	42	449	1.66	11				
	43	455	0.73	17				

[1]) d' = particle size with 38% undersize weight.

8.3.2.2 Tests carried out by Locher et al.

Locher et al. [353] investigated the effect of the shape of the particle size distribution on strength development. For two cement clinkers, with a lower and a higher alkali content, three series of tests were performed. The three series differed from each other in the fineness of the cement used, viz. 260, 360 and 460 m^2/kg, respectively. Within each series four different particle size distributions were considered as indicated in the Table 8.3. The w/c ratio was 0.5. For the alkali-rich clinker - to which we will restrict ourselves - the C_3S

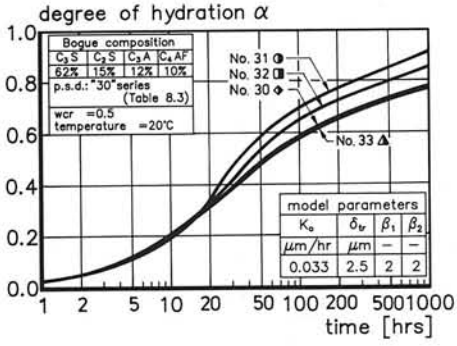

Fig. 8.6 Theoretical hydration curves according to HYMOSTRUC as a function of the particle size distribution.
PSDs taken from Locher et al. [353].

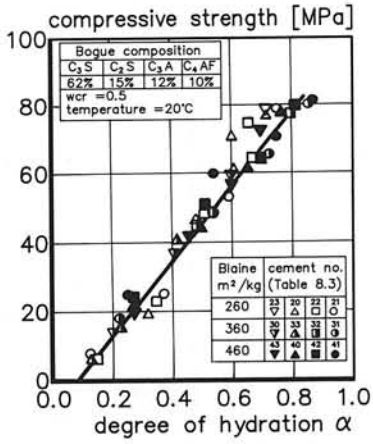

Fig. 8.7 Strength versus calculated degree of hydration. Strength data taken from Locher et al. [353].

content was about 62%. For K_0=0.033 μm/h, δ_{tr}=2.5 μm, β_1=2 and β_2=2 the calculated hydration curves for the "30-series" (see Table 8.3) are shown in Fig. 8.6. The curves in this figure illustrate the effect of the particle size distribution on the rate of hydration, the time scale being purely indicative. As in the case of Frigione's tests and in agreement with the published data, the rate of hydration is highest for a steep particle size distribution (Section 4.5.2). Since no information was given about the actual degree of hydration, a check on the accuracy of the calculated degree of hydration was not possible.

Fig. 8.7 shows a plot of the measured strength versus the calculated degree of hydration. A fairly linear correlation appears to hold, which is in good agreement with many observations on this point (Section 4.9.4). The result provides evidence that HYMOSTRUC simulates the effect of the particle size distribution on strength - and implicitly on the degree of hydration - in a reliable way.

8.3.3 Cement Fineness and Particle Size Distribution. Discussion

Model Parameters

From the comparison of Frigione's hydration data with the calculated hydration curves it can be concluded, that even for a wide range of particle size distributions - a range with extremes far beyond the limits generally utilized in practice -, HYMOSTRUC predicts the effect of the shape of the particle size distribution on the rate of hydration fairly well. It should be noted, however, that the effect of the particle size distribution on the rate of hydration is not fully accounted for in the model, since apparently the model parameters only slightly depend on the shape of the particle size distribution (see Fig. 8.5, insert).

Embedded Cement Volume and Strength

The hypothesis put forward in Section 4.10, that the embedded cement volume might be considered as a measure of the strength of the cement paste, is supported in Fig. 8.8,

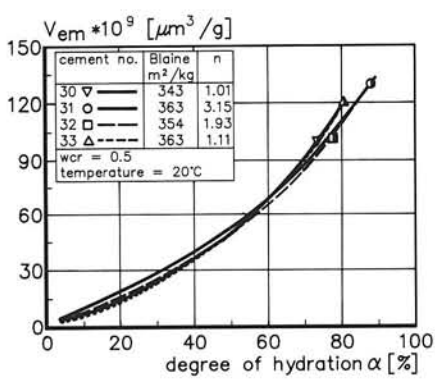

Fig. 8.8 Calculated embedded cement volume $V_{em}(\alpha)$ as a function of degree of hydration with particle size distribution as parameter. Tests of Locher et al. [353].

where the embedded cement volume $v_{em}(\alpha)$ calculated for Locher's test series is plotted against the calculated degree of hydration. Although fineness and particle size distribution of the cement varied in a wide range, an unambiguous relationship between degree of hydration and embedded cement volume appears to hold quite well, provided that the w/c ratio is constant. Knowing that strength can be considered as a linear function of the degree of hydration - which has turned out also to hold for the tests under consideration (see Fig. 8.7) - it can be concluded that strength can subsequently be considered as an unambiguous function of the embedded cement volume. We are inclined to formulate the foregoing in reverse, but it is probably more correct to state that:

> *"..... strength is a function of the embedded cement volume, i.e. of the amount of cement that is involved in generating bonds with adjacent cement particles, whereas the degree of hydration is the parameter with the help of which we are able to calculate the amount of strength-producing embedded cement".*

8.4 Effect of Water/Cement Ratio. Isothermal Tests

8.4.1 Tests by Danielsson

In Fig. 8.9 heat of hydration data (conduction calorimetry) reported by Danielsson [127] is given. This data refers to sealed cement pastes, manufactured with w/c ratios ranging from 0.25 to 0.5. The degree of hydration was obtained by dividing the measured heat of hydration by the calculated maximum heat of hydration liberated at complete hydration. The cement characteristics are also included. Since no information was provided on the particle size distribution, the R-R coefficients were taken to obtain the given Blaine surface of 312 m^2/kg. With the thus obtained particle size distribution the degree of hydration was calculated and compared with the measured degree of hydration (Fig. 8.10). The experimental

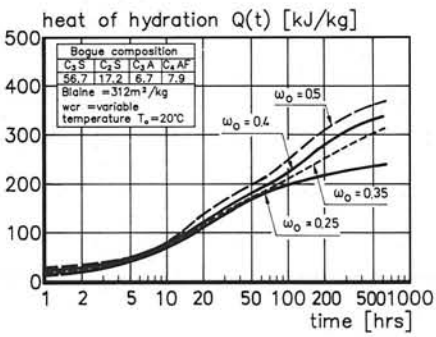

Fig. 8.9 Heat of hydration of neat pastes. Sealed curing; Danielsson [127].

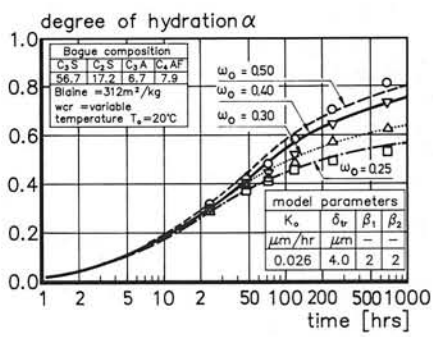

Fig. 8.10 Measured and approximated degree of hydration. Test of Danielsson [127].

data, indicated with discrete points, could be approximated satisfactorily with model parameters as indicated in Fig. 8.10.

8.4.2 Tests of Frigione et al.

In the previously mentioned paper by Frigione et al. [176] the effect of the w/c ratio on the rate of hydration on the four cements discussed in Section 8.3.2.1 was also considered. These tests are mentioned here, not because of the success of the attempts to fit the measured hydration data, but to emphasize the problems one may be faced with when using the published data for checking the reliability of hydration models. The problem considered is illustrated diagrammatically in Fig. 8.11. In that figure the measured degree of hydration for a paste with ω_0=0.4 is shown together with the hydration curve of a paste with ω_0=0.8. It appears that for cement N1 the degree of hydration at 28 days is about the same for both w/c ratios. This is in complete contrast with results obtained by Taplin (Fig. 7.11) and Danielsson (Fig. 8.10). It will be clear that *no* hydration model, at least not any granulometry and stereology-oriented hydration model like HYMOSTRUC, will be able to fit both Taplin's and Danielsson's data, and the data of Frigione, at the same time. Anyhow, caution must be exercised in all cases where only a single set of test data is used for checking the reliability of theoretical models.

Fig. 8.12 shows the measured and theoretical hydration curves for the pastes with ω_0=0.8. The model parameters for which the results were obtained are given in the insert.

8.4.3 Effect of Water/Cement Ratio. Discussion

Further to the earlier suggested ability of HYMOSTRUC to account for the effect of the w/c ratio on the rate of hydration (see Section 7.3.4), the experimental data by Danielsson

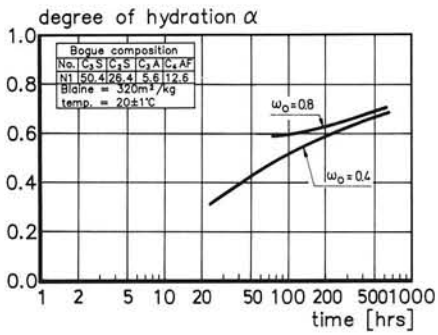

Fig. 8.11 Degree of hydration as a function of time for ω_0=0.5 and 0.8. PSD: Frigione et al. [176].

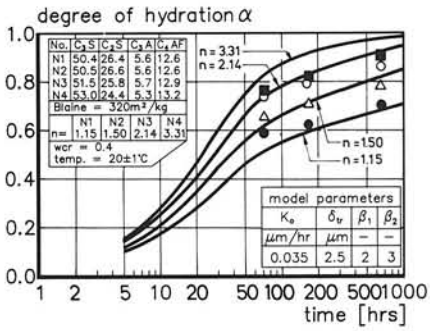

Fig. 8.12 Effect of particle size distribution on the rate of hydration. Data of Frigione et al. [176].

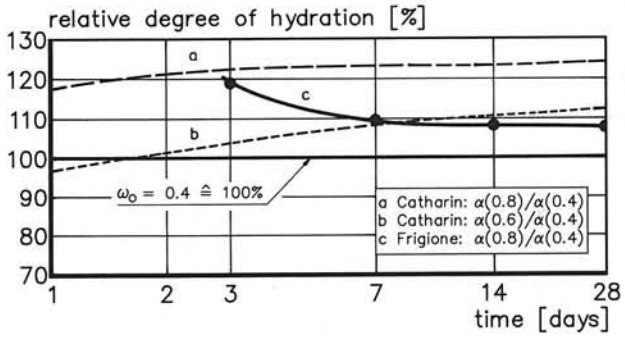

Fig. 8.13 Relative degree of hydration as a function of time for different w/c ratios. Experimental data of Catharin [93] and Frigione et al. [176].

and the quite satisfactory approximations of this data by HYMOSTRUC can be considered as a second and quite convincing check of the potential of the proposed model to simulate the effect of the w/c ratio on the rate of hydration.

In view of the discrepancy between Frigione's test data and that of Danielsson and Taplin (Section 7.3.4), the experimental work by Catharin [93] should be referred to. The latter author investigated the rate of hydration of six different cements with ω_0=0.4, 0.6, and 0.8, respectively. Fig. 8.13 shows curves representing the average values of the degree of hydration of the six cements for ω_0=0.6 and 0.8 relative to the average degree of hydration obtained for ω_0=0.4. At 28-days hydration the average degree of hydration of the pastes with ω_0=0.8 was about 24% higher than for the ω_0=0.4 series (curve a). This is about the same difference as found by Taplin and predicted using HYMOSTRUC. Frigione's data, presented in Fig. 8.13 with the solid curve c, distinctly diverges from the general trend and even exhibits a reverse trend. The comparison of this experimental data yields further arguments against the use of Frigione's hydration data as reference material.

8.5 Effect of Temperature. Isothermal Tests

8.5.1 Tests of Lerch and Ford

Introductory Remarks

In Section 6.6 a phenomenological procedure was discussed for the determination of the apparent activation energy from test data published by Lerch et al. [342]. In that procedure emphasis was placed on the effect of temperature on the rate of hydration. The actual hydration mechanisms, i.e. boundary or diffusion controlled reactions, and of the effect of structural formation on the rate of hydration, were not considered at all. These aspects form the "core" of HYMOSTRUC, whereas the temperature module as determined in Section 6.6 should be considered merely as an additional option of the model. If the stereo-

logical basis of HYMOSTRUC is sound, then it is to be expected that insertion of the temperature module in HYMOSTRUC will yield accurate hydration data when applied to Lerch and Ford's hydration tests.

Test Data

For each of the four cement types, indicated in Table 8.1, a representative cement was defined, reflecting both the *average* particle size distribution and the *average* chemical composition for each type of cement. In this way four fictitious cements were obtained, indicated as S10, S20, S30 and S40 with cement characteristics as summarized in Table 8.4.

Similarly to the averaging of the cement characteristics, the hydration data of the cements belonging to a certain cement type were averaged out yielding average hydration data for each type of cement. This data refers to neat pastes, ω_0=0.4, cured under sealed conditions at temperatures of 4.4°C, 23.9°C, 32.2°C and 40.6°C. The 32.2°C series is only considered for the Type II cement. The mean hydration values are shown in Fig. 8.14a, b,c,d as discrete points. For cement Type I, III and IV vertical bars indicate the range of hydration values observed for the individual cements.

Approximations of Hydration Data with HYMOSTRUC

For the cements defined in Table 8.4 HYMOSTRUC predicts hydration curves as indicated with solid lines in Fig. 8.14. The results are obtained with the average values of the model parameters K_0 and δ_{tr} as determined in Table 8.1 and are given in the legend of Fig. 8.14 (except δ_{tr} for Type I cement). From the comparison of the average measured hydration curves and the predictions with HYMOSTRUC it is evident that the model parameters as determined in Section 8.2.1 from the experiments at 21°C hold excellently in the temperature ranges considered.

As regards the widths of the scatter in the experimental data, note that scatter must result from (relatively small) differences in the cement composition. Particularly differences in the alkali content of individual cements might have resulted in substantial scatter in the hydration data.

Table 8.4 Characteristics of fictitious cements S10, S20, S30 and S40, representing cement Type I, II, III and IV (see also Table. 8.1).

Type of cement	denoted as	Average of x cements	Fineness [1]) [m²/kg]	PSD n	PSD b	C_3S [%] (Tab.8.1)
I	S10	7	372	0.978	0.0382	51.4
II	S20	4	314	1.003	0.0288	41.6
III	S30	3	564	1.021	0.0620	60.0
IV	S40	3	360	1.031	0.0362	24.0

[1]) Calculated fineness: particles x<0.5 μm considered as a fraction with mean particle size 0.25 μm (Compare mean Blaine values in Table 8.1).

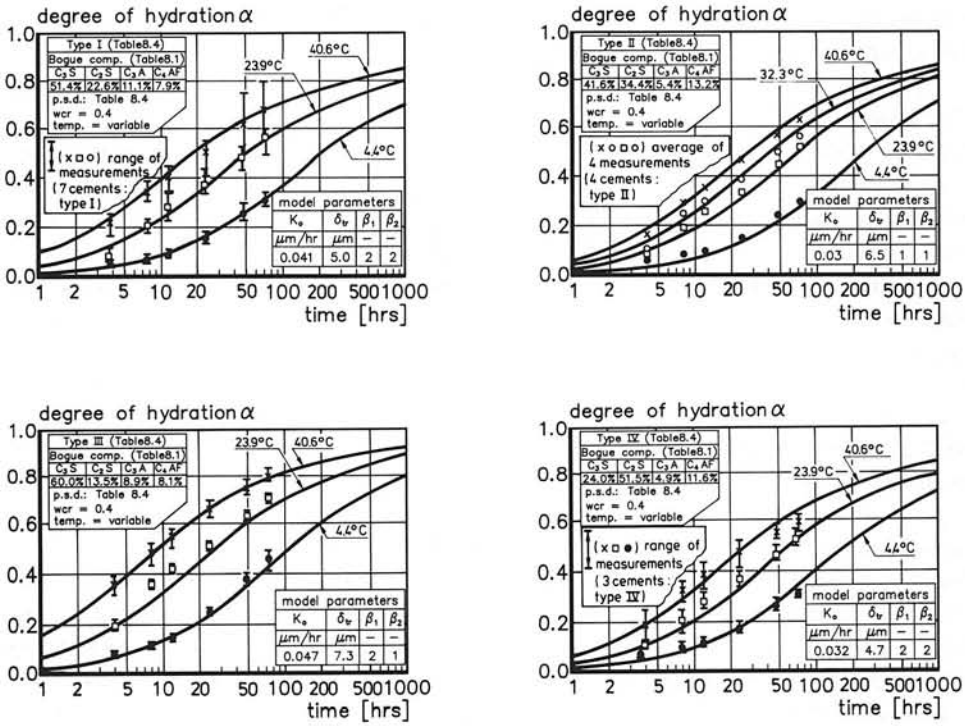

Fig. 8.14 Effect of curing temperature on rate of hydration, measured (discrete) and theoretical values (solid lines). Hydration data refer to Type I, II, III and IV cement, published by Lerch et al. [342].

8.5.2 Tests of Rakel

Degree of Hydration

Rakel [472] has carried out isothermal heat liberation and strength tests on cement pastes and mortars, respectively, with ω_0=0.4 and cured at 22°, 30°, 40° and 50°C. The cement characteristics are shown in the insert of Fig. 8.15. Discrete heat of hydration data was obtained at 3, 7 and 28 days with the heat of solution method (ASTM C 186-55). The degree of hydration was obtained by dividing this heat data by the maximum heat of hydration at complete hydration calculated from the Bogue composition of the cement. The thus obtained hydration data is shown in Fig. 8.15 as discrete points. Theoretical hydration curves generated with HYMOSTRUC are indicated in Fig. 8.15 with solid lines. The model parameters are shown in the insert.

Strength versus Embedded Cement Volume

Fig. 8.16 shows the well-known phenomenon of a positive effect of low curing tempera-

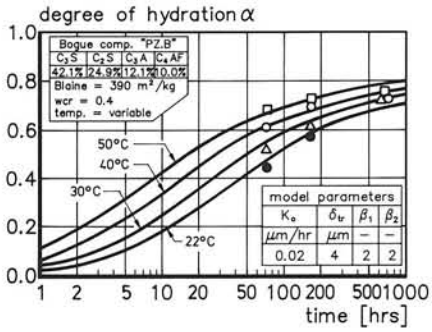

Fig. 8.15 Effect of isothermal curing temperature on rate of hydration. Discrete points: data of Rakel [472].

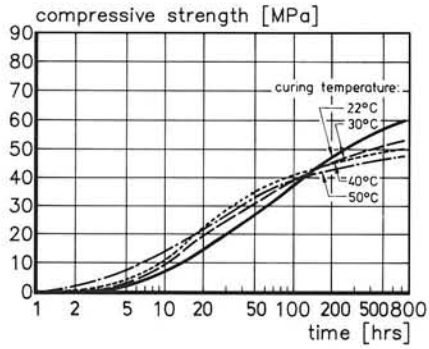

Fig. 8.16 Effect of curing temperature on strength development of mortar. After Rakel [472].

tures on final strength, i.e. at 28-day strength (Section 4.5.3). With respect to this phenomenon it is interesting to refer to the hypothesis that strength is a function of the amount of embedded cement. In Section 6.6 an option has been discussed and elaborated to account for the temperature-induced densification of the hydration products with increasing curing temperature. Less expansion of hydrating cement particles at higher curing temperatures implies a reduction of the amount of embedded cement and hence, if the hypothesis is correct, a reduction of the strength.

Let us consider now the embedded cement volume calculated using HYMOSTRUC at the degree of hydration reached at different curing temperatures after 28-days hydration. Table 8.5 shows the absolute values of the calculated amounts of embedded cement and measured 28-day strengths. The relative values of these quantities are given as well, calcu-

Table 8.5 Effect of curing temperature on compressive strength and embedded cement volume after 28-days hydration.

Curing temp.	Degree of hydration	Compressive strength at 28 d. (measured)		Embedded cement volume V_{em} at α_{28} (calculated)	
T [°C]	(measured) α_{28}	$f_c(T)$ [MPa]	$f_c(T)/f_c(22°C)$ relative	$V_{em}(T)$ [μm^3/g cement]	$V_{em}(T)/V_{em}(22°)$ relative
22	0.730	60.8	100%	145 10^9	100%
30	0.734	53.4	88%	142 10^9	98%
40	0.734	51.3	84%	134 10^9	92%
50	0.754	48.5	80%	123 10^9	85%

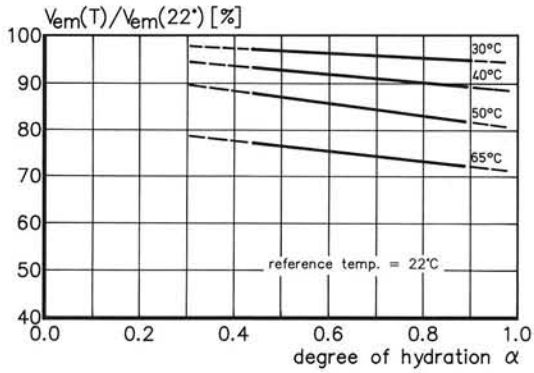

Fig. 8.17 Reduction factor allowing for the effect of curing temperature on strength development based on embedded cement volume considerations.

lated on the assumption that the embedded cement volume and the strength reached at 22°C is estimated at 100%. It appears that the relative values of both the embedded cement volume and the strength exhibit similar trends as far as their correlation with curing temperature is concerned (compare column 4 and 6). It seems valid to interpret this result as substantiating the hypothesis and that, moreover, the hypothesis seems to be able to explain, at least in part, the temperature-related strength reduction of cement pastes.

The foregoing result is shown diagrammatically in Fig. 8.17. The quotient $V_{em}(T)/V_{em}(22°C)$, plotted for different temperatures as a function of the degree of hydration, can be interpreted as a reduction factor on the strength which allows for the temperature-related decrease of strength with increasing curing temperature. Note that this reduction factor only refers to the geometry-related aspect of the strength reduction. Temperature related changes in the chemical and physical nature of the hydration products and of the bonds between these products are not considered in this factor.

8.5.3 Isothermal Temperature Effects. Summary and Discussion

The isothermal test data analyzed so far has revealed that general trends can be simulated quite satisfactorily using HYMOSTRUC. It should be borne in mind, however, that the temperature sensitivity of a particular cement may deviate quite substantially from the general trend. From the results shown in Fig. 8.14 it must be concluded that for cements of the same type deviations up to 15% have to be taken into account.

The analysis of Rakel's test data has revealed that the temperature module in HYMOSTRUC is able to explain, at least in part, both qualitatively and quantitatively the temperature-related strength reduction. This supports the hypothesis that strength development can be considered and modelled as a process of the embedding of particles. This process is adversely affected by the temperature-induced decrease of expansion of hydrating particles.

8.6 Adiabatic and Semi-Adiabatic Curing

8.6.1 Adiabatic Tests

As was explained in Chapter 1, the major aim of this project is to simulate the hydration process as a function of cement composition, particle size distribution, w/c ratio and temperature in order to be able to produce adiabatic hydration curves which will serve as the starting point for macro calculations concerning structural elements and structures as a whole. In order to check the potential of HYMOSTRUC in this area several adiabatic tests were analyzed. Test results published by Laube [329], Rakel [472], the TNO-research institute [591], the Dutch Cement Industry (denoted as "ENCI tests" [154]), and Bredero-Research Laboratories [63] will be discussed.

Effect of Initial Concrete Temperature on Adiabatic Hydration Curves
Fig. 8.18 shows the effect of the initial concrete temperature on the rate of hydration. The temperature curves refer to a concrete with a cement content of 240 kg/m^3 and 80 kg/m^3 fly-ash. In these experiments, presented by Laube [329], a well-known phenomenon was observed of a higher temperature rise in the case of low initial curing temperatures. In agreement with previously published data on this subject the phenomenon was attributed to temperature-related morphological changes of the hydration products, resulting in a relative decrease of the rate of hydration with increasing temperature. This phenomenon is modelled in HYMOSTRUC according to the option outlined in Section 6.6.3. A second factor that should be mentioned as possibly contributing to the observed phenomenon refers to the temperature dependency of the specific heat of the concrete. In [66] it has been outlined that a temperature difference of 40°C, i.e. a temperature rise from 10°C to 50°C, may account for an increase of the specific heat of about 4% for an 80% hydrated concrete.

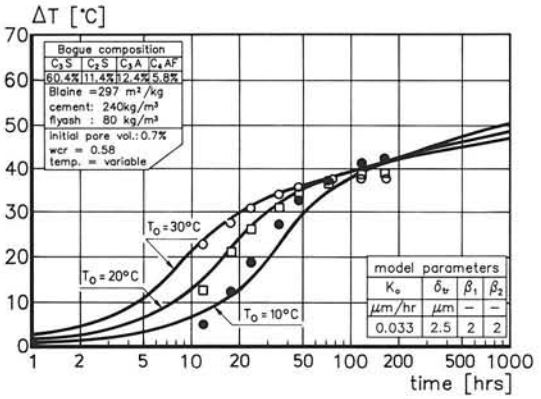

Fig. 8.18 Adiabatic temperature rise as a function of time for different initial curing temperatures. Data of Laube [329].

In the calculations, of which the results are shown in Fig. 8.18 with solid lines, the temperature dependency of the specific heat was taken into account according to [66]. The fly-ash was considered to behave as an inert filler during the first 28 days of hydration. This is, of course, a simplification of reality, and thus the calculations must be considered as indicative only. The calculated temperature curves are nevertheless interesting, since they reveal, in agreement with the measured temperatures, a higher temperature rise in the case of lower initial temperatures of the mix. The calculated differences in the temperature rise must largely be attributed to the lower specific heat of the concrete at lower temperatures.

It is further commented that the flat slope of the measured hydration curves for curing times exceeding ≈3 days is hard to simulate with HYMOSTRUC unless the value of β_2 is significantly increased. A physical background for such an increase might be sought in increased densification of the hydration products.

Effect of Water/Cement Ratio. Experiments by ENCI and Rakel

Fig. 8.19 shows the effect of the w/c ratio on the adiabatic hydration curve as determined for a concrete made with a Dutch Portland cement, class B, for ω_0=0.4 and 0.5, respectively. The experiments were carried out in the laboratories of the Dutch Cement Industry (ENCI). Cement characteristics are given in the insert of Fig. 8.19. The hydration curves were obtained for a concrete sample of which the mix composition is given in the insert as well. In the calculations the specific heat of the concrete was considered to be a function of both the degree of hydration and temperature as outlined in [66]. A good agreement was found between measured and theoretical hydration curves for the model parameters indicated in the bottom-left insert of Fig. 8.19.

In Fig. 8.20 adiabatic tests are presented carried out by Rakel [472]. The w/c ratio varied from 0.25 to 0.6. The effect of the w/c ratio on the rate of hydration is predicted fairly satisfactory with HYMOSTRUC.

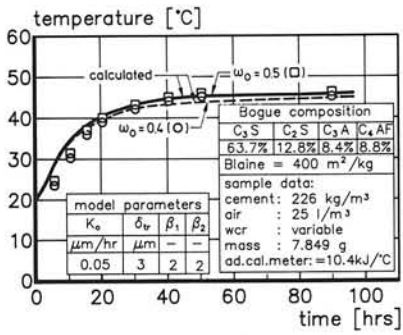

Fig. 8.19 Adiabatic hydration curves. Portland cement B. ω_0=0.4 and 0.5; T_0≈20°C. ENCI-tests [154].

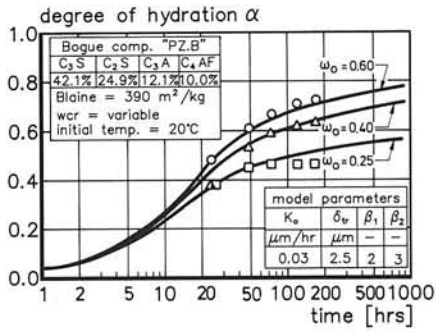

Fig. 8.20 Adiabatic hydration curves. Portland cement; ω_0=0.25, 0.4 and 0.6. Tests of Rakel [472].

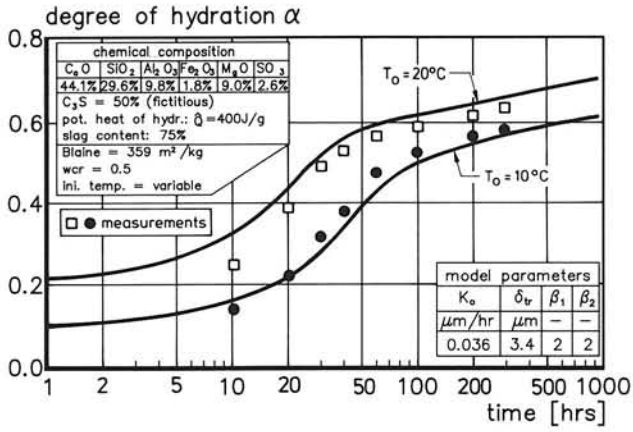

Fig. 8.21 Adiabatic hydration curves. Blast furnace slag cement. Initial curing temperature: T_0=10°C and 20°C. Tests of TNO [591].

Blast-Furnace Slag Cement

If it were true that the slope of hydration curves largely depends on the particle size distribution of the cement (see Section 5.4.1), it is to be expected that a granolumetry- and stereology-oriented simulation model like HYMOSTRUC can also be applied to simulate the hydration of a blast furnace slag cement (BFS-cement).

An extensive research program on adiabatic hydration curves of BFS-cement was recently carried out at the TNO-research institute [591]. Initial concrete temperatures were 10°C and 20°C. The measured and predicted temperatures are presented in Fig. 8.21. Note that, unlike the experiments of Laube and Rakel, the TNO-tests show a steady increase of the temperature also during the later ages. This can partly be explained by the typical reaction kinetics of BFS-cement. Possibly the particular, non-conventional way in which the adiabatic tests were carried out can also be responsible for this result.

8.6.2 Semi-Adiabatic Tests

Test Program

With the aim to check the reliability of HYMOSTRUC, particularly as regards the accuracy with which the degree of hydration can be predicted if hydration occurs under an arbitrary temperature regime, a small experimental program was developed. The program comprised hydration measurements on sealed cement pastes made from a Dutch Portland cement B, ω_0=0.4 and 0.5 and cured at temperature regimes as indicated in Fig. 8.22. At first the adiabatic temperature path was followed as determined in the ENCI tests discussed in Section 8.6.1. On reaching several prefixed temperature levels, i.e. 20°C, 26°C,

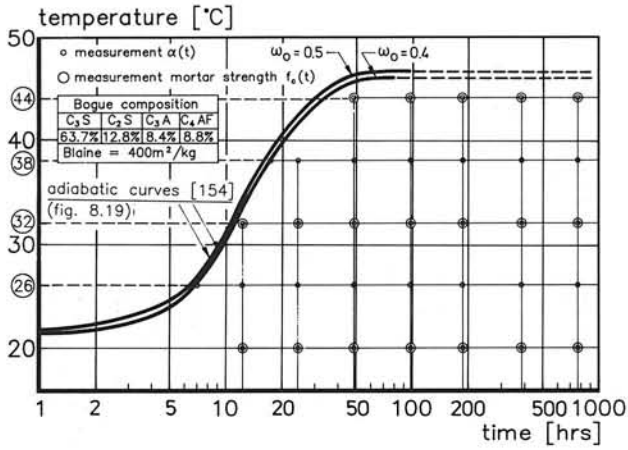

Fig. 8.22 Diagrammatical representation of curing schemes for semi-adiabatic hydration and strength tests.

32°C, 38°C and 44°C, further hydration took place isothermally at the indicated temperature levels. At discrete points of time as indicated in the test scheme of Fig. 8.22 the non-evaporable water was measured using the Penfield method (see [480]). The degree of hydration was obtained by dividing the measured non-evaporable water content by the maximum value determined from the Bogue composition of the cement according to eq. (3.5). Strength measurements were carried out on mortars cured under sealed conditions at temperature regimes as indicated for the 20°C, 32°C and 44°C series.

Hydration Data: Test Results and Theoretical Data Obtained with HYMOSTRUC

In Fig. 8.23 hydration data is given for the pastes with ω_0=0.4 and 0.5, respectively. The approximations with HYMOSTRUC are shown with solid and dashed lines. Unlike our expectations, the model parameters for which the fit was obtained (see inserts), substantially differed from those for which the adiabatic hydration data was approximated (see Fig. 8.19). A somewhat smaller K_0-value could be expected, since hydration of cement in neat cement pastes is generally expected to proceed slower than in a concrete specimen, as in the case of adiabatic tests. The well-known limited accuracy of the Penfield method [1]) may also have contributed to the observed discrepancy.

With regard to the theoretical data generated with HYMOSTRUC, note that the predicted width of the range of hydration data resulting from the difference in curing temperatures is in good agreement with the observed width of this range. The observed slow rate of reaction after 7 days hydration could not be simulated using HYMOSTRUC, unless an

[1]) The Penfield method is generally used for routine testing, when accuracy requirements are not very stringent.

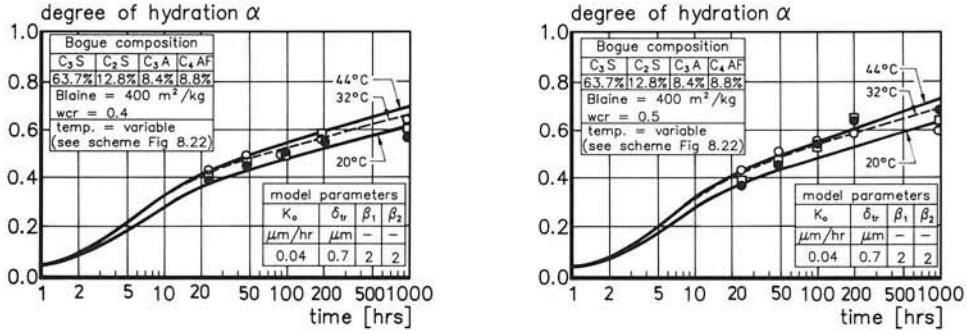

Fig. 8.23 Measured and theoretical hydration data of semi-adiabatic tests. Imposed temperature regime as indicated in Fig. 8.22.

additional increase of the diffusion resistance of the reaction products with increasing degree of hydration can be considered. Such an increase might mirror an effect of "cell interaction", which phenomenon has not been considered in HYMOSTRUC explicitly.

Strength Development

In Fig. 8.24 the strength data is expressed as a function of the degree of hydration (Fig. 8.24a) and the calculated embedded cement volume v_{em}^{pa} (Fig. 8.24b). In agreement with the published data, the relationship between strength and degree of hydration is a linear

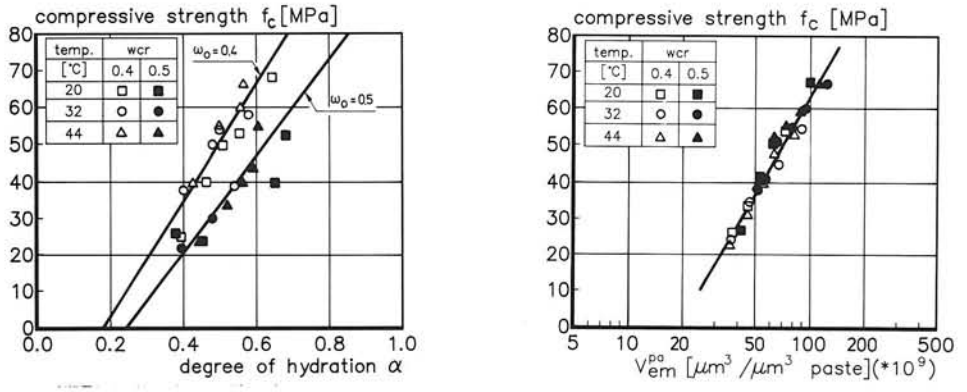

a. Strength versus degree of hydration

b. Strength versus embedded cement volume

Fig. 8.24 Strength of semi-adiabatically cured mortars as a function of degree of hydration (a) and calculated embedded cement volume v_{em}^{pa} (b).

one, whereas the w/c ratio determines the absolute values of this relationship. The relationship between the embedded cement volume v_{em}^{pa} and the strength appears to be a logarithmic one. When comparing these two figures it strikes that, unlike the f/α-relationship (Fig. 8.24), the f/v_{em}^{pa} -relationship is not distinctly affected by the w/c ratio. This brings us to the preliminary statement that:

The amount of embedded cement per unit volume of paste, i.e. the amount of cement involved in the interparticle interaction mechanism and as such considered to be a measure for the number of interparticle contact points and contact surfaces per unit of volume, is an unambiguous strength parameter, i.e. independent of the w/c ratio.

This finding is considered to be completely in line with the suggestion of those authors who have stated that it would be the number of interparticle bonds per unit of paste volume which determine the strength. More recently Lokhorst[2]) has studied the relationship between the growth of interparticle contacts on the one hand and the development of strength and stiffness on the on the other hand in more detail. His studies seem to support the reasonableness of the concept outlined in this section. Further studies, however, is still recommended in order to check the universal validity of proposed relationships.

8.6.3 Adiabatic Tests. Discussion

Accuracy of Adiabatic Temperature Calculations

The simulation of non-isothermal hydration processes is more complicated than the simulation of isothermal processes since at least two additional phenomena have to be allowed for.

Firstly, one has to allow for the temperature sensitivity of the cement, which involves selecting an apparent activation energy or alternative parameters with which the effect of the actual curing temperature on the rate of hydration can be described. The apparent activation energy depends, among other things, on the prevailing reaction mechanisms and the compound composition of the cement.

Secondly, non-isothermal calculations have to allow for the thermal properties of the specimen. These properties cannot be considered constant, but depend on the degree of hydration and the actual temperature. Disregarding or misjudgment of these effects may result in misinterpretations of observed temperature readings when the latter are used for the determination of the degree of hydration. Moreover, it should be emphasized that the high accuracy of adiabatic test devices is restricted to the relatively early stages of the hydration process, say up to one week (see Section 3.3.1.1). After that time the difference between produced heat per unit of time and heat losses to the environment is so small that the measured temperatures must be considered as a function of the type of test device

---

[2]) S.J. Lokhorst, 1997. *Deformational Behaviour of Concrete Influenced by Hydration Related Changes of the Microstructure*, TU-Delft.

rather than a characterization of the rate of reaction.

Considering these remarks it can be concluded, that the non-isothermal temperature predictions made with HYMOSTRUC are certainly encouraging. The effect of the w/c ratio and initial mix temperature on the shape of the hydration curves can be predicted quite satisfactorily.

With respect to reliability of temperature predictions exceeding 7 days hydration, it is noted that in its present stage of development HYMOSTRUC suggests a slow but steady progress of the hydration process. This was found to be in agreement with the test results of TNO, whereas tests carried out by Rakel and Laube reveal an almost total cessation of the hydration process.

8.7 Model Parameters: Quantitative Values and Accuracy. Discussion

8.7.1 Basic Rate Factor K_0

Mathematical Expression for K_0

In Section 8.2 and Fig. 8.1 it has been suggested that a correlation might exist between the basic rate factor K_0 and the C_3S content of the cement. A more complete picture of the K_0-values found in this chapter is shown in Fig. 8.25. Only those K_0-values are considered pertaining to tests with Portland cement. From this figure it can be concluded that a distinct correlation between K_0 and the C_3S content holds indeed, albeit that the scatter is quite substantial. For this correlation a parabolic expression holds quite well. A linear correlation, however, would not be bad either. For the parabolic correlation it holds that:

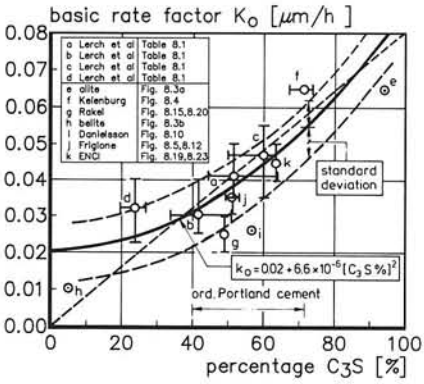

Fig. 8.25 Basic rate factor K_0 as a function of the C_3S content of the cement.

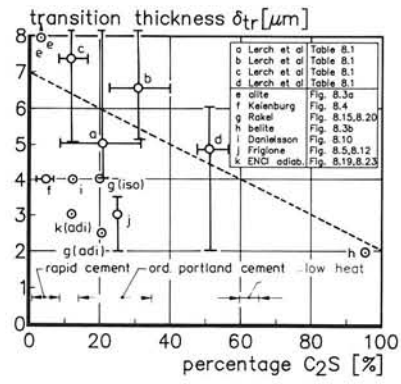

Fig. 8.26 Transition thickness δ_{tr} as a function of the C_2S content of the cement.

$$K_0 = 0.02 + 6.6\ 10^{-6} * [C_3S\%]^2 \qquad [\mu m/h] \qquad (8.1)$$

For C_3S-contents in ordinary Portland cements in the range from 40% up to 70% (see Fig. 2.2) expression (8.1) holds quite well. For the standard deviation $s(K_0)$ a value of s=0.008 μm/h was obtained. Particularly for low K_0-values the standard deviation is relative large. The effects of scatter in the K_0-values on temperature predictions will be illustrated in Section 8.8 and in Chapter 9.

Accuracy Considerations

With regard to the value of the standard deviation we refer to the accuracy considerations in Section 2.2.3 concerning the C_3S content in an arbitrary Portland cement. The *multi-method* standard deviation of the C_3S content, expressed in percentages by weight of the cement, was calculated at 6...10%. Let us assume a mean value of 8% as being representative of the standard deviation of the C_3S content and a normal distribution of the C_3S content. For a cement with a nominal C_3S content of 60%, the 16% fractiles are then defined by C_3S=52% and C_3S=68%. The K_0-values for C_3S contents of 52%, 60% and 68% calculated according to eq. (8.1) are 0.037, 0.044 and 0.051 μm/h, respectively. Obviously deviations in the C_3S content up to the magnitude of standard deviation of 8% are responsible for deviations in the K_0-values of 0.007 μm/h as compared to the mean K_0-value of 0.044 μm/h. It thus appears that the standard deviation in the K_0-values of 0.008 μm/h is, to a great extent, due to the assumed standard deviation in the C_3S content, the latter being responsible for deviations from the mean K_0-value of about 0.007 μm/h. In addition to the effect of variations in the C_3S content which appear to contribute to the scatter in the K_0-values one should consider effects of minor compounds and gypsum, which effects have not been accounted for explicitly in HYMOSTRUC.

Comparison of K_0-Values with the Literature Data

Several authors have presented values for the rate of penetration of the reaction front in hydrating cement particles. In so far that these values refer to the early stage of the reaction process, i.e. the stage when the boundary reaction is the rate controlling mechanism, these values can be compared with the K_0-values. Early penetration rate data is shown in Table 8.6. Although it is interesting to compare the data of Table 8.6 with the K_0-values presented in Fig. 8.25, it is almost impossible to deduce anything substantial from this comparison. For this purpose the majority of the published data is not sufficiently documented. However, it can be concluded that the range of published penetration rates agrees with the K_0-values found in the evaluation program in this chapter. The penetration rates for alite and C_2S determined by Tsumura [596] correspond fairly well to the K_0-value for alite and belite (Fig. 8.25, points e and h).

Table 8.6 Rate of penetration of the reaction front in cement particles and compounds (Temperature: ± 20°C)

Author	Ref.	year	reference period	material	penetration rate µm/h
Anderegg et al.	[13]	1929	0 - 24 h	cement	0.02
Krogbeumker	[314]	1972	0 - 72 h	Portland cement	0.032
Steinherz	[554]	1960	0 - 72 h	cement clinker	0.021
Tsumura	[596]	1966	first hour	alite	0.055
				C_3S	0.036
				C_2S	0.0011
Lhopitallier et al.	[343]	1948	1st mnth	cement clinker	0.042
Taplin	[572]	1968	>1000 h	alite	0.0125
				β-C_2S	0.0009
Bezjak	[50]	1980	phase-bound	alite	0.067
			phase-bound	comm. cement	0.074-0.110

8.7.2 Transition Thickness δ_{tr}

Fig. 8.26 shows the transition thickness δ_{tr} as a function of the C_2S content determined in the evaluation program. The δ_{tr}-C_2S correlation is evidently less distinct than the K_0-C_3S correlation. For the data of Lerch et al. and the alite and belite data a linear decrease of the transition thickness with increasing C_2S content seems to hold. The δ_{tr}-values found from the evaluation of the test data of Frigione, Rakel, Danielsson, Keienburg and the ENCI tests, however, are substantially lower. The only guidance that can be deduced from Fig. 8.26 is that for the majority of ordinary Portland cements the transition thickness varies between 2.5 µm and 6.0 µm. For low heat cement the transition thickness turns out to be relatively low, whereas for rapid hardening cements the best results are yielded with relatively high values of the transition thickness. Computer simulations could start with the guide values for δ_{tr} according to:

$$\delta_{tr} = -0.02 * [C_2S\%] + 4 \quad [\mu m] \tag{8.2}$$

For an explanation of the observed δ_{tr}-C_2S relationship it might be worthwhile to consider the particular characteristics of the pore structure of cement paste. In a low heat cement, i.e. a cement with a high C_2S content, the volume of capillary pores has been found to increase at the expense of micro pores (see Section 4.4.4.3). The fact that in a C_2S-rich cement the transition thickness is relatively small, points to a significant effect of the capillary pore structure on the rate of hydration. The sooner a mature capillary pore system has been built up, the sooner the reaction turns out to become diffusion controlled. Obvi-

ously it is the water transport in the capillary pore system that is of paramount importance in this respect. This conclusion is in full agreement with Parrott's statement, that the rate of cement hydration seems to be determined by the amount of water in the larger capillary pores rather than the amount of water in the porous hydrate coatings that surround residual unhydrated grains [438].

With respect to the large scatter in the δ_{tr}-values it must be emphasized that this does not necessarily jeopardize the applicability of HYMOSTRUC for practical purposes. This can easily be explained with the help of Fig. 7.14, where hydration curves are presented for different values of the transition thickness. It appeared that variations in the transition thickness are responsible for only modest changes in the course of the theoretical hydration curves and this only in the later stages of the hydration process (see also Section 8.7.3).

8.7.3 Coefficients β_1 and β_2

General remarks in view of consistency of the model

From the very outset of the evaluation programm it was assumed that the β-coefficients might exhibit a dependency on the chemical composition of the cement. The evaluation programm, however, did not reveal such a dependency. Moreover, although the variation in β-values varied from 1 to 2, the effect on the shape of the predicted hydration curves was relatively small. It this respect it is considered worthwhile to note, that the β-coefficients become operative no sooner than in the diffusion controlled stage, i.e. when the degree of hydration has reached a value between α=0.3 to 0.5 already. Until these α-values the shape of the hydration curve is determined (at least in the model) by the paste parameters like w/c ratio, the particle size distribution of the cement, the reaction temperature and, as far as the independent model parameters are concerned, *only* by the basic rate factor K_0. Beyond afore-mentioned α-values, i.e. in the stage when the degree of hydration increases up to about 0.6 to 0.8, variations in the β-values from 1 to 2 will generally cause variations in the predicted 28-day hydration values of about 5% to 10%. Variation of the same order of magnitude can be ascribed to variations in the gypsum content and the effect of minor compounds (see for example Fig. 8.4), which effects are not modelled explicitly in HYMOSTRUC. In the light of the latter fact it must be considered fruitless the search for a correlation between the β-values and the chemical composition of the cement unless we would be able to account for the effect of minor compounds and gypsum explicitly in the model.

From the foregoing a most important conclusion can be drawn as regards to the consistency and predictability of the simulation model, viz.:

> *The facts that, firstly, the K_0- and δ_{tr}-values are hardly affected by variations in the β-values and, secondly, no correlation could be established between the β-values and the chemical composition of the cement, demonstrate that the effect of the chemical composition of the cement on the rate of hydration can be accounted for by the two parameters K_0 and δ_{tr}. The correlation between these*

two parameters and the chemical composition of the cement is not affected significantly by the values of the two β-coefficients.

β-Coefficients. Guide values
For the absolute values of the β-coefficients it can tentatively be stated that:

1. The majority of test results could be approximated satisfactorily for β_1=2 and β_2=2.
2. As the hydration process progresses the β_2-values tend to increase.

Furthermore it should be noted that for detailed information about the value of β_2, i.e. the coefficient which refers to the temperature effect on the structure of the hydration products, more research is required. On the basis of the results obtained from Rakel's adiabatic tests, it is expected that the proposed method of accounting for the temperature effects has good prospects. For the time being, a value β_2=2 seems to hold reasonably well.

8.8 Predictability

8.8.1 Introductory Considerations

First indications about the predictability of HYMOSTRUC can be deduced from the fact that for the determination of the default values of the independent model parameters ignorance of even a substantial number of test data turned out hardly to affect these default values. For example, ignorance of even 20 randomly chosen tests out of the 67 that have been used for the determination of the default values presented in the foregoing, appeared to cause only a slight increase of the standard deviation of the dominant model parameter K_0 from $s(K_0)$=0.008 to 0.0095 μm/h.

To which extent the scatter in the K_0- and δ_{tr}-values might or does affect the predictability of the HYMOSTRUC, i.e. the accuracy with which (adiabatic) hydration curves can be predicted, is subject of the next Section.

8.8.2 Prediction of Adiabatic Hydration Curves

For a check of the predictability of the simulation model, calculated adiabatic hydration curves have been compared with experimental data. For the experimental results the adiabatic ENCI-test presented in Section 8.6.1 were chosen. Taking this test data, which has been used already for the determination of the independent model parameters, is considered warranted bearing in mind that ignorance of the ENCI-tests for the determination of the model parameters would *not* have changed the default values for the independent model parameters significantly (see foregoing Section 8.8.1). Actually, any randomly chosen test out of the earlier used data could have been used for checking the predictability of the simulation model!

Details of the ENCI-test have already been given in Section 8.6.1. For the default val-

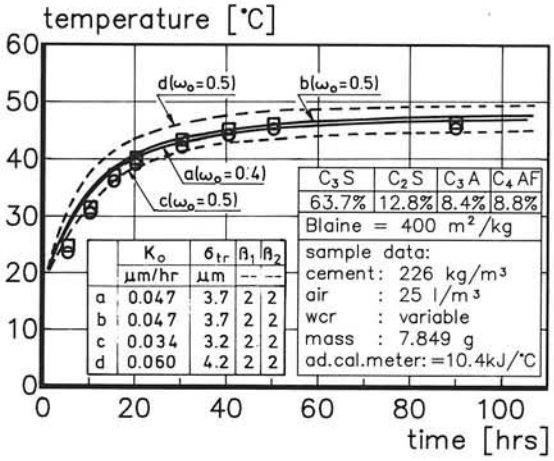

Fig. 8.27 Predicted and measured adiabatic temperatures. Experimental data: ENCI-tests [154].

ues of the four independent model parameters K_0, δ_{tr}, β_1 and β_2 as defined in the Section 8.7, the predicted adiabatic temperature curves are presented in Fig. 8.27. Curves *a* and *b* refer to mixes manufactured with ω_0=0.4 and ω_0=0.5, respectively. The default values of the model parameters with which these curves have been calculated are shown in the bottom-left insert of the figure. Experimental data are shown with discrete points.

For the mix with ω_0=0.5 also predicted temperature curves are shown calculated with K_0-values obtained by increasing the decreasing the defaults value of this parameter with 1.64*s(K_0)=1.64*0.008=0.013 µm/h, corresponding with the 5%-fractiles of this parameter. The δ_{tr}-values used in the calculations for these curves were obtained by increasing and decreasing the default values with 0.5 µm, respectively. The thus obtained model parameters are shown in the bottom-left insert of Fig. 8.27 (under *c* and *d*). The calculated temperature curves are shown with dashed lines. It can be seen that the *measured* adiabatic temperatures fall within the range bordered by these dashed curves. This result appeared to be representative of the majority of test data analyzed in this way.

Experimental hydration data are generally found to fall within the range defined by theoretical hydration curves calculated a) with values of the basic rate factor K_0 which correspond with the 5%-fractiles of this factor, b) accounting for realistic, experience-based lower and upper limit values of the transition thickness δ_{tr} and c) dummy values of the β-coefficients, viz. 2. These results confirm that with the presented simulation model reliable predictions of (adiabatic) hydration curves are possible quite good!

PART III

Applications

Evaluation and Summaries

Practical Application - Case Study

Discussion - Conclusions - Recommendations

Summaries

9 PRACTICAL APPLICATION OF HYMOSTRUC: RELIABILITY

9.1 General

With HYMOSTRUC adiabatic hydration curves can be generated. These curves are used as input for macro-level calculations concerning temperature fields, strength, stresses and risk of early-age thermal cracking in hardening concrete structures. A characteristic crack pattern caused by early temperature effects is shown in Fig. 9.1. In this chapter it will be shown to sensitive stress prediction are for variation in predicted adiabatic input curves. Uncertainties in the adiabatic input curve are the result of inaccuracies and uncertainties in the four model parameters of HYMOSTRUC, i.e. in K_0, δ_{tr}, β_1 and β_2. Emphasis will be on the influence of uncertainties in the model parameters on the predicted *probability of cracking*. The macro-level calculations in this case study are carried out using the computer program TEMPSPAN. Details of this program are discussed briefly in the next section.

9.2 Macro-Level Calculations. Program Features of TEMPSPAN

With TEMPSPAN (Eng.: TEMPerature and STRESSes) the progress of the hydration process, temperature fields, the development of material properties and the probability of cracking are analyzed in structural elements like walls and slabs.

The input consists of the adiabatic hydration curve for the concrete mix under consideration. Deviations of the actual curing temperatures from adiabatic temperatures due to heat losses to the environment are allowed for according to the "g-factor concept" as outlined in Section 5.6.2.1.

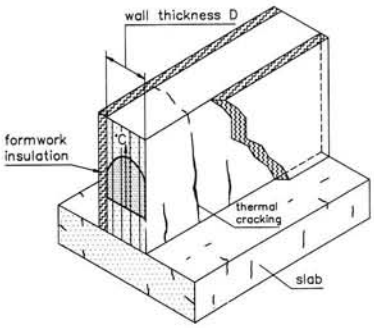

Fig. 9.1 Characteristic crack pattern in hardening concrete wall cast on a rigid slab. Surface and through-cracks.

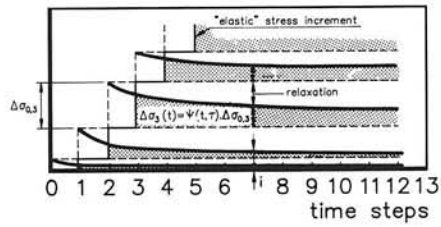

$$\psi(t,\tau) = e^{-\left[\left(\frac{\alpha(t)}{\alpha(\tau)} - 1\right) + 0.44 * \omega^{1.65} * \tau^{-d} * (t-\tau)^{n} * \frac{\alpha(t)}{\alpha(\tau)}\right]}$$

d,n = constants [66]

τ = time of application of a thermal stress increment

Fig. 9.2 Schematic representation of superposition method for stress calculations in young concrete (after [66]).

In the program the strength is determined as a function of the calculated degree of hydration, either as a direct function of this quantity or indirectly via the gel-space ratio concept (see Section 4.9). For the calculations in this case study the degree-of-hydration concept has been adopted.

In TEMPSPAN early-age stresses are calculated according to procedures proposed by the author [67,68] or, alternatively, by Vonk [607]. In both procedures early-age or maturing relaxation is formulated as a function of the progress of the degree of hydration. In this case study only the first mentioned procedure will be used. The procedure presupposes the applicability of the superposition method (see Fig. 9.2). The relaxation formula, which will not be discussed in detail here, is shown in Fig. 9.2.

9.3 Macro Calculations. Case Study

9.3.1 Construction and Mix Data

Construction Data and External Boundary Conditions

In this case study two concrete walls are considered with thicknesses 0.5 m and 1.0 m. For the temperature calculations the walls are considered to be built up of 9 elements as indicated in the Fig. 9.3a. Temperature and wind conditions at both sides of the wall, as well as the thermal properties of the moulding and stripping times, are indicated in the figure.

For the stress calculations complete restraint of the generated thermal deformations is assumed. A condition of full restraint corresponds to the stresses in the middle section of a long concrete wall cast on a rigid foundation.

Mix Data and Theoretical Adiabatic Hydration Curves

The mix data of the concrete is given in the insert of Fig. 9.3b. A Portland cement was

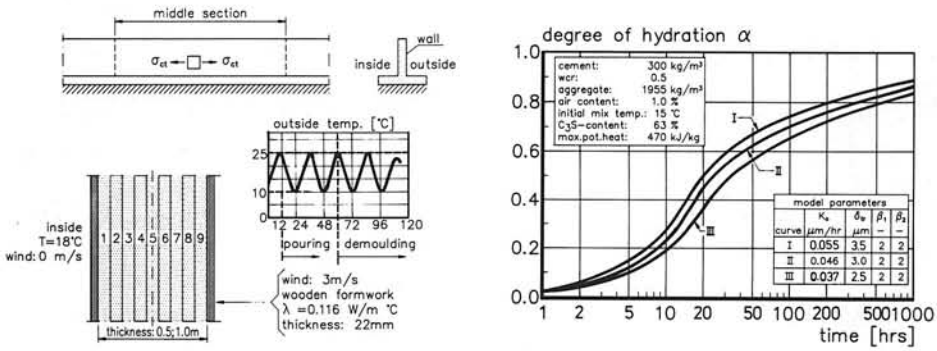

Fig. 9.3 Construction and mix data considered in the case study.
a. Concrete walls with indication of external factors of influence.
b. Theoretical adiabatic hydration curves, generated with HYMOSTRUC.

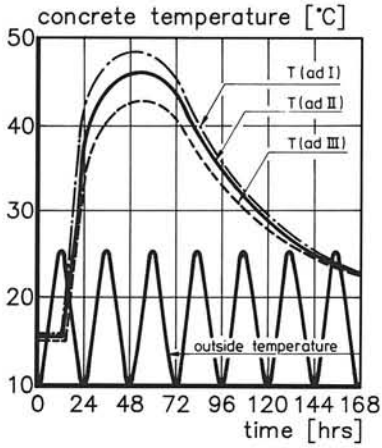

Fig. 9.4 Calculated temperature in centre of hardening concrete wall for different adiabatic input curves I, II and III.

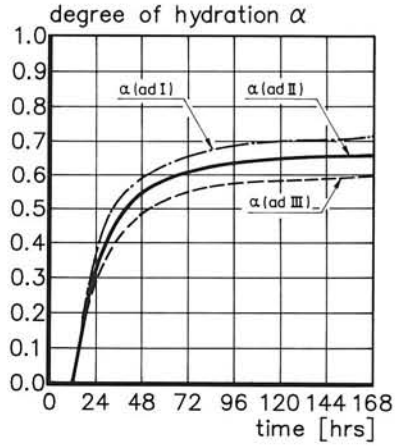

Fig. 9.5 Calculated degree of hydration in centre of hardening concrete wall for different adiabatic input curves.

used with Blaine=305 m^2/kg (R-R coefficients: n=1.12, b=0.025). C_3S-content 63%. For this concrete mix three adiabatic hydration curves have been determined using HYMOSTRUC, viz. the curves I, II and III. The model parameters for which these curves were obtained are shown in the bottom insert of Fig. 9.3b. The K_0-value of 0.046 μm/h corresponds to the mean value determined using eq. (8.1) for C_3S=63% (see Section 8.7.1). The values K_0=0.055 μm/h and K_0=0.037 μm/h correspond to the 16% fractiles for this quantity, i.e. the mean values plus or minus a standard deviation $s(K_0)$=0.009 μm/h. The δ_{tr}-values were chosen so as to cover a realistic range of values for this parameter as indicated in Fig. 8.26.

9.3.2 Case Study. Results

Temperature and Degree of Hydration

For the 1.0 m thick concrete wall the temperature and degree of hydration in the central element (el. 5) are shown in Fig. 9.4 and Fig. 9.5, respectively, for the three adiabatic hydration curves I, II, and III. As was expected, the temperatures and the degree of hydration are highest for adiabatic curve I and lowest for adiabatic curve III.

Strength and Stress Development

The relationship between the strength and the degree of hydration adopted in this study is based on the experimental results discussed in Section 8.6.2 and presented in Fig. 8.24a. The compressive strength of *mortar* was found to be a more or less linear function of the degree of hydration. For ordinary mixes the *concrete* compressive strength is generally

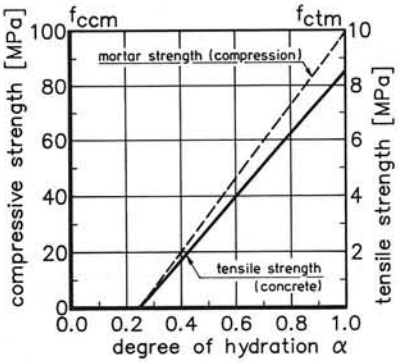

Fig. 9.6 Assumed relationship between strength and degree of hydration (based on Fig. 8.24a).

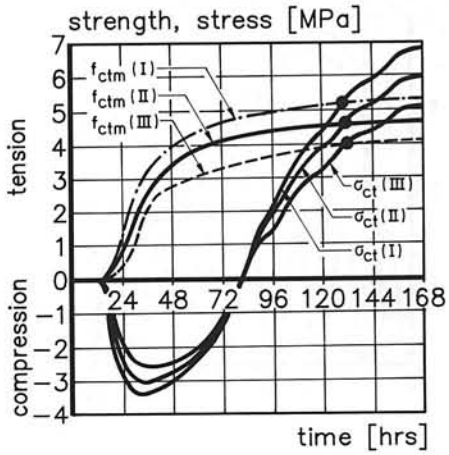

Fig. 9.7 Strength and stress in centre of a 1.0 m thick concrete wall as a function of time.

considered to be lower than the mortar strength. In line with sources quoted in Section 4.6, the concrete strength was assumed to be 16% less than the mortar strength. The concrete tensile strength was roughly estimated at 10% of the concrete compressive strength. For the mean tensile strength of a concrete with water/cement ratio ω_0=0.5 a linear function results, viz. (Fig. 9.6):

$$f_{ctm} = 11.5 * \alpha(t) - 2.8 \qquad \text{[MPa]} \tag{9.1}$$

In Fig. 9.7 the tensile strength reached in the centre of the 1.0 m thick wall is expressed as a function of time for the three adiabatic input curves together with the results of the stress calculations.

9.3.3 Probability of Cracking

From the calculated strengths and stresses it is possible to calculate the probability of cracking, provided that both the distribution functions and the standard deviations of the strength and stresses are known [67]. It is assumed that both strength and stress are *normal random variables* with mean values f_{ctm} and σ_{ctm}, respectively (Fig. 9.8). For an estimation of the standard deviation of the strength, one should remember that the strength is assumed to be a function of the degree of hydration (see eq. (9.1)). Hence, the standard deviation of the strength is linked up with the standard deviation of the degree of hydra-

tion. In Chapter 3 it was concluded, that for the degree of hydration a coefficient of variation of about 7.5% is applicable. This value of 7.5% is assumed to correspond to 1.64 times the standard deviation $s(\alpha)$ of the degree of hydration, i.e. with the 5% fractile of a normal distribution. For this value of the standard deviation of the degree of hydration the characteristic value of the tensile strength f_{ctk} can be obtained now according to:

$$f_{ctk} = 11.5 * [\ \alpha(t) - 0.075 * \alpha(t)\ ] - 2.8 \qquad \text{[MPa]} \qquad (9.2)$$

For the standard deviation $s(f_{ct})$ of the tensile strength, it follows that:

$$s(f_{ct}) = \frac{f_{ctm} - f_{ctk}}{1.64} \qquad \text{[MPa]} \qquad (9.3)$$

The standard deviation of the calculated tensile stresses $s(\sigma_{ct})$ is considered to exceed the standard deviation of the strength by about 20% [67]. It follows:

$$s(\sigma_{ct}) = 1.2 * s(f_{ct}) \qquad \text{[MPa]} \qquad (9.4)$$

For the mean value μ_z of the margin between strength and stress and for the corresponding standard deviation s_z it holds that:

$$\mu_z = f_{ct} - \sigma_{ct} \qquad \text{[MPa]} \qquad (9.5)$$

$$s_z = [\ s^2(f_{ct}) + s^2(\sigma_{ct})\ ]^{\frac{1}{2}} \qquad \text{[MPa]} \qquad (9.6)$$

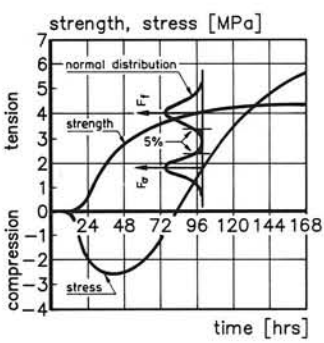

Fig. 9.8 Probability of cracking. Diagrammatical representation.

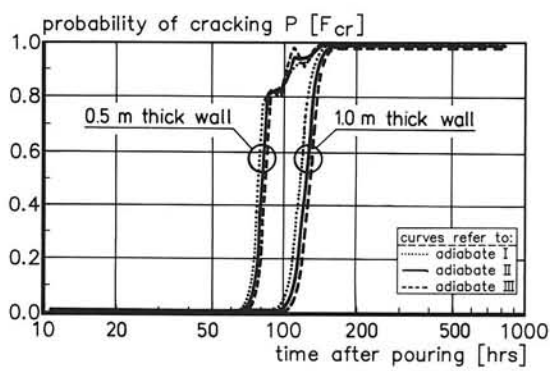

Fig. 9.9 Theoretical probability of cracking in centre of two hardening concrete walls for different adiabatic input curves.

The probability of cracking can be read off now from standard tables as a function of the quotient Φ (see also [67]):

$$\Phi = \frac{x - \mu_z}{s_z} \tag{9.7}$$

where x=0. In Fig. 9.9 the probability of cracking is shown for the central element of the 0.5 and 1.0 m thick walls for the three adiabatic input curves I, II and III. It appears that for the different input curves the probability of cracking varies within a relatively small range. The reason for the weak correlation between the input curves and the predicted moment of cracking is that the probability of cracking follows from the difference between two quantities, viz. strength and stress, which are both affected by the shape of the input curve in a similar way. A relatively rapid hydration, i.e. hydration based on adiabatic curve I, results in higher temperatures and higher stresses, but also in a higher strength. Conversely, a slowly hydrating mix, represented by curve III, results in lower temperatures and lower thermal stresses, but also in a lower strength (see also Fig. 9.7). In so far as there is a correlation between the shape of the input curve, i.e. the reactivity of the cement, and the probability of cracking, there is a tendency of decreasing probability of cracking with decreasing reactivity of the cement. This is in agreement with observations in practice.

9.4 Discussion

The aim of this case study was to illustrate the effect of uncertainties and inaccuracies in the model parameters of HYMOSTRUC on the theoretical probability of cracking in hardening concrete structures. For a realistic range of values for K_0 and δ_{tr}, - realistic in the sense that K_0-values were chosen so as to cover the values within the 16% fractile boundaries as determined in the evaluation program in Chapter 8, whereas only a modest variation in the δ_{tr}-values was considered -, it can be concluded that for the two walls dealt with in this case study the uncertainties and inaccuracies in the model parameters do *not* affect the calculated probability of cracking significantly and are certainly less significant than the effect of the wall thickness on the probability of cracking. From this observation it can be concluded that the adiabatic hydration curves generated with HYMOSTRUC are sufficiently accurate to serve as an input for parametric sensitivity studies concerning the probability of cracking in actual concrete structures. It seems that at the present stage of knowledge uncertainties in the mathematically determined probability of cracking stem from uncertainties in the external factors of influence and, moreover, the modelling of the early-age relaxation, rather than from uncertainties in the theoretical adiabatic input curves as generated by HYMOSTRUC. Future research should, therefore, preferably be focused on the early-age relaxation. In this respect the recent studies by Emborg [153] and Laube [329], as well as the phenomenological investigations by Springenschmid et al. [549,550] and Breitenbucher [64] must be considered as most worthwhile.

10 CONCLUSIONS and RECOMMENDATIONS

10.1 Objectives of the Study

The aim of this study was to develop a computer-based simulation model for hydration and structural development in Portland cement-based materials. The model should be able to generate either adiabatic, isothermal or semi-adiabatic hydration curves as a function of the chemical composition and the particle size distribution of the cement, the w/c ratio and the curing temperature. These curves could then serve as an input for macro-level calculations concerning temperature, strength and stress development in hardening concrete structures and for investigations concerning the probability of thermal cracking. Structure development and the effect of structural development on the rate of hydration should be allowed for explicitly. This, firstly, in order to enhance the consistency of the simulation model and, secondly, since it is only structural development that must be considered as the basis for the development of the majority of engineering properties such as strength and stiffness. A simulation model which takes into consideration structural development and the effects of structural formation on the rate of hydration has been termed an *integrated model*.

It must be emphasized that although many mechanisms and processes involved in hydration and structural formation can be taken into account in the integrated model presented in this study, it can not be claimed that the model describes reality in all respects. In this context reference is made to Wittmann [624]. He has pointed out very clearly that the *chemical* and *mineralogical* complexity of the xerogel, i.e. of the microstructure, in hardened cement paste necessarily leads to a certain *smearing effect*. It can be stated additionally that the fact that we are dealing with a *poly-size* powder further contributes to the complexity of the subject and compels us to consider geometry-orientated *smearing effects*. Wittmann continues by stating that because of the actual complexity of the microstructure, it is quite clear that there is no hope that we will ever be capable of modelling the microstructure of hardened cement realistically. It is obvious that if this statement holds for *hardened* cement paste, it also holds for attempts to model the development of the microstructure in *hardening* pastes. This may not prevent us, however, from developing models that allow the simulation of relevant mechanisms and processes involved in hydration and structural formation in cement-based materials as realistically and, additionally, as workable as possible.

10.2 Conclusions

With the presented integrated model, called HYMOSTRUC, the aims briefly outlined in the forgoing have been realized to a large extent. Both adiabatic and isothermal hydration curves for Portland cement-based materials were predicted sufficiently accurate for these curves to be used in macro-level calculations. The step-wise calculation procedure according to which HYMOSTRUC operates enables us to account for many non-linear pro-

cesses and mechanisms - including structure formation -, occurring either simultaneously or successively during the hydration process. Changes in the state of water in the hardening mass, i.e. considerations with regard to the effect of the relative humidity on the rate of the hydration, are dealt with as well. Many assumptions, necessary if adhering to a more classic analytical approach to the problem, need not be maintained, since the continuously changing boundary conditions are established anew at the beginning of each calculated time step.

In addition to these more general conclusions and remarks, some particular conclusions are given in the following.

1. In agreement with other studies it was found that the particle size distribution and, particularly in the later stages of the hydration process, the w/c ratio, affect the overall rate of hydration significantly.
2. Due to embedding of small particles in the outer shell of expanding large particles the rate of penetration of the reaction front of large particles is less than that of smaller particles. Obviously HYMOSTRUC appears to be capable to confirm analytically this well-known, albeit sometimes resisted, phenomenon.
3. A good correlation was found between the total amount of embedded cement embedded in the outer shells of expanding particles and strength development. This conclusion was found to hold for a wide range of particle size distributions.
4. A distinct correlation was found between the predicted effect of the curing temperature on the amount of embedded cement and on the compressive strength (experiments of Rakel).
5. The high porosity and low microhardness in the matrix-aggregate interfacial zone as observed in many experiments was in good agreement with porosity calculations carried out using HYMOSTRUC. From this observation, and bearing in mind that HYMOSTRUC is a highly stereology-oriented simulation model, it is concluded that interface phenomena exhibit a distinct stereological aspect.
6. The relationship between the rate of hydration and the relative humidity is an indirect one: the relative humidity controls the rate of hydration in so far as it determines the distribution and amount of water in the pore system of the hydrating mass.

   Note: A possible effect of internal stresses and associated extra hydration under pressure caused by drying of a sample was not investigated in the present study.
7. The accuracy of mathematical predictions of the degree of hydration based on the chemical composition of the cement (C_3S, C_2S, C_3A and C_4AF), are limited by the effects of minor components and gypsum on the hydration process. A coefficient of variation of about 5% should be considered as the best possible result.
8. Scatter and inaccuracies in generated hydration curves can largely be carried back to scatter in the C_3S contents and, moreover, to the presence of minor constituents like alkalies and gypsum, of which the effects on the rate of hydration are not considered explicitly in the present version of HYMOSTRUC.
9. For the description of hydration curves of non-Portland cement mixes HYMOSTRUC has turned out to be very well applicable, provided that the independent

model parameters are adjusted for each particular cement. Default values for the independent parameters, viz. the basic rate factor K_0 (eq. (8.1)), the transition thickness δ_{tr} (eq. (8.2)) and the coefficients β_1 and β_2 (Section 8.7.3), give good guidance already for first indications of the shape of the hydration curve of a particular cement. Obviously the basic concept of HYMOSTRUC is universal enough to cover a wide range of different cement compositions.

10. A computer-based integrated model like HYMOSTRUC enables quantification of the relevance of several non-linear mechanisms and processes, e.g. interparticle interactions, on the rate of hydration. It was concluded that ignoring the effect of particle interaction may give rise to *incorrect* interpretations of hydration mechanisms. Moreover, disregarding the interaction mechanisms makes a model in essence incapable of analyzing the development of microstructure and associated material properties. For the latter purpose the adoption of integrated models is considered to be a prerequisite.

10.3 Recommendations

In order to achieve a more universally applicable version of HYMOSTRUC the following aspects are recommended for more detailed investigations.

1. Detailed modelling of the hydration mechanisms that occur in the very early stage of the reaction process. The practical relevance of more detailed information about the development of early processes is particularly relevant to viscosity when considering workability and the development of formwork pressures.
2. Investigations with regard to the effects of alkalies, gypsum and additives and also of curing under pressure on the rate of hydration and structural formation. These effects should either be modelled explicitly and implemented in HYMOSTRUC in the form of additional modules, or result in systematic adjustment of the independent model parameters K_0, δ_{tr}, β_1 and β_2. Similar investigations are recommended for all cements other than Portland cement.
3. Investigations concerning the particular hydration features and characteristics of structural formation over the thickness of the matrix layer between aggregate particles. The promising results of the interface investigations make us believe that HYMOSTRUC can be considered a most interesting and, in essence, an adequate research tool for investigating *ribbon paste hydration* [1]).
4. Further investigations concerning the relationship between the embedded cement

[1]) Numerical simulation of ribbon paste hydration with the use of HYMOSTRUC has been dealt with by E.A.B. Koenders in his PhD-thesis: *Simulation of Volume Changes in Hardening Cement-Based Materials (TU-Delft, 1997, 171 p.)*. In that thesis due attention has been given to the actual random distribution of the cement particles in the paste and to thermo-dynamic aspects.

volume and the development of physical material properties [2]).

5. Detailed studies of the effect of curing temperature on the morphology of hydration products and on structural formation in view of the diffusion resistance of product layers.
6. Investigations concerning the relevance of and changes in the chemical composition of pore water on the rate of hydration.
7. Simulations based on a fully random distribution of the cement particles in the paste are recommended for further checks of the simulations based on the so called *pseudo-probabilistic* approach according to which HYMOSTRUC operates In this framework also those effects on the rate of hydration which disturb the randomness of particle distribution in the paste, viz. bleeding and gravitation, should be investigated [1]).
8. The promising results obtained with HYMOSTRUC warrant further development of the model in the direction of *expert systems,* with which experience-based practical knowlegde and experience can be made operational in the form of additional subroutines.

---

[2]) Additional studies on the correlation between interparticle contacts and mechanical properties, like strength and stiffness, have been performed by S.J. Lokhorst in: *Deformational Bahaviour of Concrete Influenced by Hydration-Related Changes of the Microstructure*, TU-Delft, 1997.

11 EXTENDED SUMMARY

11.1 General

In this thesis a computer-based simulation model has been presented for the kinetics of hydration and structural formation of cement-based materials. The model, indicated with the acronym HYMOSTRUC, can be characterized as *multidisciplinary*, and this in two ways. Firstly, in the model information is brought together from different disciplines, viz. chemistry, physics and stereology. Secondly, the model aims to bridge, at least in part, the gap between the material scientist and the practical engineer.

11.2 Goals

Among the macro models, i.e. calculation procedures, currently in use in engineering practice for prediction of temperature fields, strength and stresses in hardening concrete structures, the ones which explicitly correlate the early-age concrete properties with the *degree of hydration* are considered to be most important. Models of this type would be capable, in essence, to make huge amounts of information concerning the relationship between degree of hydration and material properties available and applicable for engineering practice.

The input for the majority of these numerical macro-level models consists of either an *isothermal, adiabatic* or *semi-adiabatic* hydration curve. At present these curves have to determined experimentally for each individual concrete mix and different curing conditions. There is an increasing demand, however, for computer-based simulation models with which the required input curves could be determined mathematically. In these computer-based models the hydration process should be described as a function of:

- *water/cement ratio (physico-chemical aspect);*
- *particle size distribution of the cement (granular and stereological aspect);*
- *the chemical composition of the cement (chemical aspect);*
- *the temperature regime*

An associated, and from the material science point of view, most challenging aim consisted in explicitly modelling the *effect of structure development* on the rate of hydration and investigating the correlation between the formation of microstructure and strength development. A model which explicitly accounts for the effect of structure formation on the rate of hydration has been termed an *integrated model*. HYMOSTRUC, the simulation model discussed in the next Sections, is considered such an integrated model.

11.3 Structure Formation and Strength Development. Basic Concept

The development of strength and stiffness of hardening cement-based materials must be attributed to the increasing interaction between hydrating particles. It is not surprising, there-

fore, that several authors have stated that it would be most interesting if it were possible to correlate the stiffness and strength to the *number of contact points or the total contact surface area* between hydrating particles. If it were possible indeed to establish such a correlation, one would have obtained a powerful tool for investigating the effect on strength and stiffness of all those parameters, which are assumed to affect the quality and number of contact points and contact surface area, respectively.

In view of mathematical modelling of these particle interactions the following assumptions were made:

- *Homogeneous distribution of the cement particles in the system;*
- *A temperature-dependent ratio* $\nu(T)$ *between the volumes of the reaction products and the reactant (with* $\nu_{T=20°C}=2.2$*);*
- *No differentiation between density of inner and outer product;*
- *Particles belonging to the same fraction react at the same rate.*

Based on these assumptions an algorithm has been developed with which the outward growth of hydrating particles can be determined. In this algorithm the effect of embedding small cement particles, partly or wholly hydrated, in the outer shell of expanding larger particles is taken into account (Fig. 11.1a).

The *volume of (partly hydrated) cement embedded* in the outer shell of expanding particles is expected to be a measure of the intensity with which expanding particles merge with each other and hence of the development of strength.

Another parameter that was expected to exhibit a correlation with the mechanical properties is the *embedded centre-plane area*. This quantity is defined as the total centre-plane areas of embedded cement particles (see Fig. 11.1b). Particularly those embedded particles with a radius exceeding the thickness of the outer shell of the particle in which they are embedded are assumed to contribute to the development of the strength.

11.4 Kinetics of Particle Growth and Formation of Microstructure

Most of the kinetic models currently in use for the description of the hydration process do not explicitly allow for the effect of formation of microstructure on the rate of hydration. As indicated in the preceding Section the interaction between hydrating particles can be computed, provided that some rigorous assumptions are made. The way in which the effect of structure formation on the rate of hydration is allowed for in the model will be outlined in the following. Two stages will be distinguished, viz. a first stage in which *boundary reactions*, and a second stage in which *diffusion processes* are rate controlling, respectively.

Boundary reaction

Initially, when the product layer which surrounds the hydrating particles is still very thin and the interaction between hydrating particles quite weak, the reaction is assumed to be a pure phase-boundary reaction. In this stage the *rate of penetration* $\Delta\delta_{in;x}/\Delta t$ of the reaction

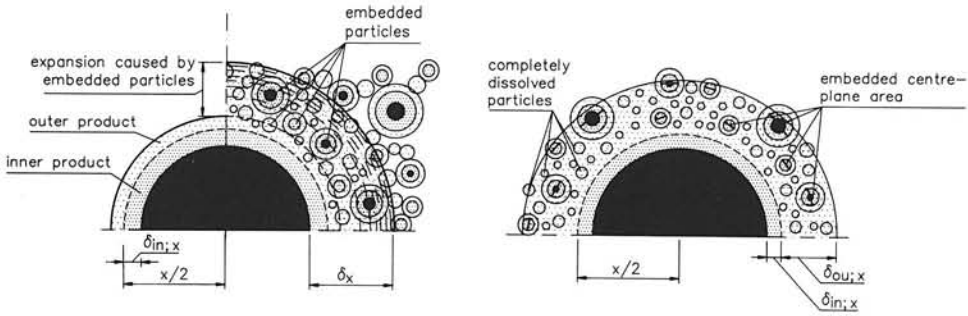

a. Embedding mechanism

b. Embedded centre-plane area

Fig. 11.1 Embedding of particles in outer shell of hydrating particles (a) and embedded centre-plane area (b); schematic.

front in a particle x [μm] during time interval Δt_{j+1} is calculated according to (see also Fig. 11.2):

$$\frac{\Delta\delta_{in;x,j+1}}{\Delta t_{j+1}} = K_0(C_3S) * F_1(\alpha_j, T_j, C_3S) \tag{11.1}$$

where K_0 [μm/h] is denoted the basic rate factor and $F_1(.)$ is a temperature function. Both $K_0(.)$ and $F_1(.)$ depend on the chemical composition of the cement, i.e. of the C_3S content, whereas $F_1(.)$ also depends on the overall degree of hydration $\alpha(t_j)$ and the actual curing temperature $T(t_j)$.

For a particle with diameter x [μm] the degree of hydration can easily be calculated from its penetration depth $\delta_{in;x,j}$. The overall rate and overall degree of hydration of a poly-size cement powder is calculated by adding up the contributions of the individual particle fractions in the time step under consideration.

Diffusion-controlled reaction

When the product layer around an individual particle x has reached the so-called *transition thickness* δ_{tr}, the boundary reaction changes into a diffusion-controlled reaction (see Fig. 11.2). The moment at which the transition thickness is reached depends on the particle size and the amount of cement embedded in the outer shell of hydrating particles. For a poly-size specimen the change from a boundary reaction into a diffusion controlled reaction will, therefore, extend over a certain period. This period roughly coincides with the significant change in the chemical composition of the aqueous phase. For the time being it was considered beyond our ability to decide whether the change of the rate controlling mechanism was the *cause* or just the *result* of the change in the chemical composition of

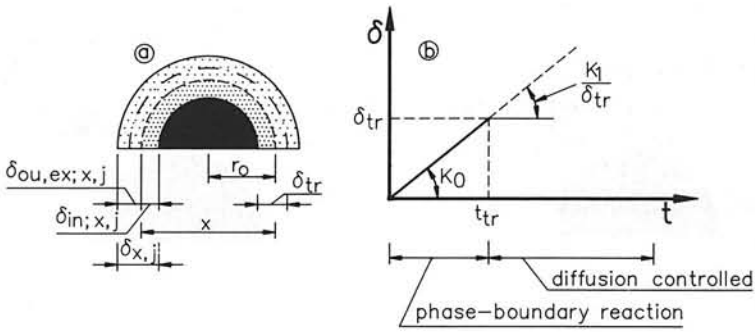

Fig. 11.2 Schematic representation of rate-controlling steps (after Section 6.5.2.2).

the aqueous phase. The coincidence of the two phenomena, however, requires consideration of only one resulting effect, which significantly simplifies mathematical modelling (see Section 11.5.3).

In the diffusion-controlled stage of the reaction the rate of penetration is assumed to be inversely proportional with the β_1-power of the total thickness $\delta_{x,j}$ [μm] of the product layer which surrounds the anhydrous cement core (Fig. 11.2). In formula form:

$$\frac{\Delta\delta_{in;x,j+1}}{\Delta t_{j+1}} = K_1(.) * F_1(.) * \delta_{x,j}^{-\beta_1} \qquad (\delta_x > \delta_{tr}) \qquad (11.2)$$

The rate factor K_1 [μm²/h] is determined so as to assure equal rates of penetration of the boundary and the diffusion-controlled reactions just prior to and after passing the transition point. At the transition point it should hold that (see eq. (11.1) and (11.2)):

$$K_1(.) = K_0(.) * \delta_{tr}^{\beta_1} \qquad (11.3)$$

Expression (11.3) inserted in (11.2) yields:

$$\frac{\Delta\delta_{in;x,j+1}}{\Delta t_{j+1}} = K_0(.) * F_1(.) * [(\frac{\delta_{tr}}{\delta_{x,j}})^{\beta_1}]^{\lambda} \qquad (11.4)$$

in which λ is an integer with the value 0 in the case of a phase-boundary reaction and 1 when the reaction becomes diffusion-controlled, i.e. when $\delta_{x,j} > \delta_{tr}$. The so-called *independent model parameters*, i.e. the basic rate factor K_0, the transition thickness δ_{tr} and the power β_1, have to be determined from suitable experimental data.

11.5 Factors Affecting the Rate of Hydration

The overall rate of hydration depends on the chemical composition and the particle size distribution of the cement, the initial w/c ratio, the curing temperature and curing conditions (with the extremes "saturated" and "sealed"). How these parameters are allowed for at particle level, i.e. the level at which the rate formula (11.4) operates, is roughly outlined in the following Sections.

11.5.1 Chemical Aspects

In order to allow for the particular hydration features and hydration rates of individual phases of Portland cement several authors have proposed the so-called *"Independent Hydration Concept"*. In this concept the compounds are assumed to hydrate separately. The overall degree of hydration of a poly-mineral cement is obtained by adding up the contributions of constituent phases.

In contrast with the independent hydration concept others have launched the *"Equal Fractional Rates Concept"*. This concept presupposes that constituent phases all hydrate at the same rate throughout the hydration process. This concept allows mathematical models to be based on the concentric inward growth of the reaction front in poly-mineral particles.

Actually both these concepts are simplifications of reality. In essence they exclude each other. In this study no attempt has been undertaken to reconcile these two concepts satisfactorily from the materials science point of view. For the development of HYMOSTRUC a more practice-oriented solution has been developed whereby the effect of the chemical composition of the cement on the rate of hydration was modelled by assuming, firstly, a *concentric inward growth of the reaction front* (as in the Independent Hydration Concept) and, secondly, that the *rate of penetration of the reaction front* depends on the chemical composition of the cement. Hence, the rate of penetration of the reaction front in a poly-mineral particle is determined as a *weighted average*, of which the absolute value is expected to depend on the chemical composition of the cement. The correlation between the rate of penetration and the chemical composition of the cement, i.e. the C_3S content of the cement, is dealt with in Section 11.6.

11.5.2 Particle Size Distribution

For the cumulative particle size distribution of the cement the Rosin-Rammler distribution has been adopted:

$$G(x) = 1 - e^{-bx^n} \tag{11.5}$$

in which the constants b (b>0) and n were determined so as to assure that $G(x \rightarrow \infty)=1$ g. The mass per fraction W(x) is found by differentiating G(x) with respect to x. The cen-

tre-to-centre distance of particles belonging to fraction W(x) is calculated by dividing the "reduced" paste volume, being the total paste volume minus the volume of all particles larger than x μm by the number of particles N_x in fraction W(x). From the thus generated spatial distribution of the particles it is relatively easy to calculate the amount of cement in the direct vicinity of the surface of either a cement or an aggregate particle.

11.5.3 Effect of Water/Cement Ratio and State of Water

In HYMOSTRUC three factors are defined which either directly or indirectly allow for the effects of both the initial w/c ratio and the state of water in the pore system on the rate of hydration. One of these factors, viz. $\Omega_1(x,\alpha_x)$, allows for a so-called *water withdrawal mechanism*. This mechanism is operative at the particle level. The value of the $\Omega_1(.)$ factor will, therefore, depend on both the particle size and the degree of hydration of the particle considered. The two other factors, viz. $\Omega_2(\alpha)$ and $\Omega_3(\alpha)$, refer to the overall state of water in the pore system. Insertion of these three factors in the rate formula (11.4) yields:

$$\frac{\Delta\delta_{in:x,j+1}}{\Delta t_{j+1}} = K_0(.)*\Omega_1(.)*\Omega_2(.)*\Omega_3(.)*F_1(\alpha,T,C_3S)*[(\frac{\delta_{tr}}{\delta_{x,j}})^{\beta_1}]^{\lambda} \qquad (11.4a)$$

Water Withdrawal Mechanism. Reduction Factor $\Omega_1(x,\alpha_x)$

Embedded particles, which are not fully hydrated and thus still require water for further hydration, will withdraw water from the so-called central particle (see Fig. 11.3). Consequently, the rate of hydration of this central particle will decrease. The amount of water used up for hydration of the embedded particles in a certain increment of time depends on the total amount of embedded cement and the increase of the degree of hydration of the embedded particles per increment of time.

The partition between the amounts of water available for hydration of the embedded cement and the central particle is determined iteratively. At low initial w/c ratios the amount of embedded cement can be so high, that all the water is used up for further hydration of the embedded cement. In that case hydration of the central particle x ceases completely ($\Omega_1(x,\alpha_x)=0$) until the rate of hydration of the embedded cement is so low so as to permit water ions to pass through the product layer again to the anhydrous core of the central particle.

Water Distribution in the Pore System. Reduction Factor $\Omega_2(\alpha)$

In the case of sealed curing conditions, the hydration process is accompanied by the gradual emptying of pores, starting with the larger ones. The local absence of water in the pore system is assumed to retard overall hydration since ions involved in the reaction process have to travel over longer distances to reach particles located adjacent to the wall of empty pores.

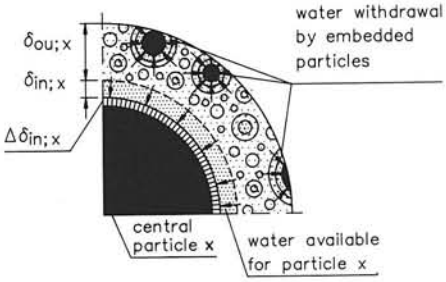

Fig. 11.3 Water withdrawal mechanism: Reduction factor $\Omega_1(x,\alpha_x)$.

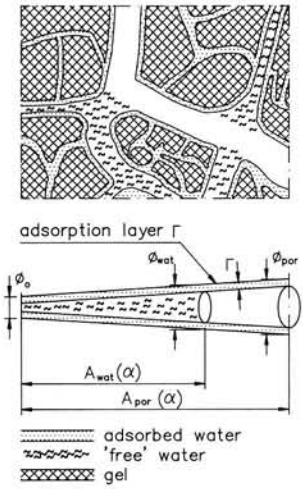

Fig. 11.4 Water distribution effects. Reduction factor: $\Omega_2(\alpha)=A_{wat}(\alpha)/A_{por}(\alpha)$.

In HYMOSTRUC the effect of local absence of water is accounted for with a reduction factor $\Omega_2(\alpha)$, being the quotient of the pore wall area $A_{wat}(\alpha)$ that is in direct contact with capillary pore water and the total pore wall area $A_{por}(\alpha)$ (Fig. 11.4).

$$\Omega_2(\alpha) = \frac{A_{wat}(\alpha)}{A_{por}(\alpha)} \tag{11.6}$$

Both $A_{wat}(\alpha)$ and $A_{por}(\alpha)$ are functions of the initial w/c ratio and also depend on the momentary values of the overall degree of hydration. Only for low w/c ratios and hydration stages close to the ultimate degree of hydration the reduction factor $\Omega_2(\alpha)$ was found to have a significant impact on the rate of reaction.

Availability of Pore Water. Reduction Factor $\Omega_3(\alpha)$

When a certain amount of cement is dissolved, a corresponding number of ions will be given off in the aqueous phase. In the case where the ion concentration remains constant there should be a balance between the rate at which ions are given off and at which they are used for the formation of reaction products. In case the ion concentration in the pore water remains constant *in spite of* a gradual decrease of the amount of water, a decrease of the rate at which the cement is dissolved and ions are given off has been presumed. This decrease might be even more pronounced if the ion concentration, i.e. the Ca^{++} concentration, in the pore water decreases as well, which is actually the case. The development of increasingly large interparticle contact surfaces and an associated decrease of the surface

area of the reactant accessible for the water must be considered as another and simultaneously operative phenomenon which will also cause a decrease the overall rate of hydration.

In HYMOSTRUC the foregoing phenomena are accounted for by a reduction factor $\Omega_3(\alpha)$. This factor depends on the initial w/c ratio ω_0 and the overall degree of hydration α according to:

$$\Omega_3(\alpha) = \frac{\omega_0 - 0.4\ \alpha}{\omega_0} \qquad (\text{for } 0.4\ \alpha<\omega_0) \tag{11.7}$$

The assumption of a constant ion concentration in the pore water is valid only in the early stage of the hydration process (say up to 70 hours for a system with $\omega_0 \approx 0.4$). As explained in Section 11.4, changes in the chemical composition of the pore water appear to coincide with the change from a boundary reaction to a diffusion-controlled reaction. The coincidence of these two phenomena considerably complicates reliable modelling of them. For the time being, HYMOSTRUC operates, therefore, without explicit allowance for changes in the pore water composition. Possible effects of such changes, however, are assumed to be implicitly reflected in the experimentally determined values of the transition thickness δ_{tr} and the coefficient β_1.

11.5.4 Temperature Effects

The curing temperature affects the rate of reaction in two different ways. Firstly one has to consider an increase of the rate of reaction at elevated temperatures. This effect is accounted for using a temperature function $F_1(.)$. A second effect refers to temperature related-changes in both the morphology of the reaction products and the pore structure. These changes are also assumed to affect the rate of reaction. This effect is accounted for by considering a temperature-dependent ν-factor, i.e. the factor that indicates the ratio between the volume of the reaction products and the reactant.

Allowance for these two temperature effects has resulted in a final equation for the basic rate (11.8):

$$\frac{\Delta\delta_{in;x,j+1}}{\Delta t_{j+1}} = K_0(.)*\Omega_1(.)*\Omega_2(.)*\Omega_3(.)*F_1(.) * \left[\left(\frac{\nu(\bar{T})}{\nu_{tr}(\bar{T})}\right)^{\beta_2} * \left\{ \left(\frac{\nu(\bar{T})}{\nu_{20}}\right)^{\beta_2} * \frac{\delta_{tr;20}}{\delta_{x,j}} \right\}^{\beta_1} \right]^{\lambda} \tag{11.8}$$

The temperature function $F_1(.)$, the temperature dependent-quantities $\nu(.)$ and $\nu_{tr}(.)$ as well as the quantity $\bar{T}$ and the coefficient β_2 will be discussed briefly in the following. For a comprehensive explanation of the term in brackets, reference should be made to the derivations in Chapter 6.

Effect of Temperature on Rate of Reaction $F_1(T,\alpha,C_3S)$

The temperature dependency of the reaction rate is accounted for using the temperature function $F_1(T_j,\alpha_j,C_3S)$ (in short: $F_1(T,\alpha,C_3S)$ or $F_1(.)$) viz.:

$$F_1(T,\alpha,C_3S) = A * e^{-\frac{AE(T,\alpha,C_3S).10^3}{R.(273+T)}} \tag{11.9}$$

where A is a constant and $AE(T,\alpha,C_3S)$ [kJ/mol] the apparent activation energy which is a function of the reaction temperature, the degree of hydration and the chemical composition of the cement, i.e. the C_3S content. R [J/mol] is the gas constant and T [°C] the actual curing temperature. From an evaluation of experimental data the following expression for the apparent activation energy was obtained:

$$AE(T,\alpha,C_3S) = p_0 * \alpha * e^{-[m*(C_3S)^n + 0.025*T^{1.5}]} + 0.33*(C_3S\%) + 30 \tag{11.10}$$

with p_0=76 kJ/mol and m and n experimentally obtained coefficients, viz. m=2.5 10^{-11} and n=6.15.

Morphology and Structure Related Temperature Effects

From the observation that curing at elevated temperatures causes a coarsening of the capillary pore structure it was concluded, that the ratio ν between the volume of the reaction products and the reactant decreases with increasing temperature. The decrease of this ratio is compatible with an increase in the density of the product layer. The effect of this densification on the rate of reaction is two-fold. Firstly, densification implies *less expansion of the product layer* and thus a *thinner diffusion barrier* and a *lower diffusion resistance* and, consequently, an *increase* in the rate of reaction. Secondly, a *denser* product only *increases* the diffusion resistance and thus causes a *decrease* in the rate of reaction.

In HYMOSTRUC the temperature-induced morphological and structural changes of the reaction products are accounted for by a temperature-dependent ν-factor:

$$\nu(\bar{T}) = 2.2 * e^{-28\ 10^{-6}\bar{T}^2} \tag{11.11}$$

in which $\bar{T}$ is the mean temperature in the hydration domain. For the mean temperature $\bar{T}(t_j)$, reached at time t_j when the overall degree of hydration is α_j it holds that:

$$\bar{T}(t_j) = \frac{1}{\alpha_j} \int_0^{\alpha_j} T(\alpha)\ d\alpha \tag{11.12}$$

Densification of the product layer is assumed to affect, i.e. to reduce, the transition thickness δ_{tr} at which the reaction changes from a phase-boundary reaction to a diffusion-controlled reaction according to:

$$\delta_{tr}(\bar{T}) = \delta_{tr,20} * \left(\frac{\nu(\bar{T})}{\nu_{20}}\right)^{\beta_2} \tag{11.13}$$

where $\delta_{tr,20}$ is the transition thickness if the reaction takes place at 20°C and ν_{20} is the ν-factor for curing at 20°C. The factor β_2 is an empirical constant to be determined from suitable experimental data (fourth independent model parameter).

The ratio between the volume of the reaction products and of the reactant at the exact moment when the temperature dependent transition thickness $\delta_{tr}(\bar{T})$ is reached is denoted as $\nu_{tr}(\bar{T})$.

11.6 HYMOSTRUC. Independent Model Parameters

11.6.1 General

With the basic rate formula (11.8) HYMOSTRUC calculates the rate of penetration, the penetration depth and the degree of hydration of individual cement particles. By adding up the amounts of hydrated cement in each particle fraction the overall degree of hydration is obtained. In this calculation procedure the effects of temperature, the w/c ratio and the particle size distribution on the overall rate of hydration are explicitly accounted for. The effect of the chemical composition of the cement on the rate of penetration is allowed for by four *independent model parameters* K_0, δ_{tr}, β_1 and β_2, to be discussed briefly in the following section.

11.6.2 Values of Independent Model Parameters

For the determination of the independent model parameters K_0, δ_{tr}, β_1 and β_2, over 60 hydration tests were analyzed, comprising 27 different Portland cements with C_3S contents varying from 15% to 75%, w/c ratios from 0.157 to 0.8, Blaine finesses from 200 to 550 m^2/kg (n-values of the R-R distribution from 0.73 to 3.14), and curing temperatures from 4.4°C to above 50°C (isothermal, adiabatic and partly adiabatic/partly isothermal).

The basic rate factor K_0 turned out to correlate directly with the C_3S content of the cement (Table 11.1, eq. (11.14)). Values ranged between 0.02 and 0.06 μm/h with a standard deviation $s(K_0)$=0.008 μm/h. For the transition thickness δ_{tr} only a slight correlation with the C_2S content could be established (eq. (11.15)).

The coefficient β_1 varied between 1 to 2, whereas for β_2 a value of 2 turned out to hold satisfactorily. Any correlation between the values of both β_1 and β_2 and the chemical composition of the cement was not found. Results are summarized in Table 11.1.

Table 11.1 Independent model parameters. Guide / Default Values

Basic rate factor K_0			
Mean value:	$K_0 = 0.02 + 6.6\ 10^{-6}\ [C_3S\%]^2$	[μm/h]	(11.14)
Standard deviation:	$s(K_0) = 0.008$ [μm/h]		
Transition Thickness δ_{tr}			
Type of cement	C_2S [%]	Transition thickness δ_{tr} [μm]	
Low heat cement	45 - 60	2 - 4	
Ordinary Portland cement	20 - 30	2 - 6	
Rapid hardening cement	5 - 20	3 - 6	
Average		2.5 - 4.0	
Mean values *(default)*:	$\delta_{tr} = -0.02 * [C_2S\%] + 4$	[μm]	(11.15)
Coefficient β_1	1 - 2	*(default = 2)*	
Coefficient β_2	2	*(default = 2)*	

11.7 Applications

11.7.1 Strength Development

A distinct correlation was found between the degree of hydration and the volume of the embedded cement (Fig. 11.5). Also the embedded centre-plane area turned out to exhibit a good correlation with the degree of hydration. These observations can be considered valuable against the background of the well-known relationship between the degree of hydration and strength. Calculations revealed that, like the relationship between strength and degree of hydration, the relationship between strength, on the one hand, and embedded cement volume and embedded centre-plane area, on the other, also depends on the w/c ratio, albeit that the effect of the w/c ratio on the latter relationships was found to be less pronounced. Moreover, the effect of temperature on the amount of embedded cement was found to be compatible with the effect of temperature on strength.

The established correlation between strength and structure formation - structure formation in terms of embedded cement volume and embedded centre-plane area - is considered to be an important step in the development of rational strength concepts.

11.7.2 Fracture Modes in Hardening Cement Pastes

The potential of HYMOSTRUC to calculate the embedded centre-plane area (see Fig. 11.1) allows the numerical substantiation of some of the observations concerning the frac-

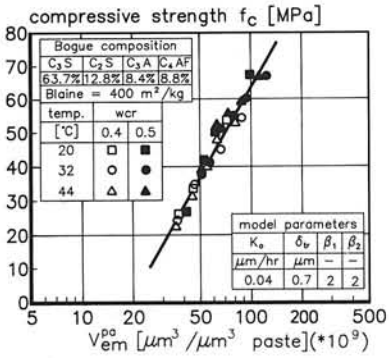

Fig. 11.5 Strength as a function of the calculated embedded cement volume (per volume unit of paste).

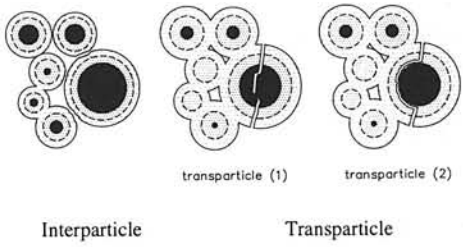

Fig. 11.6 Interparticle and transparticle fracturing (Section 7.4.4).

ture modes in cement pastes. During the hydration process, the fracture mode changes from *interparticle* to *transparticle* (Fig. 11.6). The degree of hydration at which this change in fracture mode occurs significantly depends on the w/c ratio. For ω_0=0.4 this change would take place at a degree of hydration between α=0.4 and α=0.6. Using HYMOSTRUC it can be shown quantitatively that for values of the degrees of hydration of this order of magnitude the embedded centre-plane area of some particles is so high that transparticle fracturing is likely to occur. The fact that HYMOSTRUC is able to generate quantitative information concerning the fracture mode in hardening pastes leads us to believe that the model can be applied for simulating and investigating the stereological aspects of early structure formation and strength development.

11.7.3 Interface Phenomena. Porosity

Since HYMOSTRUC allows explicitly for stereological features the model can be applied for the analysis of the effect of the spatial distribution of cement particles at aggregate surfaces on the interface characteristics. Calculations revealed that both the thickness of the matrix-aggregate interface zone, as well as trends in the development of both the degree of hydration and porosity in this zone, could be predicted reliably in so far as the stereological aspect is concerned (Fig. 11.7). This result prompts the idea to apply HYMOSTRUC for further analysis of interface phenomena, i.e. for generating ideas to modify material properties by changing the particle size distribution in the interfacial zone, for example by adding fines like fly ash or extra fines like silica fume, and for optimization purposes.

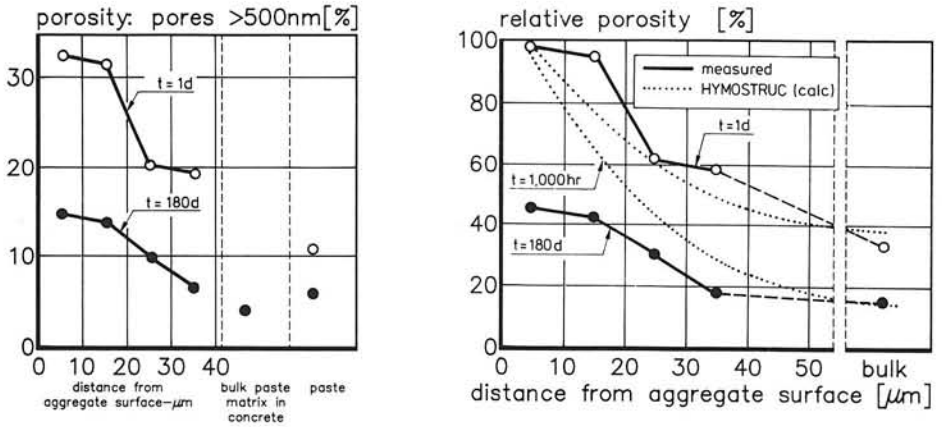

Fig. 11.7 Calculated versus measured porosity in matrix-aggregate interfacial zone (Chapter 7. Measurements of Scriverer [527]).

11.7.4 Temperature Predictions in Concrete Structures

HYMOSTRUC enables the generation of adiabatic input curves for computer programs currently in use for the determination of temperature fields in actual concrete structures (macro-level calculations). These temperature calculations are part of more comprehensive analyses of thermal stresses and of the probability of early-age thermal cracking.

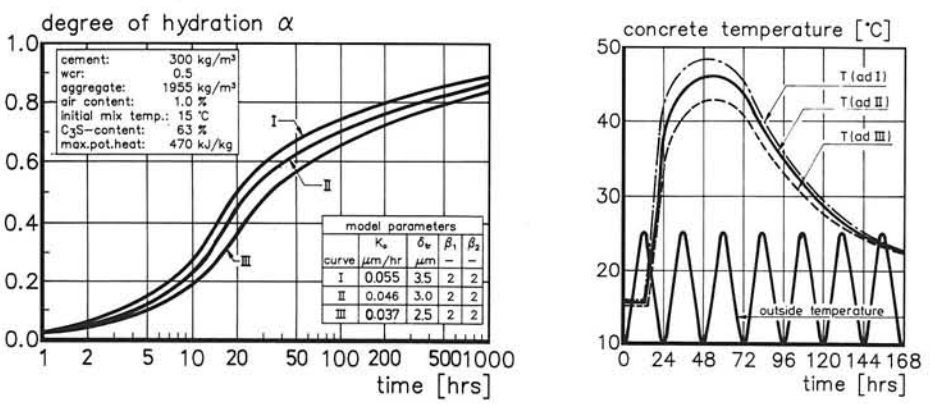

a. Hydration curves

b. Temperature fields

Fig. 11.8 Calculated adiabatic hydration curves *(a)* illustrating the effect of scatter in the independent model parameters on the shape of the curves and temperature fields *(b)* in a hardening concrete wall for different input curves.

Examples of predicted adiabatic input curves and temperature calculations in hardening concrete walls carried out on the basis of these input curves are given in Fig. 11.8a and Fig. 11.8b. Mix data is given in the insert of Fig. 11.8a. The adiabatic input curves were determined for three K_0-values, viz. the mean value according eq. (11.14) for a C_3S content of 63% as well as for the 16% lower limit and the 84% upper limit. These values correspond to the mean value decreased and increased by a standard deviation of, conservatively, $s(K_0)$=0.009 μm/h. Transition thicknesses were chosen so as to simulate - for the cement composition considered -, a rapid, a moderate and slower cement. Fig. 11.8b shows the temperatures in the core of a 1 meter thick concrete wall. Temperature calculations were carried out using TEMPSPAN, a computer program which calculates the progress of the hydration process and the associated temperatures in hardening concrete structures for a given adiabatic input curve. It appears that the consequences of the relatively large scatter in the values of the independent parameters K_0 and δ_{tr} results in maximum temperatures from 43°C for the slow cement to 48°C for the rapid cement.

11.7.5 Probability of Cracking

In the computer program TEMPSPAN the development of strength and early-age thermal stresses can be expressed as a function of time. Strength and stresses being known, the theoretical probability of cracking can be determined, provided that both the distribution functions and standard deviations of the strength and stresses are known. Results of calculations on the probability of cracking are shown in Fig. 11.9. The calculations refer to a 0.5 m and a 1.0 m thick concrete wall and have been carried out for the three adiabatic input curves presented in Fig. 11.8a. Fig. 11.9 shows that the effect of the wall thickness

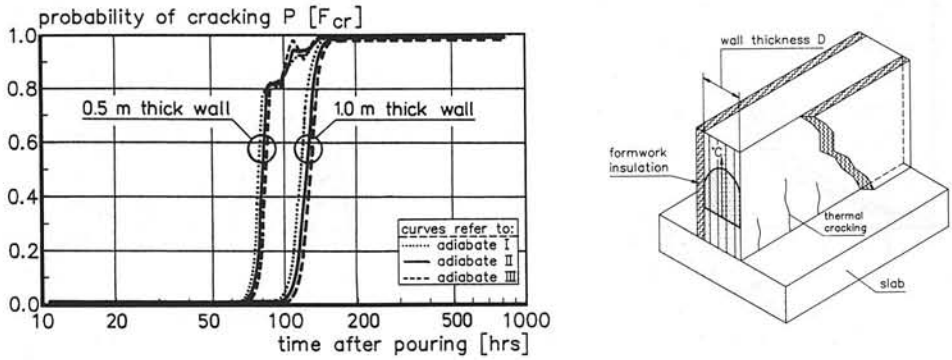

Fig. 11.9 Example of predicted probability of thermal cracking in two hardening concrete walls for the input curves of Fig. 11.8a.

on the risk of cracking dominates the effect of uncertainties in the input curves, i.e. in the scatter in the independent model parameters with which the adiabatic input curves had been calculated.

From a parametric sensitivity study it can be further concluded that the effect of un-certainties in the adiabatic input curves on the calculated probability of cracking are *less significant* than the effect of uncertainties in the modelling of early-age rheological behaviour, i.e. early-age plastic deformations and early-age relaxation. This result greatly enhances the applicability of HYMOSTRUC for executing sensitivity studies concerning the effect of changes in either the mix composition or pouring sequences, insulating schemes, cooling or heating of the concrete and time of formwork removal.

11.8 Reliability Considerations

As explained, HYMOSTRUC operates using four independent model parameters, viz. K_0, δ_{tr}, β_1 and β_2. In particular the basic rate parameter K_0 appears to be distinctly correlated with the chemical composition of the cement, i.e. the C_3S content. A standard deviation $s(K_0)$=0.008 μm/h has been determined for cements with a C_3S content ranging from 5 to 95%, approximately the range from belite to alite. About 50% of this standard deviation can be related to variations, i.e. uncertainties, in the C_3S content. The remaining part of the scatter in K_0-values as expressed in the standard deviation $s(K_0)$ must be attributed to the effect of minor constituents and gypsum (which effects have not been accounted for explicitly in HYMOSTRUC).

The curing conditions appear to affect both the K_0 and the δ_{tr}-values. Curing under saturated conditions resulted in relatively high K_0 and δ_{tr}-values in comparison with samples cured under sealed conditions. This can easily be understood since the access of water in the case of saturated curing will affect the factors $\Omega_2(\alpha)$ and $\Omega_3(\alpha)$ in the sense that their values will remain high or even close to 1. Since in the present version of HYMOSTRUC the effect of access of water on the values the $\Omega_2(\alpha)$ and $\Omega_3(\alpha)$ is not explicitly catered for, this effect is reflected in higher values of K_0 and δ_{tr}, i.e. a lower value of β_1.

With respect to the scatter in the δ_{tr}-values the possibility of a too rigorous modelling of the effect of the embedding mechanism on the rate of hydration must also be considered. The assumption of a constant density and a constant porosity of the gel products throughout the hydration process is another factor that requires critical appraisal when searching for explanations of this scatter.

The coefficient β_1 turned out to vary between 1 and 2, higher values generally occurred in later stages of the hydration process. The tendency of β_1 values to increase in later stages points to a reduction in the rate of hydration, probably due to increasing importance of merging of particles as the hydration process progresses. In this respect, the expansion mechanism operative in hydrating particles as outlined in Section 6.4.2 should be referred to. There it was stated that in the algorithm developed for the determination of the amount of embedded cement in the outer shell of a particle x in an arbitrary time step Δt, the value of the geometrical ratio of the series with which the embedding mechanism is described is assumed to be a constant throughout the iterative calculation procedure. In essence,

however, the geometrical ratio should be adjusted, i.e. increased, in each subsequent iteration step and not only when the following time step is considered. This simplification implies that *in so far* as the effect of embedding small cement particles in the outer shell of larger particles on the rate of hydration of individual particles has been modelled explicitly, one has to expect that in reality this effect will be greater than predicted with the present version of HYMOSTRUC. It is to be expected that allowance for a gradual increase of the value of the this geometrical ratio in the series will contribute to a reduction of the scatter in the values of the transition thickness.

As stated in Section 11.6.2 already, no distinct correlation could be established between the chemical composition of the cement and the two coefficients β_1 and β_2. The theoretical hydration curves generated with HYMOSTRUC even appeared to be almost independent of β_2. In so far variations in the values of the two β-coefficients exist, these variations revealed not to affect the observed K_0-C_3S and δ_{tr}-C_2S relationships significantly. This enhances the transparency and consistency of the model in the sense, that in the iterative procedures for the determination of the model parameters *one can concentrate on only two independent model parameters*, while - in the majority of cases - for β_1 and β_2 default values of 2 can be adopted.

With regard to the question of whether the scatter in the independent model parameters jeopardizes the reliability of the model, one should realize that the shape of the hydration curves does not merely depend on the values of the independent model parameters, but above all on the particle size distribution, the w/c ratio and the curing temperature of the cement. In the examples presented in Chapter 8, it has been shown that HYMOSTRUC predicts the effect of these parameters on the shape of hydration curves quite reliably. This can be considered as a strong argument in favour of the statement that the values of the independent model parameters are virtually independent of the w/c ratio, the particle size distribution and the reaction temperature.

The reliability of HYMOSTRUC should further be judged against the background of the particular aims for which the model has been developed. These main aims were, firstly, to provide the designer with a numerical tool for generating adiabatic input curves for macro-level models which can be utilized for investigating temperature fields and the probability of thermal cracking in actual concrete structures, and, secondly, to model the development of microstructure and the effect of structure development on the rate of hydration explicitly. As to the first-mentioned aim, reference should be made to Figs. 11.8a and Fig. 11.9, where it was shown that the consequences of scatter in the independent model parameters on both predicted temperature fields and the theoretical probability of cracking are relatively small and certainly acceptable for interpretations for practical purposes. With respect to the second aim, note that reliability considerations should concentrate on the consistency of the model rather than on comparison of quantitative data. The reason for this is, simply, that there is no adequate experimental data available concerning, for example, the volume of embedded cement and water withdrawal mechanisms. In so far as comparisons with experimental data are possible, these comparisons should refer to the investigated correlation between strength and the amount of embedded cement and the embedded centre-plane areas and to fracture mode analysis. The results obtained so far on these points do not give rise to doubt the basic ideas on which HYMOSTRUC is based.

11.9 Working with HYMOSTRUC

HYMOSTRUC allows the determination of the chemistry-related independent model parameters K_0, δ_{tr}, β_1 and β_2. For Portland cement-based materials guide values for these parameters are given in this report. The guide values have been inserted in HYMOSTRUC as default (Table 11.1) values, which can be used for either pure prediction purposes or for first attempts to fit new experimental data. In the latter case, when a first attempt does not yield a satisfactory fit, the parameter values have to be adjusted. Based on experience with over ninety test results it can be stated that three attempts are generally sufficient to achieve a satisfactory fit.

An operator can also take the guide values from an Info-menu. In this Info-menu the effect of variations in the parameter values are explained graphically, which significantly simplifies, i.e. shortens, the procedure for establishing the correct parameter values.

For cements other than Portland cement, for example a blast-furnace or a fly-ash cement, no guide values have been established yet. Nevertheless no more than three or four attempts will generally suffice for obtaining a good fit of experimental data.

Once the independent model parameters are known for the cement considered, HYMOSTRUC can be used for investigating the effect of variations in the particle size distribution of the cement, the w/c ratio and the curing temperature as well as variations in the concrete mix composition, on the shape of the hydration curves.

The time required for one simulation run depends on the width of the particle size distribution of the cement. For the "standard PC" in the late eighties *(AT + co-processor)*, the computation time ranged from 5 minutes for a fine cement to over 15 minutes for a coarse cement. With the currently used PC's with pentium processor the computation time is less than one minute.

HYMOSTRUC should preferably be used in combination with programs for macro-level calculations as it generates the input curves for these programs. As explained in the Chapters 7 and 8, HYMOSTRUC also generates interesting information for research on microstructural aspects, for example about the microstructure of the matrix-aggregate interfacial zone, the formation of interparticle contact areas and fracture modes.

The commercial versions of HYMOSTRUC (release 2.0, 2.1 and 3.1) are written in PASCAL (version 6.0). Research versions of HYMOSTRUC are in C. The commercial HYMOSTRUC 3.1 release runs under WINDOWS 95.

SUMMARY

In this thesis the potential for the use of computers for the simulation of the processes and mechanisms occurring in hardening cement-based materials is outlined. The major aim was

> "... to make well-established research results and experimental data in the various fields of study, such as *cement chemistry*, *physics* and *stereology*, accessible and operational for practical engineering purposes, viz. for the *prediction of adiabatic (and isothermal) hydration curves*. These curves form an essential part of the input for computer programs used for macro-level analyses of hardening concrete structures".

The multi-disciplinary character of the subject is outlined in Part I of this thesis, where granular, physico-chemical, stereological and kinetic aspects of hydration and structural formation are discussed and evaluated. Due attention has been given to accuracy considerations and to the relevance of interactions between individual processes and mechanisms insofar as they might be of importance for mathematical modelling. It was concluded that none of the models for hydration processes in cement-based materials proposed so far accounted for the simultaneous formation of microstructure and the effect this might have on the rate of hydration. A second important fact in view of mathematical modelling was that the slope of hydration curves turned out to be significantly influenced by the particle size distribution of the cement. With regard to the chemistry-related aspect of the hydration process, it had to be concluded that the important questions as to whether hydration of individual compounds of a poly-mineral cement proceeds independently or at equal fractional rates and whether hydration products are formed topochemically or through solution have not yet been answered satisfactorily.

The main features of a computer-based simulation model, called HYMOSTRUC (the acronym for HYdration, MOrphology and STRUCture development), are outlined in Part II of this thesis. The effects of the particle size distribution, the state of water and the reaction temperature on the rate of hydration are modelled explicitly. Based on a homogeneous distribution of the cement particles in the cement-water system and assuming a constant, albeit temperature dependent, ratio between the volume of the reaction products and the anhydrous cement, an algorithm was developed with which the amount of cement involved in the formation of interparticle contacts can be determined. The effect of the formation of interparticle contacts on the rate of hydration of the particles involved in the interaction process has been modelled explicitly.

The rate at which a concentric reaction front penetrates into a hydrating cement grain is described using a Basic Rate Equation. This rate equation comprises, besides factors which allow for the previously mentioned effects of the state of water, the formation of interparticle contacts and reaction temperature, four *independent model parameters*. One of these parameters, the Basic Rate Factor K_0 [μm/h], describes the *initial* rate at which a concentric reaction front penetrates into a particular cement grain. The second model parameter has been denoted the Transition Thickness δ_{tr} [μm], viz. the thickness of the product layer

at which the reaction changes from a boundary reaction into a diffusion controlled reaction. The second two independent model parameters also occur in the diffusion controlled stage. One of these factors, β_1, determines the development (linear, parabolic, cubic) of the diffusion controlled process at the particle level. The second one, β_2, refers to the effect of temperature-induced morphological changes of the reaction products on the rate of penetration.

These four model parameters have been determined in an extensive evaluation program, in which more than 60 hydration tests comprising 27 different cements were involved. In this evaluation program a distinct correlation was established between the basic rate factor K_0 and the C_3S content of the cement. The transition thickness δ_{tr} turned out to be weakly correlated with the C_2S content. No correlation could be established between the values of the coefficients β_1 and β_2 and the chemical composition of the cement. For the range in which the values of these two coefficients varied, they hardly affected the correlation between the K_0- and δ_{tr}-values and the cement composition, which substantially enhanced the reliability and applicability of the model.

The amount of cement involved in the formation of interparticle contacts was assumed to be a measure of the number of interparticle bonds per unit of paste volume and, as such, a possible strength parameter. A distinct correlation between the amount of cement (per unit volume of paste) involved in the interaction mechanism and the development of strength could also be established, which seems to confirm the validity of the previous assumptions.

Explicit allowance for the stereological aspect enabled investigation into the effect of the packing of particles in the matrix-aggregate interfacial zone on the interface properties. Results of calculated widths of the matrix-aggregate interfacial zones and porosity calculations are presented.

The potential of HYMOSTRUC to predict adiabatic hydration curves as a function of the particle size distribution of the cement, the w/c ratio, the (initial) curing temperature and the chemical composition of the cement (Portland cement), and thus to serve practical engineering purposes, is evaluated in a case study.

The structure and the main features of the simulation program have been presented in a condensed Flow Chart (Section 6.8, pp. 203-206) and in an Extended Summary (Chapter 11).

SAMENVATTING

Bij het verharden van cement-gebonden materialen, zoals cement pasta, mortel en beton, spelen zowel chemische, physische, colloidale als stereologische factoren een rol. Een consistente en tevens voor de ingenieurspraktijk toegankelijke en bruikbare modellering en simulatie van het verhardingsproces, waarbij relevante interacties tussen genoemde factoren op adequate wijze worden gehonoreerd, is vooralsnog niet voorhanden. Het leveren van een bijdrage aan ontwikkelingen op dit gebied is onderwerp van dit proefschrift. Het doel van de studie laat zich als volgt samenvatten:

> "Het met behulp van computersimulaties voor de ingenieurspraktijk toegankelijk en operationeel maken van zo goed als algemeen aanvaarde en goed gedocumenteerde informatie op het terrein van de cementchemie, physica en stereologie, voor zover deze informatie betrekking heeft op processen en mechanismen die verantwoordelijk zijn voor het verharden van cement-gebonden materialen. *Specifiek oogmerk* daarbij is het numeriek kunnen voorspellen van adiabatische (en isotherme) hydratatiekrommen. Deze krommen vormen een essentieel onderdeel van de input voor computerprogramma's, die momenteel op steeds grotere schaal worden ingezet voor het analyseren van het gedrag van beton en betonconstructies tijdens de verharding".

Het multi-disciplinaire karakter van het onderwerp wordt uiteengezet in Deel I van dit proefschrift. Daarin worden granulometrische, chemische, physisch-chemische en stereologische aspecten besproken en geëvalueerd. Bijzondere aandacht wordt daarbij geschonken aan de nauwkeurigheid, waarmee informatie op genoemde terreinen zich laat formuleren en quantificeren. Voorts wordt een overzicht gegeven van tot nu toe gepresenteerde formules en modellen op het gebied van de reactiekinetiek, voor zover deze betrekking hebben op reacties en processen in cement-gebonden materialen. In geen van deze modellen, zo bleek, wordt de interactie tussen de voortgang van het hydratatieproces en de ontwikkeling van de microstructuur van cementsteen expliciet meegenomen. Van grote invloed op de voortgang van het verhardingsproces bleek de korrelverdeling van het cement. Met betrekking tot het chemie-aspect werd geconstateerd dat belangrijke vragen, zoals de vraag of er al dan niet sprake is van een sterke wederzijdse beinvloeding van de snelheid waarmee afzonderlijke cementcomponenten hydrateren en de vraag of reacties topochemisch dan wel via de oplosfase verlopen, nog niet tot volle tevredenheid zijn beantwoord.

In Deel II van dit rapport vindt de synthese plaats van de in Deel I aangereikte informatie. Dit in de vorm van het simulatieprogramma HYMOSTRUC, de acroniem voor HYdratatie, MOrphologie en STRUCtuurvorming. De input voor dit programma bestaat uit:

1. De chemische samenstelling van het cement (vooralsnog beperkt tot Portland cement).
2. De korrelverdeling van het cement.
3. De water/cement factor, c.q. de mengselsamenstelling van de mortel of het beton.
4. De verhardingstemperatuur, i.c. storttemperatuur.

De kern van het simulatieprogramma bestaat uit een algoritme, dat, uitgaande van de

ruimtelijke verdeling van de cementkorrels in de pasta en een constante, zij het temperatuurafhankelijke, verhouding tussen het volume van het gevormde reactieproduct en het cement, in staat stelt om het verloop van het verhardingsproces te simuleren. Daarbij wordt expliciet rekening gehouden met mogelijke effecten van een physieke interactie tussen hydraterende cementkorrels, een zich continu wijzigende waterhuishouding in de pasta en de momentane reactietemperatuur op de voortgang van het verhardingsproces. Het algoritme gaat uit van een concentrish voortschrijden van het reactiefront in individuele cementkorrels. De snelheid waarmee dit reactiefront voortschrijdt wordt stapsgewijs bepaald. Voorts bevat het algoritme *vier modelparameters*. De eerste, de Basic Rate Factor K_0 [μm/uur], bepaalt de beginsnelheid van het penetratiefront in afzonderlijke korrels. De tweede parameter, de Transition Thickness δ_{tr} [μm], staat voor de dikte van de gellaag rond een cementkorrel waarbij de reactie overgaat van een oppervlaktereactie in een diffusie-gecontroleerde reactie. De derde factor, β_1, bepaalt de orde van de diffusiereactie, terwijl de vierde factor, β_2, een rol speelt in de beschrijving van het effect van de temperatuurafhankelijkheid van de microstructuur op de diffusieweerstand van de gel.

Onderzocht is of genoemde modelparameters een correlatie vertoonden met de chemische samenstelling van het cement. Daartoe is een analyse uitgevoerd van meer dan 60 hydratatieproeven met 27 verschillende cementsoorten. De Basic Rate Factor K_0 bleek sterk gecorreleerd te zijn aan het C_3S-gehalte van het cement, terwijl een zwakke correlatie tussen de Transition Thickness δ_{tr} en het C_2S-gehalte werd gevonden. Een correlatie tussen de β-coefficienten en de chemische samenstelling van het cement kon niet worden vastgesteld. Variaties in de β-coefficienten bleken *geen* noemenswaardige invloed te hebben op de K_0-C_3S en de δ_{tr}-C_2S relaties!

Op basis van het voorgaande kon de volgende conclusie worden getrokken.

> *"Bij gegeven input betreffende korrelverdeling van het cement, water/cement factor, storttemperatuur en cementsamenstelling, respectievelijk met aan de cementsamenstelling gecorreleerde dummy-waarden voor de modelparameters, zijn betrouwbare voorspellingen van isotherme en adiabatische hydratatiekrommen goed mogelijk (zie met name Par. 8.8)".*

Voorts werd gevonden dat de *hoeveelheid cement* (per volume-eenheid pasta), die direct betrokken is in het interactieproces tussen de cementkorrels en verondersteld werd een maat te zijn voor het aantal contactpunten en contactvlakken tussen de korrels onder-ling, een duidelijke correlatie vertoont met de *sterkte* van de pasta, c.q. mortel.

Het expliciet beschouwen van stereologische aspecten stelt in staat onderzoek te doen naar "wand-effecten", zoals die verondersteld worden op te treden in de matrix-toeslag interface zone. Berekeningen van de dikte van de interface zone en van de porositeit van deze zone vertoonden goede overeenkomst met resultaten van elders uitgevoerd onderzoek.

Een case-study, waarin de praktische toepasbaarheid van HYMOSTRUC wordt toegelicht, een korte discussie, conclusies en aanbevelingen, alsmede een uitgebreide samenvatting betreffende de opbouw en de belangrijkste karakteristieken van het simulatieprogramma, zijn samengebracht in Deel III van dit proefschrift en sluiten dit rapport af.

REFERENCES

Abreviations of journals, congresses and symposia

ACI(-J)	American Concrete Institute (Journal of -)
ACR	Advances in Concrete Research
ACS	American Ceramic Society
ASTM	American Society of Testing Materials
B&St	Beton- und Stahlbetonbau
BCS	British Ceramic Society
BFT	Beton- und Fertigteiltechnik
CCR	Cement and Concrete Research (Journal)
CEA	Concrete at Early Ages (RILEM Symposium)
CHCPSP	Conference on Hydraulic Cement Paste: Their Structure and Properties
CI	Concrete International (Journal)
DAfSt	Deutscher Ausschuß für Stahlbeton
ENR	Engineering News Record
HRB	Highway Research Board
IC(S)CC	International Congress (Symposium) on the Chemistry of Cements
JACS	Journal of the American Ceramic Society
JCI	Japanese Concrete Institute
JCIS	Journal of Colloidal and Interface Science
M&C	Materiaux et Construction
MCR	Magazine of Concrete Research
MRS	Materials Research Society
PCCRPC	Proceedings of Chemistry and Chemistry-Related Properties of Cement
RMC	Revue des Materiaux de Construction
RMCTP	Revue des Materiaux de Construction et de Travaux Public
SMDDHC	Symposium on Microstructural Development During Hydration of Cement
SP	Special Publication
SR	Special Report
SSPCPC	Symposium on Structure of Portland Cement Paste and Concrete
TIZ	Tonindustrie Zeitung
Z&B	Zement und Beton
ZKG	Zement, Kalk, Gips

Alphabatic list of references

1 Abrams, D., 1918, Mat. Res. Lab. Lewis Inst. Chicago, Bull. No. 1
2 Adams, L.D., 1976, CCR, Vol. 6, pp. 293-308
3 Aitcin, P-C., et al., 1986, SMDDHC, Boston, MRS, Proc. Vol. 85, pp. 261-272
4 Aitcin, P.-C., et al., 1986, CCR, Vol. 16, pp. 671-678
5 Al-Rawi, R.S., 1976, CCR, Vol. 6, No. 5, pp. 603-611
6 Aldridge, L.P., 1980, 7th ICCC, Paris, Vol. III, pp. VI-83-86
7 Aldridge, L.P., 1982, CCR, Vol. 12, No. 3, pp. 381-398
8 Alègre, R., 1961, RMC, 544, p. 1; 546, p. 181; 547, p. 218; 548, p. 247; 549, p. 300
9 Alexander, K.M., 1960, Proc. ACI, Vol. 56, pp. 377. *Ibid. Philleo [445]*
10 Alexander, K.M., et al., 1968, 5th. ICCC, Tokyo, Vol. III, 152
11 Alexander, K.M., 1972, CCR, Vol. 2, No. 6, pp. 663-680
12 Alujevic, V., et al., 1986, CCR, Vol. 16, No. 5, pp. 695-699
13 Anderegg, F.O., et al., 1929, Proc. ASTM, 29. *Ibid. Venaut [600]*
14 Anderegg, F.O., 1934, ZKG, Jhg. 23, No. 8, pp. 99-100
15 Andreasen, A.H.M., 1928, Kolloid Chem. Beihefte, Vol. 27, pp. 349-
16 Anselm, W., 1950, ZKG, Jhg. 3, pp. 267-269

17 Arrhenius, S., 1915, Quantitative Laws in Biological Chemistry, G. Bell & Sons, London
18 ASTM, Philadelphia, 1982, C 186-82. *Ibid. Killoh [293]*
19 Auskern, A.B., et al., 1976, JACS, Vol. 59, No's 1-2, pp. 29-33
20 Avdeejev, *Ibid. [54]*
21 Bajza, A., 1980, 7th ICCC, Paris, Vol. IV, pp. 329-332
22 Ball, M.C., 1983, CCR, Vol. 13, pp. 744-746
23 Balshin, M.Y., *Ibid. Fagerlund [157], Sereda et al. [532]*
24 Bamforth, P.B., Advantages from Temperature Studies, C&C Ass. Train. Centre, THD 7346
25 Barnes, B.D., 1977, ACI-J, December, pp. 612-615
26 Barnes, B.D., et al., 1978, CCR, Vol. 8, pp. 263-
27 Barnes, B.D., et al., 1979, JACS, 62, 21
28 Barnes, B.D., PhD, Perdue, *Ibid. Diamond [137]*
29 Basalla, A., 1962, ZKG, Jhg. 15, No. 3, pp. 136-140. (Disc.: No. 10, 1962, pp. 454-455)
30 Bazant, Z.P., et al., 1982, Creep and Shrinkage in Concrete Structures, J. W&S, 363 p
31 Bažant, Z.P., 1988, CCR, Vol. 18, No. 6, pp. 923-932
32 Beaudoin, J.J., et al., 1971, CCR, Vol. 1, No. 1, pp. 1-12
33 Beke, B., 1958, ZKG, Jhg. 11, No. 12, pp. 529-543
34 Beke, B., 1960, ZKG, Jhg. 13, No. 9, pp. 419-424; No. 11, pp. 520-524 (Disc. Kayser).
35 Beke, B., 1965, ZKG, Jhg. 18, No. 5, pp. 259-264
36 Beke, B., et al., 1967, ZKG, Jhg. 20, No. 6, pp. 267-270
37 Beke, B., 1970, ZKG, Jhg. 23, No. 9, pp. 401-406
38 Bemst, A. van, 1954, 27 Int. Congr. Ind. Chem., Bruss., Ind. Chim. Bel., 20, 67-70
39 Bensted, J., 1981, Advances in Cement Technology, Ed. S.N. Gosh, Perg. Press, pp. 203-264
40 Bentur, A., 1976, CCR, Vol. 6, pp. 583-590
41 Bentur, A., et al., 1979, JACS, Vol. 62, No. 7-8, pp. 362-366
42 Berestneva, Ya.Ya., et al., 1955. *Ibid. [81]*
43 Berger, R.L., et al., 1973, CCR, 3, No. 5, pp. 497-508; 4, No. 3, 1974, pp. 485-487
44 Berger, R.L., et al., 1979, JACS, Vol. 62, pp. 358-362
45 Berhane, C.J., 1983, CCR, Vol. 13, No. 1, pp. 114-118
46 Berlage, A.C.J., 1987, Strength Development of Hardening Concrete, Delft, 186 p., (in Dutch)
47 Bernal, J.D., et al., 1952, MCR, No. 11, pp. 49-
48 Bernhardt, C.J., 1956, RILEM, Symposium Winter Concreting, Sess. B II, Copenhagen
49 Betoniek 6/20, 1984, Weighted Maturity (in Dutch)
50 Bezjak, A., et al., 1980, 7th ICCC, Paris, Vol. II, pp. 111-116
51 Bezjak, A., et al., 1980, CCR, Vol. 10, No. 4, pp. 553-563
52 Bezjak, A., 1983, CCR, Vol. 13, No. 2, pp. 186-196
53 Bezjak, A., 1983, CCR, Vol. 13, No. 3, pp. 305-318
54 Bezjak, A., 1986, CCR, Vol. 16, No. 2, pp. 260-264
55 Bezjak, A., 1986, CCR, Vol. 16, No. 4, pp. 605-609
56 Blaine, R.L., 1943, ASTM-Bull., No. 123, pp. 51-55
57 Blanks, R.F., 1934, ENR, Nov., pp. 648-651
58 Bogue, R.H., 1929, Calc. of Comp. in Portl. Cem., Ind. Eng. Chem., Anal. Ed. 1, 192-7
59 Bogue, R.H., 1952, 3rd. ISCC, London. *Ibid. [81]*
60 Bogue, R.H., 1955, The Chemistry of Portland Cement, 2nd. ed., Reinhold, NY
61 Bombed, J.P., 1974, RMC, No. 687, pp. 117-122
62 Bozhinov, G., et al., 1980, 7th ICCC, Paris, Vol. IV, pp. 783-787
63 Bredero-Lab., 1989, Isoth. and Semi-isothermal Hydration and Strength Tests, Privat Documentation
64 Breitenbucher, R., 1989, Zwangspannung und Rissbildung infolge Hydratationswarme, PhD., Munic
65 Bresson, J., 1979, CERIB-report
66 Breugel, K. van, 1980, Artificial Cooling of Hardening Concrete, Delft, Res. Rep. 5-80-9
67 Breugel, K. van, 1980, Relaxation of Young Concrete, Delft, Research Report
68 Breugel, K. van, 1982, RILEM, Int. Symp. CEA, Paris, Vol. I, pp. 179-185, Vol. II, pp. 103-109
69 Brit. Cem. Ass.. *Ibid. [293]*
70 Brown, O.E., 1962, Cement, Lime and Concrete, CMLGA, pp. 45-104. *Ibid. Aitcin [4]*
71 Brown, P.W., et al., 1984, JACS, Vol. 67, No. 12, pp, 793-799. *Ibid. [581]*
72 Brown, P.W., et al., 1985, CCR, Vol. 15, No. 1, pp. 35-41
73 Brown, P.W., et al., 1986, SMDDHC, Boston, MRS, Proc. Vol. 85, pp. 83-90
74 Brownmiller, L.T., 1943, ACI-J, Vol. 14, No. 3, pp. 193-210

75 Brunauer, S., 1960, 4th ISCC, Washington, Vol. I, pp. 135-165
76 Brunauer, S., et al., 1964, The Chemistry of Cement, Ed. Taylor, Ac. Press, NY
77 Brunauer, S., et al., 1973, CCR, Vol. 3, No. 1, pp. 129-147
78 Brunauer, S., et al., 1973, CCR, Vol. 3, No. 3, pp. 279-293
79 Brunner, et al.. *Ibid. Greenberg and Chang [208], and Kondo [307]*
80 Bucchi, R., 1980, 7th ICCC, Paris, Vol. I, 1/3. *Ibid. Chatterjee, [97]*
81 Budnikov, P.P., et al., 1966, ACI-SP 90, Washington, pp. 431-446
82 Bushnell-Watson, S.M., et al., 1986, CCR, Vol. 16, No. 6, pp. 875-884
83 Byfors, J., 1980, Plain Concrete at Early Ages, Swedish C&C. Res. Inst., Stockholm, 345 p.
84 Byfors, J., 1984, B&St, H. 9, pp. 247-251
85 Capra, F., 1987, The Turning Point, Flamingo / Fontana Paperbacks, p. 516
86 Carino, N.J., 1982, RILEM, Int. Conf. CEA, Paris, Vol I, pp. 123-128..
87 Carino, N.J., et al., 1983, ACI-J, title no. 80-17, pp. 177-182.
88 Carlson, R.W., 1932, ENR, Oct. 20, pp. 461-463
89 Carlson, R.W., 1937, ACI-J, Vol. 34, Nov.-Dec., pp. 89-102
90 Carlson, R.W., 1938, ACI-J, Vol. 34, Ma.-April, pp. 497-515
91 Carter, R.E., 1961, J. Chem. Phys., 34, pp. 2010-2015
92 Catharin, P., 1966, TIZ, No. 12, pp. 554-559
93 Catharin, P., 1978, B&F, 10, pp. 539-544, 12, pp. 729-733, 1979, 1, 59-62
94 Cembureau, 1972, Paris, pp. 12. *Ibid. Killoh, [293]*
95 Cembureau. *Ibid. Killoh, [293]*
96 Chatterij, S., et al., 1971, Indian Concr. J., 45, No. 8, pp. 346-349
97 Chatterjee, A.K., 1981, Advances in Cement Technology, Ed. S.N. Ghosh, Perg. Press, pp. 203-264
98 Chatterji, S., 1976, Proc. CHCPSP, Sheffield, April, pp. 223-226.
99 Chatterji, S., 1980, 7th ICCC, Paris, Vol. III, pp. VI-5 - VI-9
100 Chopra, S.K., 1966, ACI-SP 90, Washington, pp. 9-17
101 Ciach, T.D., et al., 1971, CCR, Vol. 1, No. 1, pp. 13-25
102 Ciach, T.D., et al., 1971, CCR, 1, 2, p 143; p 159; 3, p 257; 4, p 367; 5, p 515
103 Cleemann, J., et al., 1974, ZKG, Jhg. 17, No. 7, pp. 337-343
104 Cleemann, J.O., 1987, ZKG, Jhg. 30, No. 1, pp. 29-33
105 Clover, R.E., 1937, ACI-J, Vol. 34, pp. 105-116
106 Collepardi, M., et al., 1971, JACS, Vol. 54, pp. 419. *Ibid. [413]*
107 Collepardi, M., 1972, CCR, Vol. 2, No. 1, pp. 57-65; Vol. 2, No. 5, pp. 633-636
108 Conjeaud, M., et al., 1980, 7th ICCC, Paris, Vol III, p VII-6 - VII-11
109 Cook, D.J., et al., 1986, SMDDHC, Boston, MRS, Proc. Vol. 85, pp. 201-212.
110 Copeland, L.E., et al., 1956, ACI-J, No. 52-39, February, pp. 633-640
111 Copeland, L.E., 1956, ACI-J, No. 52-55, April, pp 863-874
112 Copeland, L.E., et al., 1960, 4th ICCC, Wash., Vol. I, pp. 429-468, (incl. disc. Taplin)
113 Copeland, L.E., et al., 1962, Disc. on Ref. 4 in 4th ISCC, Wash., pp. 648-655. *Ibid. [315]*
114 Copeland, L.E., et al., 1968, 5th ICCC, Tokyo, Vol. II, pp. 387-421
115 Copeland, L.E., et al., 1971, J. Portl. Cem. Ass. Res. Develop. Lab., 9, 531
116 Courtault, B., et al., 1979, Cim., Betons, Platres, Chaux; No. 717, pp. 87-98. *Ibid. [94]*
117 Crutzeck, M.W., et al., 1987, CCR, Vol. 17, pp. 164-
118 CUR, 1956, Application of Concrete at Low Temperature, Rep. 6, p. 107 (in Dutch)
119 Currell, B.R., et al., 1985, CCR, Vol. 15, pp. 889-900
120 Czernin, W., 1954, ZKG, Jhg. 7, No. 12, pp. 460-464
121 Czernin, W., 1956, ZKG, Jhg. 9, pp. 525-530
122 Czernin, W., 1964, Zementchemie für Bauingenieure (Dutch transl., Amsterdam, 1968, 137 p.)
123 Dagleish, B.J., et al., 1980, CCR, Vol. 10, No. 5, pp. 665-676
124 Daimon, M., et al., 1971, CCR, Vol. 1, No. 4, pp. 391-401
125 Daimon, M., 1980, 7th ICCC, Paris, Vol. II, Theme III-2/1-9
126 Danielsson, U., 1956, RILEM, Symp. Winter Concreting, Sess. B II, Copenhagen
127 Danielsson, U., 1960, 4th. ISCC, Washington, Vol. I, pp. 519-526
128 Davis, R.E., et al., 1933/1934, ACI-J, pp. 413-430, pp. 485-496
129 Day, R.L., et al., 1988, CCR, Vol. 18, No. 1, pp 63-73
130 Deckers, R., et al., 1981, ZKG, No. 11, pp. 573-579
131 Delmas, P., 1976, Rev. M&C, No. 702, pp. 291-295
132 Delville, A., 1991, 1st Int. Workshop on Hydration and Setting, Dijon, Sess. II-1

133 Dent Glasser, L.S., et al., 1978, CCR, Vol. 8, No. 6, pp. 733-739
134 Detriche, C.H., et al., 1986, SMDDHC, Boston, MRS, Proc. Vol. 85, pp. 157-160
135 Detwiler, R.J., et al., 1988, CCR, Vol. 18, No. 5, pp. 823-829.
136 Diamond, S., et al., 1972, J. Coll. and Interface Sci., 38, pp. 234-244. *Ibid. [532]*
137 Diamond, S., 1976, Proc. CHCPSP, Sheffield, April, pp. 2-29
138 Daimond, S., 1976, CCR, Vol. 6, No. 3, pp. 413-416
139 Diamond, S., 1980, 7th ICCC, Paris, Vol. IV, pp. 113-123
140 Diamond, S., 1986, 8th ICCC, Rio de Jan., Vol. I, pp. 122-147
141 Diamond, S., 1986, SMDDHC, Boston, MRS, Proc. Vol. 85, pp. 21-31
142 Dmitriev, A.M., 1986, 8th ICCC, Rio de Jan., Vol. I, pp. 73-81
143 Dorner, H.W., et al., 1980, CCR, Vol. 10, No. 3, pp. 403-411
144 Double, D.D., et al., 1980, 7th ICCC, Paris, Vol. 2, II-256-260
145 Dron, R., et al., 1972, C.R. Acad. Sci., Paris, 280, pp. 187
146 Edmonds, R.N., et al., 1988, CCR, Vol. 18, No. 3, pp. 473-478
147 Efes, Y., 1980, CCR, Vol. 10, No. 2, pp. 321-242
148 Eibl J., et al., 1990, B&St, 85, No. 4, pp. 85-90
149 Eiger, A., 1931, TIZ, No. 5, pp. 1389-1390; No. 56, 1932, pp. 532-533 + 558-560
150 Eitel, W., 1941, Ztg. ang. Chemie, Vol. 54, p. 164
151 El-Jazairi, B., et al., 1980, CCR, Vol. 10, pp. 361-366
152 Emborg, M., 1986, 4th. RILEM Int. Symp. Creep and Shrinkage of Concr., Evanston, pp. 723-732
153 Emborg, M., 1989, Thermal Stresses in Concrete Structures at Early Ages, PhD., Lulea, p. 285
154 ENCI, 1986, Adiabatic Temperature rise at different w/c ratios, Privat documentation
155 Englert G., 1968, Diss. München, 90 p.
156 Fagerlund, G., 1987, Seminar on Hydration of Cement, Copenhagen, 56 p.
157 Fagerlund, G., Strength and Porosity of Concrete, paper, pp. D51-D73
158 Farran, J., 1956, Rev. Mat. Constr. Trav. Publ., 490, 491, 492
159 Feldman, R.F., 1972, CCR, 2, No. 2, pp. 123-; 2, No. 4, pp. 489-; 2, No. 6, pp. 749-.
160 Feldman, R.F., 1975, CCR, pp. 103 -; 1976, pp. 389-; 1977, pp. 469-;
161 Feldman, R.F., et al., 1976, Proc. CHCPSP, Sheffield, pp. 150-165
162 Feldman, R.F., et al., 1985, CCR, Vol. 15, No. 5, pp. 766-774
163 Feldman, R.F., 1986, 8th ICCC, Rio de Jan., Vol. 1, pp. 336-356
164 Feldman, R.F., 1986, ACI-SP-91, Ed. Malhotra, V.M., pp. 973-989
165 Fierens, P., 1975, CEMBUREAU, Paris. *Ibid. [413]*
166 Fierens, P., et al., 1976, CCR, Vol. 6, No. 3, pp. 337-342
167 Fierens, P., et al., 1982, CCR, Vol. 12, pp. 191-198
168 Fierens, P., et al., 1986, 8th ICCC, Rio de Jan., Vol. II, pp. 17-21
169 Forbrich, L.R., 1940, ACI-J, Vol. 37, pp. 161-184
170 Forbrich, L.R., 1941, ACI-J, Vol. 38, pp. 53-62
171 Forsen, L., 1935, Zement, Jhg. 24, pp. 191-197
172 Fraay, A.L.A., 1990, Fly Ash a Pozzolan in Concrete, PhD, Delft
173 Frank, A., 1935, Zement, Jhg. 24, No. 25, pp 379-381
174 Freiesleben, H., et al., 1977, Nordisk Beton, No. 1, Stockholm, pp. 2-25
175 Frens, G., 1988, Solutions (p. 24), Colloids (p. 28), Text books, Delft (in Dutch)
176 Frigione, G., et al., 1976, CCR, Vol. 6, No. 1, pp. 113-128
177 Frigione, G., et al., 1985, CCR, Vol. 15, No. 1, pp. 159-166
178 Frohnsdorff, G.J.C., et al., 1968, 5th ICCC, Tokyo, Vol. II, pp. 321-327
179 Fujii, K., et al., 1968, 5th ICCC, Tokyo, Vol. 2, pp. 362-
180 Fujii, K., et al., 1970, ZKG, Jhg. 23, No. 2, pp. 72-79
181 Fujii, K., 1974, JACS, pp. 492. *Ibid. [413]*
182 Gard, J.A., 1976, CCR, Vol. 6, No. 5, pp. 667-678
183 Gauglitz, R., et al., 1962, ZKG, No. 3, pp. 104-120
184 Gebauer, J., et al., 1966, ZKG, No. 7, pp. 303-308
185 Geiker, M., et al., 1982, CCR, Vol. 12, No. 5, pp. 603-610
186 Gilkey, H.J., 1961, ACI-J, No. 57-55, pp. 1287-1311; (Disc. pp. 1851-1978)
187 Gille, F., 1942, Zement, Jhg. 31, Aug. pp. 331-337
188 Gille, F., 1955, ZKG, Jhg. 8, pp. 128-138
189 Ginstling, A.M., et al., 1950, J. Appl. Chem., (USSR), 23, pp. 1327-1328
190 Glasser, F.P., et al., 1986, SMDDHC, Boston, MRS, Proc. Vol. 85, pp. 167-186

191 Glasser, L.S. Dent, et al., 1978, CCR, Vol. 8, No. 733-740
192 Glasstone, S., et al., 1941, The Theory of Rate Processes, McGraw Hill Book Comp., NY,
193 Glauser, A., 1962, ZKG, Jhg. 15, No. 12, pp. 529-534
194 Glauser, A., 1968, ZKG, Jhg. 21, No. 5, pp. 220-224
195 Glauser, A., 1971, ZKG, Jhg. 24, No. 6, pp. 264-267
196 Goldbeck, A.T., 1939, Crushed Stone Journal, Vol. 14, No. 5, pp. 8-
197 Goldschmidt, A., 1986, CCR, Vol. 16, pp 472-480
198 Gonnerman, H.F., 1934, ENR, Nov. pp. 651-656
199 Gorur, K., et al., 1982, CCR, Vol. 12, No. 4, pp. 447-454
200 Graf, O.. *Ibid. Grün et.al [216]*
201 Graf, O., 1930, Zement, pp. 48-49
202 Grandet, J., et al., 1980, 7th ICCC, Paris, Vol. III, pp. VII-85-89
203 Granju, J.L., 1974, M&C, Vol. 7, No. 37, pp. 25-35
204 Granju, J.L., et al., 1980, CCR, Vol. 10, No. 5, pp. 611-621
205 Granju, J.L., et al., 1984, CCR, Vol. 14, No. 2, pp. 249-256, No. 3, pp. 303-310
206 Granju, J.L., et al., 1988, CCR, Vol. 18, No. 6, pp. 886-894
207 Grant, M.R., 1987, ZKG, Jhg. 40, No. 6, pp. 319-322
208 Greenberg, S.A., et al., 1965, J. Phys. Chem. 69, pp. 553-561
209 Greene, K.T., 1962, 4th ICCC, Washington, Vol. I, pp. 359-385
210 Grindrod, P.S., 1968, ASTM-STP, 473, pp. 45-70
211 Gronow, H. Elsner von, 1935, Zement, Jhg. 24, No. 51, pp. 807-810
212 Groves, G.W., 1981, JMS, Vol. 16, No. 4, pp. 1063-1070. *Ibid. [581]*
213 Grudemo, A., 1960, 4th ISCC, Washington, Vol. 2, pp. 615-698. *Ibid. [81]*
214 Grudemo, A., The Cryst. Struct. of Cem. Hydr. - A New Gel Struct. Model; pp. -62
215 Grudemo, K., 1955, Proc. No. 26, Swedish Cem. Concr. Inst., Stockholm
216 Grün, W., et al., 1961, ZKG, Jhg. 14, No. 11, pp. 514-519
217 Gründer, W., et al., 1950, ZKG, Jhg. 3, No. 4, pp. 67-71
218 Gruteck, M.W., et al., 1969, Nature, Vol. 23, pp. 92-94
219 Guide to Compound Nomenclature, 1972, Highway Research Board, 53 p.
220 Haas, G.D. de, et al., 1975, CCR, Vol. 5, No. 4, pp. 295-320
221 Hadley, D., 1972, PhD, Thesis, Purdue Univ., 186 p.
222 Haegermann, G., 1950, ZKG, Jhg. 3, No. 3, pp. 152-155
223 Hagymassy, J., et al., 1969, JCIS, Vol. 29, No. 3, pp. 485-491
224 Hakvoort, G., 1978, Formation and dissolution of $AgMO_3$ compounds, PhD, Delft, p. 212
225 Halstead, P.E., 1962, 4th ICCC, Washington, Vol. I, pp. 321-324
226 Hansen, T.C., 1970, ACI-J, May, pp. 404-407
227 Hansen, W., et al., 1978, Proc. Mat. Res. Symp., Vol. 85, pp. 105-114
228 Hansen, W., et al., 1986, SMDDHC, Boston, MRS, Proc. Vol. 85, pp. 105-114.
229 Hansen, W.C., 1963, ACI-J, pp. 141-156.
230 Harmelen, A.H.J. van, Simulation of Temperature Dev. in Girder-Box Bridge, Delft, (unpublished)
231 Harrisson, A.M., et al., 1985, CCR, Vol. 15, No. 5, pp. 775-780
232 Hasselmann, D.P.H., 1962, JACS, 1962. *Ibid. [503]*
233 Hedin, R., 1945, Swedish Cem. and Concr. Res. Inst., Stockholm
234 Heinz, 1987, (Atkins, P.W.) Physical Chemistry, 3rd. ed., Oxford Un. Press
235 Helbig. *Ibid. Gründer et al. [217]*
236 Helland, S., 1986, Nordisk Betong, 1-2-1986, pp. 63-70
237 Hellmich, K., 1984, B&St, No. 2, pp. 42-46
238 Helmuth, R.A., 1980, 7th ICCC, Paris, Vol. III, pp. VI-0/19 - VI-0/29
239 Henk, B., 1966, Betonstein Zeitung, No. 8, pp. 461-470
240 Herdan, G., 1960, Small Particle Statistics, Butt. & Co., Ltd.
241 Herrmann, A.G., 1975, Praktikum der Gesteinkunde, Springer Verlag. *Ibid. [480]*
242 Highway Research Board, 1972, SR 127, Washington DC., 53 p.
243 Hime, W.G., 1968, ASTM-STP 473, pp. 3-19
244 Ho, D.W.S., et al., 1989, CCR, Vol. 19, No. 3, pp. 457-464
245 Hochdahl, O., 1972, ZKG, Jhg. 25, No. 12, pp. 593-598
246 Horden, W.C., et al., 1986, Cement, No. 12, pp. 49-52
247 Hraste, M., 1974, CCR, Vol. 4, No. 6, pp. 915-923
248 Hsu, Th.T.C., et al., 1963, ACI-J, Title no. 60-14, pp. 209-224

249 Hsu, Th.T.C., et al., 1963, ACI-J, Title no. 60-25, pp. 465-486
250 Huang Cheng-yi, et al., 1985, CCR, Vol. 15, pp. 285-294.
251 Huber, H., 1987, Z&B, Jhg. 32, No. 4, pp. 148-149
252 Huber, H., 1988, Z&B, Jhg. 33, No. 3, pp. 162-163
253 Hughes, D.C., 1985, MCR, Vol. 37, No. 133, pp. 227-233
254 Hunt, C.M., 1966, ACI-SP 90, Washington, pp. 112-122
255 Hutchinson, C.S., 1974, Lab. Handb. of Petrogr. Techn., J. W & S., NY
256 Iwasaki, N., et al., 1976, Rev. 30th Gen. Mtg. Cem. Assoc. Japan, pp. 213-215
257 Jambor, J., 1963, MCR, Vol. 15, No. 45, pp. 131-142
258 Jambor, J., 1976, Proc. CHCPSP, Sheffield, April, pp. 175-188
259 Jambor, J., 1986, 8th ICCC, Rio, Vol. II, pp. 363-368
260 Jander, W, 1927, Ztg. anorg. allg. Chem., 163, pp. 1-30
261 Jap. Stand. Spec. for Des. and Constr. of Concr. Struc., 1986, Part 2, Ch 15, pp. 132-151
262 Jaspers, M.J.M., 1951, Rev. M&C, No's 429-432. *Ibid. [600]*
263 Jawed, I., et al., 1977, CCR, Vol. 7, No. 6, pp. 719-730
264 Jelenic, et al., 1978, CCR, Vol. 8, 173-
265 Jennings, H.M., 1979, CCR, Vol. 9, No. 4, pp. 501-506
266 Jennings, H.M., 1981, Advances in Cement Technology, Ed. Ghosh, Perg. Press, pp. 349-396
267 Jennings, H.M., et al., 1981, JACS, 64, pp. 567-572
268 Jennings, H.M., 1986, SMDDHC, Boston, MRS, Proc. Vol. 85, pp. 291-300
269 Jennings, H.M., 1991, 1st Int. Workshop on Hydration and Setting, Dijon, Sess. III
270 Jia, W., et al., 1986, 8th ICCC, Rio de Jan., Vol. II, pp. 460-465
271 Jonassen, J.-E., 1982, RILEM, Int. Conf. CEA, Paris, Vol. II, pp. 213-218
272 Jong, J.G.M. de, et al., 1967, J. Appl. Chem., Vol. 17, pp. 246. *Ibid. [413]*
273 Jons, E.S., et al., 1980, 7th ICCC, Paris, Vol. IV, pp. 514-519.
274 Jons, E.S., 1982, CCR, Vol. 12, pp. 167-178
275 Kaempfe, F., 1955, ZKG, Jhg. 8, No. 3, pp. 77-84
276 Kalousek, G.L., 1951, ACI-J, September, pp. 77-90
277 Kantro, D.L., et al., 1962, J. Phys. Chem., 66, pp. 1804. *Ibid. [413]*
278 Kantro, D.L., et al., 1966, ACI-SP 90, Washington, pp. 309-327. *Ibid. [138]*
279 Kapranov, W.W., 1975, CCR, Vol. 5, pp. 15-24
280 Kargin, V.A., et al., 1961. *Ibid. [81]*
281 Karni, J., 1974, M&C, Vol. 7, No. 39, pp 197-200
282 Karsch, K.H., et al., 1963, ZKG, Jhg. 16, No 5, pp. 165-169
283 Kawamura, M., 1972, CCR, Vol. 2, No. 5, pp. 507-520
285 Kayser, W., 1961, ZKG, Jhg. 14, No. 11, pp. 520-524
284 Kayser, W., 1965, PhD, Karlsruhe
286 Kayyali, O.A., 1978, M&C, Vol. 18, No. 10, pp. 259-262
287 Keienburg, R.R., 1976, PSD. and Norm Strength of PC, PhD, Karlsruhe, 111 p. (in German)
288 Keil, F., 1967, ZKG, Jhg. 20, No .5, pp. 201-213
289 Keil, F., 1971, Zement, Springer Verlag, 439 p. (in German). *Ibid. Powers [462]*
290 Keller, H., 1937, B&E, Jhg. 36, No. 14, pp. 231-235; No. 15, pp. 249-255
291 Kendall, K., et al., 1983, Phil. Transact. of the Royal Soc., A 310, pp. 139-153
292 Khalil, S.M., et al., 1977, M&C, Vol. 10, No. 56, pp. 67-72
293 Killoh, D.C., 1988, ACR, Vol. I, No. 3, pp. 180-186
294 Kittl, P. et al., 1980, 7th ICCC, Paris, 1980, Vol. II, pp. II - 7-11
295 Kjellsen, K.O., 1987, Seminar on Hydration of Cement, Copenhagen/Aalborg, 11 p.
296 Kjellsen K.O., at al., 1990, CCR, Vol. 20, No. 2, pp. 308-311
297 Kjellsen K.O., et al., 1990, CCR, Vol. 20, No. 6, pp. 927-933
298 Kjellsen K.O., et al., 1991, CCR, Vol. 21, No. 1, pp. 179-189
299 Klieger, P., 1958, ACI-J, pp. 1063-1081
301 Knofel, D., 1979, ZKG, Jhg. 32, No. 9, pp. 448-454
300 Knofel, et al., 1969, ZKG, Jhg. 22, No. 22, pp. 471-476
302 Knudsen, T., 1980, 7th ICCC, Paris, Vol. II, pp. I - 170-175
303 Knudsen, T., 1984, CCR, Vol. 14, No. 5, pp. 622-630
304 Knudsen, T., 1986, 8th ICCC, Rio de Janeiro, Vol. II, pp. 369-374
305 Knudsen, T., 1987, Seminar on Hydration of Cement, Copenhagen/Aalborg, p 8.
306 Kondo, R., 1965, Int. Symp. ACSBP, SCI, London. *Ibid. [430]*

307 Kondo, R., et al., 1968, 5th ICCC, Tokyo, Vol. II, Sess. II-4, pp. 203-248
308 Kondo, R., et al., 1969, JACS, Vol. 52, pp. 503. *Ibid. [413]*
309 Koster, H., et al., 1986, CCR, 16, pp. 207-214; 16, pp. 893-901; 17, 1987, pp. 22-30
310 Kramer, H., 1960, ZKG, Jhg. 13, No. 12, pp. 572-579.
311 Kratzer, K., 1981, Z&B, Jhg. 26, No. 3, pp. 118-123
312 Kristmann, M., 1987, CCR, Vol. 17, No. 7, pp. 649-658
313 Kristulovic, R., et al., 1980, 7th ICCC, Paris, Vol. II, pp. II - 153-159
314 Krogbeumker, G, et al., 1972, ZKG, Jhg. 25, No. 9, pp. 417-418
315 Krokosky, E.M., 1970, M&C, Vol 3, No. 17, pp 313-323
316 Kroone, B., et al., 1961, MCR, 13, No. 39, pp. 127-132; 14, No. 40, 1962, pp. 43-46
317 Kühl, H., 1930, Leningrad. *Ibid. [81]*
318 Kühl, H., 1930, Zement, Jhg. 19, pp. 604-608; Jhg. 20, 1931, p. 196. *Ibid. [217]*
319 Kühl, R., 1958, VDZ, Dusseldorf, H. 22
320 Kuhlmann, K., et al., 1985, ZKG, Jhg. 28, No. 4, 169-178; No. 9, 528-534, No. 10, 586-588
321 Kuzel, H.-J., et al., 1991, 1st Int. Workshop on Hydration and Setting, Dijon, Sess. I-3.
322 Lach, V., et al., 1980, 7th ICCC, Paris, Vol. IV, p.776-781
323 Langton, C.A., et al., 1980, CCR, Vol. 10, pp. 449-454
324 Larbi, J.A., et al.. *Ibid. [324]* and privat communication
325 Larbi, J.A., et al., 1989, Stevin report 25, 11-89-11/C, 10 p.
326 Larbi, J.A., et al., 1990, Cement, No. 10, pp. 13-19 (in Dutch)
327 Larbi, J.A., et al., 1990, MRS, Symp. Proc., Vol. 178, pp. 127-138
328 Larrard, F. de, 1989, CCR, Vol. 19, No. 2, pp. 161-172
329 Laube, M., 1990, Constitut. Mod. for Calc. Temp. Stress. in Mass Concr., PhD, 1990, 251 p., (Germ.)
330 Lawrence, C.D., 1966, ACI-SP 90, Washington, pp. 378-391
331 Lawrence, F.V., et al., 1973, CCR, 3, No. 2, pp. 149-161; 4, No. 3, 1974, pp. 481-483
332 Lazonder, J.M., et al., CUR-report No. 32, Dutch Concrete Society
333 Le Chatelier, H., 1900, Bull. de la Soc. d'encouragement pour l'industrie nationale, 1900
334 Le Chatelier, H., 1905, McGraw Publ. Co. New York
335 Le Sueur, P.J., et al., Proc. PCCRPC, BCS, pp. 179-191
336 Lea, F.M., et al., 1935, JSCI, 54, 63 T. *Ibid. [121]*
337 Lea, F.M., 1970, The Chemistry of Cement and Concrete, 3rd. ed., Edward Arnold Ltd.
338 Lehmann, H., et al., 1965, TIZ, No. 15/16, pp. 337-350
339 Lentz, C.W., 1966, ACI-SP 90, Washington, pp. 269-283
340 Lerch, W., et al., 1935, Zement, 24. Jhg., No. 11, pp. 155-158; No. 12, pp. 169-172.
341 Lerch, W., 1946, PCA Bull. 12, (Also: Proc. ASTM., Vol. 46)
342 Lerch, W., et al., 1948, ACI-J, Vol. 44, pp. 745-795
343 Lhopitallier, P., et al., 1948, XXI Congr. Chem. Ind., Bruxelles. *Ibid. [600]*
344 Lindner, B., et al., 1969. *Ibid. [480]*
345 Linsbauer, H., et al., 1989, Z&B, Jhg. 34, No. 1, pp. 35-37
346 Liu Chong Xi, 1987, ZKG, Jhg. 40, No. 2, pp. 103-108
347 Locher, F.W., 1955, ZKG, Jhg. 8, pp. 301-308
348 Locher, F.W., 1960, ZKG, Jhg. 13, No. 9, pp. 389-394
349 Locher, F.W., 1961, ZKG, Jhg. 14, No. 12, pp. 573-580
350 Locher, F.W., 1964, ZKG, Jhg. 17, No. 5, 1964, pp. 175-182
351 Locher, F.W., 1966, ACI-SP 90, Washington, pp. 300-308
352 Locher, F.W., et al., 1966, TIZ, No. 12, pp. 547-534
353 Locher, F.W., et al., 1973, ZKG, Jhg. 26, No. 8, pp. 349-355
354 Locher, F.W., et al., 1976, ZKG, Jhg. 29, No. 10, pp. 435-442
355 Locher, F.W., 1976, Beton, H. 7, pp. 247-249; No. 8, pp. 283-285
356 Ludwig, N.C., et al., 1956, ACI-J, Title no. 52-43, pp. 673-687
357 Ludwig, U., 1968, ZKG, No. 2, pp 81-90; No. 3, pp 109-119; ZKG. No. 4, pp 175-180
358 Lyubimova, T. Yu, et al., 1962, Colloid. J., 24, pp. 491-498
359 Maage, M., et al., 1988, Proc. FIP-Symp., Israel, pp. 53-60
360 Maage, M., et al., 1988, CI, pp. 34-39
361 Maatjes, E., et al., 1986, Cement, No. 5, pp. 44-52
362 Maatjes, E., et al., 1989, Cement, No. 3, pp. 56-62
363 Mai, Y.W., et al., 1985, CCR, Vol. 15, pp. 995-1002
364 Mai, Y.W., et al., 1986, CCR, Vol. 16, pp. 646-652

365 Malhotra, V.M., et al., 1983, CI, pp. 40-46
366 Malinine, Y.S., et al., 1980, 7th ICCC, Paris, Vol. VI, pp. 195-198
367 Mallinson, L.G., 1987, 1st Int. Conf. Concr. for Haz. Prot., Edinburgh, pp. 299-318
368 Maso, J.C., 1980, 7th ICCC, Paris, Vol. I, Sub-theme VII-I
369 Massaza, F., et al., 1980, 7th. ICCC, Paris, Vol. III, pp. VII - 16-21
370 Massazza, F., et al., 1986, 8th ICCC, Rio de Jan., Vol. I, pp. 158-180
371 Matoushek, F., 1947, Schw. Arch. angewandte Wiss. & Tech., Cah. 2,3
372 Mayers, A.H., 1990, Camber Development in Prestressed Girders, Delft, (in Dutch)
373 McHenry, D., 1937, ACI-J, Vol. 34, pp. 117-125
374 McIntosh, J.D., 1956, Proc. Symp. Winter Concreting, RILEM, Copenhagen, Sess. B-II, 17 p.
375 Mehta, P.K., 1976, CCR, Vol. 6, No. 2, pp. 169-182
376 Mehta, P.K., et al., 1980, 7th ICCC, Paris, Vol. III, pp. VII-1-5
377 Mehta, P.K., 1986, 8th ICCC, Rio de Jan., Vol. I, pp. 113-121
378 Mehta, P.K., 1986, 8th ICCC, Rio de Jan., Vol. III, pp. VII - 1-5
379 Meissner, H.S., 1933, ACI-J, Sept.-Oct., pp. 21-26
380 Menetrier, D., et al., 1979, CCR, Vol. 9, No. 4, pp. 473-482
381 Menetrier, D., et al., 1980, CCR, Vol. 10, No. 3, pp. 425-432
382 Menetrier, D., et al., 1980, CCR, Vol. 10, No. 5, pp. 697-701
383 Meric, J.P., 1980, 7th ICCC, Paris, Vol. I, Sub-theme 1-4
384 Michaelis, W., 1909, Chem. Zeitung, 5, p. 9
385 Midgley et al., 1971, CCR, Vol. 1, pp. 101-
386 Mikhail, R.Sh., et al., 1964, Can. J. of Chem., 42, pp. 426-438
387 Mills, R.H., 1966, ACI-SP 60, Washington, pp. 406-424
388 Mills, R.H., 1969, Int. Conf. Structure and solid mechanics, Southampton, 68
389 Mindess, S., 1986, 8th ICCC, Rio, Vol. I, pp. 115-157
390 Min-Hong Zhang, et al., 1990, CCR, Vol. 20, No. 4, pp. 610-618
391 Mino, I., et al., 1986, 8th ICCC, Rio de Jan., Vol. II, pp. 167-172
392 Monteiro, P.J.M., 1985, PhD. Thesis, Berkeley
393 Monteiro, P.J.M., et al., 1986, 8th ICCC, Rio de Jan., Vol. II, pp. 433-437
394 Monteiro, P.J.M., et al., 1986, CCR, Vol. 16, pp. 127-134
395 Moore, A.E., 1980, 7th ICCC, Paris, Vol. III, pp. VI-97-102
396 Mori, H., et al. 1968, 5th ISCC, Tokyo, Paper II-73, pp. 349-360
397 Mukerji, J., 1981, Advances in Cement Technology, Ed. S.N. Ghosh, Perg. Press, pp. 265-288
398 Muller-Hesse, H., et al., 1956, ZKG, Jhg. 9, pp. 386-389
399 Naredi, R., 1964, ZKG, Jhg. 17, No. 7, pp. 302-313
400 Neville, A.M., 1973, Properties of Concrete, Pitman Publ., 687 p.
401 Newkirk, T.F., 1952, 3rd ICCC, London, pp. 151-168
402 Newmark, N.M., 1938, ACI-J, Vol. 34, March-April, pp. 104-1/5
403 Nonat, A., et al., 1991, 1st. Int. Workshop on Hydration and Setting, Dijon, Sess. II
404 Novak, D., 1973, ZKG, Jhg. 26, No. 7, pp. 312-315
405 Nyame, B.K., et al., 1980, 7th ICCC, Paris, Vol. III, pp. VI-181-185
406 Nykanen, A., 1956, Proc. RILEM Symp. Winter Concreting, Copenhagen, Sess. B-II, 19 p.
407 O'Conner, T.L., et al., 1958, J. Phys. Chem., Vol. 62, pp. 1195-1198. *Ibid. [5.25]*
408 Oberholster, R.E., 1986, 8th ICCC, Rio, Vol. I, pp. 323-335
409 Odler, I., et al., 1966, ZKG, Jhg. 19, No. 6, pp. 276-281
410 Odler, I., et al., 1972, CCR, Vol. 2, pp. 463-480
411 Odler, I., et al., 1972, CCR, Vol. 2, pp. 577-589
412 Odler, I., et al., 1978, CCR, Vol. 8, pp. 525-538
413 Odler, I., et al., 1979, CCR, 9, pp. 239-248; 9, pp. 277-284; Disc. 9, pp. 799.
414 Odler, I., et al., 1981, ZKG, Jhg. 34, No. 9, pp. 445-449
416 Odler, I., et al., 1982, CCR, Vol. 12, No. 1, pp. 13-20
415 Odler, I., et al., 1982, World Cement Tech., pp. 216-222
417 Odler, I., et al., 1983, CCR, Vol. 13, No. 4, pp. 447-482
418 Odler, I., et al., 1985, CCR, Vol 15, pp. 320-330; Vol 15, pp. 401-410
419 Odler, I., 1986, CCR, 16, pp. 207-214; 16, pp. 893-901; 17, 1987, pp. 22-30.
420 Odler, I., et al., 1986, SMDDHC, MRS, Boston, Proc. Vol. 85, pp. 33-38
421 Odler, I., et al., 1989, CCR, Vol. 19, No. 2, pp. 295-305
422 Oliew, G., et al., 1980, 7th ICCC, Paris, Vol IV, p. 291-294

423 Ollivier, J.P., 1981, PhD, Thesis, Toulouse
424 Orr, D.M.F, 1982, Symp. CEA, RILEM, Paris, Proc. Vol. I, pp. 57-61
425 Osbaeck, B., 1979, ZKG, Jhg. 32, No. 2, pp. 72-88
426 Osbaeck, B., 1980, 7th ICCC, Paris, Vol. II, pp. II-135-140
427 Osbaeck, B., 1987, Seminar Hydration of Cement, Copenhagen, 1987, 19 p.
428 Ottewill, F.R.S., 1983, Developments in Hydraulic Cement, Ed. Hirsch, Roy. Soc., London, pp. 67-77
429 Owens, P.L., et al., 1980, 7th ICCC, Paris, Vol. IV, pp. 811-815
430 Oyefesobi, S.O., et al., 1976, CCR, Vol. 6, pp. 803-810
431 Pancrazi, R. et al., 1986, 8th ICCC, Rio de Jan., Vol. II, pp. 75-78
432 Papadakis, M., et al., CERIB-publ., Technique, No. 8
433 Papadakis, M., et al., 1969, Man. Lab. d'Essais Cim., Mortar, Beton, Ed. Eyrolles, Paris
434 Parcevaux, P., 1984, CCR, Vol. 14, pp. 419-430
435 Parrott, L.J., et al., 1984, C&CRPC, Ed. D. Glasser.
436 Parrott, L.J., et al., 1984, JACS, 67, 4, pp. 233-237
437 Parrott, L.J., 1986, SMDDHC, Boston, MRS, Proc. Vol. 85, pp. 91-104
438 Parrott, L.J., et al., 1986, 8th ICCC, Rio de Janeiro, Vol. II, pp. 46-50
439 Parrott, L.J., et al., 1990, CCR, Vol. 20, No. 6, pp. 919-926
440 Parry-Jones, G., et al., 1989, CCR, Vol. 19, No. 2, pp. 228-234
441 Penfield, S.L., 1894, Amer. J. Sci., 48, p. 30
442 Perow, W.A., et al., 1954, Feinmahlung der Erze, VEB Verlag Techn., Berlin
443 Peterson, E., 1965, Chem. Reaction Analysis, Prentice-Hall, NY. *Ibid. [452]*
444 Petscharnig, F., 1987, Z&B, Jhg. 32, No. 4, pp. 162-163
445 Philleo, R.E., 1966, ACI-SP 90, Washington, pp. 175-185
446 Plowman, C., 1984, CCR, Vol. 14, pp. 238-248
447 Plowman, J.M., 1956, MCR, pp. 13-22
448 Pojiarvi, H., et al., 1977, ZKG, Jhg. 20, No. 11, pp. 586-591
449 Polak, A.Ph., et al., 1980, 7th ICCC, Paris, Vol. III, pp. VI - 108-113
450 Pommersheim, J.M., et al., 1979, CCR, Vol. 9, No. 6, pp. 765-770
451 Pommersheim, J.M., et al., 1980, 7th ICCC, Paris, Theme VI, pp. 195-200
452 Pommersheim, J.M., et al., 1982, CCR, Vol. 12, No. 6, pp. 765-772
453 Pommersheim, J.M., 1986, SMDDHC, Boston, MRS, Proc. Vol. 85, pp. 301-306
454 Pommersheim, J.M., et al., 1986, CCR, Vol. 12, pp. 440-450
455 Popov, L.N., 1980, 7th ICCC, Paris, Vol. III, p. VI-192-194
456 Popovics, S., 1968, B&Z, No. 11, pp. 587-590
457 Popovics, S., 1979, Concrete making materials, McGr.-Hill. B. Comp., Washington, 370 pp.
458 Popovics, S., 1980, 7th ICCC, Paris, Vol. III, pp. VI-47-51
459 Popovics, S., 1985, ACI-J, No. 82-11, April, pp. 136-145
460 Popovics, S., 1987, CCR, Vol. 17, No. 5, pp. 821-838
461 Postaciogly, B., 1959, Rev. Construction, Dec.
462 Powers, T.C., et al., 1946/1947, ACI-J, Part 1-9
463 Powers, T.C., 1947, Proc. HRB, 27, Washington DC, pp. 178-188. *Ibid. [173]*
464 Powers, T.C., et al., 1948, PCA Bull. 22. *Ibid. [490]*
465 Powers, T.C., 1958, JACS, Vol. 41, No. 1, January, pp. 1-6
466 Powers, T.C., 1960, 4th ISCC, Washington, Paper V-1, pp. 577-609
467 Powers, T.C., 1968, C&C Ass., London, pp. 319-344. *Ibid. [623]*
468 Pratt, L.D., et al.. *Ibid. [141]*
469 Pratt, P.L., et al., 1983, Developments in Hydraulic Cements, Ed. Hirsch et.at., Roy. Soc., pp. 93-103
470 Prosen, E.J., et al., 1985, CCR, Vol. 15, No. 4, pp. 703-710
471 Rahman, A.A., et al., 1982, CCR, Vol. 12, No. 1, pp. 33-38
472 Rakel, K., 1965, Beitrag z. Bestimmung d. Hydratationswarme von Zement, PhD, Aachen. 149 p.
473 Ramachandran, A.R., et al., 1986, SMDDHC, Boston, MRS, Proc. Vol. 85, pp. 33-38
474 Ramachandran, A.R., et al., 1986, 8th. ICCC, Rio de Jan., Vol. II, Theme 2.1, pp. 225-230
475 Rammler, E., 1940, VDI-Ztg, Beihefte Verfahrenstechnik, H. 5, pp. 150-160
476 Rammler,E.. *Ibid. Gründer et al. [217]*
477 Rastrup, E., 1954, MCR, September, pp. 79-90
478 Rastrup, E., 1956, Winter Concreting, RILEM-Symp. Copenhagen, Session B II
479 Rayment, D.L., et al., 1982, CCR, Vol. 12, No. 6, pp. 753-764
480 Rechenberg, W., et al., 1976, ZKG, No. 11, pp. 512-516

481 Regourd, M., et al., 1975, RMC, No. 693, pp. 73-87; CCR, 1976, Vol. 6, pp. 733-740
482 Regourd, M., et al., 1980, Ann., No. 387, pp. 83-96
483 Regourd, M., 1985, Very High Strength Cement-Based Materials, Ed. Young, MRS., 42, pp. 3-17
484 Regourd, M., 1986, SMDDHC, Boston, MRS, Proc. Vol. 85, pp. 187-200. *Ibid. [3]*
485 Rehbinder, P.A.. *Ibid. Jambor [257]*
486 Reinhardt, H.W., et al., 1982, RILEM Symp. CEA, Paris, Vol. I, pp. 211-226
487 Relis, M., et al., 1977, CCR, Vol. 7, pp. 673-680
488 Relis, M., et al., 1980, JACS, 63, pp. 690-
489 Rexford, 1943, ACI-J, Vol. 14, No. 6, pp. 212/1-3
490 Richartz, W., et al., 1965, ZKG, Jhg. 18, No. 9, pp. 449-459
491 Ritt, H.G., et al., 1961, TIZ, No. 85, pp. 52-
492 Ritzmann, H., 1968, ZKG, Jhg. 21, No. 9, pp. 390-396
493 Robson, T.D., 1962, London Contractors Record. *Ibid. [82]*
494 Rockwood, N.C., 1949, ACI-J, 23, 1051, Nov. 205 (Auszug: ZKG, 2, 1949, 220)
495 Rodger, S.A., et al., 1986, SMDDHC, Boston, MRS, Proc. Vol. 85, pp. 13-20.
496 Roelfstra, P.E., 1988, Beton Numerique, PhD, EPFL, Lausanne, Sw, p. 177
497 Roelfstra, P.E., et al., 1985, M&C, Vol. 18, No. 107, pp. 327-335
498 Röhling, S., et al., 1989, A microstructure-based model etc., Privatly received doc.
499 Röhling, S., et al., Model for Kinetics of Struct. Form. and Strength Dev., Priv. Comm.
500 Röhling, S., 1990, Methods for Calculating Temperature, subm. to RILEM TC 119; Privat. comm.
501 Rordam, S., 1933, RMCTP, Jan. 1933, No. 280. *Ibid. Venaut [600]*
502 Rosin, P., et al., 1933, Zement, No. 8, pp. 427-433
503 Rossler, M., et al., 1985, CCR, Vol. 15, No. 2, pp. 320-330; No. 3, pp. 401-410
504 Roth, W., 1970, Heat of Hydration and Degree of Hydration of Portland Cement, PhD, Aachen
505 Roy, D.M., et al., 1972, CCR, Vol. 2, No. 3, pp. 349-366
506 Roy, D.M., et al., 1973, CCR, Vol. 3, Nr. 6, pp. 807-820
507 Roy, D.M., et al., 1982, ACI-J, pp. 444-457
508 Rumpf, H., 1966, ZKG, No. 8, pp. 343-353
509 Rumyantsev, P.F., 1980, 7th ICCC, Paris, Vol. III, pp. VI - 79-82
510 Sabri, S., et al., 1980, 7th ICCC, Paris, Vol. III, pp. VI-52-55
511 Sadouki, H., 1987, PhD Thesis, Ec. Polytechn. Lausanne, 295 p.
512 Saito, M., et al., 1986, CCR, Vol. 16, pp. 653-662
513 Sandri, R., 1933, Zement, Jhg. 22, No. 43, pp. 593-644
514 Santarelli, L., et al., RMC, No. 544, pp. 13-19
515 Sarkar, S.L., 1985, CCR, Vol. 15, No. 3, pp. 549-552
516 Sarkar S.L., 1990, CCR, Vol. 20, No. 3, pp. 398-406
517 Saul, A.G.A, 1951, MCR, No. 6, pp. 127-
518 Schlüssler, K.H., 1986, CCR, Vol. 16, pp. 215-226
519 Schonert, K., 1979, ZKG, Nr. 1, pp. 1-9
520 Schwiete, H.E., et al., 1960, Z&B, No. 16, pp. 25-29. *Ibid. [75]*
521 Schwiete, H.E., et al., 1966, Symp. SPCPC, ACI-SR-90, pp. 353-367
522 Schwiete, H.E., et al., 1966, TIZ, 90, pp. 562-574
523 Schwiete, H.E., et al., 1970, ZKG, No. 12, pp. 581-588
524 Scrivener, K.L., 1984, PhD Thesis, Imperial College, Univ. London
525 Scrivener K.L., et al., 1984, Proc. British Ceramic Society, pp. 207-219
526 Scrivener, K.L., 1986, 8th ICCC, Rio de Jan., Vol. II, pp. 389-393
527 Scrivener, K.L., et al., 1988, ACR, Vol. I, No. 4, pp. 230-237
528 Sebok, T., 1986, CCR, Vol. 16, pp. 461-471
529 Seidel, K., 1955, ZKG, Jhg. 8, No. 5, pp. 153-162
530 Seki, S., et al., 1969, ACI-J, March, pp. 198-201
531 Sereda, P.J., et al., 1966, Symp. SPCPC, ACI-SR-90, pp. 58-73
532 Sereda, P.J., et al., 1980, 7th ICCC, Paris, Vol.I, Sub-theme VI-I
533 Setzer, M.J., 1977, DAfSB, Heft 280, Wilhelm Ernst & Sohn, pp. 43-117
534 Shah, S.P., et al., 1986, Int. Conference on the Structure of Concrete, CCA., London, pp. 82-92.
535 Shebl, F.A., et al., 1985, CCR, 15, pp. 747-757
536 Shein, V.I., 1980, 7th ICCC, Paris, Vol. I, Sub-Theme VI-3, pp. VI-3/1-9
537 Shi-Ping, J., et al., 1989, CCR, Vol. 19, No. 3, pp. 487-496
538 Skalny, J., et al., 1980, 7th ICCC, Paris, Vol. I, subtheme II-1

539 Skalny, J., et al., World of Cement Techn., 9, pp. 183-195. *Ibid. [450]*
540 Skvara, F., et al., 1980, CCR, Vol. 10, No. 2, pp. 253-262
541 Slegers, P.A., et al., 1977, CCR, Vol. 7, No. 1, pp. 31-38
542 Smith, M.A., et al., 1974, CCR, Vol. 7, No. 1, pp. 31-38
543 Solovyanchik, A.R., et al., 1990, Privat communication and paper, 9 p.
544 Soroka, I., 1972, CCR, Vol. 2, No. 2, pp. 551-558
545 Soroka, I., et al., 1976, Proc. CHCPSP, Sheffield, April, pp. 87-90
546 Soroka, I., 1983, Bull. ACS, 62, pp. 695-697, 703. *Ibid. [547]*
547 Soroka, I., 1986, CCR, Vol. 16, pp. 495-504
548 Splittgerber, H., 1976, CCR, Vol. 6, No. 1, 1976, pp. 29-36
549 Springenschmid, R., et al., 1986, B&F, H. 11, pp. 704-711
550 Springenschmid, R., et al., 1988, B&St, H. 4, pp. 93-97
551 Stein, H.N., 1962, Rec. trav. chim. Pays-Bas, 81, pp. 881-889
552 Stein, H.N., et al., 1964, J. Appl. Chem., Vol. 14, pp. 338
553 Stein, H.N., 1968, Disc. Kondo *Ibid. [307]*, pp. 248
554 Steinherz, A.R., 1960, RMCTP, No. 536. *Ibid. Venaut [600]*
555 Steinour, H.H., 1944, Ind. Eng. Chem., 36, pp. 840-
556 Steinour, H.. *Ibid. Rahman et al. [471]*
557 Stichting Betonmortelcontrole, Ann. Reports.
558 Stockhausen, N., 1976, Proc. CHCPSP, Sheffield, April, pp. 219-222
559 Strelkov, M.I., 1962, Kiev. *Ibid. [81]*
560 Stroeven, P., 1973, Some Aspects of the Micromechanics of Concrete, PhD, Delft, 329 p.
561 Struble, L., et al., 1980, CCR, Vol. 10, pp. 277-286.
562 Stucke, M.S., et al., 1976, Proc. CHCPSP., Sheffield, April, pp. 31-51
563 Swenson, E.G., 1956, RILEM, Symp. Winter Concreting, Copenhagen, Sess. A., pp. 3-38
564 Swenson, J.A., et al., 1936, J. of Res. Nat. Bur. of St., Vol. 14, Paper 777
565 Sylvan, P., 1964, ZKG, Jhg. 17, No. 7, pp. 299-301
566 Tadros, M.E., et al., 1974, JACS, *Ibid. [413]*
567 Tammann, G., 1925, Ztg. anorg. allg. Chem., 149, pp. 21-98
568 Tang, F.J., et al., 1988, ACR, Vol. I, No. 2, pp. 67-74
569 Taplin, J.H., 1959, Aust. J. Appl. Sci., 10, pp. 329-345
570 Taplin, J.H., 1962, 4th ISCC, Washington, Vol. I, pp. 263-266
571 Taplin, J.H., 1962, 4th ISCC, Washington, Vol. I, paper IV-3, pp. 465-467.
572 Taplin, J.H., 1968, 5th ICCC, Tokyo, paper II-70, pp. 337-348
573 Taplin, J.H., Disc. with Kondo *Ibid [307]* pp. 249-250
574 Taplin, J.H., *Ibid. Fagerlund [156]* (dealing with f/α relationship)
575 Tashiro, C., et al., 1977, CCR, Vol. 7, No. 5, pp. 545-552
576 Taylor, E., 1932, RMCTP, No. 274
577 Taylor, H.F.W., 1950, J. Chem. Soc., London
578 Taylor, H.F.W., 1964, The Chemistry of Cements, Ac. Press, London-NY
579 Taylor, H.F.W., 1968, 5th ICCC, Tokyo, Vol. II, pp. 1-27
580 Taylor, H.F.W., et al., 1984, CCR, Vol. 14, pp. 565-573
581 Taylor, H.F.W., 1986, 8th ICCC, Rio de Jan., Vol. I, pp. 82-110
582 Taylor, H.F.W., 1986, SMDDHC, Boston, MRS, Proc. Vol. 85, pp. 47-54
583 Taylor, H.F.W., 1990, Cement Chemistry, Acad. Press, London, 475 p.
584 Tazawa, E., et al., 1983, Transact. JCI, Vol. 5, pp. 119-126
585 Tenoutasse, N., 1967, ZKG, No. 10, pp. 459-467
586 Tenoutasse, N., et al., 1974, Ind. Chem. Belge, pp. 761. *Ibid. [413]*
587 Tetmayer, 1883, Deutsche Topfer- und Ziegler-Ztg., p. 234
588 Tezuka, Y., et al., 1986, 8th ICCC, Rio de Jan., Vol. II, Theme 2.2, pp. 323-329
589 Thorvaldson, T., et al., 1930, JACS, 52, pp. 3927-3936
590 Timachev, V.V., et al., 1980, 7th ICCC, Paris, Vol. IV, pp. 347-352
591 TNO-IBBC Lab., Adiabatic Temperature Rise in Concrete, Rep. B-88-940 & B-89-320, Rijswijk, NL
592 Tognon, G.P., et al., 1980, 7th ICCC, Paris, Vol. III, pp. VII-133-137
593 Tognon, G.P., et al., 1980, 7th ICCC, Paris, Vol. III, pp. VII - 75-80
594 Traetteberg, A., et al., 1974, CCR, Vol. 4, No. 2, pp. 203-221
595 Trettin, R., et al., 1980, 7th ICCC, Paris, Vol. IV, pp. 163-167
596 Tsumura, S., 1966, ZKG, Jhg. 19, No. 11, pp. 511-518

597 Turriziani, A.R., et al., 1965, Ind. Ital. Cem.. *Ibid. [541]*
598 Uchikawa, H., 1986, 8th ICCC, Rio, Vol. I-III, pp. 249-280
599 Vavian, H.E., 1966, ACI-SP 90, Washington, pp. 19-25
600 Venaut, M., 1961, Rev. M&C., 549, pp. 333-351; 552, pp. 393-406, 552, pp. 434-443
601 Verbeck, G.J., 1960, 4th ISCC, Washington, Paper IV-3, pp. 453-465
602 Verbeck, G.J., et al., 1968, 5th ISCC, Tokyo. Ibid. [295]
603 Verbeck, G.J., et al., 1950, Proc. ASTM, Vol. 50, pp. 1235-1262. *Ibid. [477], [342]*
604 Vidick, B., 1987, CCR, Vol. 17, No. 5, pp. 845-847
605 Vivian, H.E., 1966, Symp. SPCPC, ACI-SP-90, pp. 18-25
606 Vollet, D.R., et al., 1986, 8th ICCC, Rio de Jan., Vol. II, pp. 330-336
607 Vonk, R.A., et al., 1988, Cement, No. 7/8, pp. 53-57
608 Vyrodov, I.P., 1980, 7th ICCC, Paris, Vol. II, pp. II/12-17
609 Wagner, L.A., Proc. ASTM, Vol. 33, Part II, pp. 553-570
610 Walz, K., et al., 1966, Beton, 11, pp. 35-48
611 Walz, K., 1970, Beton, No. 11, pp. 499-503.
612 Werner, D., et al., 1928, Zement, pp. 1002-1005, pp. 1071-1076
613 Werthmann, E., 1982, Z&B, Jhg. 27, No. 3, pp. 131-133
614 Whiting, D., et al., 1977, CCR, Vol. 7, No. 1, pp. 53-60
615 Wieland, W., 1959, ZKG, Jhg. 12, No. 11, pp. 516-519
616 Williamson, R.B., 1972, Progress in Materials Science, Vol. 15, pp. 189-285
617 Wischers, G., 1981, Beton, No. 9, pp. 337-340; No. 10, pp. 385-389
618 Wischers, G., et al., 1982, Beton, No. 9, pp. 337-341; No. 10, pp. 379-386
619 Wittmann, F.H., 1966, ZKG, Jhg. 19, No. 9, pp. 448-451
620 Wittmann, F.H., 1973, JACS, Vol. 56, No. 8, pp. 409-415
621 Wittmann, F.H., et al., 1974, CCR, Vol. 4, No. 3, pp. 389-397
622 Wittmann, F.H., 1976, Proc. CHCPSP, Sheffield, April, pp. 96-117
623 Wittmann, F.H., 1977, DAfSt, Heft 290, Wilh. Ernst & Sohn, Berlin, pp. 43-101
624 Wittmann, F.H., 1980, 7th ICCC, Paris, Vol. I, Sub-theme VI-2, pp. VI-2/1-14.
625 Wittmann, F.H., 1982, RILEM Symp. CEA, Paris, Vol II, Sess. VI, pp. 187-201
626 Woods, H., et al., 1932, ENR, Oct., pp 435-437
627 Woods, H., 1933, ENR, pp. 431-433
628 Wu, X., et al., 1933, CCR, Vol. 13, pp. 277-286
629 Wührer, J., 1950, ZKG, Jhg. 3, pp. 148-151
630 Yamaguchi, G., et al., 1960, ZKG, No. 10, pp. 467-478
631 Yong, K., et al., 1961, ACI-J., Oct., pp. 459-469
632 Young, J.F., et al., 1973, CCR, Vol. 3, No. 6, pp. 689-700
633 Young, J.F., et al., 1977, CCR, Vol. 7, No. 6, pp. 627-636
634 Young, J.F., et al., 1977, JACS, pp. 193
635 Young, J.F., et al., 1986, SMDDHC, Boston, MRS, Proc. Vol. 85, pp. 313-322
636 Young, J.F., et al., RILEM TC-68, M&C, pp. 377-382
637 Young, J.F., et al., Doc. prepared by RILEM TC69, 27 p.
638 Yudenfreund, M., et al., 1972, CCR, Vol. 2, pp. 313-330
639 Zacedatelev, I.B., 1980, 7th ICCC, Paris, Vol. II, pp. II - 71-75
640 Zagar, L., et al., ZKG, pp. 282-284
641 Zhi-Yuan, C., et al., 1986, 8th ICCC, Rio de Jan., Vol. II, pp. 449-453
642 Zimbelmann, R., 1978, B&F, No. 2, pp. 89-96
643 Zimbelmann, R., 1987, CCR, Vol. 17, pp. 651-660
644 Zimbelmann, R., 1989, B&St, No. 5, No. 84, pp. 116-120
645 Zur Strassen, H., Zur Frage der nicht-selektieven Hydratation der Zementminerale, 3 p.

NOTATIONS AND SYMBOLS

A	=	accumulated centre-plane area (per g cement)	[μm^2]
A_{por}	=	total pore wall area	[μm^2]
A_{wat}	=	pore wall area in contact with (bulk) pore water	[μm^2]
AE	=	apparent activation energy	[kJ/mol]
a_c	=	coefficient of thermal diffusivity	[m^2/s]
a_x	=	centre-plane area of particle x	[μm^2]
C	=	(ion) concentration	
C_w	=	water concentration factor (eq. 5.37)	[--]
D	=	diffusion coefficient	[$\mu m^2/s$]
d	=	thickness of spherical product layer	[μm]
E	=	activation energy	[kJ/mol]
F	=	particle fraction	
$F(T)$	=	temperature functions (index 1 or 2)	
f	=	strength	[MPa]
G_c	=	amount (by weight) of cement in mix	[kg/m^3]
$G(x)$	=	cumulative mass distribution of poly-size cement powder	[g]
g	=	temperature sensitivity factor (Section 5.6.2)	
I_x	=	cell (with central particle x)	[μm^3]
K_0	=	basic rate factor	[$\mu m/h$]
K_1	=	rate constant (diffusion reaction)	[$\mu m^2/h$]
L	=	centre-to-centre particle distance	[μm]
N	=	number of particles per gram cement	
O	=	surface area of reactant	[μm^2]
O_x	=	surface area of particle x	[μm^2]
Q	=	heat of hydration	[J/g]
Q^{max}, Q	=	maximum heat of hydration at complete hydration	[J/g]
R	=	universal gas constant	[J/K.mol]
$R_{...}$	=	outer radius of expanding particles	[μm]
RH	=	relative humidity	
r_0	=	radius of anhydrous particle	[μm]
S_x	=	rib size of cubic cell I_x	[μm]
SS	=	specific surface	[m^2/kg]
s	=	standard deviation	
T	=	temperature	[°C]
$\bar{T}$	=	"weighted" temperature (eq. 6.98)	[°C]
t	=	time	[h or sec]
V_x	=	volume of particle fraction F_x	[μm^3]
$V_{...}$	=	pore volume (capillary, total)	[cm^3/cm^3]
V_w	=	initial water volume in paste	[cm^3/cm^3]
v_x	=	volume of particle with diameter x	[μm^3]
W_x	=	mass of particle fraction F_x	[g]
w	=	amount of water (Section 6.5.4.2)	[g]
x	=	particle diameter (also used as particle counter)	[μm]
Y_x	=	radius of spherical cell with central particle x	[μm]

$\alpha(t)$	=	degree of hydration at time t	[--]
$\beta_{..}$	=	independent model parameters (index 1 or 2)	
β_{RH}	=	reduction factor, accounting for relative humidity effects	
Γ	=	thickness of adsorption layer	[μm] or [Å]
δ	=	thickness of layer of reaction products	[μm]
ζ	=	volumetric density factor	[$\mu m^3/\mu m^3$]
η	=	stereometric correction factor (expr. 6.22)	[--]
Θ	=	absolute temperature	[K]
κ	=	temperature factor (eq. 5.52)	[--]
λ	=	parameter, indicating the type of reaction process (Section 6.5.2)	
$\lambda_{..}$	=	Embedded/Free ratio (Section 6.4.3)	[--]
ν	=	ratio: volume of hydration products / reactant	[--]
ρ	=	specific mass	[g/cm^3]
σ	=	stress	[MPa]
ϕ	=	pore diameter	[μm] or [Å]
χ	=	stereometric conversion factor (= $(4.\pi/3)^{1/3}$)	[--]
$\Omega_1(x,\alpha_j)$	=	reduction or partition factor (water withdrawal mechanism)	[--]
$\Omega_2(\alpha_j)$	=	reduction factor, allowing for distribution of water	[--]
$\Omega_3(\alpha_j)$	=	reduction factor, allowing for amount of water	[--]
ω_0	=	water/cement ratio	[--]

INDICES

Superscripts

c	=	cubic
L	=	local
s	=	spherical

Subscripts

a	=	aggregate
ad	=	adsorbed (water at pore walls)
c	=	concrete
cap	=	capillary (in V_{cap})
ce	=	cement
chsh	=	chemical or Le Chatelier shrinkage (in V_{chsh}, Section 6.5.5.2)
ct	=	strength index: tension
ctk	=	concrete tensile strength index, characteristic value
ctm	=	concrete tensile strength index, mean value
em	=	embedded (- cement volume, - centre plane area)
fr	=	free (- particles; i.e. not embedded particles; - water)
in	=	inner (- product, - shell)
in	=	penetration depth of reaction front (in: δ_{in})
j	=	time index, indicating subsequent time steps
ma	=	matrix
ou	=	outer (- product, - shell)
pa	=	paste
por	=	pores (in V_{por})
sh	=	shell
tr	=	transition (in: δ_{tr})
u	=	ultimate
w	=	water
x	=	particle with diameter x [μm]

ACKNOWLEDGEMENTS

The research project, which has resulted in this book, was performed while the author was employed at the Faculty of Civil Engineering of the Delft University of Technology. Actually this second edition is a modified version of the author's PhD-thesis in 1991.

The author wishes to express his sincere thanks to Professor E.M. Theissing (†) for his enthusiastic and practice-oriented support in the early stage of the project and for establishing contact with the laboratories of the Dutch Cement Industry and Bredero-Bouw. His sudden death in 1985 was a great loss to many and also to me. I was honoured that Professor F.H. Wittmann of the ETH-Zürich and Professor J.M.J.M. Bijen of the Delft University of Technology were willing to take over the supervision of the project jointly. They followed the study with stimulating criticism and suggestions, for which they are most gratefully acknowledged.

The discussions with Dr. G. Hakvoort of the Faculty of Chemistry and Dr. P. Stroeven of the Faculty of Civil Engineering concerning reaction kinetics and stereological aspects of structural development, respectively, have been most elucidating and encouraging and are gratefully mentioned. The discussions with Dr. J.A. Larbi on different aspects of the cement paste-aggregate interfacial zone are gratefully mentioned as well.

I wish to thank the Dutch Cement Industry, in particular L.H. Goessens (B.Sc. (†)) and Dr. W. van Loo of ENCI-Maastricht, for conducting adiabatic tests and for the supply of cement samples.

I am greatly indebted to H. Schinkel (M.A.) for stimulating discussions and for coordinating the experimental work carried out at the Bredero Laboratories. I wish to thank Mr. Mak (B.Sc.) for executing the isothermal and semi-adiabatic hydration and strength tests.

Colleagues of the Department of Concrete Structures and students who have been involved in the research project are acknowledged for their stimulating collaboration. I would like to mention in particular F. Lindhout (B.Sc.), Mr. T. Steijn and Mr. H. Spiewakowski. Their enthusiastic and indispensable support concerning the development of the software and preparation of almost all the drawings in this thesis is most gratefully acknowledged. I wish to thank Dr. C.R. Braam for reading carefully the preliminary version of this thesis and his critical remarks.

The permission of Dr. P.L. Pratt (†) of Imperial College, Dr. J.L. Parrott of the British Cement Association and Dr. K. Scrivener for reproducing several photos and of the Royal Society of London for using material from the Royal Society's Philosophical Transactions, Series A, for illustrating purposes is gratefully mentioned.

All those who inspired the author the publish a second edition of this book are gratefully acknowledged. I would like to mention in particular professor P.C. Aïtcin of Sherbrooke University (Can) for his encouraging comments and discussions and for stimulating me to have this book reprinted.

Many thank to mrs. Ina van der Ende for her practical advices, particularly for preparing the front cover.

The financial support by the Section of Concrete Structures of the Faculty of Civil Engineering of the Delft University of Technology of and DIANY ANALYSIS B.V. is gratefully acknowledged.

Klaas van Breugel was born in Oude Niedorp in the north-western part of The Netherlands on the 21th of March 1952. He left secondary school (MULO-B) in 1968 and went to Amsterdam to study at the Technical Institute of Civil Engineering. He was awarded a bachelors degree in 1973.
He continued to study at the Faculty of Civil Engineering at the Delft University of Technology where he was awarded his masters degree in 1979. During this study he served in the army for a 16 month period. On completion of his studies he was employed in the Department of Concrete Structures of the Faculty of Civil Engineering. There he supervised a large number of research projects on the behaviour of concrete protective structures under extreme loading conditions and thermal problems in hardening concrete structures.

At present the author is a senior lecturer and researcher. His main topics and Temperature Effects in Concrete Structures, Early-Age Concrete and Concrete Structures for Environmental Protection. He participates in several task groups of the FIP, RILEM and CUR and is a member of the Dutch Concrete Society, STUVO, STUTECH, IABSE and the American Concrete Institute